TR 82-25

THE GEOLOGY, GEOCHEMISTRY AND SILICATE MINERALOGY OF THE UPPER CRITICAL ZONE OF THE NORTH-WESTERN BUSHVELD COMPLEX, AT RUSTENBURG PLATINUM MINES, UNION SECTION

by

W. J. DE KLERK, B.Sc (Hons)

Thesis presented for the degree of Master of Science in the Department of Geology, Rhodes University, Grahamstown.

January, 1982

DECLARATION

All work in this thesis is the original work of the author except where specific acknowledgement is made to the work of others.

SIGNED: _____

W.J. DE KLERK
Johannesburg Consolidated Investment Co.,
Fundamental Geological Research Dept.,
James Park Complex,
P.O. Box 976,
Randfontein,
1760

January, 1982

ABSTRACT

Rustenburg Platinum Mines, Union Section, is located in the mafic phase of the north-western sector of the Bushveld Complex. This part of the Complex is characterised by transgressions of Upper zone ferrogabbros across the lower sequence of mafic rocks. These transgressions have effectively isolated a roughly triangular segment of Lower, Critical and Main zone rocks. It is in the upper part of the Critical zone that the Merensky Reef, with a strike length of 9,5 km, is found to suboutcrop below a 2-3 m black turf soil cover and it constitutes the orebody being mined at Union Section.

Underground mining and development have exposed a stratigraphic succession from the Middle Group chromitites to within the lower part of the Main zone gabbros. A detailed investigation of a 100 m stratigraphic succession was undertaken in the upper part of the Critical zone, which includes the Bastard Reef, Merensky Reef, Pseudo Reef, UG 2 and UG 1 layers. Stratigraphic descriptions are presented for both a normal and potholed succession, as well as a description of pothole characteristics. The variations of Merensky Reef thickness, pothole distribution and structure of the ore body are also discussed.

Forty seven whole-rock major- and trace-element analyses were carried out on selected samples from both normal and potholed successions, although more emphasis was placed on the former. These samples were taken from just below the UG 1 to above the Bastard Reef. Trace elements determined included Sr, Rb, Y, Nb, Zr, Cr, Co, Ni, Cu and V. The cyclical nature of the layering is clearly defined by breaks in the trends of both the major- and trace element analyses, although some elements are strongly

influenced by the modal proportions of the main mineral phases. Although major breaks are observed for individual elements, insignificant variation of the $Mg/Mg+Fe^{2+}$ ratio is observed throughout.

New electron microprobe data are presented for the main silicate phases olivine, orthopyroxene, clinopyroxene and plagioclase, while only a limited number of analyses were carried out on the spinel phase. There would appear to be a reversal of the expected fractionation trend from the hanging wall of the UG 2 to the Pseudo Marker layer. There is an upward increase of the Fo content of the olivine from $Fo_{76,7-81,6}$. A similar trend is observed for the orthopyroxene analyses. The Merensky unit, as a whole, exhibits a gradual decrease in the Mg end member of the Ca-poor pyroxenes from $En_{78,5-74,1}$. Cumulus plagioclase was found to be markedly more calcic ($An_{72,8-81,7}$) than the intercumulus phase ($An_{56,3-71,9}$). A further feature of the cumulus plagioclase is that strong zonation was observed with the cores of individual crystals being consistently lower in Ca relative to their margins.

CONTENTS

PAGE

ABSTRACT

1. INTRODUCTION 1

2. PREVIOUS WORK 3

3. REGIONAL GEOLOGICAL SETTING 6

4. DETAILED DESCRIPTION OF UPPER CRITICAL ZONE STRATIGRAPHY 12

4.1 Introduction 12

4.2 Role of mine geologist 12

4.3 Sources of data 13

4.3.1 Underground Mapping 13

4.3.2 Underground Diamond Drilling 13

4.3.3 Surface Diamond Drilling 14

4.3.4 Surface Mapping 14

4.3.5 Surface Grid Geomagnetics 15

4.3.6 Regional Airborne Geomagnetics 15

4.4 Nomenclature 15

4.5 Stratigraphic Description 17

4.5.1 MG 4 Chromitite 17

4.5.2 UG 1 Chromitite Layer 20

4.5.3 UG 2 Chromitite Layer 27

4.5.4 Pseudo Reef Unit..... 29

4.5.5 Pseudo Marker and Pothole Marker Layers .. 31

4.5.6 Merensky Reef Unit..... 32

4.5.7 Bastard Reef Unit..... 35

4.5.8 Potholed Succession 37

PAGE

5. REGIONAL GEOLOGICAL FEATURES OF THE MERENSKY REEF AND ITS IMMEDIATE HANGING- AND FOOTWALL 38

5.1 Introduction 38

5.2 Potholes and their distribution 38

5.3 Pothole Structures 40

5.3.1 Contact Reef 41

5.3.2 Pothole Reef 43

5.3.3 Lens Reef 45

5.4 Variation in thickness of Merensky Reef ... 48

5.4.1 Normal Merensky Reef 48

5.4.2 Pothole Merensky Reef 50

5.5 Structure of Merensky Reef 51

5.6 Dykes 51

5.6.1 Dykes of the Pilanesberg Alkaline Province 53

5.6.2 Dolerite Dykes 53

5.7 Faulting 54

5.8 Intrusive Pegmatites and Pegmatoids 55

5.8.1 Pegmatites 55

5.8.2 Pegmatoids 55

5.9 Linear Features 57

6. SAMPLING PROCEDURE 59

6.1 Introduction 59

6.2 Normal Succession 59

6.3 Potholed Succession 63

7. PETROGRAPHY 64

7.1 Introduction 64

7.2 Igneous layered rocks and their nomenclature 64

PAGE

7.3 Anorthosite 69

7.4 Norites 72

7.5 Pyroxenites 77

7.6 Harzburgites 84

8. MINERALOGY 92

8.1 Introduction 92

8.2 Olivine 92

8.3 Pyroxenes 101

8.4 Feldspars 113

8.5 Spinels 124

9. MAJOR-ELEMENT GEOCHEMISTRY 130

9.1 Introduction 130

9.2 Major Element Variation Diagrams 130

9.3 Major Elements vs. Stratigraphic Height ... 132

10. TRACE-ELEMENT GEOCHEMISTRY 150

10.1 Introduction 150

10.2 Incompatible Trace Elements 151

10.2.1 Rubidium (Rb) 151

10.2.2 Zirconium (Zr) and Niobium (Nb) ... 153

10.2.3 Yttrium (Y) 154

10.3 Compatible Trace Elements 155

10.3.1 Strontium (Sr) 156

10.3.2 Chromium (Cr) 159

10.3.3 Cobalt (Co) 160

10.3.4 Nickel (Ni) 161

10.3.5 Copper (Cu) 163

PAGE

10.3.6 Vanadium (V) 164

11. DISCUSSION AND CONCLUSIONS 176

APPENDICES 183

ACKNOWLEDGEMENTS 187

REFERENCES 188

LIST OF FIGURES

		PAGE
FIGURE 1:	Subdivision of the upper Critical zone used by various workers	4
FIGURE 2:	Regional geological map of the Western Bushveld Complex, showing the major linear features	7
FIGURE 3:	Geological setting of Union Section ..	9
FIGURE 4:	IUGS classification and nomenclature of the igneous rocks	16
FIGURE 5:	Stratigraphic column of the upper Middle Group chromitite layers exposed in Spud Shaft	18
FIGURE 6:	Four stratigraphic columns of the upper Critical zone along strike, at Union Section	21
FIGURE 7:	Stratigraphic and strike variations of the UG 2 chromitite layer in the Spud shaft area	28
FIGURE 8:	Geological map of mine workings	39
FIGURE 9:	Schematic section of a pothole	42
FIGURE 10: a and b	Detailed dip sections illustrating the variability of potholes	47
FIGURE 11:	Thickness contour plan for normal Merensky Reef	49
FIGURE 12:	Structure contour (strike) plan of Union Section for the top contact of the Pseudo Reef	52
FIGURE 13: a and b	Plan and section of the underground development in the normal and potholed areas used for the study sections	60
FIGURE 14:	Study section through the upper Critical zone, showing the sampling positions	61
FIGURE 15:	Subdivisions of each core sample used in the present study	62

PAGE

FIGURE 16:	Rock types and sample positions in the study section	65
FIGURE 17:	Types of cumulus textures (Wager,Brown and Wadsworth, 1960)	66
FIGURE 18:	Estimated modal percentage of the main mineral phases in each sample	91
FIGURE 19:	Position of samples used for the electron microprobe mineral analyses of the four main silicate minerals	93
FIGURE 20:	Molecular percent forsterite (Fo) of the olivines, plotted against stratigraphic height	95
FIGURE 21:	Ni (ppm) plotted against weight percentage of MgO for olivines of the Karoo Province and for the Upper Critical zone	98
FIGURE 21a:	Detail of the Ni vs. MgO for olivines from the Bushveld upper Critical zone	99
FIGURE 22: a and b	Ca-Mg-Fe ternary diagrams for Union Section pyroxenes	103
FIGURE 23:	Atomic percent Mg in orthopyroxenes plotted against stratigraphic height .	105
FIGURE 24: a - f	Variation diagrams for Union Section pyroxenes using weight percent FeO as the abscissa	108
FIGURE 25: a - c	Or-Ab-An ternary diagrams for plagioclase feldspars	115
FIGURE 26:	Molecular percent An of Union Section plagioclase plotted against stratigraphic height	116
FIGURE 27: a and b	Diagrams illustrating the Ca distribution between the cores and margins of cumulus and intercumulus plagioclase grains	118
FIGURE 28:	Molecular percent Or plotted against molecular percent An for all Union Section plagioclase analyses	124
FIGURE 29:	Variations in composition of some chromite from the upper Critical zone, plotted against stratigraphic height .	127

PAGE

FIGURE 30:	Triangular diagram depicting Cr-Al-(Fe^{3}+2Ti) variations in some spinels of the upper critical zone	128
FIGURE 31: a - l	All major elements plotted against weight percent MgO	135
FIGURE 32: a - p	Major elements plotted against stratigraphic height	139
FIGURE 33: a and b	Plot of Zr vs. Y and Rb vs. Y (ppm.) .	152
FIGURE 34: a - i	Trace elements (in ppm) plotted against weight percent MgO	166
FIGURE 35: a - k	Trace elements (in ppm) plotted against stratigraphic height	169
FIGURE 36:	Triangular diagram depicting V-Co-Ni whole-rock variations for the upper Critical zone, part of the Main zone and other intrusive bodies	180
FIGURE 37:	Possible crystallization sequence of the upper Critical zone	180

LIST OF PLATES

			PAGE
PLATE 1	a:	Layered leuconorite and chromitite blebs	19
	b:	"Cross-bedded" layered leuconorite	
	c:	Post-crystallization deformation of layered leuconorite	
PLATE 2	a:	Complete UG 1 chromitite with continuous chromitite stringers	22
	b:	Bifurcation of continuous UG 1 footwall chromite stringers	
	c:	Very fine layered chromitite in anorthosite	
	d:	"Cross-bedded" fine layered chromitite in anorthosite	
PLATE 3	a:	Non-continuous UG 1 chromitite stringers in anorthosite	24
	b:	Slump structures of non-continuous chromitite stringers in leuconorite below the UG 1	
	c and d:	Discrete chromitite blebs in leuconorite below UG 1	
PLATE 4	a:	Undisturbed UG 1 chromitite layer.	26
	b:	Top contact of the UG 1 chromitite showing vertical intercumulus plagioclase stringers	
	c:	Thin chromitite layer, 1,5 m below the UG 2 with near vertical intercumulus plagioclase stringers	
	d:	Typical UG 2 chromitite layer	
PLATE 5	a:	Pseudo Marker layer showing the Pothole Marker and upper part of the Pseudo Reef	33
	b:	"Strepie" marker layer (inch-scale layering) within leuconorite	
	c:	Corona texture within leuconorite.	
	d:	Contact between the poikilitic anorthosite and leuconorite in the footwall of the Merensky Reef	
PLATE 6	a:	Fairly thin, normal Merensky Reef.	36
	b:	Detail of the Merensky Reef bottom contact	
	c:	Detail of the Merensky Reef top contact	
	d:	Contact of the Bastard Reef and underlying poikilitic anorthosite.	

PAGE

PLATE 7	a:	Contact Merensky Reef on leuconorite	44
	b:	Dimpling of the contact Merensky Reef into the poikilitic anorthosite (mottled)	
	c:	Lens Merensky Reef	
PLATE 8	a:	Pegmatitic gash vein in feldspathic pyroxenite	56
	b:	Iron-rich intrusive pegmatoid in poikilitic anorthosite	
	c:	Late stage pegmatoidal intrusion or replacement body which has disrupted the layering	
	d:	Coarse-grained pegmatite in layered leuconorite	
PLATE 9	a:	Intercumulus pyroxenes in a plagioclase adcumulate	73
	b:	Large oikocryst of clinopyroxene in a poikilitic anorthosite	
	c:	Cumulus orthopyroxene rimmed by clinopyroxene in a norite	
	d:	Cumulus orthopyroxene with optically continuous intercumulus orthopyroxene in a norite	
	e:	Cumulus chromite with embayments into the cumulus orthopyroxene in a feldspathic pyroxenite	
	f:	Cumulus olivine and orthopyroxene in a granular feldspathic harzburgite .	

LIST OF TABLES

		PAGE
TABLE 1:	Olivine analyses by microprobe ...	100
TABLE 2:	Pyroxene analyses by microprobe ..	110
TABLE 3:	Plagioclase analyses by microprobe	121
TABLE 4:	Chromite analyses by microprobe ..	129
TABLE 5:	Major element analyses (inclusive of H_2O^+, Co_2 and L.O.I.) and CIPW weight percent norms	144
TABLE 6:	Major element analyses (where $Fe_2O_2/FeO=0,2$) and CIPW weight percent norms	147
TABLE 7:	Whole-rock trace element analyses.	173
TABLE 8:	Partition coefficients for trace elements in plagioclase, clinopyroxene, orthopyroxene, olivine and biotite	175

INTRODUCTION

Union Section of Rustenburg Platinum Mines (South 24°56', East 27°9'), is situated 20 km due north of the Pilanesberg Alkaline Complex, and 18 km west of the village of Northam in the north-western sector of the Bushveld Complex. It is here that a roughly triangular segment of Lower, Critical and Main zone rocks of the Bushveld Complex, with an average dip of 19° to the south-east and a strike length of 9,5 km, is exposed.

Mining operations, which commenced in the early 1940s, on the Merensky Reef have been carried out on the farms Zwartklip 405 KQ, Turfbult 404 KQ, Haakdoorn 6 JQ, and Spitzkop 410 KQ (See Figure 3). The international border between the Republic of South Africa (to the north) and the newly independent Republic of Bophuthatswana (to the south), effectively divides the mine along the Turfbult 404 KQ - Zwartklip 405 KQ boundary (Figure 8).

The upper portion of the Critical zone is well exposed by mining operations, in the form of stopes on the Merensky Reef and its associated footwall development. The stratigraphic sequence of a selected normal succession was studied from 4 m below the UG 1 chromitite to 17 m above the Bastard Reef, and that of a pothole succession from 4 m below the UG 1 chromitite to 30 m above the Bastard Reef.

A detailed geochemical study of the rocks in the 100 m stratigraphic succession was undertaken by the author, as few studies of this nature have been done before, with the exception of 10 whole-rock analyses by Van Zyl (1970) in a 780 m section. Detailed studies by the mining company have naturally been undertaken on the economically important

elements within the immediate reef zone.

This study was initiated in order to document the author's geological knowledge of the mine, to produce new and more detailed whole-rock geochemical data (major- and trace-elements) and to present new mineralogical analyses of the main silicate phases: olivine, orthopyroxene, clinopyroxene and plagioclase feldspar. Only a limited number of spinel analyses are presented. The emphasis of the investigation was largely on the documentation of the geology and geochemistry and not the origin of the layering within this portion of the complex.

2. PREVIOUS WORK

Aspects of the geology of the mafic phase of the Bushveld Complex in the north-western Transvaal have been investigated and described by various authors including Wagner (1929), Wasserstein (1936), Van der Walt (1941), Fuller (1951), Coertze (1958, 1962, 1970 and 1974), Feringa (1959), Cousins (1959), Ferguson and Botha (1963), Wager and Brown (1968) and Van Zyl (1970). Included in the literature of the geology in the area are numerous "in-house" JCI memoranda and mining, mineralogical, exploration and research reports.

Wasserstein (1936) described the "breaks" or Gap areas in the continuity of the Critical zone and hence the Merensky Reef and chromitite layers, north of the Pilanesberg, and suggested that these layers had been displaced by faults.

Feringa (1959) drew up structural sections of borehole logs from Union Section using the Bastard Reef as a datum. His interpretation of these sections was that there had been gentle folding of the layers which underlie the Merensky Reef. Feringa (op.cit.) also pointed out that the borehole evidence strongly suggested that the Merensky Reef and its hanging wall formations represented a younger heave of magma than that which formed the footwall layers. He also went further to suggest that the folded floor had possibly been exposed at surface and that the Merensky Reef and associated hanging wall had been extruded. Cousins (1959) in his discussion of Feringa's (op.cit.) paper, supported this extrusive hypothesis, and pointed out that there was sufficient parallel evidence from other localities in the Bushveld Complex. Coertze (1959), in his discussion, pointed out that, had Feringa (op.cit.) used a lower datum to draw his structural sections, then a gentle folding of the Merensky and Bastard Reef would have been observed. The anti-

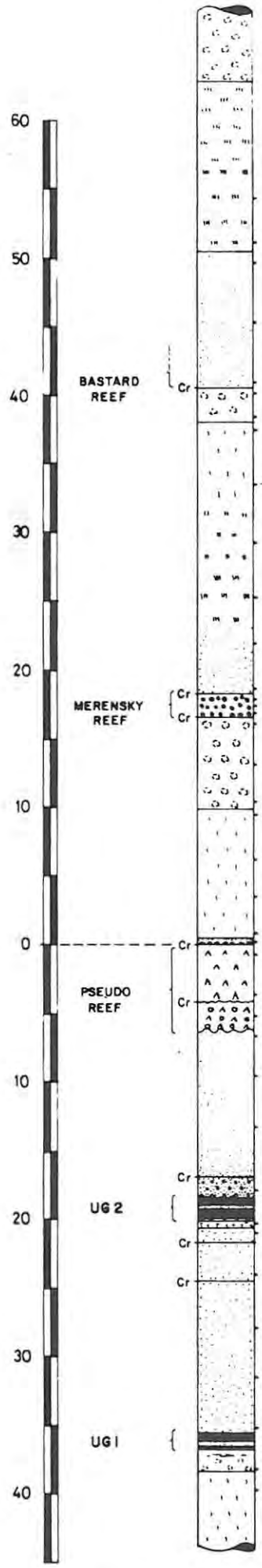

Feringa (1959)	Wager and Brown (1968)	Van Zyl (1970)	S A C S (1980)	This Study
Subzone 8 Anorthositic Group 53 m	Macro-Rhythmic Units (MRU) Bastard Merensky MRU	Norite-Anorthosite Unit Bastard Reef Sub-unit	Upper part of the Rustenburg Layered Suite of the Western Bushveld Complex	Bastard Unit
Subzone 7 Pyroxenitic Group				
Subzone 6 Anorthositic Group	Merensky MRU	Merensky Reef Sub-unit		Merensky Unit
Subzone 5 Pyroxenitic Group				
Subzone 4 Anorthositic Group	Pseudo-Reef MRU	Pseudo-Reef Sub-unit	Mathlagame Norite-Anorthosite Upper Sub-zone of the Critical Zone (≡ Winter=veld Norite Anorthosite of the Eastern Bushveld Complex)	Footwall Unit
Subzone 3 Pyroxenitic Group	MRU			Upper Pseudo Unit Lower UG 2 Unit
Subzone 2 Pyroxenitic Group	MRU			UG 1 Unit
Subzone 1 Anorthositic Group 122 m		Basal Sub-unit		Basal Unit

Figure 1

clinal features would in fact become depressions and this has since been found to be the case, these depressions being in the form of potholes.

Van Zyl (1970) made a study of borehole cores and limited mine workings at Union Section on the farm Swartklip 405 KQ, and concluded that the rock types intersected in the upper Critical zone could be divided into four main sub-units (Figure 1). He explained the rhythmic layering of these sub-units by postulating different heaves of homogeneous magma, which were emplaced at intervals, after which fractional crystallization and gravitative differentiation took place. Van Zyl (op.cit.) also concluded that textural relationships between the chromite and silicate phases indicated that the chromitite layers were not early crystal accumulations. He suggested that the chromite in these rocks unmixed as a chromiferous liquid at an early stage, after the crystallization of some silicates, and that it then settled as a result of gravity.

Various workers at Union Section, notably Feringa (1959), Wager and Brown (1968), and Van Zyl (1970), subdivided the Upper Critical zone into subzones, sub-units and macro-rhythmic units (Figure 1). Wager and Brown (op.cit.) simply re-interpreted the 8 subzones that Feringa (op.cit.) had presented, and they introduced the macro-rhythmic unit (MRU) concept to the upper Critical zone layers. Wager and Brown (op.cit.) recognised each MRU as having a melanocratic base, grading upwards into a leucocratic top. For the purpose of this investigation the study section has been divided into a number of units (Figure 1), because this term does not carry any genetic overtones, but rather divides the upper Critical zone into well-defined lithologies or lithological groups, which have distinct mineralogical, chemical and petrological characteristics.

3. REGIONAL GEOLOGICAL SETTING

Union Section of Rustenburg Platinum Mines is situated within the north-western sector of the Bushveld Complex. This part of the Complex differs from other parts, in that it is characterised by a number of major transgressions and truncations of large sectors of the Lower, Critical and Main zone assemblages, by rocks of the Upper zone (Figures 2 and 3). Two major transgressions of this type, known as the northern and southern Gap areas, bound Union Section to the north-east and south-west respectively, effectively isolating a triangular segment of Lower, Main and Critical zone rocks. A 9,5 km stretch of Merensky Reef with a north-easterly strike occupies the central part of this segment and constitutes the ore body being mined at Union Section.

Lower, Critical and Main zone rocks are generally poorly exposed and are largely covered by a layer of black turf soil 1 to 2 m. thick. The base of the Bushveld Complex in the area is marked by a narrow (7 m. wide) resistant and metamorphosed quartzite layer in the vicinity of the Bierspruit, which dips steeply at 65° to the south-east. This is overlain by pyroxenites and harzburgites of the Lower zone and basal part of the Critical zone. The LG (Lower Group) chromitite layers (nomenclature of Cousins and Feringa, 1964) are present within the upper part of the pyroxenites (lower Critical zone) but not one of the chromitite layers has been mined in this sector of the Bushveld Complex. The harzburgite layers have well-developed cappings of secondary birbirite, consisting of resistant opaline silica and semi-lateritic material. Rocks of the upper Critical and Main zones are poorly exposed, except for minor outcrops of poikilitic anorthosite and norite.

Upper zone rocks of the Gap areas are very poorly

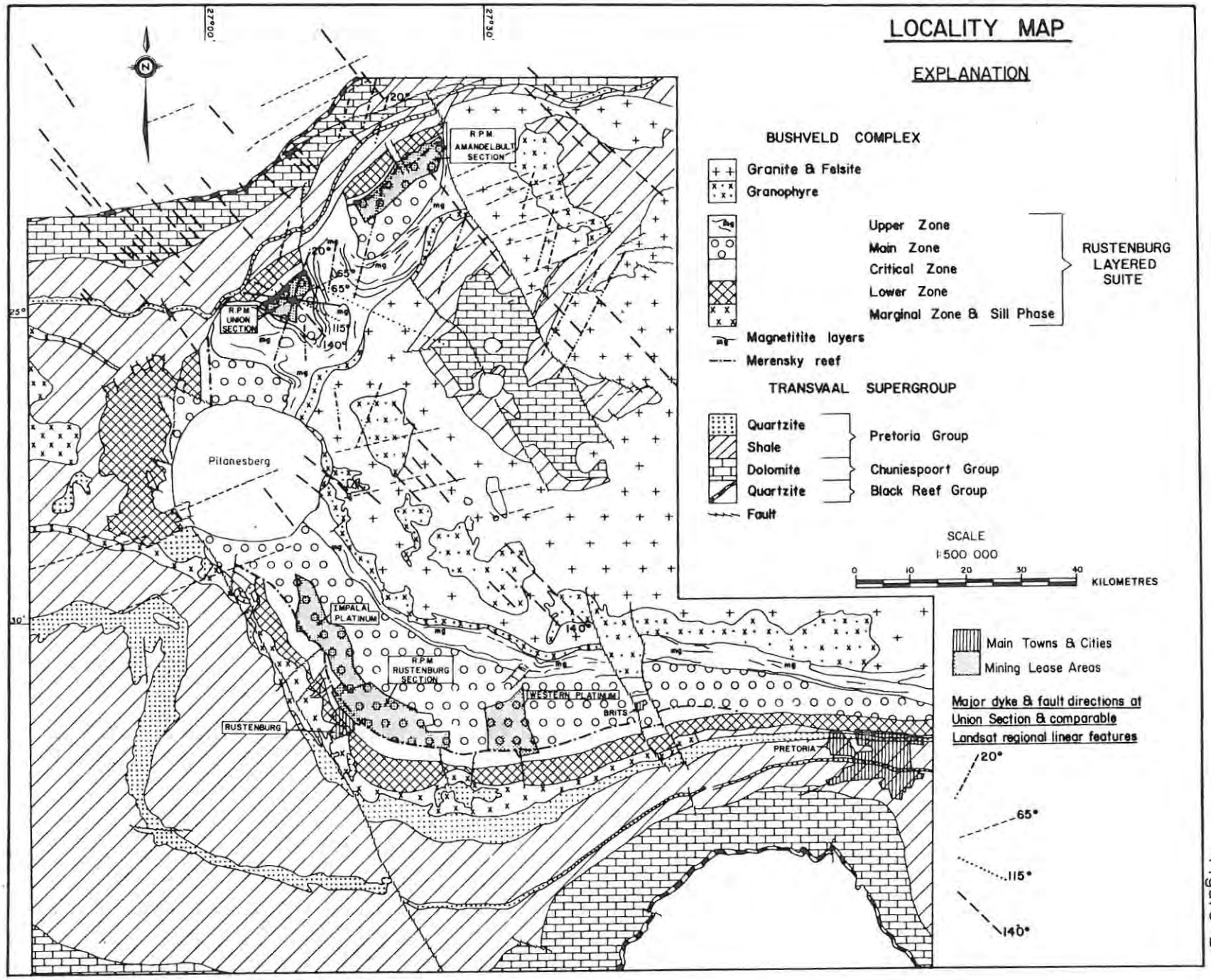
LOCALITY MAP
EXPLANATION
BUSHVELD COMPLEX
Granite & Felsite
Granophyre
Upper Zone
Main Zone
Critical Zone
Lower Zone
Marginal Zone & Sill Phase
RUSTENBURG LAYERED SUITE
Magnetitite layers
Merensky reef
TRANSVAAL SUPERGROUP
Quartzite
Shale
Pretoria Group
Dolomite
Quartzite
Chuniespoort Group
Black Reef Group
Fault
SCALE
1:500 000
0 10 20 30 40 KILOMETRES
Main Towns & Cities
Mining Lease Areas
Major dyke & fault directions at Union Section & comparable Landsat regional linear features
20°
65°
115°
140°
R.P.M. AMANDELBULT SECTION
R.P.M. UNION SECTION
R.P.M. RUSTENBURG SECTION
IMPALA PLATINUM
WESTERN PLATINUM
Pilanesberg
RUSTENBURG
BRITS
PRETORIA
27°00'
27°30'
25°
30'

Figure 2

exposed, but, in striking contrast to the rocks of the lower succession described above, give rise to dark red and brown soils, thereby allowing for the easy delimitation of their extent. The Upper zone rocks are characterised by the presence of vanadium bearing titaniferous magnetite layers, which form useful stratigraphic marker layers. These magnetite layers dip towards the centres of the trough-like transgressions, and the layers also follow the Gap cut-off, effectively enveloping the segment of Lower Critical and Main zone rocks at Union Section. They indicate a structure in the Gap areas in which the Upper zone assemblage completely transgresses and truncates the lower stratigraphy, eventually abutting against the Transvaal floor rocks (Figure 3).

Owing to lack of detailed information, there is as yet no unanimity on the origin and detailed structure of the Gap areas. Feringa (1958) and Cousins (1959) maintain that faulting with a throw of approximately 2300 m. was responsible for the displacement of the Lower, Critical and Main zones, and for the subsequent emplacement of the younger ferrogabbros of the Upper zone into the Gap areas. Coertze (1974) suggests that the ferrogabbros occurring in the Gap areas are intrusive. He considers each Gap to be an intrusion of magma, which, in places, completely obliterated the underlying Critical and Main zone rocks. Viljoen and Feuchtwanger (1977), consider the evidence for such an hypothesis as rather scant. Firstly, they point out that the size of the gravity anomaly over the Gap area is far too small for the amount of denser rock (ferrogabbro) that would have to be present, should Coertze's theory be valid. Secondly they say that the continuity of the ferrogabbros north and southwards from the Gap areas seems to suggest that they form an integral part of the main bulk of the Upper zone, rather than separate injections.

Walraven and Darracott (1976) conclude from a study of

GEOLOGICAL SETTING OF UNION SECTION

0 1000 2000 3000 4000 5000
metres

KEY

- Hills
- Main road
- Single track railway line
- Minor stream

GEOLOGICAL EXPLANATION

TRANSVAAL SUPERGROUP
- Quartzite
- Shale and sandy shale

LOWER ZONE
- Bronzitite
- Harzburgite with birbiritic capping

CRITICAL ZONE
- LG-6 Chromitite
- MG Chromitite
- Norite, anorthosite and minor bronzitite with chromitite layers
- UG-2 Chromitite
- Merensky reef

MAIN ZONE
- Norite, anorthosite, gabbro
- Spotted norite
- Anorthosite

UPPER ZONE
- Magnetite gabbro, troctolite, olivine gabbro
- Magnetitite seam

- Iron-rich dunites and pegmatoid
- Magnetite dunites and pegmatoid

From underground workings and surface magnetics
- Pilansberg dyke
- Diabase dyke
- Major fault
- Dip

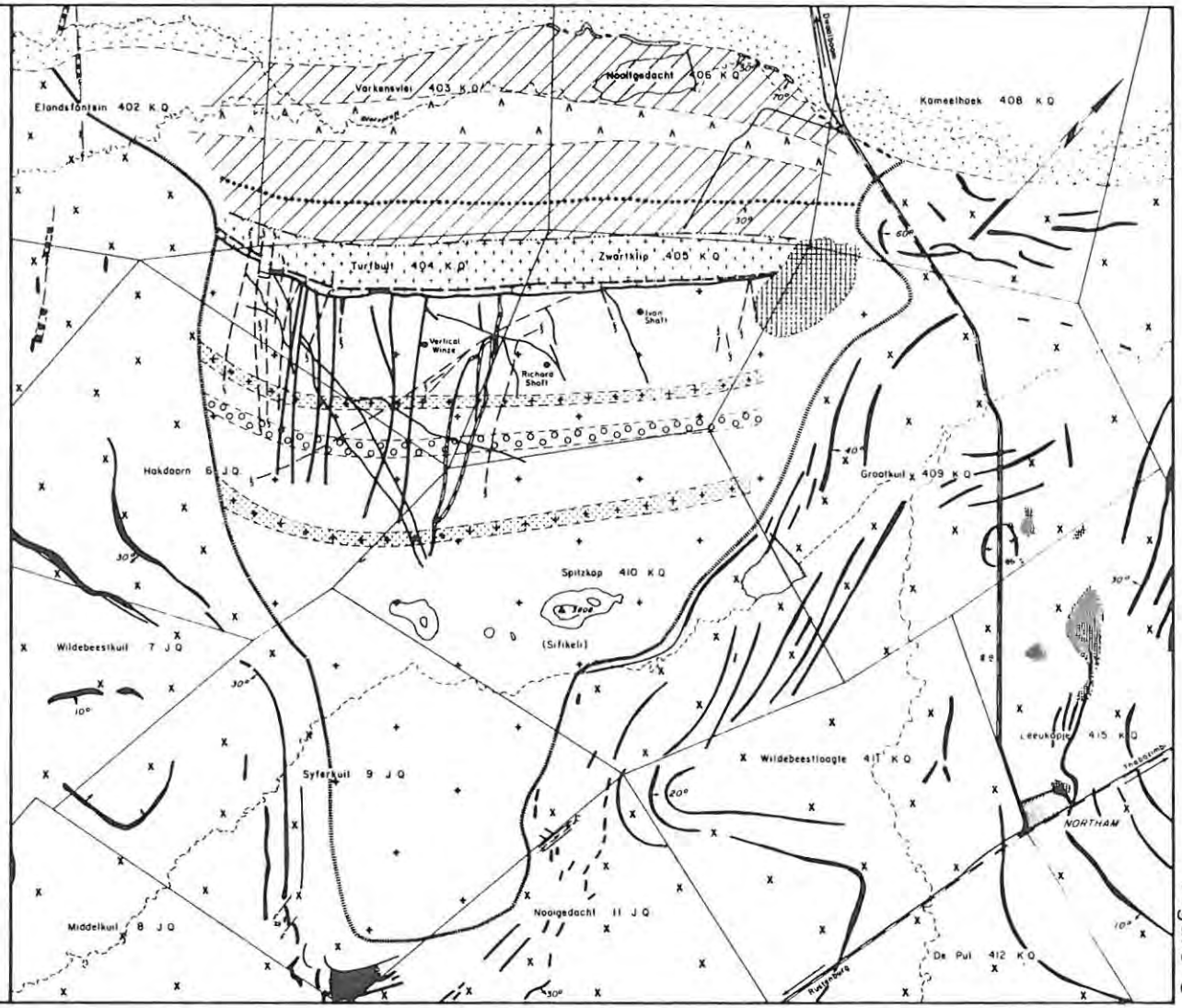

Figure 3

the acid rocks of the Bushveld Complex, east of the Pilanesberg, that a series of north-west trending synclines and anticlines exists in this area. A major anticlinal structure is considered to trend through a granophyric sheet in the acid rocks of the Bushveld to the south-east and then to extend through the Union Section area. Two synclinal axes to the north-east and south-west of the above area are projected in a north-westerly direction through the northern and southern Gap areas.

The regional geological maps (Figure 2 and 3) as well as the Landsat image (Frontispiece) of the area, show the Transvaal floor rocks to the north-west of both Gap areas to be anticlinal in form, while the sector containing the Merensky Reef and associated marker layers is synclinal and abuts against the anticlinal feature. This would imply that the relationship of the Bushveld Complex to the floor rocks in the western Bushveld area is similar to relationships in the eastern Bushveld as described by Button (1975) and could mean that the Merensky Reef never occurred in the Gap areas.

It has been stated above that the gravity values over the gaps are smaller than would normally have been anticipated. The reasons for this could be twofold: either the ferrogabbro is only thinly developed, or there is an upwarping of the Transvaal floor rocks. The latter postulate would fit the geological observation outlined above. Although there is evidence, therefore, for an anti-formal feature below the Gap area, the observed distribution of ferrogabbro would suggest the later development of a syn-formal structure. How this feature might have developed is a matter for speculation. Viljoen and Feuchtwanger (1977) suggested that graben faulting was probably operative in part. However, rather than a straightforward down-faulted block being developed, they consider pivotal faulting to have been responsible for producing the Gap areas. The

axis of the hinge is postulated to have developed parallel to the strike of the Magaliesberg quartzite. Tilting of the Pretoria Group sediments along this hinge axis resulted in their being slightly upfaulted and taking on a steeper dip, with the outcrop moving in a south-easterly direction. Simultaneously the portion of floor rocks below the present Gaps to the south-east of the hinge zone was downfaulted and attained a steeper dip, thereby allowing for the emplacement of Upper zone material.

The direction of the postulated graben faults is north-west, which parallels a major direction of faulting and dyke emplacement seen at Union Section (discussed later). The dykes form part of the Pilanesberg swarm in the area. It would thus appear that the structural grain that controlled the faulting, which in turn gave rise to the Gap area graben, has persisted, and is manifested in post-Bushveld faulting and dyke intrusion. As might be expected, prominent drag on the faults, and a substantial steepening are observed at the north-east extremities of the Lower, Critical and Main zones at Union Section (discussed later), as well as at the south-western extremity of Amandelbult Section. At the south-western part of Union Section, numerous subsidiary faults (exposed in underground mine workings) parallel to the graben edge are manifested in the Critical zone. These faults are probably part of a major dislocation and are considered to be situated along the contact between the Upper zone rocks of the Gap areas and the Transvaal floor rocks.

4. DETAILED DESCRIPTION OF THE STRATIGRAPHY OF THE UPPER CRITICAL ZONE

4.1 Introduction

The upper part of the Critical zone and the base of the Main zone of the Bushveld Complex are routinely exposed by underground workings at Union Section. Exposures generally extend from 20 metres below the uppermost of the Middle Group (MG) chromitite layers, to a level approximately 300 metres above the base of the Main zone gabbros, a vertical interval of some 680 metres (see Figures 5 and 6). Figure 5 represents a short borehole through those MG chromitite layers which have been exposed in the deepest mine working at Spud shaft, while Figure 6 represents stratigraphic columns along strike (columns 1-3), which have been compiled from numerous underground boreholes, underground mapping and surface boreholes from each area.

4.2 Role of mine geologist

The fundamental responsiblities of the mine geologists at Union Section could be summarised as follows:

a) To document the geology of the ore body and its environs by regularly visiting current development and stoping faces in each section.

b) To evaluate the ore body, in co-operation with the survey and sampling departments, and to try and improve on the existing evaluation methods.

c) To monitor the grade-control, in co-operation with the mining and survey departments.

d) to participate in the on-mine exploration and research programmes in order to maintain or increase the ore reserves.

A sound knowledge of various geophysical mapping techniques and exploration diamond-drilling operations (surface and underground) is essential.

4.3 Sources of Data

4.3.1 Underground Mapping The detailed geology of the above stratigraphic succession (Figure 6) has been determined principally from underground mapping of the main tramming haulages, cross-cuts, reef raises and winzes, stopes and any other underground excavations. Routine daily underground mapping is done on a scale of 1:1000, excepting areas of special interest, such as geologically disturbed zones, which are mapped on a scale of 1:500, i.e. a plan and dip section (Figure 10a and b). This detailed mapping (1:500 and 1:1000) is later transferred to a 1:5000 master geological plan, which is used in all evaluation and planning exercises.

Stope-face mapping is also of considerable importance in monitoring the variations in reef thickness, fault and dyke positions and in mapping in the positions of the so-called "cut-offs" of potholes. Accurately co-ordinated and elevated survey stations in the stopes help in the construction of the strike contour plan of the mine (Figure 13).

4.3.2 Underground Diamond-drilling Further details of the upper Critical zone are obtained from underground diamond-drilling. A X U size (3,5 cm) core is recovered, and to date 320 underground boreholes have been drilled. This drilling is co-ordinated by the geological staff and is usually directed at the more geologically disturbed areas on the mine. Diamond-drilling is also routinely used for short-term evaluation purposes, which require data relating to both the grade and attitude of the

ore body. An average of 300 metres of core is drilled per month and all core is logged and sampled before being discarded. Detailed logging records are kept of each hole, and a normal (right-angle) stratigraphic section of each hole is drawn up, in which the angle and direction of each hole, and the local attitude of the layering in the area are taken into account.

4.3.3 Surface Diamond-drilling To date 47 surface boreholes have been drilled. These boreholes have been used to prove and evaluate the ore-body beyond the limits of present mining activity. A careful check has to be maintained during drilling to determine any deviation from the intended direction of the borehole. As in the case with dipping strata, the vertical boreholes from surface tend to deflect up-dip, i.e. in a north-westerly direction. This deflection must be kept within the acceptable limits of ore-body intersection, which permit no more than a 10° deviation from a normal intersection. Any deflection is plotted on a plan, and the final ore body intersection and the true elevation above or below mean sea-level is calculated. This calculation is done after all the borehole survey results are submitted by the drilling contractors. The true thickness of all the layers intersected is also calculated, after the deflection of the borehole has been taken into account.

4.3.4 Surface Mapping Surface exposure of the Lower, Critical and lower Main zone rocks is rather limited in the Union Section area because of a thick (1 to 5 m) turf soil overburden. The Lower and lower Critical zone rocks are poorly exposed, as they are covered by alluvium from the Bierspruit, which runs almost parallel to the strike direction. Outcrops of Main zone gabbros are exposed in the Pyramid Gabbro hills, 5 km. south-east of the Merensky reef sub-outcrop (See frontispiece, Landsat image). The position

of the Merensky Reef sub-outcrop was determined by numerous prospecting trenches in the 1920s (Wagner, 1929)

4.3.5 Surface Grid Geomagnetics Cheaper and more sophisticated geomagnetic mapping techniques were employed to probe problematic areas in advance of the mining front. To date, five detailed surface geomagnetic surveys have been completed, forming a mosaic primarily over the south-western sector of the mine. These surveys have clearly demarcated all the dykes, dunitic pipes and cross-cutting iron-rich pegmatoids in these areas. Where mining operations have advanced into the survey areas, a very good degree of correlation between underground geological features and geomagnetic anomalies has been confirmed.

4.3.6 Regional Airborne Geomagnetics A regional airborne geomagnetic survey was flown over a large area from the northern limit of the Pilanesberg, in an arc, to the eastern limit of the Amandelbult section of R.P.M., just south of Thabazimbi. This survey included an area from the Transvaal Sequence floor-rocks to well within the Main zone gabbros. The results of this survey are not fully processed yet.

4.4 Nomenclature

The nomenclature and classification of the rocks in this study are based on the recommendations of the IUGS subcommission on the systematics of igneous rocks (Streckeisen 1976). Figure 4 shows the common gabbroic and ultramafic rocks in the tetrahedron, plagioclase-orthopyroxene-clinopyroxene-olivine. For noritic and gabbroic rocks, a plagioclase content of 35-65% is considered as normal. Part of Shand's(1943) colour-index classification has been retained, and the prefixes mela- and leuco- are used to

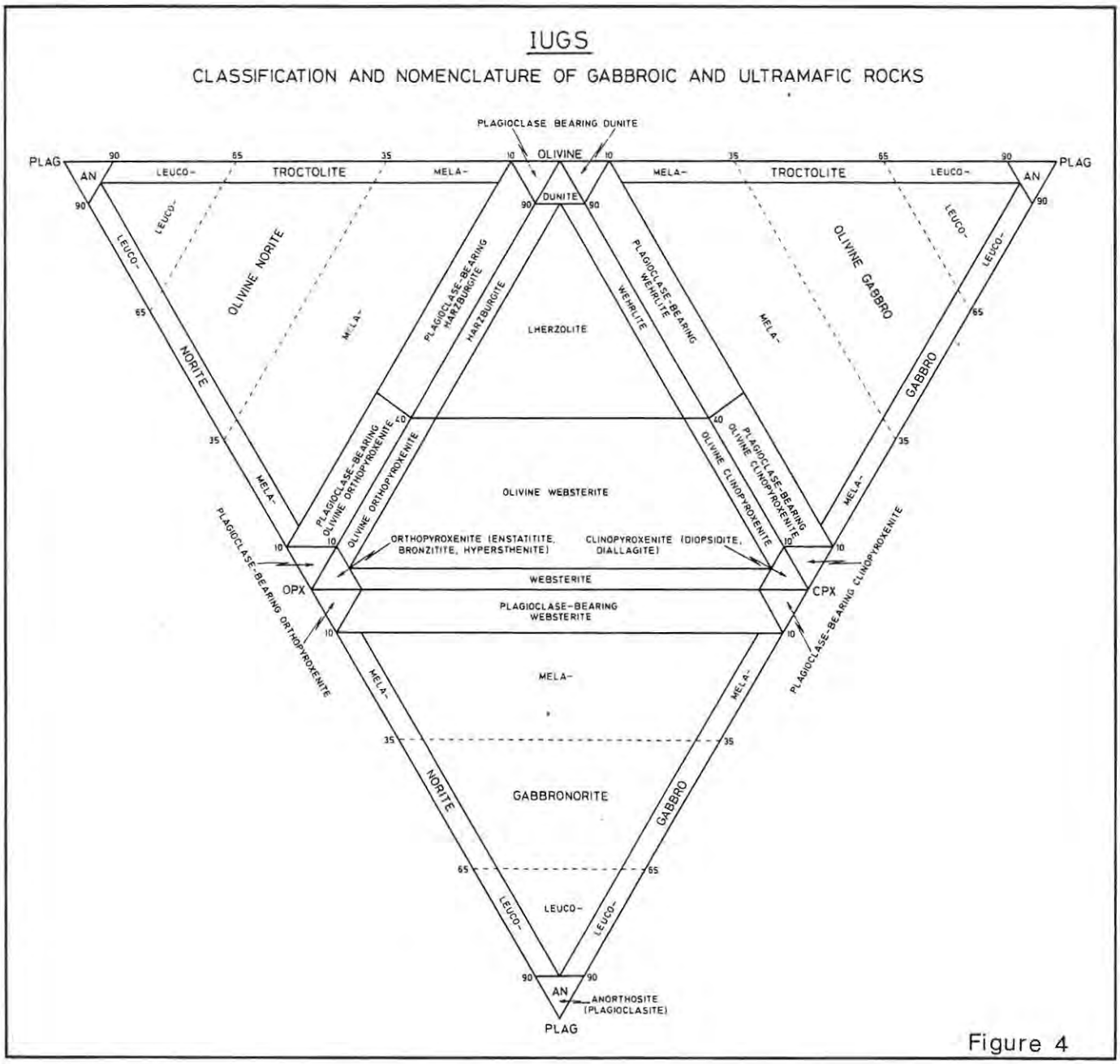

Figure 4

designate the more felsic and mafic rock types respectively, in comparison with normal types. Rocks that contain more than 65% plagioclase are termed leuco-, whereas rocks that contain less than 35% plagioclase are termed mela-.

As all the noritic and pyroxenitic rock types in the study section contain a greater concentration of ortho-pyroxene than clinopyroxene, the prefix ortho- has been

dropped in this study, to simplify rock descriptions, e.g. plagioclase-bearing orthopyroxenite has been simplified to feldspathic pyroxenite, i.e. the rock has no more than 10% plagioclase.

The majority of rock types in this study section are medium-grained, i.e. mineral grains are between 1 and 5 mm in diameter. Those rocks that are extremely coarse-grained, i.e. grain-size greater than 5 mm, are termed pegmatoidal, e.g. pegmatoidal feldspathic harzburgite or pegmatoidal feldspathic pyroxenite.

4.5 Stratigraphic Description

4.5.1 MG 4 Chromitite 280 metres below the well-developed UG 1 chromitite layer lie the MG 4 chromitite layers, a 4-metre wide series of chromitites, which form the uppermost of the so-called Middle Group chromitite layers. These layers are exposed in the deepest workings of Spud Shaft, i.e. 20 level, which is 1030 metres below the shaft collar. An underground borehole was drilled from 20 level downward to locate any further MG chromitite layers (See Figure 5). A further series of chromitites are thought to be part of the MG 3 layers, but the last chromitite could represent the MG 2.

The thick unit between the MG 4 chromitite and the UG 1 consists predominantly of norite with some fine-grained feldspathic pyroxenite layers. The immediate hanging wall of the MG 4 chromitite is a fine-grained pyroxenite which grades upwards to a fine-grained melanorite. Closer to the UG 1 the norite becomes more leucocratic and medium-grained, with a distinctly layered texture. This distinctive zone is 5 to 8 metres thick, and is referred to locally as the "streaky" norite (See Figure 6 and Plate 1a).

Figure 5

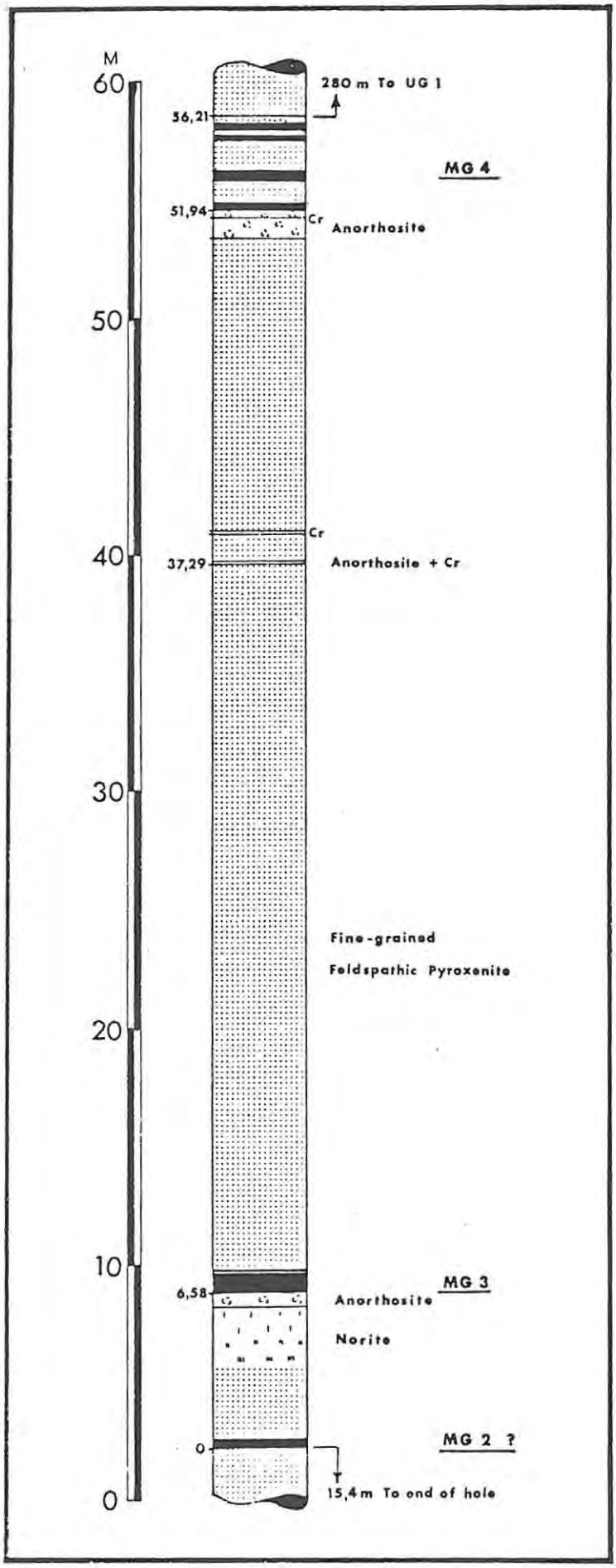
M
60
50
40
30
20
10
0
56,21
51,94
37,29
6,58
0
280 m To UG 1
MG 4
Cr
Anorthosite
Cr
Anorthosite + Cr
Fine-grained
Feldspathic Pyroxenite
MG 3
Anorthosite
Norite
MG 2 ?
15,4 m To end of hole

PLATE 1

a. Fine scale layering of cumulus orthopyroxene in the "streaky" leuconorite, 4 m below the UG 1 chromitite. Note the small discrete chromitite blebs in a zone of orthopyroxene depletion, above the prominent layering.

b. Distortion of the regular layering in the "streaky" leuconorite 4 m below the UG 1, creates the effect of igneous cross-bedding. This is most likely caused by limited post-crystallization plastic flow of the crystalline mush before final solidification.

c. Slumping of a feldspathic pyroxenite Xenolith, highly charged with disseminated chromite which has distorted the layered leuconorite 4 m below the UG 1. The xenolith is rimmed by a zone 2 cm thick, which is devoid of pyroxene. The layering directly below the xenolith has been compacted and it would appear as if the plagioclase has been expelled. Note the flow-fold structure in the leuconorite below the layered zone.

PLATE 1

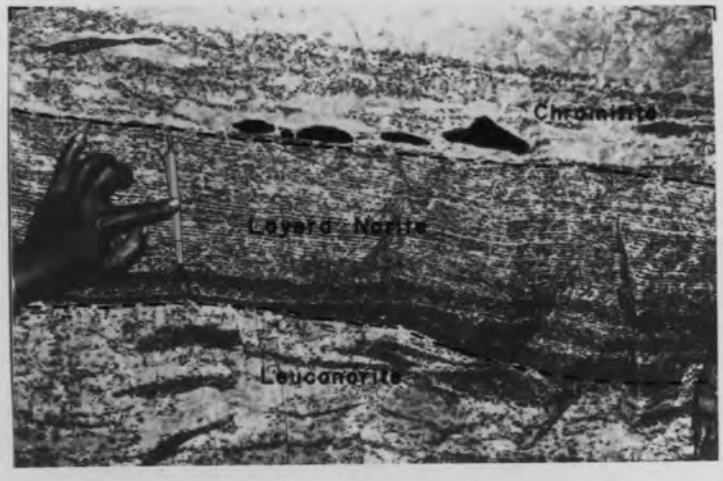
Chromitite
Layered Norite
Leucanorite

a

b

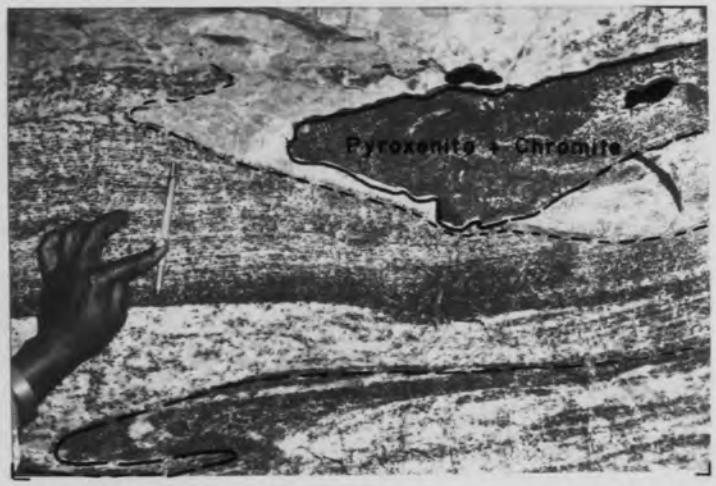
Pyroxenite + Chromite

c

It is in this "streaky" norite that a type of "cross-bedding" and disruption of the layering is developed. These structures are explained by post-crystallization "plastic" flow (movement) and deformation of the primary layering (Plate 1b and c). Overlying the streaky norite and forming the immediate footwall of the UG 1 is an anorthosite layer of between 1 and 3 metres in thickness, which contains a variety of chromitite layers, blebs and stringers. This rock type is more conveniently described together with the UG 1 chromitite layer.

4.5.2 UG 1 Chromitite Layer The UG 1 chromitite is a composite interval forming the first of the so-called Upper Group of chromitite layers of the Critical zone. It can generally be divided into a main upper chromitite and a complicated assemblage of footwall layers, stringers and lenses, enveloped by anorthosite (See Figure 6).

Two types of UG 1 stringers are recognised, viz., continuous and non-continuous. The continuous stringers comprise very regular and continuous layers of chromitite which are generally greater than 0,5 cm but less than 20 cm in thickness. The contact between the stringers and the host anorthosite is invariably sharp, and the layers anastomose in a very distinctive way within the anorthosites (Plate 2a and b).

Interpretations of these structures in the footwall include the hypothesis of separate intrusions of a unique magma (Coertze, 1974), and turbulent mixing of plagioclase at the top of a cyclic unit, with chromite deposited at the bottom of the following unit (Vermaak, 1976). Sampson (1932) suggested that the underlying crystallised anorthosite cracked, and chromite-bearing residual magma intruded these cracks. Cameron (1978) concluded that these structures originated through flow, and that the chromitite layers penetrated along fractures into the anorthosite from the

Figure 6

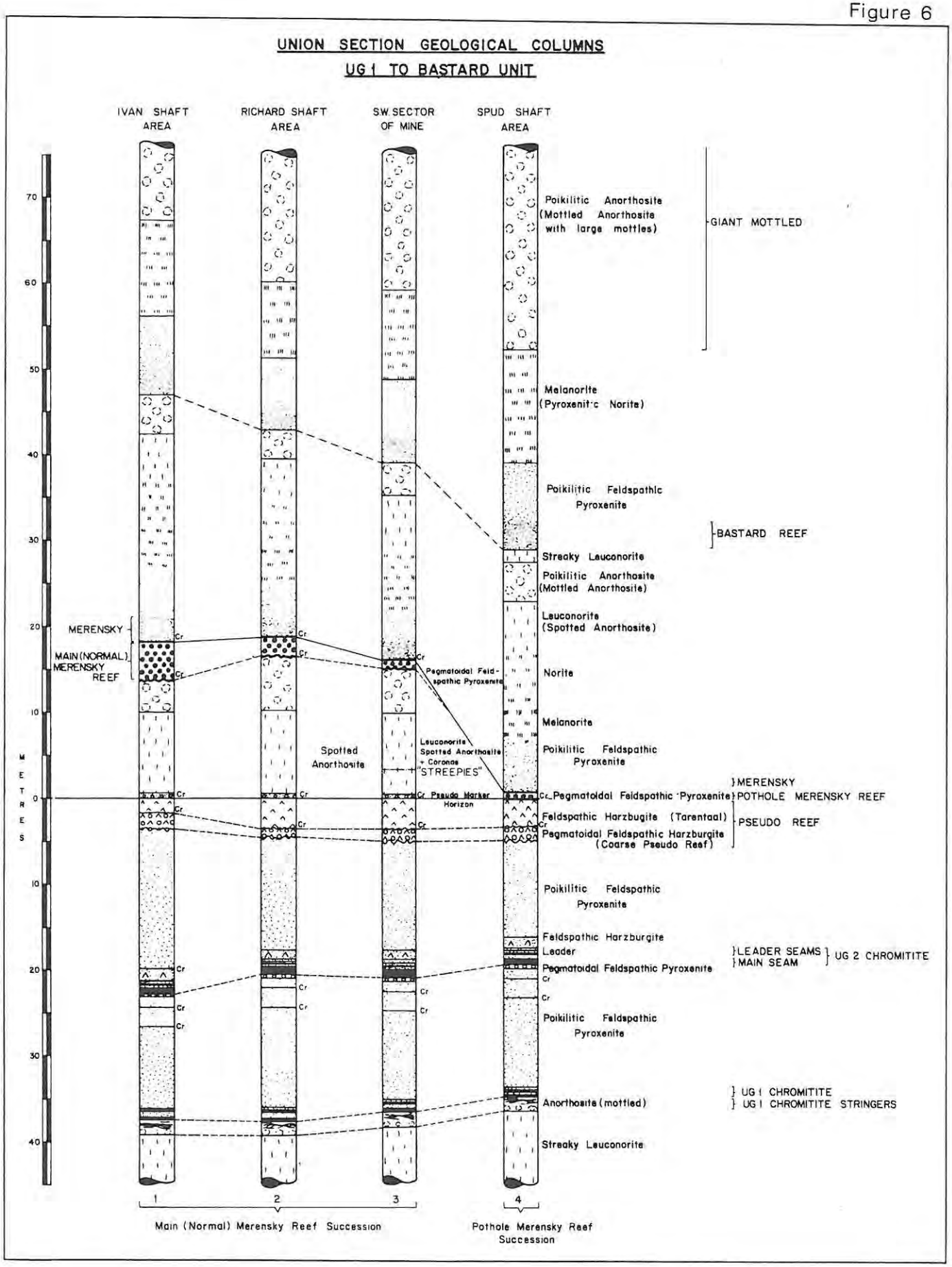
UNION SECTION GEOLOGICAL COLUMNS
UG 1 TO BASTARD UNIT
IVAN SHAFT AREA
RICHARD SHAFT AREA
S.W. SECTOR OF MINE
SPUD SHAFT AREA
METRES
70
60
50
40
30
20
10
0
10
20
30
40
Poikilitic Anorthosite (Mottled Anorthosite with large mottles)
GIANT MOTTLED
Melanorite (Pyroxenitic Norite)
Poikilitic Feldspathic Pyroxenite
BASTARD REEF
Streaky Leuconorite
Poikilitic Anorthosite (Mottled Anorthosite)
Leuconorite (Spotted Anorthosite)
MERENSKY
MAIN (NORMAL) MERENSKY REEF
Pegmatoidal Feldspathic Pyroxenite
Norite
Melanorite
Spotted Anorthosite
Leuconorite Spotted Anorthosite + Coronas "STREEPIES"
Poikilitic Feldspathic Pyroxenite
Pseudo Marker Horizon
Pegmatoidal Feldspathic Pyroxenite
MERENSKY
POTHOLE MERENSKY REEF
Feldspathic Harzburgite (Tarentaal)
Pegmatoidal Feldspathic Harzburgite (Coarse Pseudo Reef)
PSEUDO REEF
Poikilitic Feldspathic Pyroxenite
Feldspathic Harzburgite
Leader
Pegmatoidal Feldspathic Pyroxenite
LEADER SEAMS
MAIN SEAM
UG 2 CHROMITITE
Poikilitic Feldspathic Pyroxenite
Anorthosite (mottled)
UG 1 CHROMITITE
UG 1 CHROMITITE STRINGERS
Streaky Leuconorite
Cr
1
2
3
4
Main (Normal) Merensky Reef Succession
Pothole Merensky Reef Succession

PLATE 2

a. Continuous UG 1 chromitite layers in anorthosite, showing the typical patterns of bifurcation and convergence. In this case it is rather difficult to explain why only the upper layer of chromitite has been disrupted by "footwall" anorthosite material.

b. Detail of the continuous UG 1 chromitite layers in the anorthosite footwall. Well illustrated here are the bifurcation, convergence, and variable thickness of individual chromitite layers. Note the dimpling effect of the top contact of some of the chromitite layers. This feature is not uncommon.

c. Fine-scale layered concentrations of UG 1 chromitite within the anorthosite. Note that the fine chromitite layers abut abruptly on the flanks of the dimpled upper contact, instead of being warped around the undulations.

d. Fine-scale layering of UG 1 chromitite in the anorthosite, creating the effect of cross-bedding in this two-dimensional plane.

PLATE 2

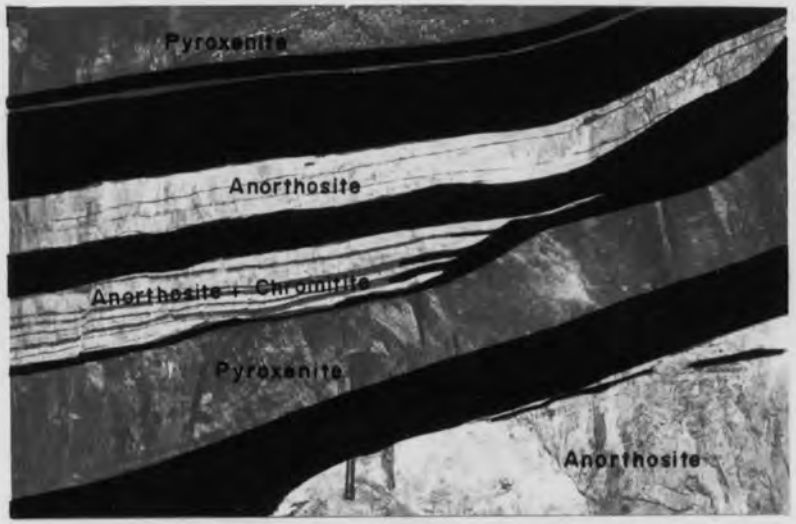
Pyroxenite
Anorthosite
Anorthosite + Chromitite
Pyroxenite
Anorthosite

a

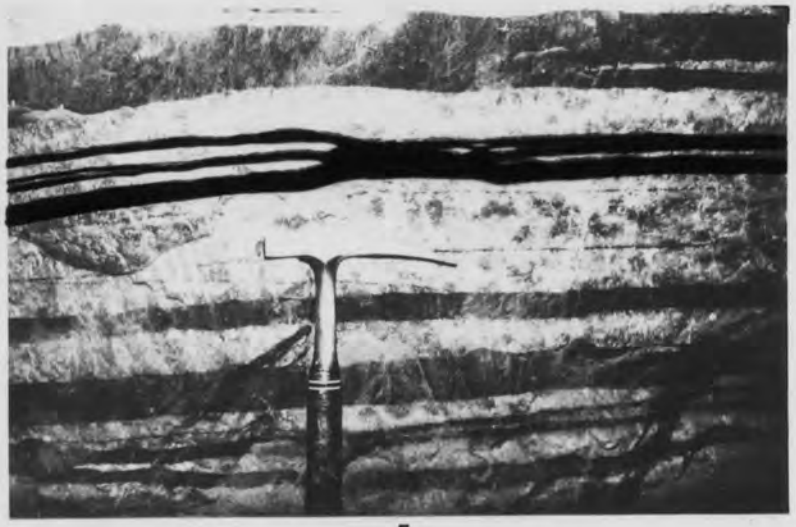

b

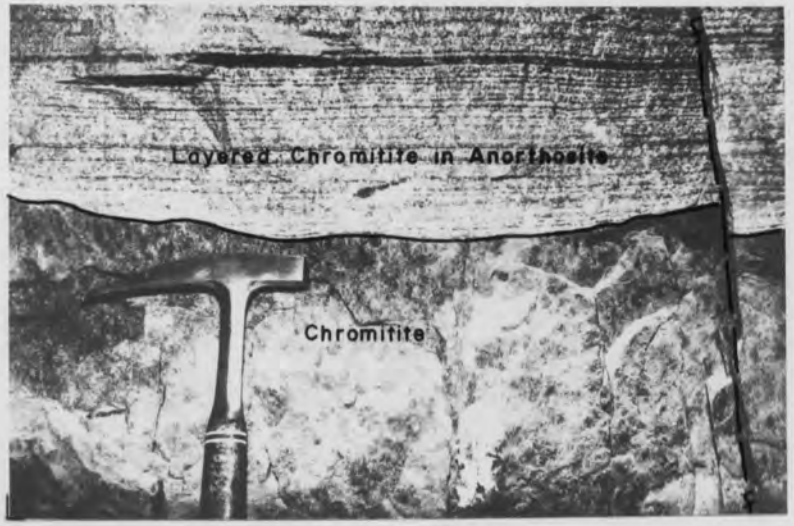
Layered Chromitite in Anorthosite
Chromitite

c

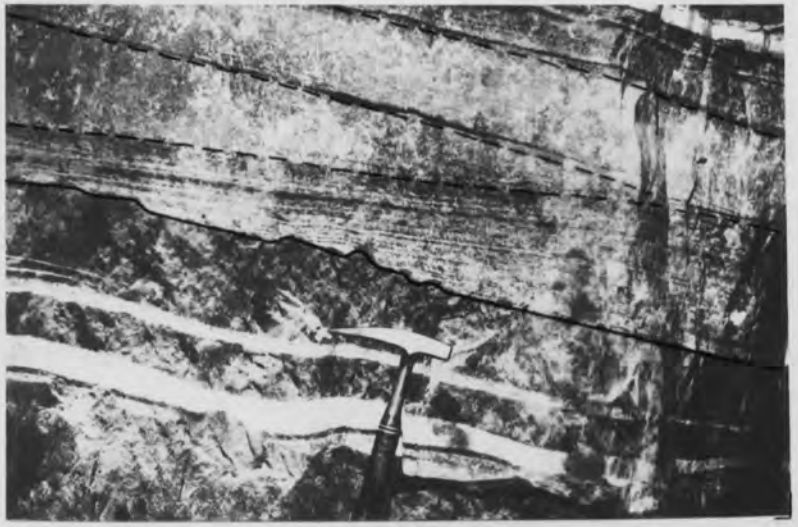

d

overlying UG 1 differentiation units. Lee (1981) suggests that these structures and layering in the anorthosite of the UG 1 are analogous to sandstone dykes and sills in shale. He says that the layered system of chromite above and anorthosite below was in metastable equilibrium, and the potential energy was sufficient to initiate and propagate fractures in the underlying anorthosite. Lee (op. cit.) also states that the chromite mush behaved as a fluid (similar to a heavy quicksand) which filled these fractures. The growth of the horizontal fractures would be comparable to brittle rupture, which, once started, proceeds very rapidly and does not stop before the energy of the system is expended. This type of UG 1 stringer is very much akin to the well-known UG 1 chromitite stringers developed at Dwars River and elsewhere in the Bushveld Complex.

In some areas, numerous very fine-scale chromitite layers of less than 0,5 cm in thickness are finely "bedded" in the host anorthosite. Very often a distinctive type of "crossbedding" or truncation structure is developed in these finely-bedded chromitite layers (Plate 2 c and d).

The non-continuous UG 1 chromitite stringers would appear to owe their origin to post-crystallization movement and dismembering of the chromitite in the anorthosite. The stringers consist of irregular blebs, lenses and bands of chromitite which often have diffuse contacts with the host anorthosite. These chromitite bands are generally elongated and display a pseudo-stratification conformable with the regional layering (Plate 3 a and b). Small-scale flow and fold structures are also often developed in these dismembered stringer lenses. These have been described by Van Zyl (1970) as "chromitite migmatites".

An additional variety of discrete chromitite blebs occurs at the interface of the basal anorthosite and the

PLATE 3

a. Non-continuous UG 1 footwall stringers, blebs and lenses of chromitite within anorthosite. Van Zyl (1970) called this feature a "chromitite migmatite". The post-crystallization plastic flow, which has caused the disruption of the chromitite, did not disturb the regularity of layering in the leuconorite and this would suggest that it was already solid.

b. Slumping of the non-continuous UG 1 chromitite through the anorthosites. Once again note the distortion of the cumulus pyroxene layers which have been slump-folded in places.

c & d. Discrete chromitite blebs which have distorted and truncated the regular layering in the leuconorite approximately 4 m below the UG 1. The chromitite blebs are rimmed by a halo of anorthosite 2 cm thick.

PLATE 3

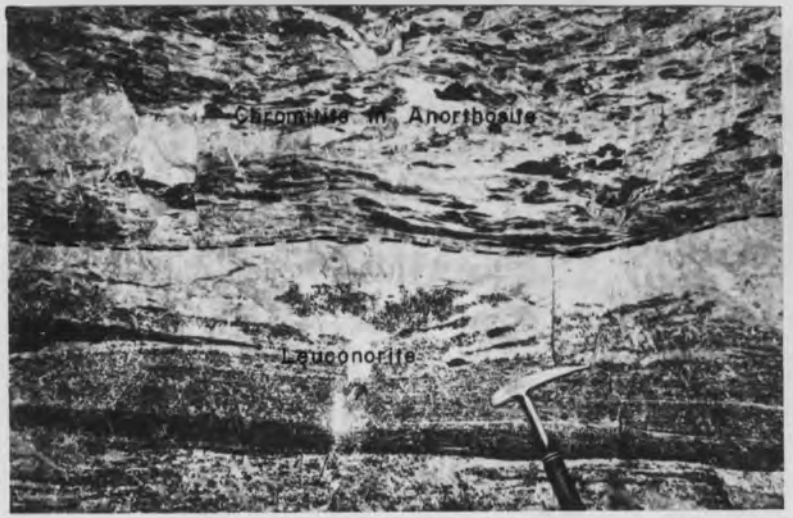
Chromitite in Anorthosite
Leuconorite

a

Chromitite
Leuconorite

b

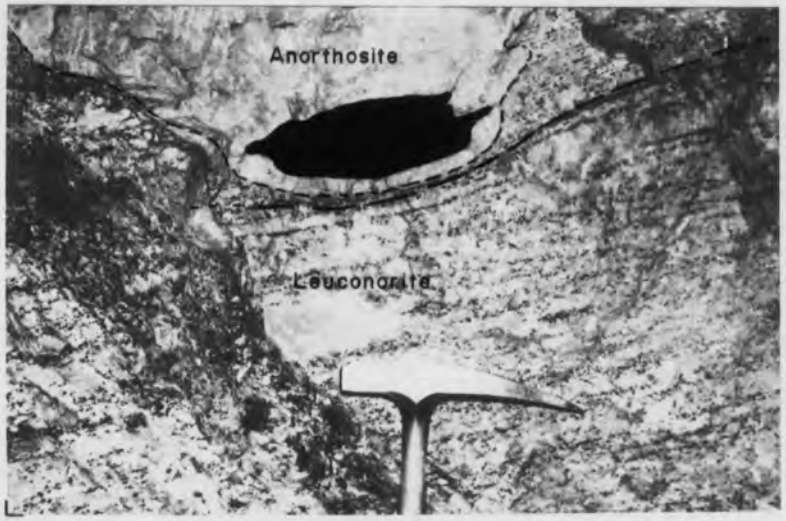
Anorthosite
Leuconorite

c

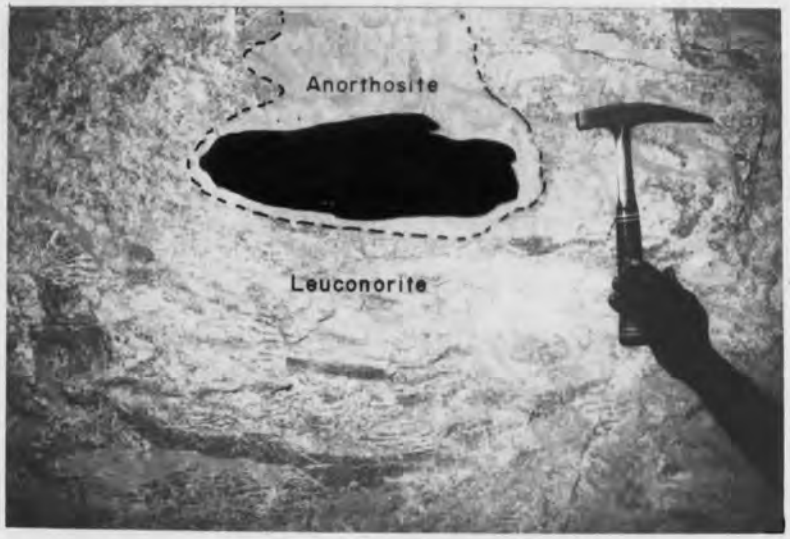
Anorthosite
Leuconorite

d

layered or "streaky" leuconorite, approximately 4 metres below the UG 1, and invariably distorts the regular layering of the leuconorite below it. These blebs vary in size from 6 to 40 cms., and usually have an oblate-spheroid shape. A rim or halo of anorthosite, usually 1 cm thick, surrounds these chromitite blebs (Plate 3 c and d).

In some exposures in the mine, the UG 1 has no footwall chromitite stringers, which suggests that there has been no disturbance of the layer (Plate 4a). In such instances two main chromitite layers, (the top 57 cm and the bottom 28 cm thick) are developed and are separated by medium-grained pyroxenite, 32 cm thick, which has a high concentration of disseminated chromite throughout. The two main chromitite layers are fine-grained with well-packed chromite crystals, the upper layer often having fairly large (1 cm diameter) generally spherical oikocrysts of orthopyroxene scattered throughout. These orthopyroxene oikocrysts have a very high concentration of chromite chadacrysts.

The feldspathic pyroxenite directly above the top chromitite exhibits a structure which is superficially reminiscent of amygdaloidal structure. The intercumulus feldspar is often concentrated in vertical 'schlieren', originating at the upper contact of the underlying chromitite layer. These feldspathic vein-like structures only penetrate the feldspathic pyroxenite for a mere 20 to 40 cm above the top chromitite contact (Plate 4 a and b). These coarsely crystalline plagioclase stringers, which are orientated perpendicular to the layering, apparently originate at the interface of two distinct rock types, and may represent evidence for the existence of intercrystal liquid (Lee, 1981).

A 15 metre poikilitic feldspathic pyroxenite unit

PLATE 4

a. Undisturbed UG 1 layer. The footwall anorthosite has only a limited number of non-continuous chromitite stringers. The anorthosite is overlain by a 28 cm-thick layer of chromitite, followed by pyroxenite and then by a 57 cm thick layer of chromitite. Note the vertical orientation of intercumulus plagioclase in the poikilitic feldspathic pyroxenite above the UG 1.

b. Vertical intercumulus plagioclase, above the UG 1 chromitite, only penetrates the poikilitic feldspathic pyroxenite for 20-30 cm. In this example the UG 1 chromitite has a 5 cm leader layer, separated from the main chromitite by 8 cm of pyroxenite.

c. Vertically orientated intercumulus plagioclase above the 1 cm undulating chromitite, which is found 1,5 m below the UG 2. Note that, compared to the poikilitic feldspathic pyroxenite below the 1 cm chromitite, there is a much higher concentration of intercumulus plagioclase, and the pyroxene crystals are coarser-grained above the chromitite.

d. UG 2 chromitite layer with a footwall pegmatoidal feldspathic pyroxenite. There are two leader layers, above the main chromitite, with the upper leader showing bifurcation in the centre of the photograph to form a total of 3 leader layers towards the right hand side of the photograph. Note the ovoid pyroxenite lens near the top of the main layer, immediately above the hammer head.

PLATE 4

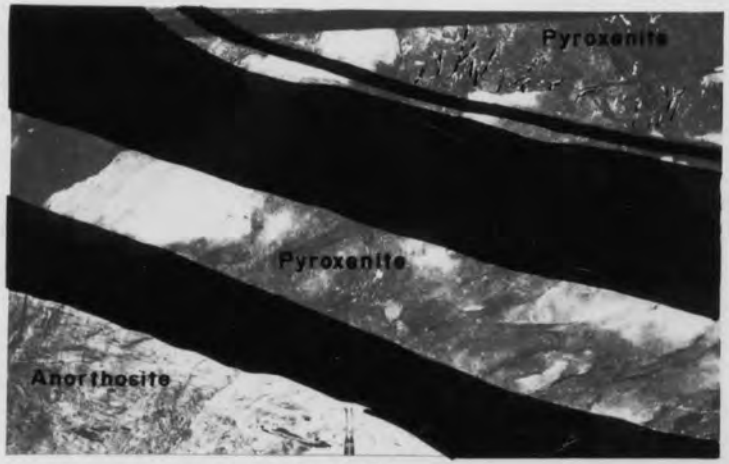

a

b

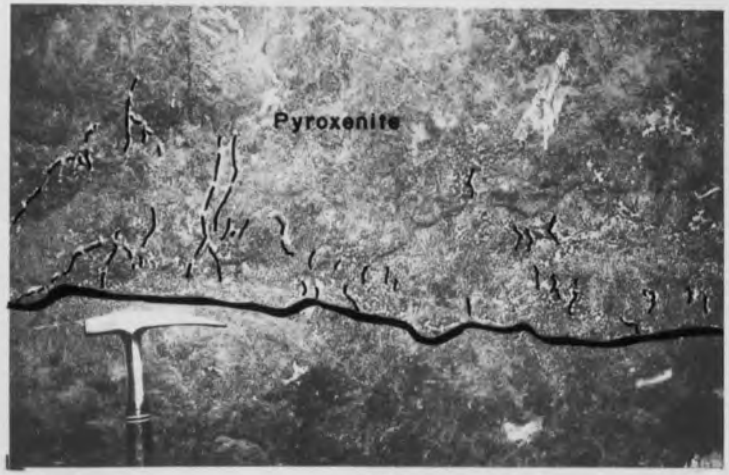

c

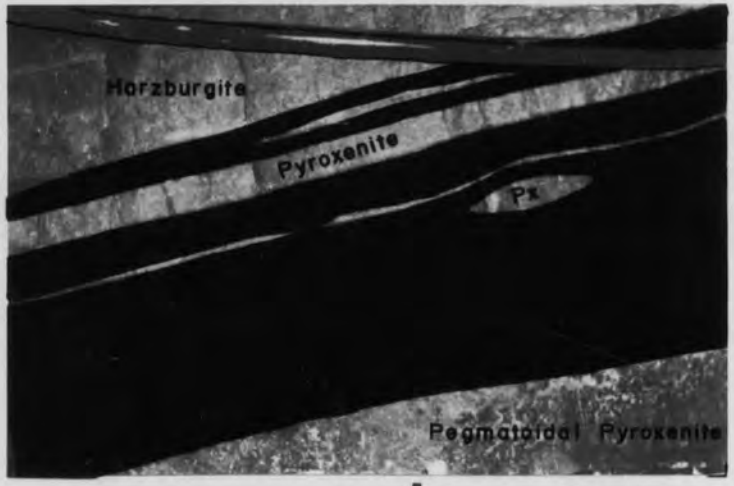

d

0 20cm

occurs between the UG 1 and UG 2 chromitites and shows no sign of differentiation (Figure 6). It contains two persistent 1 cm chromitite layers 1,5 and 3,5 metres respectively below the main UG 2 chromitite. The pyroxenite above the uppermost of these chromitites has the same characteristics as that just above the UG 1 as described above, i.e. vertical pipe-like feldspar stringers. These feldspar stringers appear to "stream off" the top of the 1 cm chromitite, and occasionally reach the pegmatoidal feldspathic pyroxenite of the UG 2 (Plate 4 c).

4.5.3 UG 2 Chromitite Layer This layer of chromitites is divided into a main chromitite and the overlying leader layers (Figure 6 and Plate 4 d). The main UG 2 chromitite averages 78 cm in thickness, and displays only slight variations in thickness along strike. Its immediate footwall is invariably formed by a pegmatoidal feldspathic pyroxenite layer which averages 50 cm in thickness, and contains a 2 cm chromitite layer some 4 to 6 cm below the base of the main UG 2 chromitite. The thickness and number of the leader chromitite layers vary across the mine, due largely to bifurcation and coalescence of seams, as shown in Plate 4 d. In the Ivan Shaft and Richard Shaft areas there are only two 10 cm wide leaders above the main layer, separated from each other by a fine-grained pyroxenite. In the Spud Shaft area there are typically three or sometimes more leaders. These variations are illustrated in Figure 7. The pyroxenite separating the first and second leaders has a rather high concentration of disseminated chromite, and the pyroxenite-chromitite contacts are rather diffuse and gradational over about 2 cm.

The upper two leader layers characteristically have poikilitic orthopyroxene crystals of up to 1 cm in size, scattered in the chromitite, and these oikocrysts have a very high concentration of disseminated chromite throughout. The thickness of the pyroxenites between the leaders is

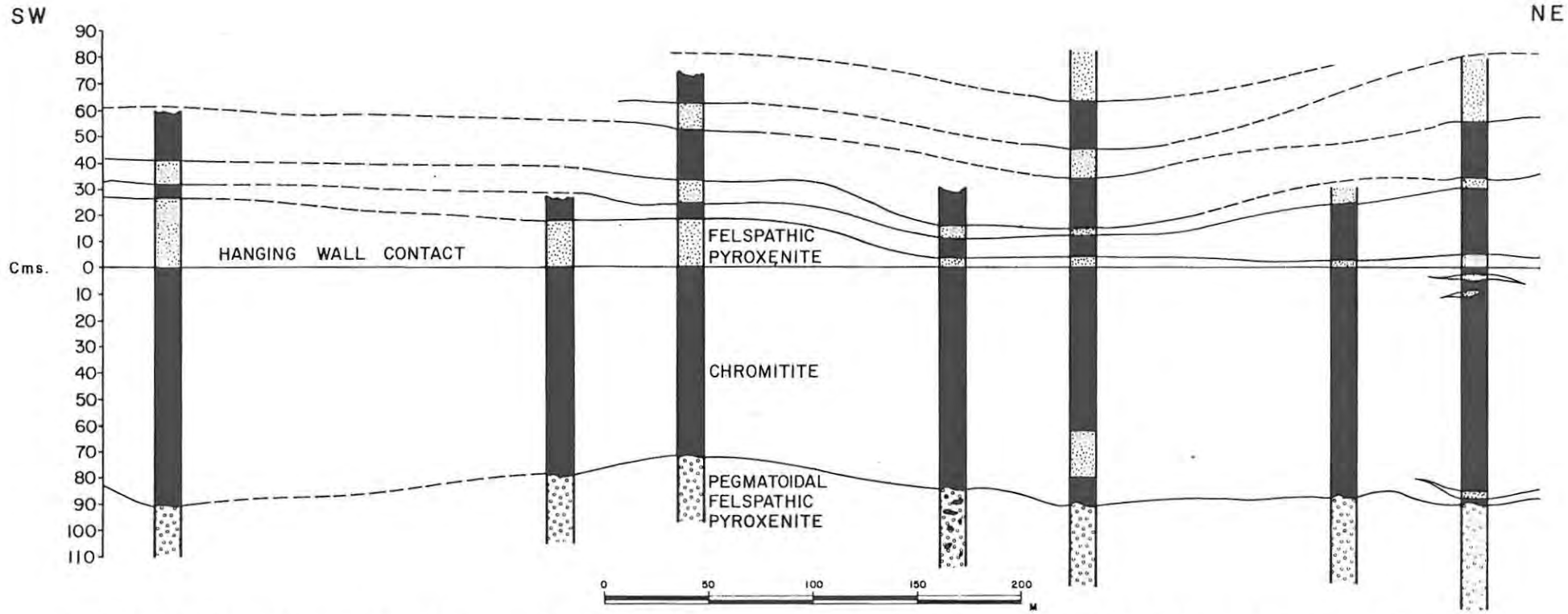

VARIATIONS IN UG.2 HORIZON IN THE VICINITY OF SPUD SHAFT.

Figure 7

usually very consistent, but local variations do occur, when one or two or all the leaders are updomed away from the main layer (Plate 4 d).

The immediate hanging wall of the UG 2 is a medium-grained feldspathic harzburgite which is some 2 metres thick. The upper contact of this harzburgite unit is rather gradational with a decrease in the olivine concentration upward to a poikilitic feldspathic pyroxenite. The olivine in the harzburgite has been serpentinised to varying degrees, giving the rock a dark appearance. Near the top of the harzburgite unit, about 1,5 metres above the top UG 2 leader, a thin 0,5 to 1 cm wide persistent but patchy chromitite layer is found. This layer is sometimes disrupted and only small blebs of chromitite are then observed at this position. The poikilitic feldspathic pyroxenite is 12 metres thick, and the concentration of clinopyroxene oikocrysts tends to increase towards the Pseudo Reef.

4.5.4 Pseudo Reef Unit This unit is divided into an upper and lower portion. The lower or coarse-grained Pseudo Reef is a pegmatoidal feldspathic harzburgite with large subhedral olivine crystals (1 to 1,5 cm) and intercumulus feldspar. Large poikilitic orthopyroxene (bronzite) crystals of up to 4 cm in diameter partly or wholly enclose the olivine and feldspar. The olivine crystals have been severely serpentinised and thin-section study shows only small, unaltered olivine relicts.

A lacework of fine magnetite and alteration products, including chlorite, serpentine, iddingsite, bowlingite and talc are typically derived from the pyroxenes and olivines. The unit could be described as a heteradcumulate and is usually 1,5 metres thick. The lower contact with the underlying poikilitic feldspathic pyroxenite undulates

considerably (Figure 6).

The upper Pseudo Reef has an average thickness of 3 metres but local variations of up to 5 metres have been encountered. Exposures of this layer in underground workings have a distinctive 'mottled' texture. Large ovoid anhedral orthopyroxene oikocrysts (3 to 4 cm in diameter) poikilitically enclose smaller subhedral to anhedral olivine chadacrysts. These oikocrysts appear to be evenly spaced at about 10-12 cm intervals throughout the rock. The interstitial material between the orthopyroxene oikocrysts is made up of cumulus olivine crystals (3-5 mm grain size) and intercumulus plagioclase, constituting a feldspathic harzburgite. It is this cumulus olivine with intercumulus plagioclase which gives the rock its distinctive spotted texture similar to the plumage of a guineafowl, and hence its colloquial name of "Tarentaal".

An irregular, 0,5 to 1 cm chromitite layer is developed at the contact between the lower and upper Pseudo Reef units. Associated with this chromitite (immediately above and below) is an increase in the amount of disseminated base metal sulphides. This sulphide mineralization decreases rapidly in both directions away from the chromitite layer. Local, rather patchy, high concentrations of sulphides have been seen in the upper Pseudo unit, and an analysis yielded very high platinum group element (PGE), copper and nickel values, but generally the mineralization is confined to 20 cm on either side of the chromitite layer noted above. The upper contact of the "Tarentaal" is bounded by a well-packed, medium- to fine-grained chromitite layer 1 cm wide. This chromitite is very persistent and occurs over virtually the entire property (Plate 5 a). Again PGE, Cu and Ni sulphides are associated with the chromitite, and both the sulphides

and values persist up to 20 cm below the chromitite (Figure 6).

Associated with the top chromitite contact is a very well-defined serpentinised slip plane, which is also evident over the whole mine area (Plate 5 a and 7 c). There is no documentation or other evidence of displacement on the bedding plane slip or possible fault, although slickensides are evident along most exposures, and the displacement, if any, seems to have been in the dip direction. Cousins (1964), noted a similar type of "bedding fault" which is 9,1 metres below the Merensky Reef at Rustenburg Section. Measurement of the displacement of dykes indicates a lateral movement of some 7,6 metres. The dip slip plane at Union Section undulates with a small amplitude (10 cm) over a very large area (20 m) from 5 cm below the top chromitite contact, to 5 cm above this chromitite. In many places the chromitite layer is eliminated by the slip.

Acicular actinolite-tremolite crystals up to 20 cm long have been observed, and are orientated with their long axes parallel to the dip direction (See Plate 5 a and especially Plate 7 c).

4.5.5 Pseudo Marker and Pothole Marker Layers

Olivine is a major constituent of this marker layer, which commences with a pegmatoidal feldspathic harzburgite 20 cm thick. This passes upwards into a feldspathic pyroxenite, followed by a medium-grained melanorite. The top of the Pseudo Marker is defined by a very persistent anorthosite layer known as the Pothole Marker, 1 to 2 cm thick (Plate 5 a).

The Pseudo Marker is of considerable importance as it occupies the same stratigraphic elevation as the pothole Merensky Reef. As will be discussed later, the

Pseudo Marker changes character as a pothole is approached, and grades into the pegmatoidal pothole reef. At the same time the well-defined Pothole Marker (1-2 cm anorthosite) becomes fragmented and disappears.

Overlying the Pothole Marker anorthosite is a unit of leuconorite (spotted anorthosite) 10 metres thick. This leuconorite unit has a very distinctive zone of parallel layering developed over 80 cm in the Spud Shaft area and south-western sector of the mine, locally known as the "Strepies" (Plate 5 b, Figure 6). This banding, which is 4 metres above the top chromitite of the Pseudo Reef, is very similar to the so-called "inch-scale layering" which is found at Stillwater (Hess, 1960). Layers of orthopyroxenes are separated from each other by layers of anorthosite, and the thickness of the individual layers of anorthosite decreases away from the centre of the layered zone.

Another distinguishing feature of this leuconorite is a clustering of the orthopyroxene crystals, which also develop a halo or rim of plagioclase. The orthopyroxene clusters are about 0,5 to 1 cm in size, and have a rather diffuse outline. This texture is locally referred to as a "corona" texture (Plate 5 c and d).

Above the leuconorite is a unit of poikilitic anorthosite (mottled) some 4 to 5 metres thick, which forms the footwall of the Merensky reef. The contact between the leuconorite and the poikilitic anorthosite is rather sharp, and a persistent dark band of intercumulus orthopyroxene is taken as the boundary between the two (Plate 5 d).

4.5.6 Merensky Reef Unit By definition, the Merensky Reef is a coarse-grained pegmatoidal feldspathic pyroxenite of varying thickness, which is bounded by thin,

PLATE 5

a. The Pseudo Marker layer showing the 1 cm thick basal chromitite and associated dip slip, which overlies the upper Pseudo reef unit. The Pseudo Marker layer consists of a lower feldspathic harzburgite which grades into a feldspathic pyroxenite, and finally a melanorite. The thin anorthosite layer, called the Pothole Marker, at the top contact, is usually 1 cm thick.

b. "Strepies" marker layer, which is found within a massive leuconorite, 4 m above the Pseudo Marker, is made up of strongly layered anorthosite and pyroxenite. These orthopyroxene and anorthosite layers are thicker towards the centre.

c. "Corona" texture within the massive leuconorite consists of cumulus orthopyroxene clusters surrounded by irregular anorthosite rims. This texture is only found in the Footwall unit leuconorites.

d. The contact between the leuconorite (with prominent corona texture) and the overlying poikilitic, or mottled anorthosite which forms the footwall of the Merensky Reef. This contact, as with other poikilitic anorthosite/leuconorite contacts in the study section, is characterised by persistent layering of intercumulus pyroxene.

PLATE 5

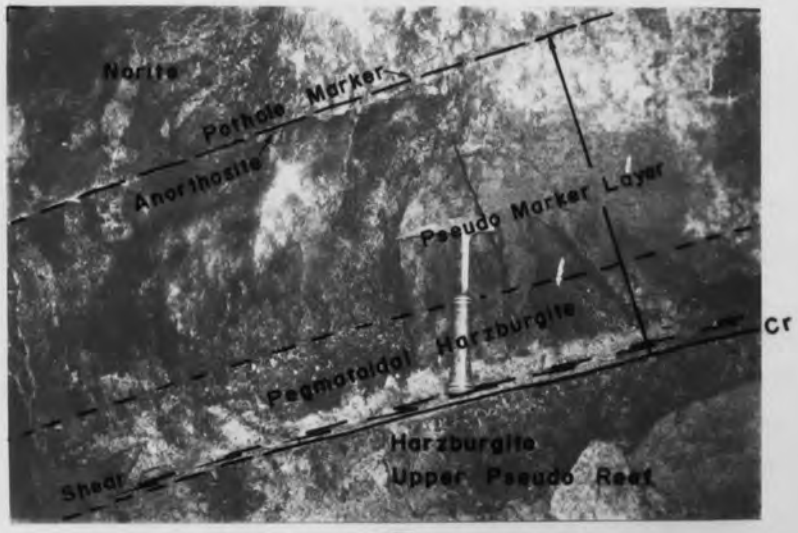
Norite
Potholes Marker
Anorthosite
Pseudo Marker Layer
Pegmatoidal Harzburgite
cr
Harzburgite
Upper Pseudo Reef
Shear

a

"Strepies"
Leuconorite

b

"Coronas"
Leuconorite

c

Poikilitic Anorthosite
Leuconorite
"Coronas"

d

over- and underlying chromitite layers, and contains significantly high PGM, Cu and Ni values (Plate 6 a). At Union Section the pegmatoidal reef contains significantly high concentrations of olivine (Fo 79,8 - 78,6) and is thus more correctly termed a pegmatoidal feldspathic harzburgite. Zoning and layering are apparent within the reef, however, and the olivine is found to be more concentrated in the lower part of the reef than at the top, which may be wholly devoid of this phase.

The bottom chromitite layer of the Merensky Reef has a characteristically dimpled contact with the footwall poikilitic anorthosite (Plate 6 b). The poikilitic anorthosite has a very low concentration of mafic minerals over 1 to 4 cm at this contact, and this is much more evident when the Merensky Reef is underlain by the leuconorite (See Plate 7 a).

Immediately above the upper contact of the Merensky Reef is a poikilitic feldspathic pyroxenite, more commonly referred to as the "Merensky" or Merensky Pyroxenite (Plate 6 c). This is a medium-grained pyroxenite, and is somewhat more feldspathic than the pyroxenite that occurs in the vicinity of the UG 2. The first 15 - 25 cm is generally well-mineralised and contains essentially the same base metal sulphides as the Merensky Reef. PGM content drops off rapidly over the first 20 cm, while a slight increase in Cu and Ni may occur. This pyroxenite layer extends over 3 to 4 metres, and often displays a very well-developed joint pattern. These joints may be well serpentinised and are orientated approximately at right angles to the layering.

A gradual, transitional change takes place upwards from the Merensky pyroxenite, with the development of a melanorite followed by a norite and finally a leuconorite. The transition extends over 11 to 12

metres with the uppermost leuconorite forming a 4 metre thick unit which is very similar to the leuconorite below the Merensky Reef, but without the pyroxene crystal clustering (coronas). Overlying this leuconorite is a poikilitic anorthosite (mottled anorthosite) some 3 to 4 metres thick, which forms the top of the Merensky unit and the footwall of the Bastard Reef. The contact between the leuconorite and the poikilitic anorthosite is again very sharp, and a consistent dark band of intercumulus pyroxenite demarcates their boundary.

When the Merensky Reef is in pothole condition, the poikilitic anorthosite is slightly thicker (4,5 to 5 metres) and is often overlain by a 1,5 metre layer of strongly layered leuconorite (See Figure 6, column 4). This leuconorite is often slightly darker, with irregular (1 - 1,5 cm wide) anorthosite layering parallel to the strata. Very fine, disseminated sulphides are usually found within this layered leuconorite.

4.5.7 Bastard Reef Unit The basal contact of the Bastard Reef poikilitic pyroxenite has a well-developed slip plane (Plate 6 d). Again no evidence of displacement has been recorded, although slickensides are evident and a distinctly mylonitic character, extending for 20 cm, has been exposed in places. The base of the Bastard pyroxenite is very sharp and sometimes contains a very thin chromitite layer. The Bastard Reef is basically a poikilitic feldspathic pyroxenite some 8 to 9 metres thick, which gradually becomes more feldspathic towards the top. Occasionally some coarse-grained pegmatoidal development is seen in the lower 10 to 20 cm, and fine-grained, disseminated base metal sulphides may also be observed in this basal portion. This unit generally carries low levels of PGM, Cu and Ni. Overlying the Bastard pyroxenite is a medium-grained

PLATE 6

a. Narrow normal Merensky Reef showing the footwall poikilitic (mottled) anorthosite, sharp basal contact with the chromitite layer, pegmatoidal reef, sharp upper contact with the chromitite layer and the hanging wall Merensky feldspathic pyroxenites. This type of narrow reef would be characteristically found close to a pothole edge.

b. Detail of the basal Merensky Reef contact. The pegmatoidal feldspathic harzburgite of the reef is underlain by the basal chromitite layer with its dimpling of the footwall poikilitic anorthosite.

c. Detail of the Merensky Reef upper contact, showing the pegmatoidal feldspathic pyroxenite and the upper chromitite layer, overlain by hanging wall Merensky poikilitic feldspathic pyroxenite. The upper part of the reef is characteristically more pyroxenitic, as opposed to the harzburgite lower down.

d. Contact of the Bastard Reef pyroxenite with the underlying poikilitic anorthosite of the Merensky unit. Note the slip plane at this contact and the small pegmatitic gash vein in the Bastard pyroxenite.

PLATE 6

Merensky Pyroxenite
Merensky Reef
Poikilitic Anorthosite

a

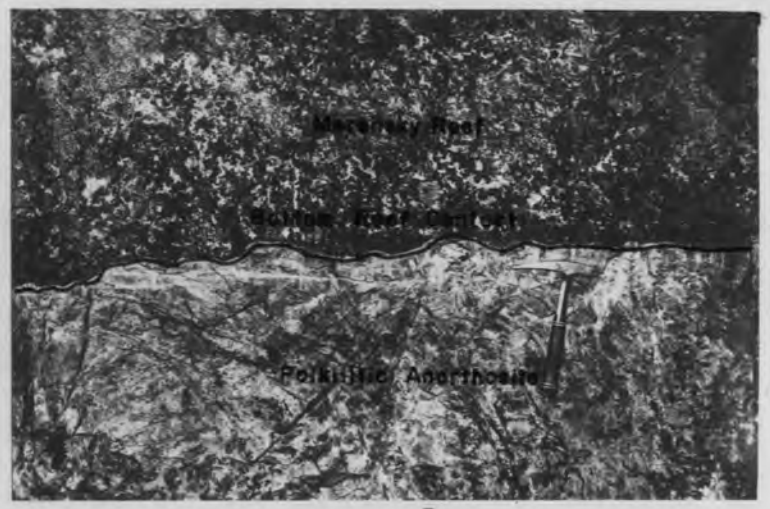
Merensky Reef
Bottom Reef Contact
Poikilitic Anorthosite

b

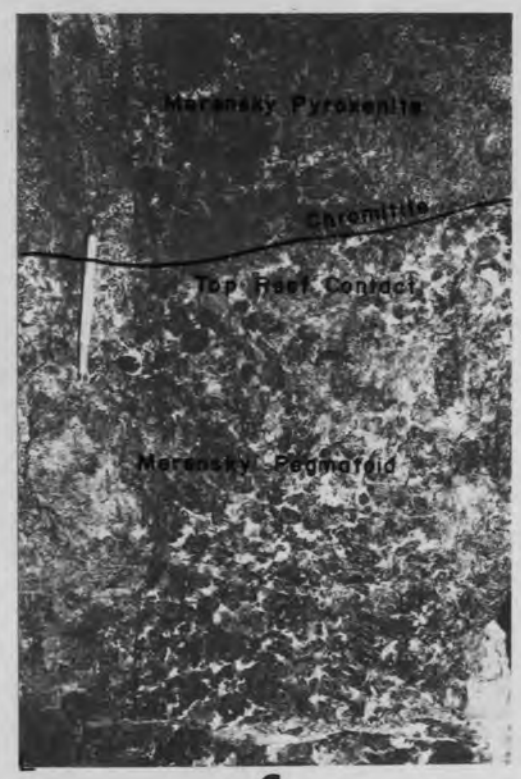
Merensky Pyroxenite
Chromitite
Top Reef Contact
Merensky Pegmatoid

c

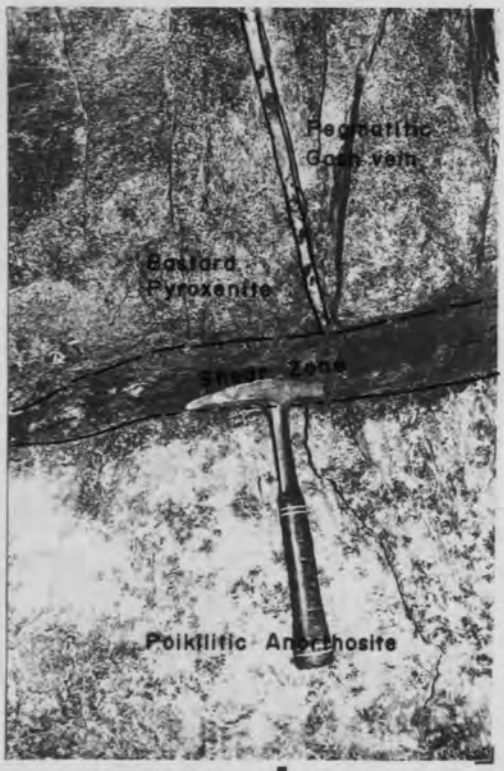
Pegmatitic Gash vein
Bastard Pyroxenite
Shear Zone
Poikilitic Anorthosite

d

melanorite some 11 metres thick. The interface between these two units is gradational over about 3 metres. The melanorite has a layered structure which gives it a streaky appearance towards the top.

The uppermost layer of the Bastard unit is a very well-developed and persistent poikilitic anorthosite, known colloquially as the "Giant Mottled". The layer is 13 to 15 metres thick and occurs 59 metres above the normal elevation of the Merensky Reef; it marks the top of the Critical zone of the Bushveld Complex (Vermaak, 1976).

The contact between the melanorite and the poikilitic anorthosite of the "Giant Mottled" is rather sharp and is marked by some dark bands of intercumulus pyroxene. The mottles are also larger than normal, attaining a size of 6 cm in diameter, but these become smaller towards the top of the layer.

4.5.8 Potholed Succession The above description of the upper Critical zone pertains to the normal stratigraphic succession. As will be discussed later, the Merensky reef is characterised by the presence of potholes, where the reef plunges down and truncates its immediate footwall stratigraphy.

Pothole Merensky Reef develops at the level of the Pseudo Marker layer and thus its immediate footwall becomes the Pseudo reef feldspathic harzburgite. The entire normal Merensky Reef footwall succession, which averages about 14 metres, is completely eliminated in the pothole succession, as shown in column 4 of Figure 6. There is a definite thickening of the layers above the Merensky Reef in the potholed succession, and a distinctive feature is the appearance of a streaky leuconorite above the poikilitic anorthosite at the top of the Merensky unit (Figure 6).

5. REGIONAL GEOLOGICAL FEATURES OF THE MERENSKY REEF AND ITS IMMEDIATE HANGING- AND FOOTWALL

5.1 Introduction

The Merensky Reef ore body at Union Section is characterised by regional differences in the reef thickness, dip and strike, and is geologically disturbed by faults, dykes, intrusive pegmatoidal bodies and pothole structures (See Figure 8).

5.2 Potholes and their distribution

The nature of potholes has been briefly noted in a previous section (4.5.8). They are of major importance at Union Section, accounting for approximately 35% of the area mined to date where normal succession should have been expected. The regional distribution of potholes, and the three main reef types within these features, viz. contact, pothole and lens reef, are shown schematically in Figure 9. They vary considerably in size, shape and frequency. The lowest frequency, and also the smallest potholes, occur in the north-eastern part of the mine, in the Ivan Shaft area, where they tend to be nearly circular in plan view (Figure 8). These latter potholes vary in size from about 50 metres to about 500 metres (long axis), and there appears to be no preferred orientation, although there is a suggestion that their longer axes are aligned parallel to the direction of dip, i.e. south-east. It is no coincidence that the thickest development of Merensky Reef occurs in this sector of the mine, which has only a few, small potholes (See Section 5.4).

The nature of the potholes changes significantly to

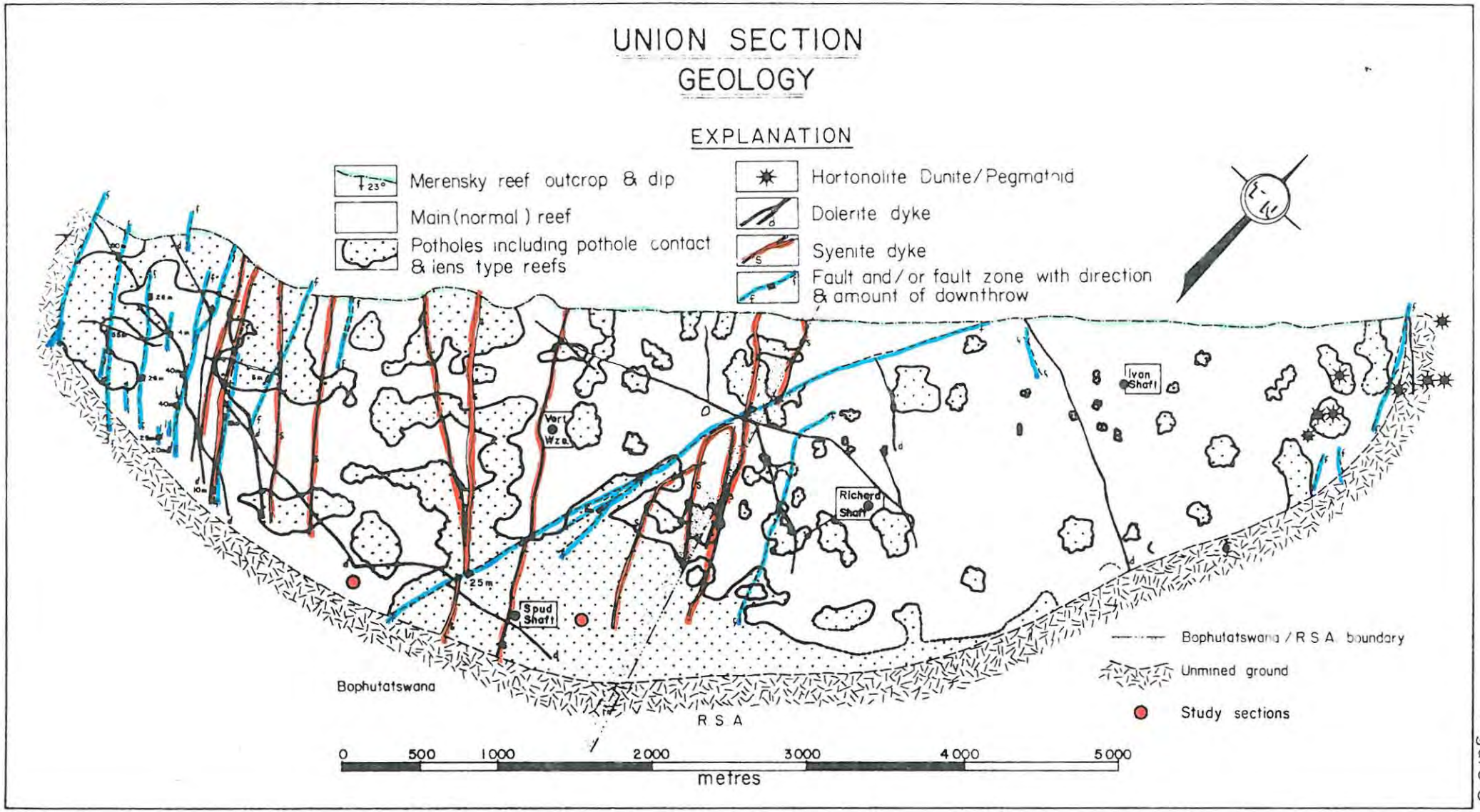
UNION SECTION
GEOLOGY
EXPLANATION
Merensky reef outcrop & dip
Main (normal) reef
Potholes including pothole contact & lens type reefs
Hortonolite Dunite/Pegmatoid
Dolerite dyke
Syenite dyke
Fault and/or fault zone with direction & amount of downthrow
Bophutatswana / R S A boundary
Unmined ground
Study sections
Vert Wze
Richard Shaft
Ivan Shaft
Spud Shaft
Bophutatswana
R S A
0 500 1000 2000 3000 4000 5000
metres

Figure 8

the south of a line running approximately east-west through the 22 Vertical Winze (see Figure 8). Large, irregular and interconnected potholes now become the dominant feature. The two largest of these are in the extreme south-western part of the mine in the Spud Shaft area. These larger potholes are characterised by the fairly substantial development of contact reef between normal and pothole reef.

In addition, the Spud Shaft pothole, which is the largest encountered thus far, is characterised by the development of so-called lens reef conditions, as described later. The normal reef, in the vicinity of the potholes of regional extent, is also considerably reduced in thickness, generally 1 to 2 metres (See Section 5.4).

In the area of present mining, the Spud Shaft pothole is 4,4 kilometers in extent, and at depth opens out into an even larger feature. In the region in which development will be taking place over the next decade, the dominant reef type will thus be pothole reef with only small amounts of normal reef. The reef conditions at depth are thus completely different from those at Ivan Shaft, where mining first commenced at Union Section.

5.3 Pothole Structure

At Union Section, as elsewhere in the Bushveld Complex, a pothole is an area from which part of the normal Merensky Reef footwall succession is missing. As noted earlier, in a pothole, the Merensky Reef and overlying poikilitic pyroxenite plunge down abruptly from their normal stratigraphic level and sharply transgress the footwall sequence of the normal Merensky Reef. This transgression eliminates about fifteen metres of the footwall sequence down to the Pothole Marker, and at this elevation pothole reef develops. Potholes vary greatly in shape, from ovoid or circular in

plan, to irregular and amoeboid. They vary in diameter from a few tens of metres to several kilometers, and their distribution has not yet been successfully correlated with other structural features.

A number of very distinctive features are associated with potholes, and these are schematically portrayed in Figure 9. At the edge of a pothole, the top and bottom chromitite layers of the normal Merensky Reef converge until the pegmatoidal portion of the reef disappears and only a composite chromitite layer persists. At this point the hanging wall poikilitic pyroxenite virtually comes into contact with the footwall anorthosite (Figure 9). Once the two chromitite layers have converged, the reef is called contact Merensky Reef. The convergence of the two chromitite layers, with accompanying thinning of the pegmatoidal reef, usually takes place over about 10 to 20 metres, but this does vary locally. The gradient of thinning of the pegmatoid is usually less, if a large pothole is approached, and vice versa. On a regional scale, the lower the incidence of potholes, the greater is the thickness of the normal Merensky Reef, and this will be discussed later. In areas of high pothole density the normal Merensky Reef rarely attains a thickness of more than 2,5 metres (Figure 11).

A number of different types of reef development occur within a pothole, and these are referred to as contact, pothole and lens reefs.

5.3.1 Contact Reef Contact reef forms at the point of convergence of the top and bottom chromitite layers of the normal Merensky Reef. Strictly speaking, this should not be called a "reef", because there is no pegmatoidal development at all, but for mining purposes the term contact reef applies to the chromitite layer, hanging wall Merensky Pyroxenite and footwall leuconorite. It is invariably found on the margins of potholes, and can be considered to

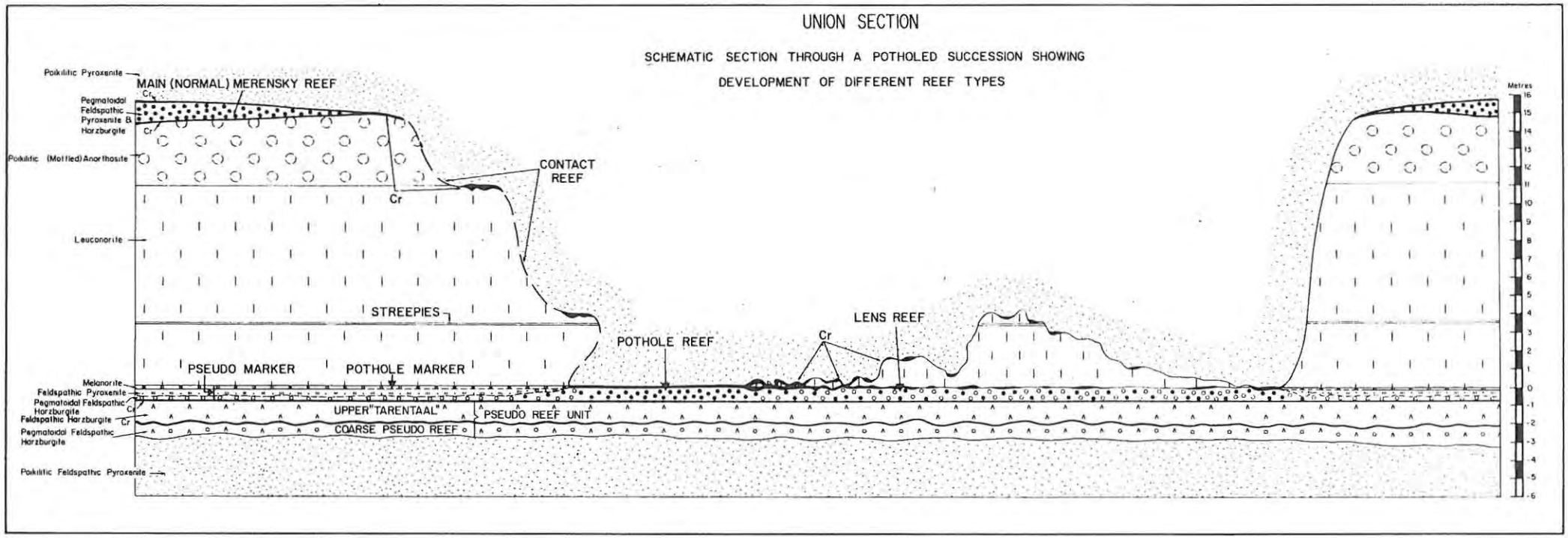
UNION SECTION
SCHEMATIC SECTION THROUGH A POTHOLED SUCCESSION SHOWING
DEVELOPMENT OF DIFFERENT REEF TYPES
Poikilitic Pyroxenite
MAIN (NORMAL) MERENSKY REEF
Pegmatoidal Feldspathic Pyroxenite & Harzburgite
Poikilitic (Mottled) Anorthosite
CONTACT REEF
Leuconorite
STREEPIES
LENS REEF
POTHOLE REEF
PSEUDO MARKER
POTHOLE MARKER
Melanorite
Feldspathic Pyroxenite
Pegmatoidal Feldspathic Harzburgite
Feldspathic Harzburgite
UPPER "TARENTAAL"
PSEUDO REEF UNIT
COARSE PSEUDO REEF
Pegmatoidal Feldspathic Harzburgite
Poikilitic Feldspathic Pyroxenite
Cr
Metres

Figure 9

represent the transition between normal and pothole reef (Plate 7 a and b). Contact reef can sometimes continue on the same elevation as the normal reef for short distances, although in extreme cases it has been traced for up to 8 metres at the normal reef elevation.

Once the contact reef starts to truncate the footwall succession, the chromitite thins out and only a pyroxenite-anorthosite rock contact with occasional chromite grains is developed. The angle of the transgression across the footwall rocks can vary from only a few degrees to 90° or more, creating a "flick-back" or overturned situation in the latter case (Figure 9).

Flattening of the contact reef transgression through the footwall stratigraphy may occur locally at any layer between the normal reef elevation and the pothole reef elevation. Preferred flattening however, takes place at the leuconorite-poikilitic anorthosite contact (Figure 10 b in centre) and on the "strepies" marker layer within the leuconorite. The stabilised contact reef chromitite can vary in thickness, but is usually between 3 and 8 cm thick. Localised thickening of the chromitite layer does take place in dimples in the footwall and at these localities the chromitite can attain a thickness of 20 cm in extreme cases (Figure 9, Plate 7 b). It is only in these "stable" contact reef areas that the PGM values associated with the pyroxenite, chromitite and footwall anorthosites or norites are high enough to warrant mining over narrow stope widths.

5.3.2 Pothole Reef Pothole reef is defined as commencing at the point at which the contact reef settles onto the Pseudo Marker layer. At this position, the character of the Pseudo Marker layer changes completely. The well-developed stratification of the Pseudo Marker described earlier, (4.4.5), disappears, and the whole Marker layer becomes coarse-grained and pegmatoidal. The first sign

PLATE 7

a. Contact of the Merensky pyroxenite and associated basal chromitite with Footwall unit leuconorite on the margin of a pothole. This contact is rather irregular and has a 2 cm anorthosite zone which parallels the contact. This is known as contact Merensky Reef.

b. Contact of the Merensky pyroxenite and associated basal chromite with the Footwall unit poikilitic anorthosite on the margin of a pothole. In the depression of this contact there is a higher concentration of disseminated chromitite, and the feldspathic pyroxenite is more pegmatoidal.

c. Lens-type Merensky Reef, which is a reconstituted Pseudo Marker layer (See Plate 5a) and is at the same stratigraphic level. The basal 1 cm chromitite and associated dip slip overlying the upper Pseudo Reef is well illustrated. The lens reef is a pegmatoidal feldspathic harzburgite throughout, and is overlain by a lens of leuconorite. Note that the Pothole Marker anorthosite layer has disappeared, and that there is now a zone of anorthosite (higher than the Pothole Marker position) at the contact between the harzburgite and leuconorite.

PLATE 7

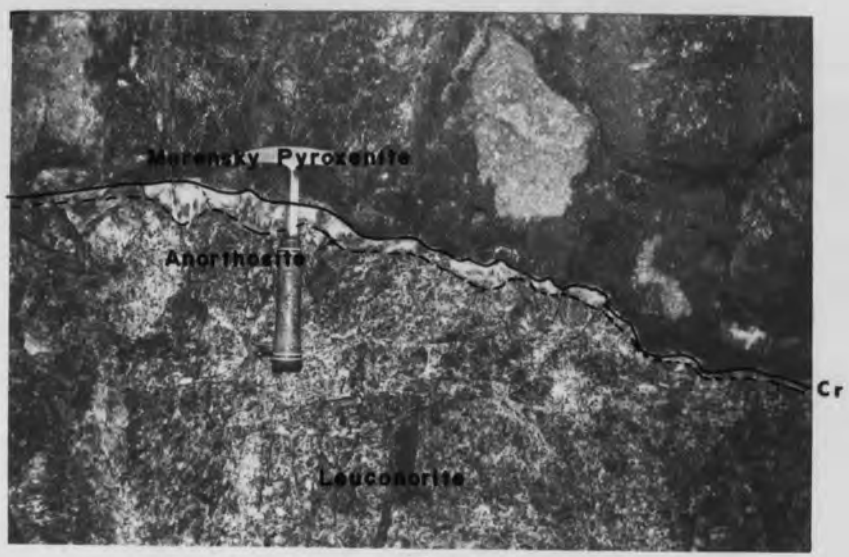

a

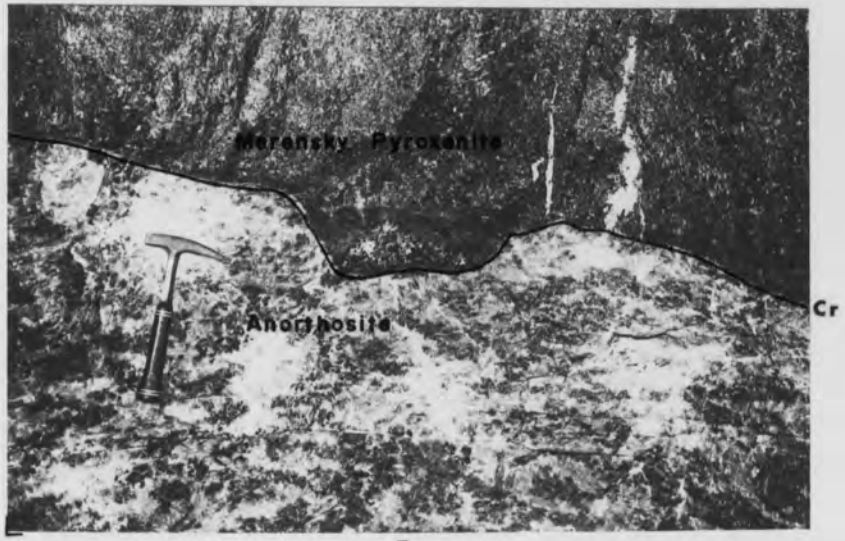

b

c

449

of approaching pothole reef is the fragmentation of the anorthositic Pothole Marker, which disappears completely in the pothole reef. A well-developed (1 cm thick) Pothole Marker anorthosite is taken as good evidence for normal reef conditions in the area.

The pothole reef is a pegmatoidal feldspathic pyroxenite and harzburgite (Wagner, 1929, p.114) and has the same characteristics as the normal reef, including high PGM, Cu and Ni values. Instead of having an anorthosite footwall, however, the footwall of the pothole reef is the feldspathic harzburgite of the upper Pseudo Reef (Tarentaal), and the bottom chromitite layer of pothole reef is in fact the top contact of the Pseudo Reef (Figure 9). The top chromitite of the pothole reef in part appears to represent contact reef lying on reconstituted Pseudo Marker.

5.3.3 Lens Reef Incomplete removal of the footwall succession between the normal Merensky Reef and the Pseudo Marker occurs in places in the larger potholes. In such places, lenses of leuconorite or anorthosite occur sporadically, and are particularly abundant in the Spud Shaft pothole. They occur immediately above the Pseudo Marker, and individual lenses can vary in size from 0,1 m to over 100 metres in lateral extent. Lenses also vary in thickness from only 2 cm to 6 metres. Thick lenses often contain remnants of the "Strepies" Marker layer, which testifies to their origin as relict footwall components that were not completely removed by whatever process is responsible for the formation of these features.

The noritic lenses are characterised by the development of chromitite and disseminated chromite along their flat basal contacts, as well as by the presence of much more erratic and lenticular chromite along their very uneven upper contacts (Figure 9 and Plate 7 c). Disseminated chromite and chromitite stringers are found associated with base metal

sulphides in the lenses. PGM values are also associated with the chromitite along the top and bottom contacts of the noritic lenses, and are also present within the partly reconstituted Pseudo Marker in the immediate footwall. Values in the latter are lower than in adjoining well-developed pothole reef that does not have hanging wall noritic lens material.

Where the lenses are thin, they can be mined out together with their chromitite layers and pegmatoidal pyroxenite and harzburgite, forming the lens reef on pothole elevation (Plate 7 c). Where a lens is thicker than 6 metres, the upper irregular contact is also termed contact reef (Figure 9). The irregular nature of this contact makes efficient mining virtually impossible, although good values occur in places. In such areas of thick lens development, mining is confined to the Pseudo Marker or lens reef elevation, where values are, however, somewhat less than in pothole reef outside the lens areas. In such instances the noritic lens, together with its overlying chromitite layer and poikilitic pyroxenite, are left in the hanging wall of the stope.

Two detailed Dip sections illustrating the various pothole features discussed above are presented in Figure 10 a and b. Figure 10 a illustrates a gradual transgression of the contact reef through the footwall anorthosites and leuconorites as far as the pothole reef, some 300 metres down dip from the normal reef "cut-off" totrue pothole reef. The contact reef was flattened over 70 metres, in the centre of the section on the poikilitic anorthosite-leuconorite contact. This area of contact reef was mined successfully at a narrow stope width of 76 cm. Closer to the pothole reef, lenses of leuconorite are trapped between the Merensky pyroxenite and the pegmatoidal pyroxenite of the Pseudo Marker, forming in this case a small area of lens reef.

Figure 10

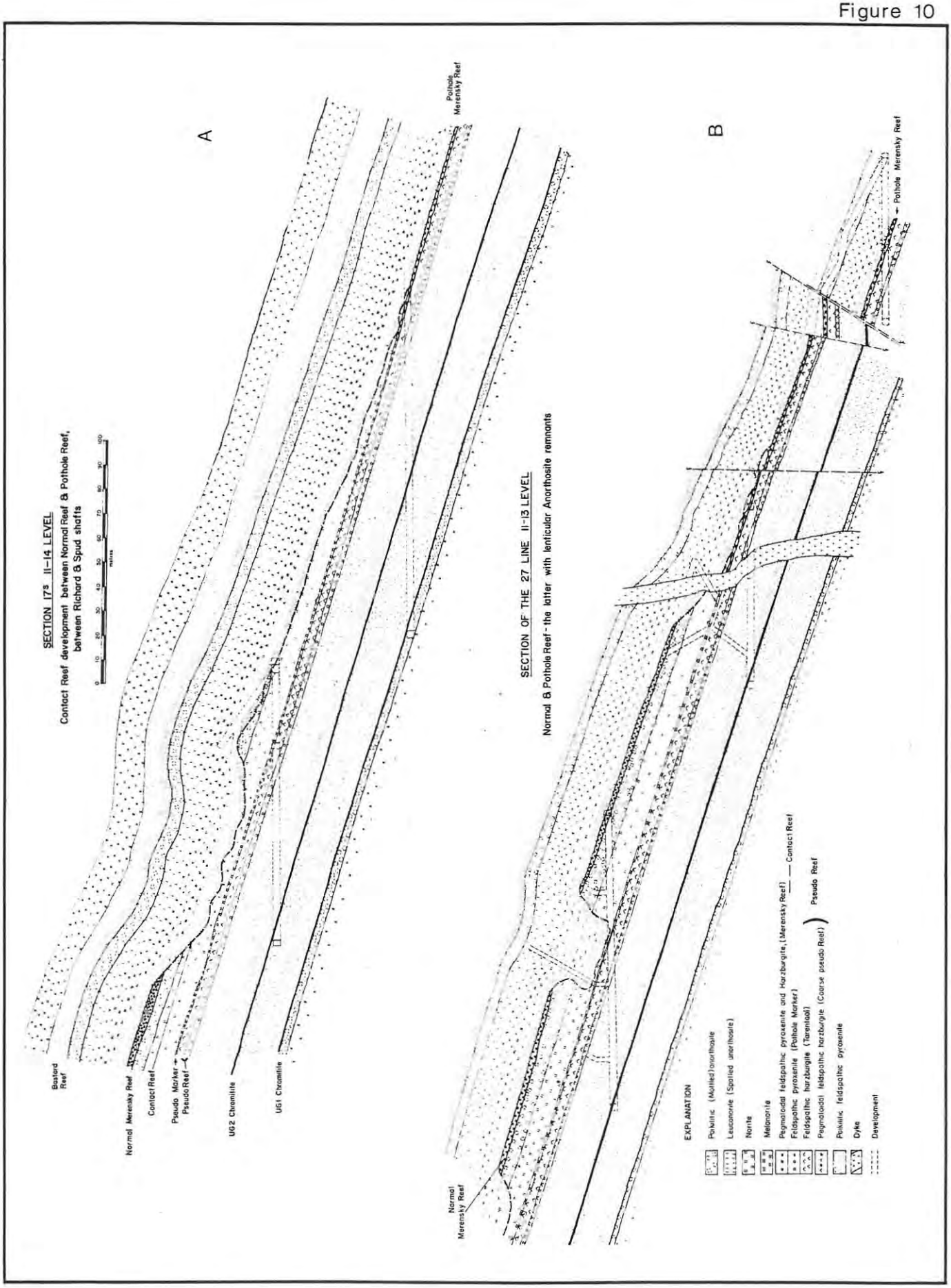
SECTION 17S 11-14 LEVEL
Contact Reef development between Normal Reef & Pothole Reef, between Richard & Spud shafts
Metres
A
Bastard Reef
Normal Merensky Reef
Contact Reef
Pseudo Marker
Pseudo Reef
UG2 Chromitite
UG1 Chromitite
Pothole Merensky Reef
SECTION OF THE 27 LINE 11-13 LEVEL
Normal & Pothole Reef - the latter with lenticular Anorthosite remnants
B
Normal Merensky Reef
Pothole Merensky Reef
EXPLANATION
Poikilitic (Mottled) anorthosite
Leuconorite (Spotted anorthosite)
Norite
Melanorite
Pegmatoidal feldspathic pyroxenite and Harzburgite, (Merensky Reef) — Contact Reef
Feldspathic pyroxenite (Pothole Marker)
Feldspathic harzburgite (Tarentaal)
Pegmatoidal feldspathic harzburgite (Coarse pseudo Reef) — Pseudo Reef
Poikilitic feldspathic pyroxenite
Dyke
Development

In Figure 10 b, the complexity of multiple pothole development is well-illustrated, and all features of potholing are evident, i.e. thinning of normal reef, "flick back", pothole cut-offs, contact reef, lens development, and true pothole reef. Also shown is the position of the development haulages, crosscuts and raises. The mining problems created by these pothole structures are obvious.

5.4 Variation in thickness of Merensky Reef

The Merensky Reef (both normal and pothole) varies considerably in thickness from the north-eastern to south-western part of Union Section. In order to monitor this variation in thickness, all available data from surface and underground boreholes, as well as from underground sampling records, have been used in the construction of an isopach map (Figure 11). This plan refers only to normal reef, as data for pothole reef thickness are scanty, and compilation of these data is not yet complete.

5.4.1 Normal Merensky Reef Data are difficult to come by in many areas, particularly in areas of thick reef development, where only the uppermost part of the reef is mined, and the lower part is thus not exposed. Sufficient data were acquired, however, for the construction of a regional normal reef thickness contour map, which is considered to give a reasonably good indication of regional trends in reef thickness variation (Figure 11).

It is evident that the normal Merensky Reef attains its greatest thickness in the Ivan Shaft area, from where it thins gradually along strike and down dip. Thus at Richard Shaft, some 2 km south of Ivan Shaft the thickness is 4 metres, while at the 22 Vertical Winze 2 km south-west of Richard Shaft, it averages about 1 metre (Figure 11).

UNION SECTION

MERENSKY REEF ISOPACH AND POTHOLE MAP

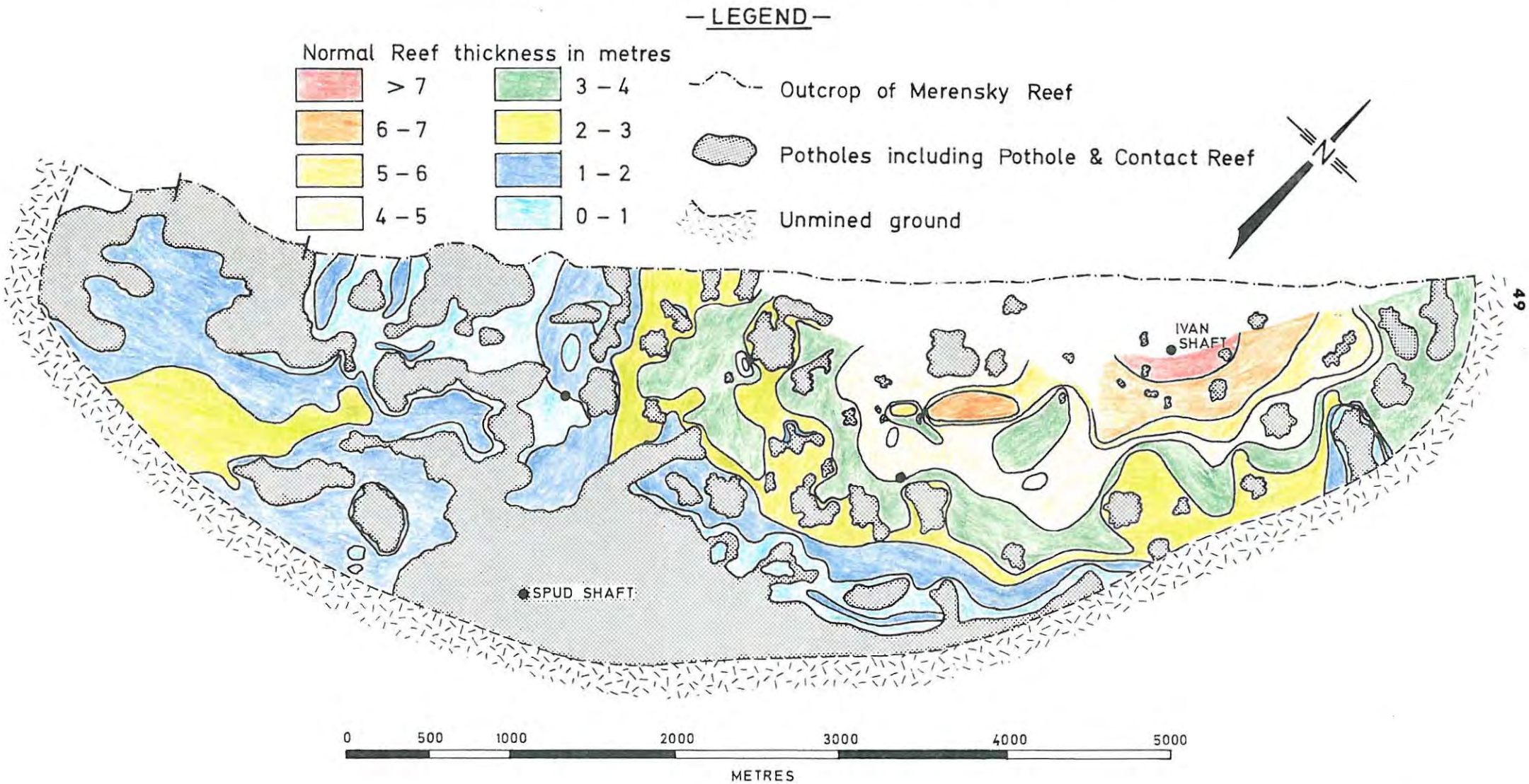

A close relationship is evident between normal reef thickness and the size and abundance of potholes. Thus in the region of thick reef development at Ivan and Richard Shafts, only a few, relatively small potholes are developed. The frequency and size of potholes generally increases in all directions away from this area, and this correlates well with the gradual thinning of the Merensky Reef. From an east-west line, drawn roughly between the 22 Vertical Winze and Richard Shaft, an abundance of large, irregular and frequently interconnected potholes is evident; normal Merensky Reef in between is generally less than 2 m in thickness. The down-dip areas of Richard and Ivan Shafts in the area of current mining activity also generally have a normal Merensky Reef thickness of less than 3 m (Figure 11).

Although data from underground are hard to come by, observations invariably show a second order, local, rapid thinning in the vicinity of individual potholes. One example 1,5 km east of Ivan Shaft (Figure 11), exhibits rapid thinning from 3 metres to zero at the pothole edge, over a distance of 30 metres. If one proceeds southwards from Richard Shaft to Spud Shaft, a gradual thinning of the normal reef from the trace of the 3 metre isopach line to the edge of the large regional pothole in the Spud Shaft area takes place over about 700 m. It thus appears that the rate of thinning of the normal Merensky Reef bears a broad relationship to the size of the approaching pothole.

5.4.2 Pothole Merensky Reef Pothole reef thickness in the majority of potholes exposed, has been very consistent at 76 cm, but isolated, abnormal thicknesses of the pegmatoid of up to 3 m, have been observed. No thinning of pothole reef towards the edges of potholes has been documented. Recent drilling down dip of the present mining limits however, indicates that the pothole reef in the very large Spud Shaft pothole, thins quite considerably

to about 15 cm. This narrow reef contains conspicuous base metal sulphides and very high PGM values.

5.5 Structure of Merensky Reef

As noted, the Merensky Reef at Union Section has been traced for a distance of 9.5 km at surface between the northern and southern Gap areas.

The dip of the Merensky Reef, and associated layers of the upper Critical zone, is variable. A gradual and steady increase in the angle of dip, as the north-eastern limits are approached, is evident from regional structure contours constructed for the top of the Pseudo Reef (Figure 12). This accompanies a gradual swing in strike to the north, as the northern Gap area is approached. Thus in the 22 Vertical Winze-Spud Shaft area the dip is 20°; at Richard Shaft it is 22°; while at Ivan Shaft it has steepened to 24°. In the extreme north-east, close to the northern Gap area, a pronounced swing has resulted in a significant steepening to 30° (Figure 12).

No such steepening is evident to the south-west as the southern Gap area is approached. Here a number of large north-east trending faults result in an apparent swing in the reef, by successive fault blocks being displaced to the north-east as the southern Gap area is approached (Figure 13).

5.6 Dykes

As can be seen in Figure 8, there are two dominant dyke directions and types, namely:

a) Northwest - trending dykes of Pilanesberg affinity, which could be described as diabasic types.

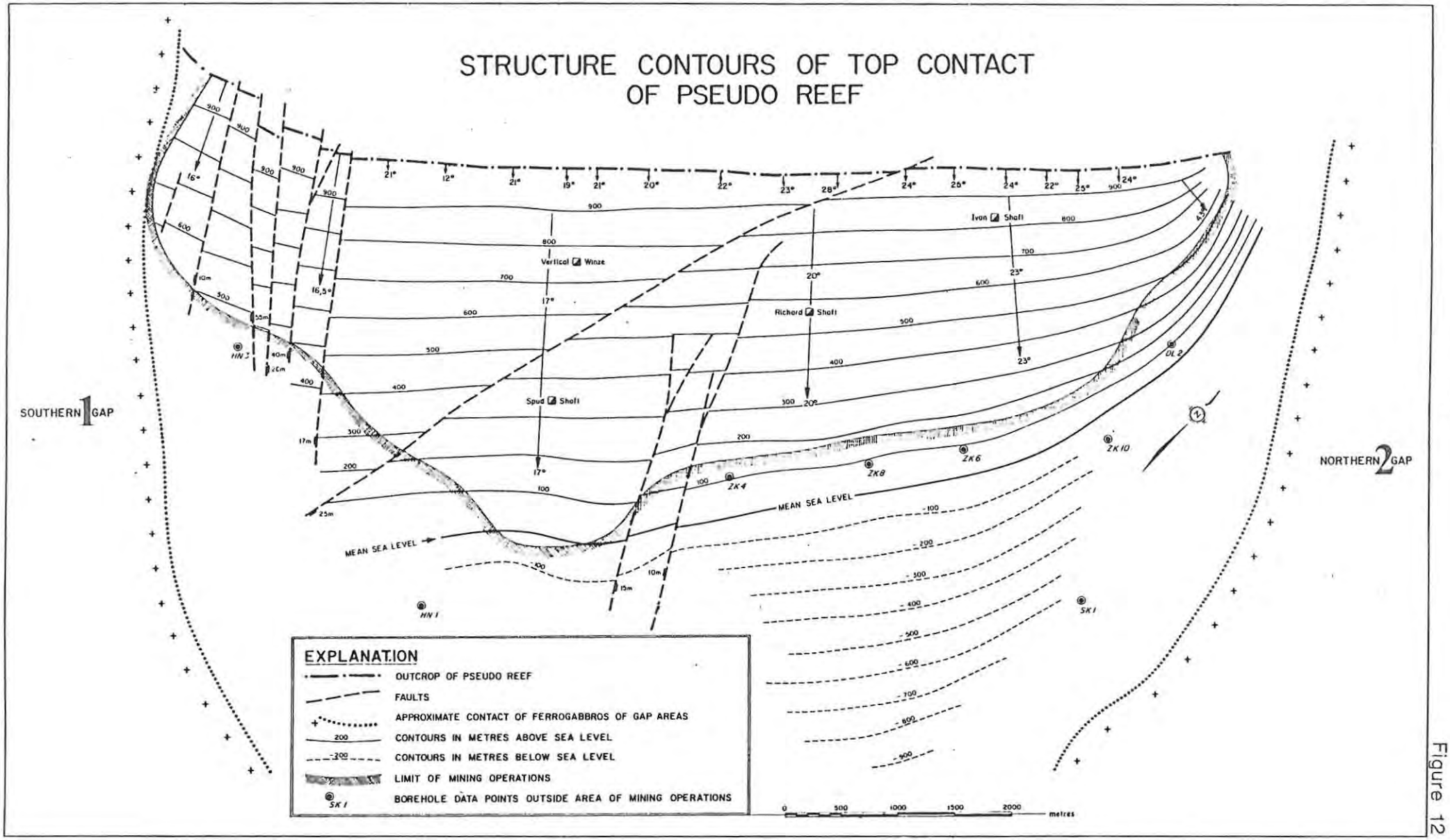
STRUCTURE CONTOURS OF TOP CONTACT
OF PSEUDO REEF
SOUTHERN 1 GAP
NORTHERN 2 GAP
Vertical Winze
Spud Shaft
Richard Shaft
Ivan Shaft
MEAN SEA LEVEL
HN 2
HN 1
ZK 4
ZK 8
ZK 6
ZK 10
SK 1
DL 2
EXPLANATION
OUTCROP OF PSEUDO REEF
FAULTS
APPROXIMATE CONTACT OF FERROGABBROS OF GAP AREAS
CONTOURS IN METRES ABOVE SEA LEVEL
CONTOURS IN METRES BELOW SEA LEVEL
LIMIT OF MINING OPERATIONS
BOREHOLE DATA POINTS OUTSIDE AREA OF MINING OPERATIONS
0 500 1000 1500 2000 metres

Figure 12

b) Roughly east-trending dykes, which are doleritic in character.

5.6.1 Dykes of the Pilanesberg Alkaline Province These dykes are part of the Pilanesberg Alkaline Province as described by Ferguson (1973), and trend along a bearing of 140°. They are generally thick (25 to 60 metres) vertical dykes which are medium-grained over most of their width, but have a fine-grained chill phase of 1 to 2 m in thickness on their margins, in contact with the country rocks. These fine-grained chill rocks are seen in thin section to be fresh dolerites, but the medium-grained cores are diabasic in character. The dolerite chills display the characteristic ophitic texture, and there is the occasional larger phenocryst of augite which has a very distinct hour-glass texture in thin section. The diabase cores of these dykes are medium-grained, and have undergone more alteration than the chilled margins. The pyroxenes are altered to chlorite and serpentine, and the plagioclase crystals are saussuritised to varying degrees. The contacts with the country rocks are sharp, but in some places the contacts are zones of minor shearing.

These dykes characteristically have a negative magnetic signature, arising from strong remanent magnetization approximately anti-parallel to the present earth's field direction of -60° from the horizontal. Gough (1956), in his work on the palaeomagnetism of the Pilanesberg dyke swarm, reported that the negative anomalies are due to a stable remanent magnetization having an inclination of +69°.

5.6.2 Dolerite Dykes These dykes are rather narrow (8 to 10 m) and vertical, and consist of fine-grained dark dolerites. Their contacts with the country rocks are sharp, but they sometimes have minor shearing on the contacts. Magnetically they have a positive signature, which indicates normal magnetization, and they postdate the larger Pilanesberg

dykes described above.

5.7 Faulting

Normal faulting is the most prominent style of faulting at Union Section, and the dip of the faults is usually close to 90°. Very little major faulting is observed in the north-east sector of the mine, although numerous small faults (with a displacement of less than 3 m), shears and joints are associated with the northern Gap area cut-off.

Dr. M.J. Viljoen (1981, pers. comm.) has recognised a number of prominant lineament directions which are illustrated in Figure 2. The faults, which constitute part of these lineaments, are summarised as follows:

a) In the south-western part of the mine, a swarm of seven major faults, with displacements varying from 4 - 55 m, are developed, and they have a consistent direction which averages 140° and parallels the Pilanesberg dyke direction. A large fault with numerous small (<3m) faults occurs in the north-eastern part of the mine with a 140° direction. Viljoen et al.(1981,in press) considers these faults in the south-west and north-east of the mine to be related to, and perhaps represent part of the major graben fault system invoked earlier (Chapter 3)to explain the cut-off of the Critical zone and the development of the northern and southern Gap areas.

b) A major fault with a 20° direction cuts through the central part of Union Section and has a downthrow of 25 m to the east and a left lateral movement of 115 m.

5.8 Intrusive Pegmatites and Pegmatoids

5.8.1 Pegmatites In the poikilitic feldspathic pyroxenites above the UG 1, UG 2, Merensky Reef and the Bastard Reef, pegmatitic "gash veins" between 10 and 20 cm thick are well-developed. A gash vein was originally used to define vertical solution joints in limestone, and is confined to single formations. In some respects, they resemble fissure veins, and in the Union Section context they are vertical, thin pegmatitic bodies, which have a strike parallel to the prominant 140° direction described earlier. These gash veins consist essentially of very coarse-grained plagioclase, hornblende, biotite and quartz, and display a distinctive comb structure (Plate 8 a). The general attitude of the gash veins is vertical, but variations of up to 10° from the vertical may occur. These pegmatitic gash veins have a strike which corresponds very closely to the 140° direction (at right angles to strike).

5.8.2 Pegmatoids These are generally coarse-grained, intrusive, irregular, ultramafic bodies, which appear to be the results of migration and crystallization of late-stage intercumulus fluids which have, in some cases, been forcefully injected into the semi-consolidated crystalline mush. This forceful injection often distorts the primary layering, as can be seen in Plate 8 a, b and c.

Crosscutting, iron-rich pegmatoids are found predominantly in the north-eastern sector of the mine, and appear to be genetically related to the dunite in the northern Gap area (Figure 3). Trenching on surface beyond the limits of mining has revealed the presence of a dunite intrusive, and this dunite could account for the numerous pegmatoids exposed by underground workings. Elsewhere on the mine, isolated pegmatoids usually occur in close proximity to potholes, and within the larger potholes.

PLATE 8

a. Pegmatitic gash vein in the poikilitic feldspathic pyroxenite between the UG 1 and UG 2 chromitite layers. These pegmatitic veins only occur in the pyroxenites (Plate 6 d), and consist essentially of hornblende, plagioclase, biotite and quartz.

b. Crosscutting iron-rich intrusive pegmatoid in the poikilitic (mottled) anorthosite below the Merensky Reef. These pegmatoidal pyroxenite bodies are usually best-developed in the more anorthositic rock types, and vary greatly in size.

c. Very coarse-grained intrusive pegmatite in the poikilitic anorthosite 8 m below the UG 1 chromitite. Here the "mottles" have been elongated and drape the pegmatite. Some of the larger hornblende crystals are 20 cm long and have a characteristic comb texture.

d. Coarse-grained pegmatite in the layered leuconorite 5 m below the UG 1 chromitite. Here there has been almost no distortion of the layering.

PLATE 8

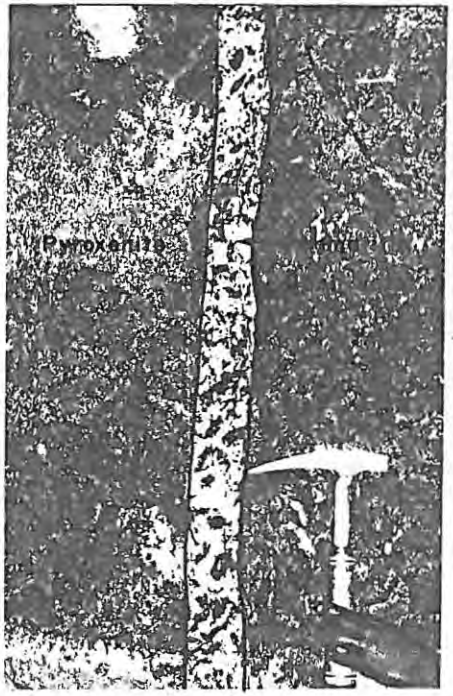

a

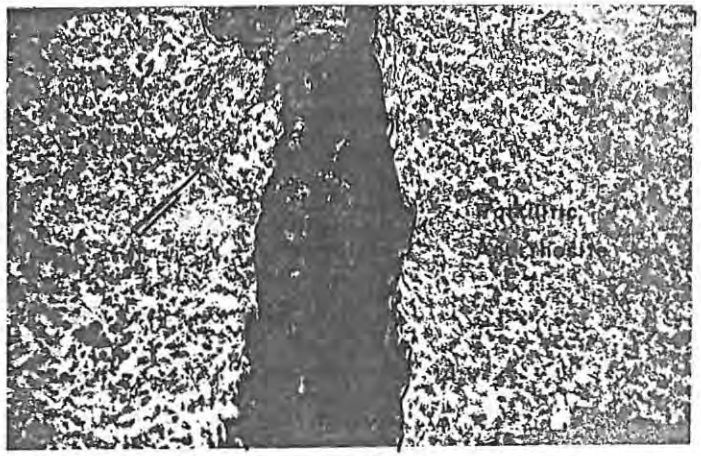

b

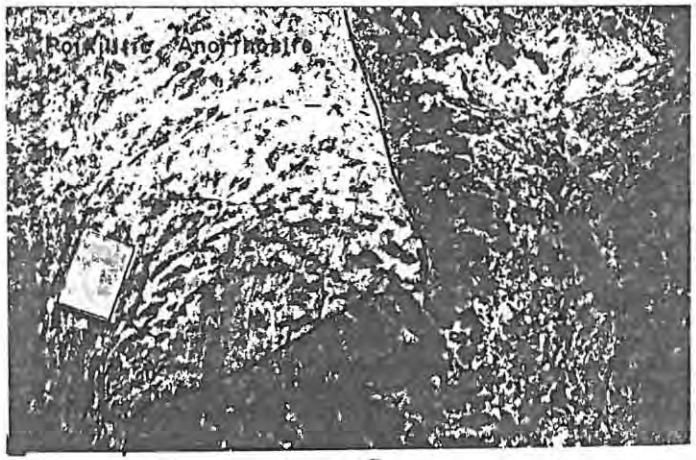

c

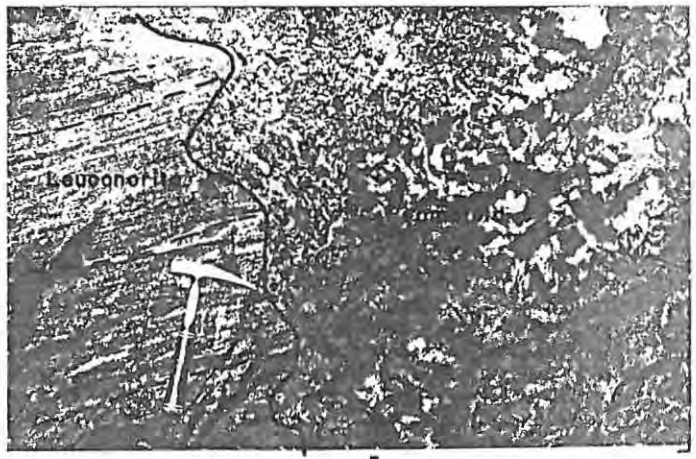

d

The dark, iron-rich pegmatoids have a tendency to be emplaced in, or to replace, the more feldspathic rock types in the upper Critical zone. The result is that one often finds intrusive iron-rich pegmatoids replacing the poikilitic anorthosite and anorthosites below the Merensky Reef, Bastard Reef and UG 1 respectively (Plate 8 b). This replacement does not always alter or disturb the overlying layers to any significant degree, but in isolated instances the iron-rich pegmatoids do replace all the rock types and transgress the layering.

5.9 Linear Features

The major dyke and fault directions at Union Section, discussed above (Section 5.6, 5.7) are shown as single, linear features centred on the mine area in Figure 2. Five major directions are evident; four of these correlate well with the regional linear features obtained from the interpretation of LANDSAT images. The latter have been extracted from the compilation of Lee (1981).

The most striking set of linear features has a direction of 140° and is correlated with the Pilanesberg dyke swarm. These linear features are well developed in the dolomite to the north-west of Union Section, as well as in the Bushveld granites to the south-west. They correspond perfectly to the trend of the Pilanesberg dykes as seen at Union Section, as well as to the parallel set of major faults (Figures 3 and 8).

A set of linear features with a direction of 65° is well developed in the granite terrain to the north of the Crocodile river fragment, as well as within, and to the east and west of the Pilanesberg alkaline complex. This direction is equated with the direction of a number of dolerite dykes at Union Section (Figures 3 and 8).

Only one linear feature with a 115° direction was noted, extending from the Crocodile river fragment to Union Section. This corresponds with the trend of a few dolerite dykes in the mine.

Finally, a set of linear features with a 20° direction extends northwards from Union Section and is also seen to the north of the Crocodile river fragment. It corresponds with the direction of a major fault which cuts diagonally across the centre of the mine (Figures 3 and 8).

The 100° dyke direction developed towards the south-west of Union Section does not appear to have an analogue among the regional satellite linear features which have been mapped. Similarly, a very strong set of north north-west trending linear features, which are well developed in sediments of the Transvaal Sequence on the western side of the Pilanesberg, are not manifested by major dyke or fault directions at Union Section.

6. SAMPLING PROCEDURE

6.1 Introduction

From July 1978 to December 1980, detailed mapping and data compilation of the upper Critical zone were carried out as part of the author's daily work while in the employ of Rustenburg Platinum Mines, Union Section, as mining geologist. In 1979, a number of underground diamond drill boreholes were carefully sited to compile an undisturbed normal Merensky Reef succession and a representative pothole reef succession. Figure 13 a and b illustrate the positions of these intersections in the mining area.

6.2 Normal Succession

A total of four boreholes was drilled, at right angles to the layering on the 13-30 South crosscut, some 1030 m south-west of Spud Shaft, to intersect an undisturbed normal Merensky Reef succession. The positions of the various boreholes, making up a composite column, B235, are illustrated in Figure 13 b. A total of 40 core samples was selectively taken throughout this composite column in order to sample each horizon represented in the succession (Figure 14). An average core-length of 48 cm was sampled at each location, as illustrated in Figure 15, and for the coarser rock types such as the Merensky Reef, Pseudo Marker, Pseudo reef and the pegmatoidal pyroxenite footwall of the UG 2, a larger sample of 10 kg was collected from exposures in the stope and crosscut at 13-30 South.

This area of normal Merensky Reef was chosen because the closest pothole in the vicinity is greater than 200 m away, and is thought to have had very little effect on the

Figure 13

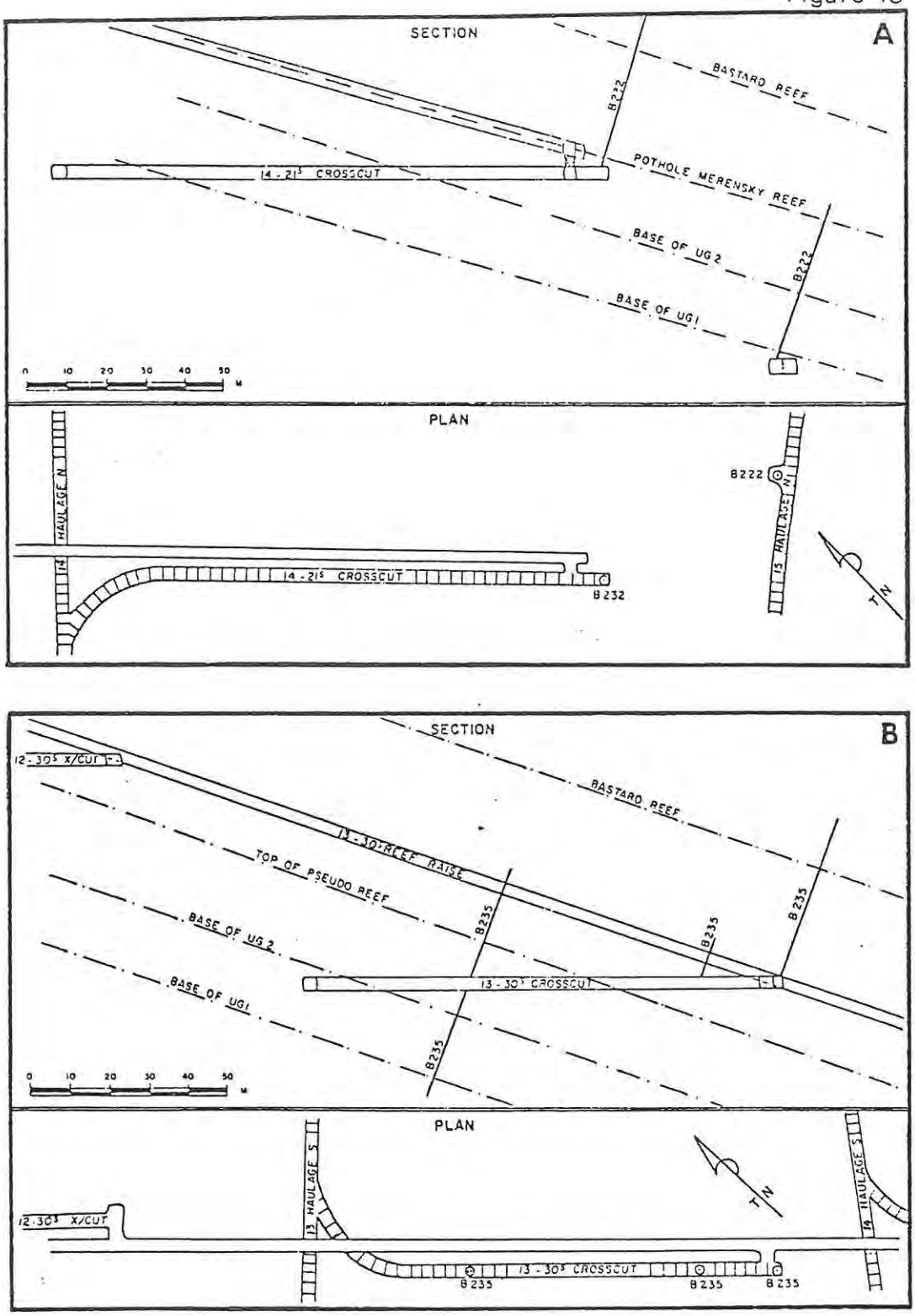

Figure 13 a and b: Plan and section diagram illustrating the underground borehole sampling localities. Boreholes B232 and B222 were drilled for a pothole succession (A) and B235 was drilled for a normal succession (B).

Figure 14

STUDY SECTION THROUGH UPPER CRITICAL ZONE SHOWING SAMPLING POSITIONS

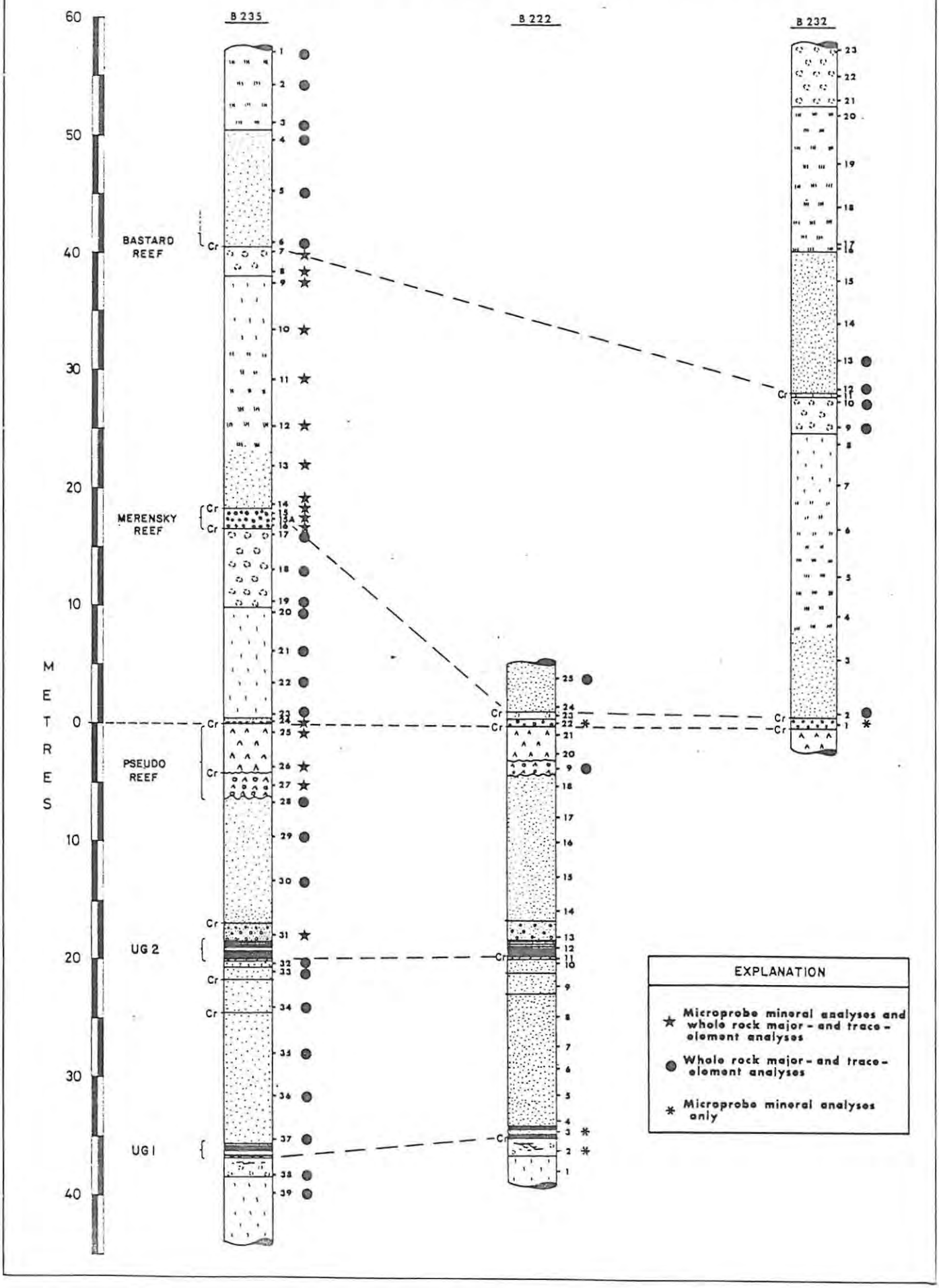

Figure 15

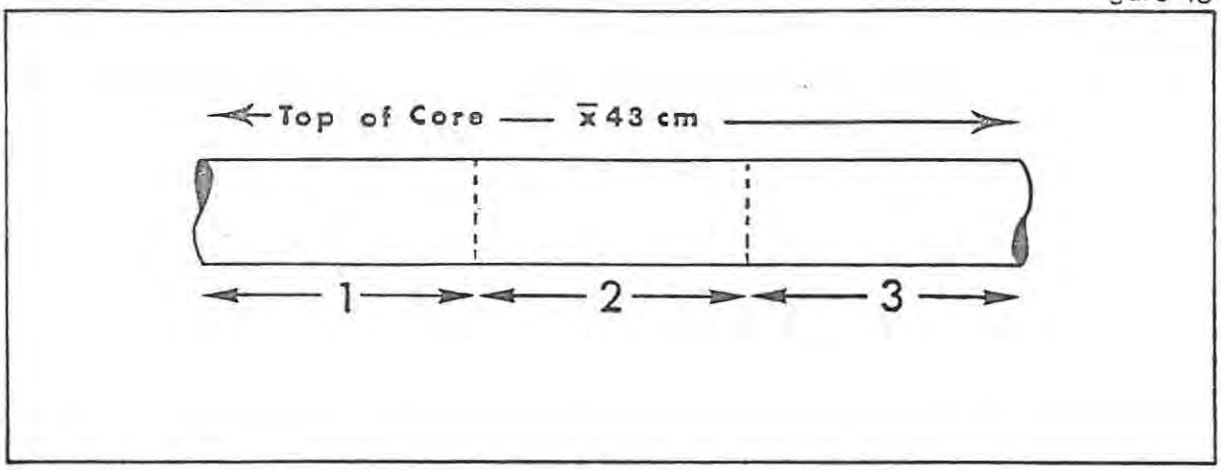

Figure 15: Diagram showing the position of various samples from each sampling locality. Positions 1 and 3 were combined and used for whole rock major - and trace - element analyses. Position 2 was used to cut thin sections for election microprobe and optical studies, and the remainder was retained as a library specimen.

chemistry and mineralogy of the normal succession. Each core sample was divided into three sections for the preparation of the various specimens used in the study (Figure 15). The top and bottom of the core sample, i.e. positions 1 and 3 in Figure 15, were combined and used for whole-rock major- and trace-element analyses. These two segments of core were thoroughly cleaned, and all serpentinised slips and flaws in the sample were ground off, so that only a fresh, unaltered sample would be used for the analyses. The samples were split in a jaw crusher, crushed to ±120 mesh size in a manganese steel swing mill, and then crushed to ±300 mesh size by hand in an agate mortar. Powder briquettes, using approximately 4 grams of fine powder, were prepared for X.R.F. analysis of all trace elements except Cu and Ni.

Core from position 2 in Figure 15 was used to cut thin sections and polished thin sections for microprobe mineral analyses. The remainder of the core from position 2 has been retained as a library specimen (5-10 cm long).

6.3 Potholed Succession

The potholed succession was drilled in the large Spud Shaft pothole, 450 m to the north-east of the shaft from 15 haulage North and the 14-21 South crosscut. Two boreholes, B222 and B232, were drilled to make up a composite Pothole column (Figure 13 a). Borehole B222 intersected Lens Reef, which is rather common in the Spud Shaft area. The B232 borehole exposed good Pothole Reef and thus afforded an ideal opportunity of seeing whether there were any mineralogical variations between the Pseudo Marker layer, Lens Reef and Pothole Reef, which are all on the same stratigraphic layer.

Only seven samples from the pothole succession were used for whole-rock major- and trace-element analyses. These seven samples were chosen to see if there was any lateral chemical variation along the same stratigraphic horizon from the normal to pothole succession. Equivalent stratigraphic samples (two in each case) were chosen from the Bastard Reef feldspathic pyroxenite, the Bastard Reef footwall poikilitic anorthosite (or the top of the Merensky unit) and from the Merensky pyroxenite. The lower pegmatoidal Pseudo Reef from the pothole succession was also sampled.

A total of 48 samples was taken from both pothole succession boreholes (Figure 14), and thin sections were cut from each sample. Microprobe polished thin sections were prepared for samples B232/1, B222/2, B222/3 and B222/22. The same method of sample preparation used for the normal succession was used for the seven pothole succession samples.

7. PETROGRAPHY

7.1 Introduction

In this chapter the petrography of the upper Critical zone in both the normal and potholed succession is discussed and includes all layers from just below the UG 1 chromitite to the top of the poikilitic anorthosite (Giant mottled anorthosite), which demarcates the top of the Bastard unit and the top of the Critical zone (Figure 16). The different rock types are described in sequence of increasing colour index, and an estimated modal percentage of the main mineral phases is presented in Figure 18. In all cases the thin sections were cut parallel to the layering of the Complex, i.e. at right angles to the bore-hole core.

7.2 Igneous layered rocks and their nomenclature

McBirney and Noyes (1979) point out that there are two basic processes which have been proposed to account for crystal fractionation during solidification of large intrusions.

Briefy, they are:

a) Crystals nucleate and grow mainly under the roof of the magma chamber and move, under the influence of gravity, to accumulate on the floor (Wager, 1968).

b) Crystals nucleate and grow essentially in situ (Jackson, 1961).

The concept of crystal settling is at present under

Figure 16

STUDY SECTION THROUGH UPPER CRITICAL ZONE SHOWING SAMPLING POSITIONS

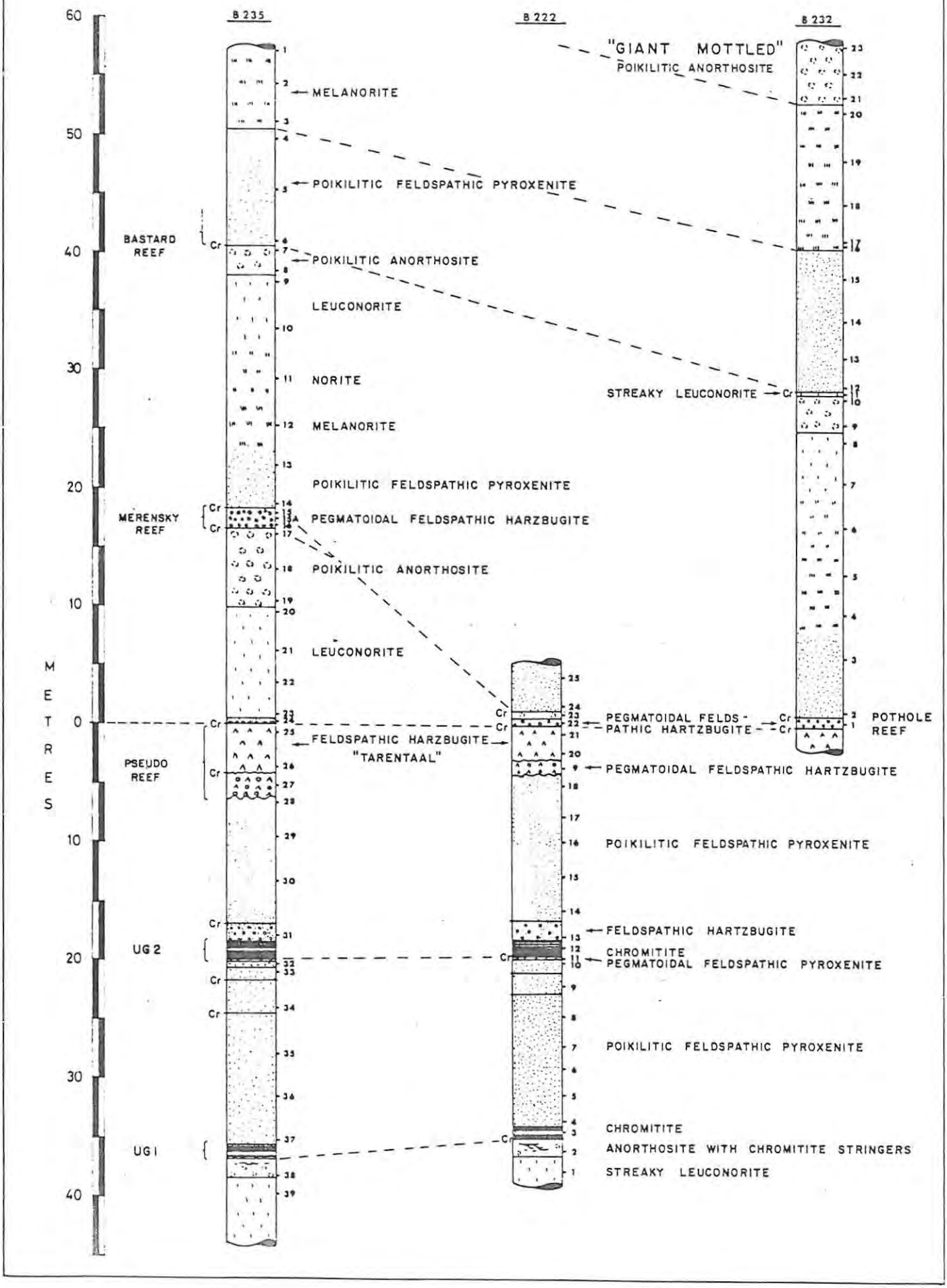

Figure 17

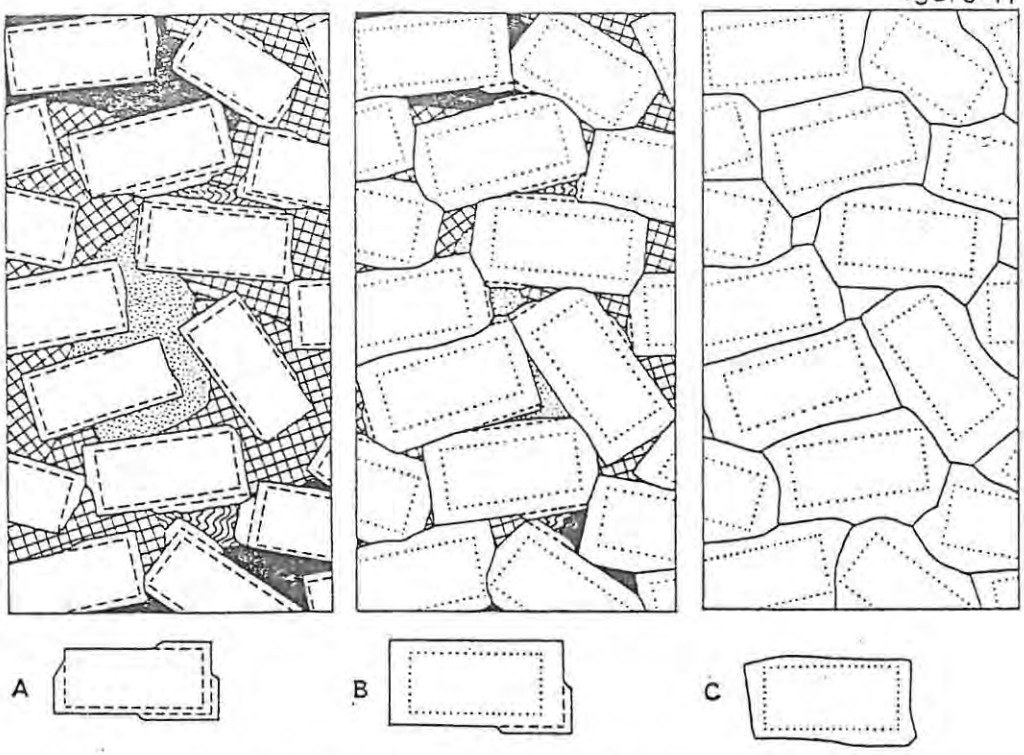

Figure 17: Diagrammatic representation of plagioclase cumulates formed from basaltic magma. A, extreme plagioclase orthocumulate; B, plagioclase mesocumulate; C, extreme plagioclase adcumulate.
After Wager, Brown and Wadsworth (1960).

critical review (McBirney and Noyes, 1979; Irvine, 1980), and appears to be much less important than was originally believed, but this does not seem sufficient reason to abandon the terminology that has been developed for cumulus processes. The cumulate terminology developed by Wager, Brown and Wadsworth (1960), which has strong genetic overtones, is retained for the present discussion, but it ignores the actual process of crystal pile accumulation.

Igneous rock types which have formed by crystal pile accumulation due to the gravity settling of crystals from a magma, have been termed cumulates (Wager, Brown and Wadsworth, 1960). Cumulus crystals first nucleate in the magma, and grow for a while as primocrysts within the magma, and are then removed from suspension to become attached to any of the boundary surfaces of the intrusion, (floor, wall or roof).

The cumulus crystals remain partially enclosed in intercumulus liquid, which has the composition of the now somewhat modified contemporary magma, and the intercumulus liquid could eventually solidify as intercumulus material. The various types of cumulus processes and their products found most commonly at Union Section are described below (Figure 17).

a) Adcumulates

If one starts with a plagioclase crystal mush on the floor of a magma chamber, and the distances to the liquid-crystal interface are not too great, and if the channels to the overlying magma are kept open, two-way diffusion of ions between the intercumulus liquid and overlying magma reservoir may take place. This would permit continued growth of the plagioclase crystals of the mush at the expense of the intercumulus liquid, a process which could continue until the liquid was exhausted or the rock was wholly crystalline. This would result in a monomineralic assemblage called a plagioclase adcumulate (Figure 17 c). The continued growth of plagioclase and the absence of intercumulus phases was attributed by Wager, Brown and Wadsworth (1960) to the simultaneous operation of two processes: diffusion of plagioclase components from the magma to the crystals, and the consequent squeezing out of inappropriate liquid by the growing cumulus crystals.

If accumulation of plagioclase primocrysts on the floor

were more rapid, the mush might become too thick for ionic diffusion to be effective, in which case some or all of the intercumulus liquid might be trapped. Hess (1960) suggests that pure anorthosite may represent very slow accumulation of crystals on the floor, and increasing amounts of interstitial pyroxene (orthopyroxene or clinopyroxene) may indicate more rapid rates of accumulations.

b) Orthocumulates

If the rate of accumulation of crystals becomes so rapid as to prohibit effective diffusional exchange altogether, the resulting cumulus rock will consist of cumulus crystals and interstitial postcumulus material of variable composition. Rocks approaching such a state are frequently observed and are called orthocumulates.

A fairly common texture in layered intrusion is the poikilitic enclosure of euhedral or subhedral phases by later anhedral crystals of different minerals. The euhedral phase could be interpreted as the primocrysts, and the anhedral poikilitic crystals as the minerals formed by in situ crystallization of intercumulus or trapped liquid. This texture would be typical of an orthocumulate.

c) Mesocumulates

These rock types are intermediate in character between orthocumulates and adcumulates, and are by far the commonest type. Here limited two-way diffusion takes place, and only a limited amount of adcumulus growth occurs on the primocrysts.

d) Heteradcumulates

These rocks form when nucleation of a mineral species in the intercumulus liquid occurs, and this mineral grows

in the intercumulus space by adcumulus growth, and poikilitically entraps the primocryst cumulus phase or phases. Once again, limited two-way diffusion between the overlying magma and the intercumulus liquid takes place.

7.3 Anorthosites

Anorthosites from the study section include the following samples: B235/7, 8, 17, 18, 19 and 38, B222/2 and 23, and B232/9, 10, 21, 22 and 23 (See Figure 16).

In the anorthosites, 0-5% of the rock is made up of large skeletal poikilitic crystals of clinopyroxene, orthopyroxene, and minor biotite, which are interstitial to the cumulus plagioclase.

Van Zyl (1970) distinguished two types of anorthosite at Union Section and he termed them pure anorthosite, and mottled anorthosite. Strictly, an anorthosite is a monomineralic rock-type, and hence would, by definition, be pure. The term "mottled anorthosite" has been widely used in the literature and on the platinum mines, as a descriptive textural term to signify presence of the diffuse pyroxenes which typify this rock-type. The strict petrological name for this rock would be a poikilitic anorthosite. The large "mottles" which are from 2-6 cm in diameter are optically continuous intercumulus crystals, and in this study these are mainly clinopyroxene and orthopyroxene within a plagioclase adcumulate. The pyroxene mottles thus represent the oikocrysts, and the feldspar within the "mottles", the chadacrysts.

All the anorthosites in the study section are holocrystalline and Van Zyl (1970) gives an average volumetric mineral composition of a typical anorthosite as: plagio-

clase - 93%, orthopyroxene - 4%, clinopyroxene - 2% and accessory biotite and spinel - 1%.

The plagioclase, in all cases, occurs in two distinct textural types, namely small (0,3-0,5mm) cumulus subhedral to euhedral crystals, and larger (1-3,5mm) anhedral adcumulus crystals. The smaller plagioclase crystals are often found poikilitically enclosed in the skeletal intercumulus pyroxene oikocrysts and also tend to cluster loosely together away from the pyroxene.

The larger, anhedral plagioclase crystals are, in many cases, zoned and display strained extinction. They also often poikilitically enclose the smaller grains of plagioclase towards their margins.

Both ortho- and clinopyroxene form large intercumulus concentrations which range in size from 1-6 cm in diameter, and are regularly spaced throughout this rock type. These intercumulus pyroxene concentrations are quite often in optical continuity, but the intercumulus clinopyroxene, and, more rarely, the orthopyroxene, tends to occur rather as discrete intercumulus crystals, or at best, only a few grains in close association within the larger "mottles" are in optical continuity (Plate 9 a). The amount of intercumulus pyroxene seen in each thin section is largely dependent on where the sample was taken within the anorthosite layer, i.e. the thin section could be cut in the anorthosite itself, or through a "mottle", as in sample B232/22 where the entire slide is cut through a large oikocryst of clinopyroxene (Plate 9 b).

Biotite also occurs as intercumulus oikocrysts, which enclose euhedral chadacrysts of plagioclase, which also project into the biotite in typical subophitic texture (B232/21). In most cases, however, the biotite only occurs as small discrete intercumulus grains. The

disseminated euhedral chromite is only found in those anorthosites which are adjacent to chromitite concentrations (B235/7, 17, 38, B222/2, and 23). Here the chromite grains, which range in size from 0,1-0,3mm tend to lie at the triple point junctions of the cumulus plagioclase crystals. In some cases, disseminated chromite is also found poikilitically enclosed towards the margins of the larger plagioclase crystals.

Intercumulus disseminated base metal sulphides occur in the foot-wall anorthosites of the Bastard and Merensky Reefs (B235/7 and 17), and also in the lens of anorthosite between the Mẽrensky pyroxenite and the Lens Reef (B222/22). These sulphides occur at grain boundaries and triple point junctions of the plagioclase, and the plagioclase is invariably saussuritised around the sulphide grain. The dominant sulphide is pyrrhotite, in association with subsidiary chalcopyrite, and these composite grains have a grain size of between 0,1 and 0,4 mm.

Saussuritization of the plagioclase is found most commonly associated with small fractures and cracks throughout the anorthosite. These pervasive fractures acted as feeder channels for the hydrothermal fluid. Generally the degree of saussuritization is highest in the immediate footwall anorthosites of the Merensky and Bastard Reefs (B235/7 and 17), and more generally in close proximity to fault and fracture zones within the upper Critical zone.

If only the anorthosite between the "mottles" were considered, then this rock would be described as a typical plagioclase adcumulate. As the mottles are generally skeletal clinopyroxene and/or orthopyroxene which are intercumulus to the plagioclase, this rock would by convention be termed a heteradcumulate. Only those

anorthosites which do not contain any poikilitic mottles are adcumulates, e.g. the UG 1 footwall (B235/38 and B222/2) while all the other poikilitic anorthosites throughout the section are heteradcumulates.

7.4 Norites

Norites, throughout the study section, are represented by the full range, from leuco- to melanorite types, and these ranges are best represented in the Bastard, Merensky, Footwall and Basal units. They are gradational, without any sharp contacts, from leucocratic at the top to melanocratic towards the base of each unit. The norites, which make up part of each of the upper three units, are represented by samples B235/1-4, 9-12 and 20-23 for the normal succession. Samples B232/3-8 and 16-20 represent norites from the pothole succession while sample B232/11, which forms the footwall of the Bastard Reef, represents a norite not found in the normal succession. Other norites from the study section are the streaky leuconorites approximately 4 m below the UG 1 (B235/39 and B222/1), which are well illustrated in Plate 1, making up the remaining norites from the study section.

All these norites are made up of varying proportions of cumulus subhedral prismatic orthopyroxene and plagioclase crystals with minor amounts of intercumulus anhedral clinopyroxene, orthopyroxene, biotite and base metal sulphides.

A dominant feature of the plagioclase in the norites is the occurrence of a bimodal distribution of plagioclase grain sizes in the more leucocratic types. The smaller grains of plagioclase, which are between 0,2 and 0,5 mm are subhedral to euhedral in form, while the larger plagioclase grains are anhedral and from 1,5 to 3,5 mm in

PLATE 9

a. Poikilitic (mottled) anorthosite where the intercumulus pyroxene is made up both of clinopyroxene and orthopyroxene. It is only the orthopyroxene that is, in this case, optically continuous.
B235/18.

b. Poikilitic (mottled) anorthosite where the section has been cut through a large clinopyroxene oikocryst (mottled). Note the extreme euhedral nature and variable grain size of the cumulus plagioclase.
B232/22.

c. Cluster of cumulus orthopyroxene crystals which have small chadacrysts of plagioclase within them, are rimmed by a large, optically continuous, intercumulus clinopyroxene crystal. The optically continuous intercumulus clinopyroxene extends for 21 mm, forming a diffuse "mottle" within the leuconorite.
B235/10.

d. Cumulus orthopyroxene with optically continuous intercumulus branchings away from the core. The cumulus orthopyroxene is partially rimmed by intercumulus clinopyroxene. This texture would suggest that orthopyroxene was the first crystalline phase, and that plagioclase started to crystallize before orthopyroxene had ceased, forming a sub-ophitic texture.
B235/9.

PLATE 9 (continued)

e. In this poikilitic feldspathic pyroxenite there is a fairly high concentration of disseminated cumulus chromite, both as inclusion in the orthopyroxene and in the intercumulus plagioclase. The orthopyroxene crystals are generally subhedral, but where they are in contact with other orthopyroxenes, annealing has taken place. Note the way the orthopyroxene has grown around the chromite crystal, which is surrounded by intercumulus plagioclase. The intercumulus plagioclase is one large crystal, 1 cm in diameter, which poikilitically encloses all the other phases. Note also the numerous parallel clinopyroxene exsolution lamellae within the orthopyroxene.
B222/9.

f. In the granular feldspathic harzburgite above the UG 2, olivine occurs as both subhedral cumulus grains, and also as anhedral intercumulus crystals. Here the former are seen in association with cumulus orthopyroxene, and all these phases are enveloped by intercumulus plagioclase.
B222/13.

PLATE 9

a

b

c

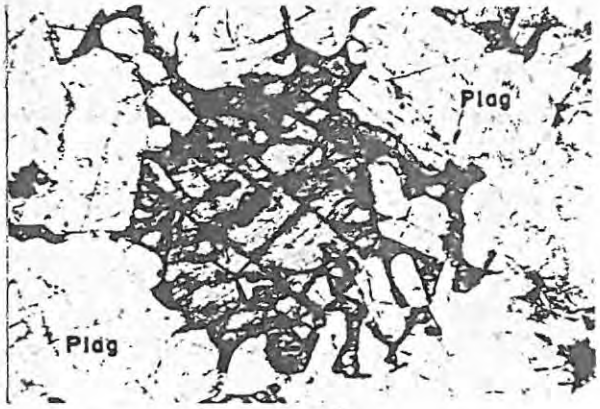

d

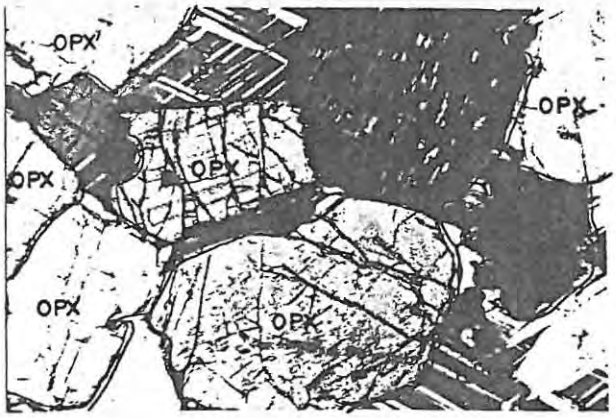

e

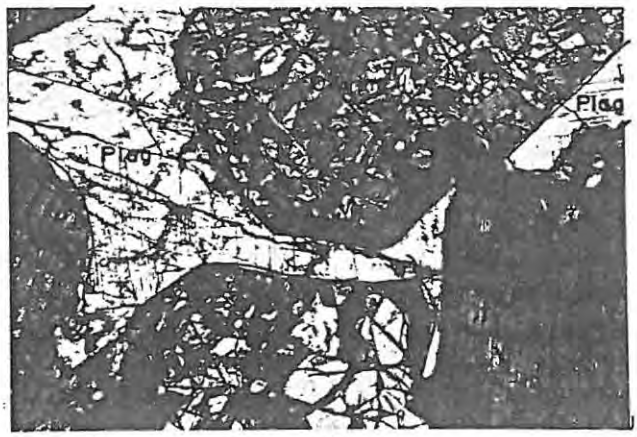

f

0 1 2 3 mm

diameter. The smaller grains are often poikilitically or partially enclosed in the cumulus orthopyroxene, and also form loose clusters around the orthopyroxene, giving the rock a sub-ophitic texture (Plate 9 c and d).

The cumulus orthopyroxene crystals are generally anhedral in form, with numerous embayments of smaller plagioclase laths (Plate 9 d). The orthopyroxene grains in the norites of the Bastard, Footwall and Basal units are smaller in size than those of the Merensky unit, the former being 1-1,8 mm and the latter 1,5-3 mm respectively. It would appear as if the orthopyroxene and the smaller grains of plagioclase started to crystallize simultaneously. At a later stage the smaller plagioclase grains crystallized more rapidly than the orthopyroxene because the subhedral plagioclase surrounding the cumulus orthopyroxene had intercumulus orthopyroxene interstitial to it. The intercumulus orthopyroxene is in optical continuity to the primary orthopyroxene (Plate 9 d). This texture has the effect of forming a diffuse zone of orthopyroxene, similar to that of a "mottle", around the cumulus core. In the Bastard and Merensky units, notably samples B235/1, 2 and 10, loose clusters of individual anhedral orthopyroxene and smaller plagioclase crystals are completely rimmed and in some cases enclosed by intercumulus clinopyroxene (Plate 9 c). In B235/10 (Plate 9 c) the intercumulus clinopyroxene forms a large diffuse "mottle" or oikocryst which is 2,1 cm in diameter and poikilitically encloses numerous subhedral orthopyroxene and small subhedral plagioclase crystals.

In stratigraphic comparable samples, B235/12 and B232/4, from the Merensky unit in both normal and pothole succession, (Figure 16), the orthopyroxene has two dominant habits. One forms stumpy prismatic crystals, between 2,5 and 3 mm, with small plagioclase inclusions,

and the other forms laths, generally 4-6 mm long and 1 mm wide. These laths are randomly orientated with their long axes within the plane of layering and make up approximately 40% of the orthopyroxene within this layer.

The norite footwall of the Bastard Reef, in pothole succession only (B232/11), has a very well-developed igneous lamination which is parallel to the regional layering. Tabular grains of plagioclase, 1-1,5 mm in diameter and 0,5-0,7 mm thick, lie in the plane of layering, while acicular laths of orthopyroxene, 2-3,5 mm long and 0,6 mm thick, are clearly randomly orientated, with their long axes in the plane of layering. This norite layer is rather similar to the 'needle norite' which is approximately 1000 ft. above the Merensky Reef, in a zone 100 ft. thick, from the Eastern Transvaal (Willemse, 1969). A section cut, parallel to the layering, shows individual subhedral laths of orthopyroxene in random orientation to each other, while the subhedral to anhedral plagioclase grains are generally rounded. Once again there are two plagioclase grain sizes, the smaller being from 0,4-0,6 mm, while the larger grains are between 1 and 2,5 mm. The smaller grains occur as loose clusters around the orthopyroxene laths and are sometimes poikilitically enclosed within these laths, while the larger anhedral crystals develop away from the cumulus orthopyroxene. Also evident is the occurrence of small, disseminated grains of base metal sulphides (0,5 mm), which are usually associated with the cumulus orthopyroxene. All the sulphide grains have a halo of alteration products which is invariably made up of a felted intergrowth of penninite, with its characteristic "berlin blue" interference colour.

Accessory minerals within the norites include clinopyroxene, biotite and base metal sulphides (See Figure 18). Intercumulus clinopyroxene occurs in four dominant forms,

namely:

a) as exsolution lamellae in the cumulus orthopyroxene,
b) as partial rimmings to the cumulus orthopyroxene and associated small plagioclase crystals,
c) as skeletal poikilitic crystals which enclose both the cumulus orthopyroxene and small plagioclase, and lastly,
d) as a discrete anhedral intercumulus phase.

Biotite usually occurs as very small intercumulus grains associated with the cumulus orthopyroxene, and only accounts for approximately 0,5% of the norites. The base metal sulphides are seen only in the Bastard, Merensky and Footwall units, with a greater concentration in the Merensky unit and towards the base of each of the units. These sulphides are predominantly made up of pyrrhotite and chalcopyrite, between 0,2-0,5 mm, and occur as interstitial intergrowths between the dominant silicate phases, without any noticable preferred bias to any one silicate.

During crystallization of the norites there was a certain degree of two-way diffusion between the intercumulus liquid and the overlying magma, which has resulted in limited adcumulus growth of the plagioclase and orthopyroxene primocrysts. It follows therefore that all the norites are mesocumulates.

7.5 Pyroxenites

According to the IUGS classification of the igneous rocks (Streckeisen, 1976, Figure 4), a pyroxenite must have more than 90% pyroxene and less than 10% plagioclase. As can be seen in Figure 18, the estimated modal percentage of plagioclase in all the pyroxenites is from 0-5 percent

higher than the 10% classification limit. Wagner (1929), described the pyroxenites as 'pseudo-porphyritic pyroxenitic diallage norites'. Van Zyl (1970) in his examination, noted the poikilitic nature of the clinopyroxene in places, but termed these rocks porphyritic melanorites and bronzitites. On closer examination, the large, irregularly spaced, clinopyroxene "phenocrysts" were found to enclose poikilitically numerous primary euhedral orthopyroxene oikocrysts. Because the crystallization habit of the plagioclase in these rocks is no different from that in the norites and anorthosites (being intercumulus as opposed to cumulus), and because there is only a marginally higher amount of plagioclase present, the name poikilitic feldspathic pyroxenite is retained in this study (IUGS, Plagioclase-bearing orthopyroxenite).

The feldspathic pyroxenites throughout the study section in both the normal and potholed succession are represented in four units (Figure 16), namely:

Bastard unit - B235/5, 6, B232/12, 13 and 14.
Merensky unit - B235/13, 14, B232/2, B222/24 and 25.
UG 2 unit - B235/28, 29, 30, B222/14, 15, 16, 17 and 18.
UG 1 unit - B235/32, 33, 34, 35, 36, 37, B222/3, 4, 5, 6, 7, 8, 9, 10 and 11.

The cumulus orthopyroxene crystals throughout the study section generally have two distinctive habits of crystallization:

a) Stumpy medium-grained (1-4mm) prismatic crystals which are subhedral to euhedral in form, are the more common type;

b) lath-like medium-grained crystals are also evident. These laths are usually 2-6 mm long and no wider than 1 mm.

In all cases, both crystalline habits of the orthopyroxenes display fine exsolution lamellae which are parallel to 100 and composed of diopsidic clinopyroxene. The lamellae are between 0,001 and 0,002 mm thick and are generally spaced 0,005 to 0,01 mm apart. In many instances these lamellae are poorly developed towards the margins of the orthopyroxene crystals. The tips of the narrowing lamellae extend to the crystal faces. Jackson (1961) suggested that this is a primary border effect caused by the local reduction of unit volume from which Ca^{2+} can migrate during the exsolution.

The presence of these lamellae is indicative of the fact that the orthopyroxene crystals have undergone a certain amount of sub-solidus re-equilibration. Hess (1960) has noted that orthopyroxenes of the Bushveld type, with their characteristic exsolution lamellae, appear to be identical in bulk composition to those without exsolution lamellae found in most volcanic and hypabyssal rocks.

Evidence of post-depositional deformation is exhibited by bent clinopyroxene exsolution lamellae, which give the individual orthopyroxene crystals a strained extinction effect (B235/5, 28, B222/4 and 18). An unusual feature of this effect is that only a limited number of crystals in the same sample display this distortion.

Lath-like orthopyroxene crystals would appear to be more common in those pyroxenites which underlie pegmatoidal rock types, e.g. B235/28 and 33 from the normal succession, and B222/10 and 18 from the potholed succession. In common with this feature, there also appears to be an upward increase in the concentration of the clinopyroxene

oikocrysts in the UG 2 unit. Genetically, these two petrographic features in the pyroxenites may be related in some way. It would also appear as if a certain amount of resorbtion of an earlier lath-type of orthopyroxene has occurred. Relict crystals of an earlier orthopyroxene phase, which are in optical continuity, are separated from each other and are poikilitically enclosed in both subhedral lath orthopyroxenes and prismatic orthopyroxenes (B235/28).

Clinopyroxene in these orthopyroxenites occurs in four basic forms, namely:

a) as fine exsolution lamellae between 0,001 and 0,002 mm within the subhedral and euhedral orthopyroxene crystals. In places these lamellae do widen and form irregular clinopyroxene exsolution blebs within the orthopyroxene.

b) as intercumulus grains which often form partial rimmings to the cumulus orthopyroxene crystals.

c) as large (0,5-1,5 cm) anhedral oikocrysts which poikilitically enclose orthopyroxene. These oikocrysts are randomly distributed throughout the pyroxenites at intervals of between 10 and 20 cm. Because these oikocrysts are so widely spaced within the pyroxenites, it is rather difficult to estimate their bulk modal percentage in the rock. Nevertheless it is evident from underground exposures that there is a gradual increase in concentration of the clinopyroxene oikocrysts towards the top of the UG 2 unit. Those thin sections with clinopyroxene oikocrysts are B222/6, 7, 10, 12 and 14.

d) Lastly, clinopyroxene occurs more rarely as subhedral cumulus grains within the orthopyroxenite (B222/15).

The plagioclase in these pyroxenites is interstitial to the chromite, ortho- and clinopyroxene, and forms large (1-1,5 cm) anhedral grains. These large plagioclase crystals in effect poikilitically enclose all the other cumulus oxide and silicate phases. In the majority of cases the plagioclase shows strong zoning (B235/28). It would appear as if this type of plagioclase was the last crystallization phase of the poikilitic feldspathic pyroxenites. Another less common form of the plagioclase occurs as small subhedral rounded inclusions which are poikilitically enclosed in the larger cumulus orthopyroxenes.

Those pyroxenites which are in close proximity to chromitite concentrations i.e. the UG 1, UG 2 and smaller chromitite layers and disseminations, generally have a much higher concentration of disseminated cumulus chromite throughout, e.g. 12% in B222/3. Once again, two crystallization habits of the orthopyroxenes occur. Smaller euhedral prismatic crystals (0,8-1,2 mm) and larger lath-like crystals (2-2,5 mm) occur and the lath crystals appear to be loosely clustered together. It is in these larger orthopyroxene crystals that one finds the cumulus chromite (<0,1-0,35 mm) being poikilitically enclosed.

The disseminated chromite is also often poikilitically enclosed in the intercumulus plagioclase (Plate 9 e), and more rarely in the clinopyroxene. When the chromite is poikilitically enclosed within the orthopyroxene it often has a thin rim or halo of biotite (B235/30), clinopyroxene (B235/29) or plagioclase (B235/29) around individual grains, but not all the chromites display this phenomenon. More commonly, when the disseminated cumulus chromite is hosted by the intercumulus plagioclase, embayments into the cumulus orthopyroxene are observed (B235/29, 34, 37, B222/3 and 9). Here the chromite grains are rimmed by a thin halo of intercumulus plagioclase and both the

chromite and plagioclase indent in the subhedral orthopyroxene grains (Plate 9 e). The paragenetic sequence in this type of texture would suggest that chromite and orthopyroxene started to crystallize at about the same time. Plagioclase preferentially nucleated on the margins of the chromite crystals and acted as a buffer to the growth of the larger orthopyroxenes. In some instances the chromite crystal, with its halo of plagioclase, is poikilitically enclosed in the orthopyroxene (B235/29), but the more common form is only a partial embayment.

Henderson (1975) has reported a similar texture from the Rhum intrusion, but more commonly the rounded spinel crystals are situated in the embayments of olivine. He reported that these spinels are more aluminous than the smaller spinels outside the orthopyroxene or olivines. Henderson (1975) has also noted that as the proportion of mesostasis rises (i.e. plagioclase), the crystals tend to be larger and to be richer in Fe and poorer in Al. Large anhedral chrome-spinel crystals between the cumulus silicates are Al rich and often show a reaction relationship with the cumulus olivine, in that the crystal form of the olivine is corroded and embayed adjacent to the chromite.

Base metal sulphides, predominantly pyrrhotite, pentlandite and chalcopyrite, are quite common in the vicinity of mineralised layers, e.g. Bastard Reef (B235/6 and B235/12), Merensky pyroxenite (B235/14, B222/24 and B232/2) and the footwall of the Pseudo Reef (B235/28 and B222/18). Extremely small base metal sulphide grains are sporadically found in the orthopyroxenites throughout the study section (e.g. B222/14).

Biotite occurs as an intercumulus accessory mineral in all the feldspathic pyroxenite and rarely exceeds

3 percent of the rock.

Although the majority of the feldspathic pyroxenites throughout the study section are medium-grained, coarse-grained pegmatoidal types do also occur. In some instances the upper 20-30 cm of the coarse pegmatoidal Merensky Reef contains very little or no olivine and is therefore, in reality, a pegmatoidal feldspathic pyroxenite (not sampled in this study). More commonly the footwall of the UG 2 chromitite is a pegmatoidal feldspathic pyroxenite which is well illustrated in Plate 4 d (B235/32 and B222/11). Here the subhedral orthopyroxene grains are between 1 and 1,5 cm in diameter and poikilitically enclose both cumulus chromite and small anhedral, almost tricuspate, plagioclase grains, which are all in optical continuity with each other. This could possibly suggest that the plagioclase was interstitial to some earlier cumulus phase (olivine?) which has been replaced by the larger orthopyroxenes. Sample B222/11 is a bit more unusual because, apart from the normal suite of minerals, hornblende and quartz are also present. The hornblend is late magmatic and has formed at the expense of the pyroxene, while the quartz is interstitial to the other minerals and occurs as late-stage infilling. The biotite from this locality is anomalously very dark red (fox red) to pale brown, which indicates a higher TiO_2 content.

Alteration of the poikilitic feldspathic pyroxenites is not very common, but where present, the intercumulus plagioclase has only discrete spots of saussuritization present and the orthopyroxene is altered to a felted intergrowth of antigorite and chlorite. This type of alteration appears to be confined to zones of minor shears and fractures, e.g. B222/12.

The poikilitic feldspathic pyroxenite layers could be described as typical heteradcumulates. The large

intercumulus oikocrysts are both the ubiquitous plagioclase and the scattered clinopyroxene oikocrysts.

7.6 Harzburgites

The harzburgites represented in the study section include the following samples, from the base upward:

a) the hanging wall of the UG 2 (B235/31 and B222/13),
b) lower pegmatoidal Pseudo Reef (B235/27 and B222/13),
c) upper Pseudo Reef (B235/25, 26 and B222/20, 21),
d) the Pseudo Marker layer in a normal succession (B235/24),
e) Lens Reef (B222/22),
f) Pothole Reef (B232/1) and
g) the Merensky Reef in normal succession (B235/15, 15a, and 16).

In all cases there is a certain amount of intercumulus plagioclase and these rocks should, by the IUGS classification (Figure 5), be termed plagioclase-bearing harzburgites, but a less cumbersome term, feldspathic harzburgite, is used throughout this discussion.

There are macroscopically three distinct varieties of this rock type, namely:

a) Pegmatoidal feldspathic harzburgite which is represented by samples B235/15, 15a, 16 (normal Merensky Reef), B235/24 (Pseudo Marker layer), B222/22 (Lens Reef), B232/1 (Pothole Reef), B235/27 and B222/19 (Lower Pseudo Reef unit).

b) Coarse-grained feldspathic harzburgite of the Upper Pseudo Reef unit ("Tarentaal"), represented by samples B235/25, 26, B222/20 and 21.

c) Medium-grained feldspathic harzburgite forming the hanging wall of the UG 2 chromitite, which is represented by samples B235/31 and B222/13.

Both feldspathic harzburgite types, a) and b) above, have a poikilitic texture, while type c) is subhedral and equigranular. These two basic textural types were also recognised by Jackson (1961) in the Stillwater harzburgites. The equigranular harzburgite above the UG 2 (B235/31 and B222/13) is composed essentially of prismatic subhedral orthopyroxene crystals (≈55%), with a grain size of between 1 and 3 mm. These orthopyroxene crystals in many cases poikilitically enclose small 0,1-0,2 mm euhedral grains of cumulus chromite. Once again the orthopyroxene characteristically has clinopyroxene exsolution lamellae parallel to 100. Clinopyroxene also forms as intercumulus material and as large oikocrysts, 0,8 to 1,5 cm in diameter, scattered throughout the layer. These oikocrysts poikilitically enclose both orthopyroxene and olivine. In some cases the clinopyroxene appears to have resorbed the subhedral orthopyroxene, because isolated relicts of orthopyroxene within the clinopyroxene are in optical continuity with adjacent subhedral orthopyroxene.

The olivine is normally in excess of 40%, but may make up as little as 35% of the rock, when it is more correctly to be termed a feldspathoidal olivine pyroxenite. In most cases the olivine is anhedral and commonly interstitial to the cumulus orthopyroxene, and in many cases exhibits embayments into the orthopyroxene. Isolated cases of relict chadacrysts of orthopyroxene are found in the olivine. These relicts of orthopyroxene are in optical continuity with adjacent cumulus orthopyroxene.

It appears that the olivine has partially resorbed and replaced the orthopyroxene. This texture is not uncommon. Schwellnus (1956) noted forsteritic olivine characteristically interstitial to orthopyroxene in the

peridotite layers, a few hundred feet below the Main Chromitite seam in the Eastern Bushveld Complex. He ascribed the texture to replacement of pyroxenite by dunitic magma. Willemse (1969) suggested that pressure had an effect on the relative sequence of formation of olivine and pyroxene only at comparatively low pressure.

Alteration of the olivine is not as severe as in the other harzburgite layers, with only about 15% of the olivine being serpentinised in both samples. The common alteration products are serpentine, talc, fine magnetitic stringers, iddingsite and bowlingite. Expansion cracks, which radiate outward from the partially serpentinised olivine, are well-developed in the large, intercumulus plagioclase crystals of B222/13.

Plagioclase, as in the feldspathic pyroxenites, is interstitial to both the orthopyroxene and olivine, and forms large, 1-1,5 cm intercumulus crystals which are especially well-developed in B222/13. Plagioclase makes up 8% of this sample. The sample B235/31, from the normal succession, is rather anomalous in that the thin section cut is devoid of plagioclase, while in hand specimen intercumulus plagioclase is evident. Intercumulus biotite forms a common accessory mineral in B235/31, making up approximately 4% of the rock, while B222/13 has only trace amounts of intercumulus biotite. The biotite is characteristically pleochroic, from pale yellow to tan. Disseminated euhedral cumulus chromite is found in both samples and is enclosed predominantly in the orthopyroxene crystals, and more rarely in the olivine. These chromite grains are small and vary in diameter from 0,1-0,3 mm.

The upper Pseudo Reef, commonly referred to as the "Tarentaal" or "Guineafowl", is represented by samples B235/25 and 26 in the normal succession and B222/20 and 21 in the Lens succession (Figure 16). This unit is

characteristically made up of altered olivine (62%), orthopyroxene (26%) and plagioclase (11%), with accessory biotite (0,7%) and clinopyroxene (0,2%) and minor chromite.

The orthopyroxene occurs as large, 3 cm diameter oikocrysts which poikilitically enclose subhedral rounded grains of primary olivine between 1 and 4 mm in size. The large spheroidal poikilitic crystals are evenly spaced at about 10 cm intervals throughout the layer. Once again the orthopyroxene has the ubiquitous parallel clinopyroxene exsolution lamellae, and numerous expansion cracks radiate outwards from the olivine chadacrysts, which have been partially serpentinised.

The olivine, as mentioned above, occurs as chadacrysts in the larger orthopyroxene crystals, and also as rounded anhedral cumulus crystals between 2,5 and 4 mm in diameter throughout the rock unit. These latter olivines are almost completely serpentinised (90%), while the olivines within the intercumulus plagioclase and orthopyroxene oikocrysts are only partially serpentinised (20%). Once again the alteration products of the olivine are serpentine, talc, magnetite stringers, bowlingite and iddingsite, and only subhedral pseudomorphs after olivine remain.

Isolated relict rounded kernels of original olivine remain in these serpentine pseudomorphs. Generally the orthopyroxene in all the rock types throughout the study section shows a much greater resistance to alteration and serpentinisation, but where alteration of the bronzite crystals has occurred, the alteration product is invariably antigorite. It would thus appear as if the orthopyroxene and the intercumulus plagioclase have armoured the enclosed olivines against severe serpentinisation. Hess (1960) believes that the original serpentinisation of the Stillwater rocks took place during the cooling of this complex, and the same could quite well apply to the Bushveld rocks.

Irvine (1981, pers. comm.) has noticed that the cumulus olivine grains between the large orthopyroxene oikocrysts have a definite preferred long axis alignment, which is at right angles to the layering. This is almost identical to the vertical alignment of the olivine grains in some of the Muskox dunite and peridotite layers (Irvine, 1980, p.360). This vertical fabric appears to be confined to the more compacted parts of the Muskox layered series and Irvine (op.cit.) suggests therefore, that this alignment was caused by the flow of the intercumulus liquid as it was expelled from the compacting layers. The postulate might be that the flow was sufficient to lift the cumulus grains, perhaps to a depth of a meter or so below the surface of accumulation and to jostle them enough to rotate them into parallel orientation.

The plagioclase is, in all cases, intercumulus to the olivine, and shows varying degrees of saussuritization; it takes on a milky pale green colour in hand specimen. Intercumulus biotite usually occurs at the grain boundaries between the orthopyroxene and olivine, but in B235/26 the biotite is associated with serpentine and magnetite stringers. Here the biotite is strongly distorted and has numerous magnetite stringers thorughout which lie parallel to the distorted basal biotite cleavage. Euhedral cumulus chromite, between 0,1 and 0,2 mm, is found disseminated throughout the unit and is poikilitically enclosed in all the dominant silicate phases; it constitutes approximately 1% of the total rock unit.

The remaining feldspathic harzburgites are all coarse-grained pegmatoidal types and include:

a) lower Pseudo Reef (B235/27 and B222/19)
b) basal portion of the Pseudo Marker layer (B235/24)
c) Lens Reef (B222/22)
d) Pothole Reef (B232/1)
e) Merensky Reef (B234/15, 15a and 16).

These rock units are all essentially the same with regard to their grain size, silicate mineralogy and their mutual relationships, but because they are so coarse-grained, it is rather difficult to study them in a single thin section. Nevertheless, a reasonable understanding is achieved if one considers all the thin sections representing the various samples of these rocks. Apart from their grain size differences, they are very much akin to the upper Pseudo Reef (Tarentaal) unit with regard to their textures and mineralogy.

In all the above pegmatoidal feldspathic harzburgites large anhedral orthopyroxene oikocrysts, between 3 and 4 cm in size, poikilitically enclose anhedral grains of olivine, clinopyroxene and cumulus euhedral chromite. Once again the orthopyroxene has shielded the enclosed olivine crystals from severe serpentinisation.

The olivine grains are generally anhedral and sometimes have an almost amoeboid appearance, being intercumulus to the orthopyroxene. An unusual phenomenon in the intercumulus plagioclase is the presence of small (0,4 mm) enclosed tabular grains of orthopyroxene, which are all in optical continuity with each other (B222/19). These small chadacrysts appear to be optically related to larger orthopyroxene grains which rim the anhedral olivine on the edges of the intercumulus plagioclase. Partial resorption of once-larger orthopyroxene, and subsequent nucleation of plagioclase, may be postulated to explain this type of texture. Another feature of interest in the intercumulus plagioclase is the presence of acicular biotite needles, only 0,01 mm in thickness, and ranging from 0,15 to 1,9 mm in length. These biotite crystals are, in most cases, related to adjoining orthopyroxene and olivine grains, and penetrate the latter minerals for short distances. Where these biotite needles are at right angles to the plagioclase twinning, the regularity of the twinning is disrupted

across the biotite (B232/1).

The extent and nature of secondary alteration is quite varied; it is not uncommon to find completely saussuritised intercumulus plagioclase and fresh plagioclase in the same thin section. The intercumulus plagioclase in the partially serpentinised feldspathic harzburgites is fresh, as a rule, but in highly serpentinised harzburgites, the plagioclase, which is saussuritised, takes on a light-green colour in hand specimens. Alteration is clearly related to fractures, which provide channelways for the infiltration of alteration fluids. Secondary mineral assemblages are dependent on the nature of the co-existing mafic minerals, and include penninite, chlorite, tremolite, serpentine and talc.

Figure 18

ESTIMATED MODAL PERCENTAGE OF THE MAIN MINERAL PHASES

8. MINERALOGY

8.1 Introduction

The silicate mineralogy of the upper Critical zone consists essentially of four primary minerals: olivine, orthopyroxene, clinopyroxene and calcic plagioclase. The only abundant secondary minerals are serpentine and biotite. The former is limited to the olivine-bearing rock types, and the latter is closely related to the feldspathic harzburgites. High concentrations and disseminations of chromian spinels are also found throughout the study section.

Representative electron microprobe analyses of the four main silicate phases of the Merensky Unit are presented in this chapter. Samples that were used for these analyses are B235/7-16 (including 15a). Further microprobe analyses for olivine, pyroxene and plagioclase were done on those samples which contain olivine as a cumulus phase. These samples were represented by the feldspathic harzburgite above the UG 2 (B235/31), the Pseudo Reef (B235/25 and 26), Pothole Marker layer (B235/24), Lens Reef (B222/22) and Pothole Reef (B232/1). The latter three samples are on the same stratigraphic level but represent lateral variations in the hanging wall (Figure 19). Although a study of the chromite in the upper Critical zone was not undertaken, a number of analyses of chromite were done by the author from the same study section. These results are also presented.

8.2 Olivine

The olivine group of minerals has orthorhombic symmetry and a structure which consists of independent

Figure 19

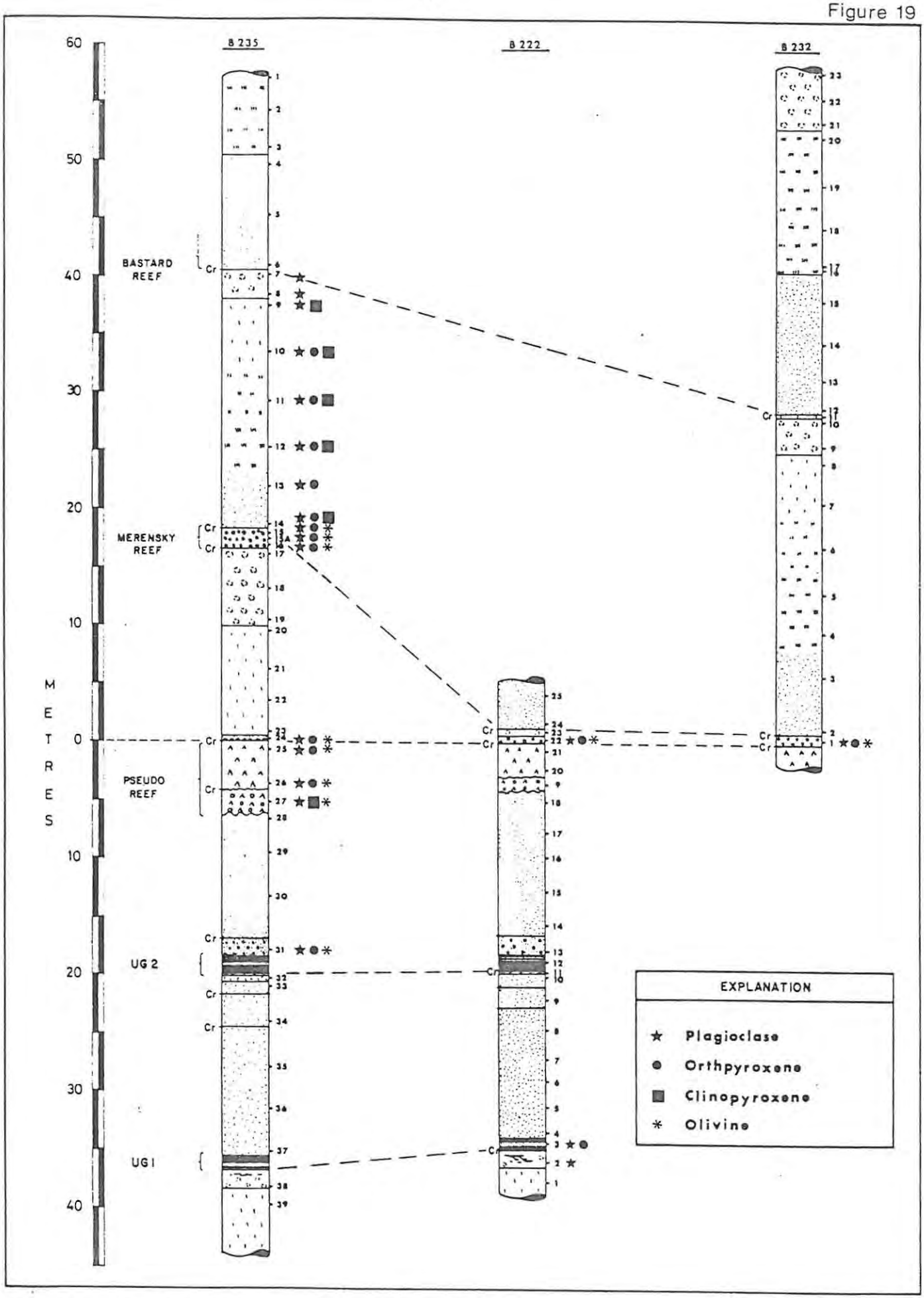

Figure 19: Diagram showing the positions of samples used for the electron microprobe mineral analyses, and the minerals that were analysed.

SiO_4 tetrahedra linked by divalent cations in six-fold coordination. There are two nonequivalent six-fold coordinated sites in the olivine structure: M_1 and M_2. The two most important cations in the M sites are Fe and Mg, and these elements approach random distribution between M_1 and M_2 (Birle et al., 1968). The almost complete disordering of Fe and Mg between M_1 and M_2 sites is explained by Burns (1970b) in terms of Crystal Field Theory.

The common ferromagnesian olivines form a solid solution series between forsterite (Mg_2SiO_4) and fayalite (Fe_2SiO_4). Within this basic framework, there is minor substitution by Ni, Cr, Mn and Ca for Fe and Mg. The partitioning of Ni into olivine, in particular, has received considerable attention over the past few years (Sato, 1977; Hart and Davis, 1978; Leeman and Lindstrom, 1978), and there is a wealth of information available on estimated olivine/liquid distribution coefficients, these ranging between 4,8 and 34 (Leeman and Lindstrom, op.cit.).

In Figure 20 the molecular percent Fo is plotted against stratigraphic height. The range in Fo content for the normal succession is $Fo_{76,7}$ to $Fo_{81,6}$, and there appears to be no zonation of the olivines between the margins and cores of the analysed crystals. A notable feature of the olivine mineralogy from the UG 2 hanging wall (B235/31) to the Pseudo Marker layer (B235/24) is the upward increase of the Mg component from $Fo_{76,7}$ to $Fo_{81,6}$, in extreme samples (range of $Fo_{4,9}$). A different pattern of olivine composition in a pothole succession is suggested by the lower Fo content for both the Lens and Pothole Reefs (B232/1 and B222/22).

The Merensky Reef has a uniform olivine composition of $Fo_{78,6}$ to $Fo_{79,5}$, a range of $Fo_{0,9}$. Again, there is a suggestion of a reversed fractionation trend within

Figure 20

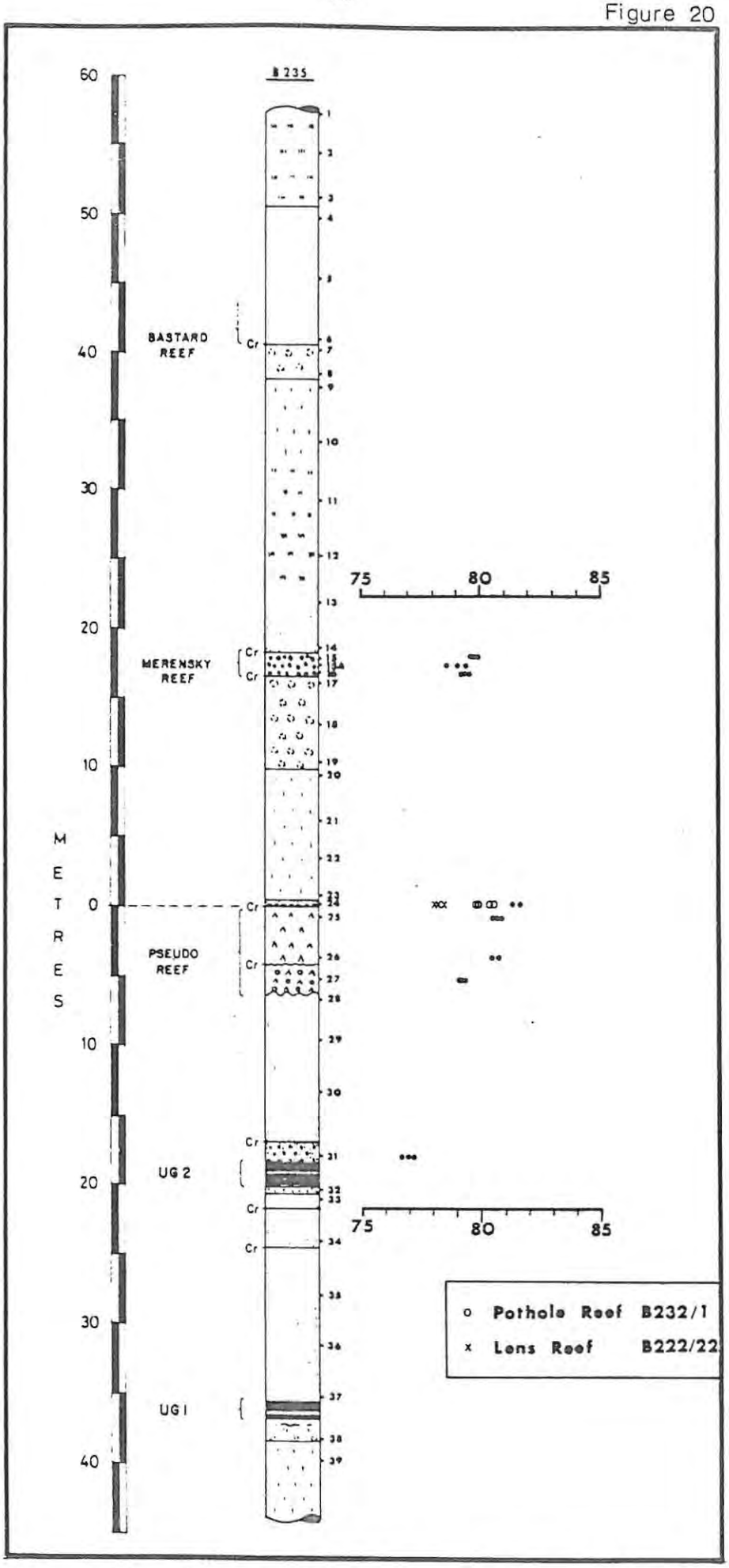

Figure 20: Plot of Molecular % Fo for olivines against stratigraphic height in normal, pothole B232/1 and lens B222/22 successions.

the Reef, with Mg being higher at the top contact of the Merensky Reef. Olivine appears for the last time in the lower part of the Bushveld Complex in the Merensky Reef, and then it once again reappears in the upper zone with a much lower Fo content.

The lateral compositional variation of the olivines in a particular layer is illustrated by the analyses of samples of the Peudo Marker (B235/24), Lens Reef (B222/22) and the Pothole Reef (B232/1). The Pseudo Marker layer (B235/24), from a normal succession, has a compositional range of $Fo_{81,3-81,6}$. The Lens Reef (B222/22), which was sampled some 1500 m to the north-east of the normal succession, has a compositional range of $Fo_{78,1-78,5}$, while the Pothole Reef (B232/1), which was sampled 53 m to the east of the Lens succession, has a composition of $Fo_{79,7-80,6}$.

As this layer undergoes a process of reconstitution and recrystallization, from the Pseudo Marker to the Pothole Merensky reef, it could be expected that a lateral variation in the bulk chemistry of the layer would exist. There does appear to be a slight iron enrichment from the normal to pothole succession. The Lens Reef (B222/22) has a much higher iron content of $Fo_{78,1-78,5}$, which may be due to small-scale local lateral variations.

In Figure 21, Ni contents in ppm are plotted against weight percent MgO for all the olivine occurrences in the upper Critical zone. For comparison, a variety of Karoo data are included in this diagram (Mitchell, 1980). The upper Critical zone olivines and those of the Elephants Head Dyke fall at the high Mg, high Ni end of the trend in Figure 21. The cumulus nature of the Elephants Head olivines, and their effect on MgO content of the host rock, are discussed by Eales and Marsh (1979). The trend in Figure 21, for the Karoo data as pointed

out by Mitchell (1980), is hyperbolic, with Ni content of the olivines decreasing rapidly from the Elephants Head to the low-Ni olivines in the Drumbo Basalt Member. This type of relationship reflects a high distribution coefficient for Ni, and consequently a lower Ni content for olivines from more evolved rocks (Mitchell, 1980).

The field for the Bushveld olivines in Figure 21 and 21a suggests that they are Ni-enriched, relative to those of the Karoo Province, and that their trend does not conform to that of the Karoo rocks, but is more linear (vertical). The MgO content of the olivines is restricted and has values of between 40 and 43 weight percent, while the Ni content is far more variable (between 2500 and 4100 ppm). With regard to the magma from which these olivines crystallized, these high Ni values could reflect one of two things, namely:

a) that the magma was Ni-rich, or
b) the olivine crystallized from a very large volume of magma, and this small amount of olivine therefore had very little influence on the total Ni content.

The olivine from the normal, pothole and lens Merensky Reefs is enriched in Ni, compared to that from the Pseudo Marker, Pseudo Reef and the hanging wall of the UG 2 (Figure 21a). The latter rocks are all relatively sulphide-poor, compared to the Merensky Reef. This observation is in marked contrast to the pattern one would expect to see, where Ni would preferentially be partitioned into the sulphides, hence the olivines in these sulphide-rich rocks would be Ni-depleted.

Possible explanations for this anomaly are as follows:

a) That olivine was the first phase to crystallise

Figure 21

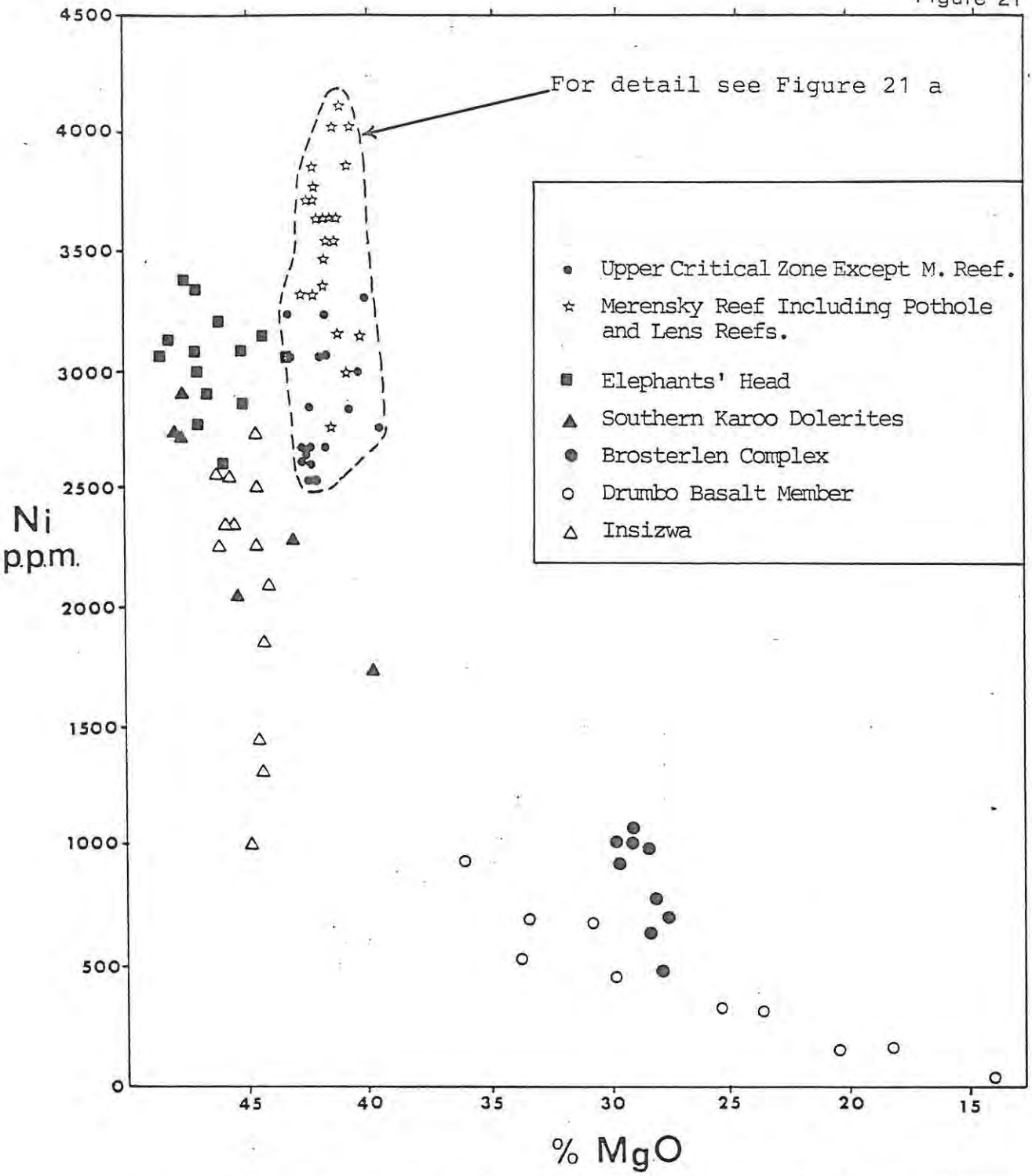

Figure 21: Plot of Ni (ppm) vs. weight % MgO for olivines from the Karoo igneous province and the field for the upper Critical zone.

Sources of information: H.V. Eales (Elephant's Head, Insizwa); J.S. Marsh (Southern Karoo Dolerites); A.A. Mitchell (Brosterlen, Drumbo) and the present study.

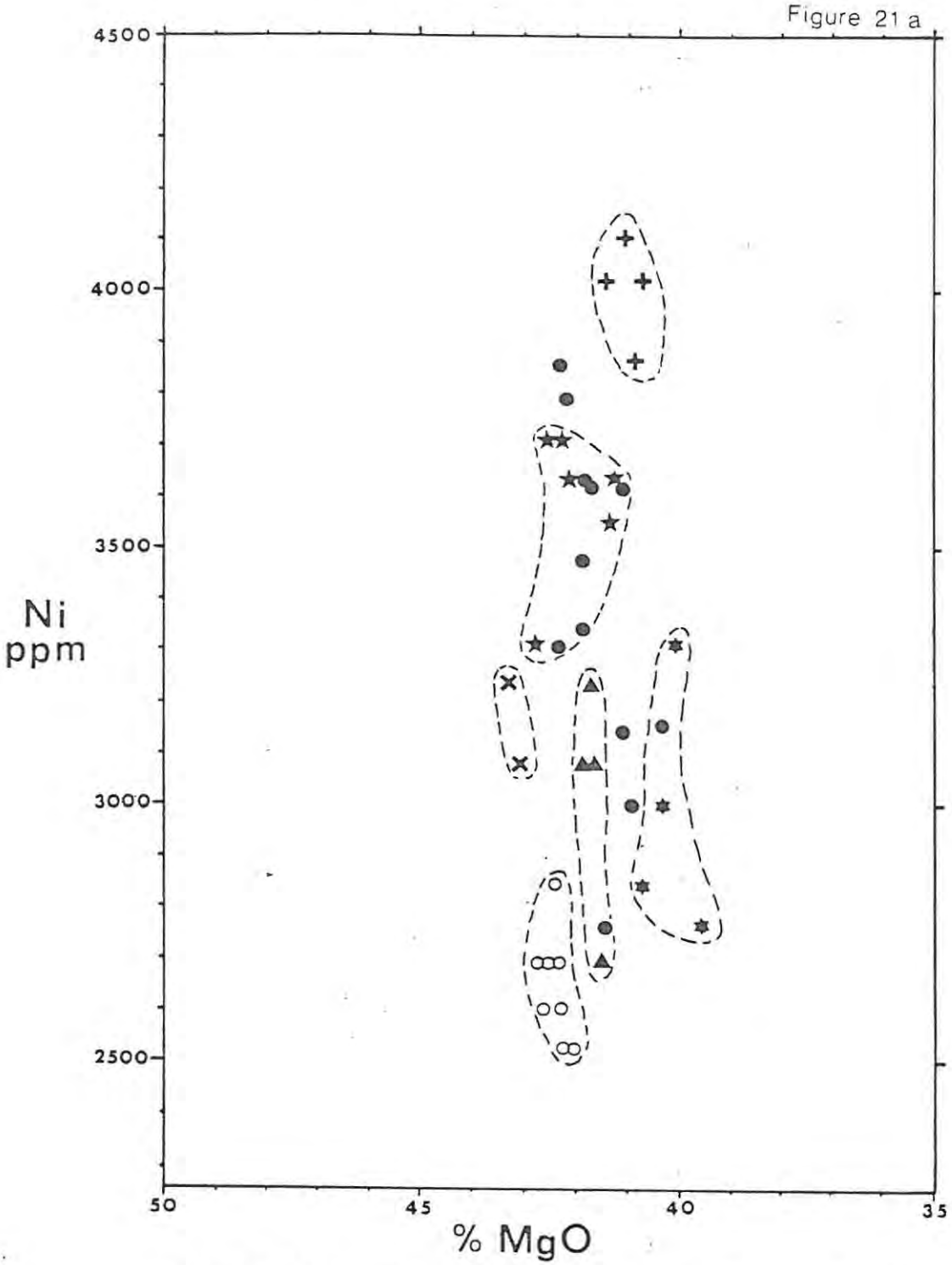

Figure 21 a: Detail of the upper Critical zone olivine plot of Ni (ppm) vs. weight % MgO.

● Normal Merensky Reef (B235/15, 15A, 16)
✚ Lens Merensky Reef (B222/22)
★ Pothole Merensky Reef (B232/1)
✕ Pseudo Marker Layer (B235/24
▲ Lower Pseudo Reef (B235/27)
o Upper Pseudo Reef (B235/25, 26)
✱ UG 2 Hangingwall (B235/31)

TABLE 1: OLIVINE ANALYSES BY MICROPROBE

	B232/1 REMNANT	B232/1 REMNANT	B232/1(1) MARGIN	B232/1(1) CORE	B232/1(1) MARGIN	B232/1(1) CORE	B222/22 REMNANT	B222/22 REMNANT	B222/22 REMNANT	B222/22 REMNANT	B235/24 MARGIN	B235/24 CORE	B235/25(1) MARGIN	B235/25(1) CORE	B235/25(1) MARGIN	B235/25(1) CORE	B235/26 MARGIN	B235/26 CORE	B235/26 CORE	B235/26 CORE
SiO_2	39,30	39,11	39,17	39,25	39,27	39,37	38,95	39,03	39,00	38,94	39,59	39,99	33,93	39,44	39,26	39,47	39,59	39,42	39,57	39,53
FeO	17,57	17,47	18,52	18,60	17,97	18,73	19,73	19,75	19,83	19,70	17,06	17,27	17,78	18,06	17,77	17,84	17,81	17,91	17,66	17,89
MgO	41,37	41,26	42,08	42,51	42,77	42,33	41,08	40,85	40,74	41,47	43,29	43,14	42,74	42,52	42,47	42,57	42,05	42,25	42,65	42,27
NiO	0,45	0,46	0,46	0,47	0,42	0,47	0,52	0,49	0,51	0,51	0,41	0,39	0,34	0,34	0,36	0,34	0,32	0,32	0,33	0,33
TOTAL	98,69	98,30	100,23	100,82	100,43	100,89	100,28	100,12	100,08	100,62	100,35	100,79	100,19	100,35	99,86	100,22	99,77	99,90	100,21	100,02
Molecular %																				
Fo	80,38	80,41	79,82	79,90	80,58	79,72	78,35	78,26	78,13	78,54	81,55	81,33	80,79	80,47	80,68	80,68	80,53	80,51	80,74	80,53
Fa	19,15	19,10	19,71	19,61	19,00	19,80	21,11	21,23	21,34	20,94	18,03	18,27	18,86	19,18	18,95	18,97	19,14	19,16	18,92	19,13
Ni-oliv	0,47	0,49	0,47	0,49	0,42	0,48	0,54	0,51	0,53	0,52	0,42	0,40	0,35	0,35	0,37	0,35	0,33	0,33	0,34	0,34
TOTAL	100,00	100,00	100,00	100,00	100,00	100,00	100,00	100,00	100,00	100,00	100,00	100,00	100,00	100,00	100,00	100,00	100,00	100,00	100,00	100,00
Ni ppm	3550	3629	3629	3708	3314	3708	4103	3866	4024	4024	3235	3077	2683	2683	2840	2683	2525	2525	2604	2604

	B235/27 MARGIN	B235/27 CORE	B235/27 MARGIN	B235/27 CORE	B235/31 CORE	B235/31 MARGIN	B235/31 CORE	B235/31 MARGIN	B235/15 MARGIN	B235/15 CORE	B235/15 MARGIN	B235/15 CORE	B235/15A REMNANT	B235/15A MARGIN	B235/15A CORE	B235/15A MARGIN	B235/15A CORE	B235/16 MARGIN	B235/16 CORE	B235/16 CORE
SiO_2	39,17	39,22	39,18	39,32	38,60	38,65	38,86	38,47	39,50	39,34	39,40	39,36	39,48	39,49	39,25	39,32	38,85	39,23	39,36	39,13
FeO	19,29	19,14	19,08	19,31	21,08	21,11	20,87	20,97	18,83	18,62	18,67	18,59	18,84	19,20	18,91	18,77	18,94	18,65	18,97	18,84
MgO	41,74	41,67	41,70	41,80	39,57	40,75	40,31	40,08	42,22	41,90	42,29	42,27	40,88	40,37	41,88	41,42	41,12	41,35	41.73	41.93
NiO	0,41	0,34	0,39	0,39	0,35	0,36	0,38	0,42	0,48	0,46	0,42	0,49	0,38	0,40	0,42	0,35	0,42	0,46	0,46	0,44
TOTAL	100,60	100,36	100,35	100,82	99,60	100,87	100,42	99,94	101,02	100,32	100,78	100,71	99,58	99,46	100,46	99,86	99,33	99,69	100,52	100,34
Molecular %																				
Fo	79,07	79,23	79,25	79,10	76,70	77,19	77,18	76,96	79,59	79,66	79,80	79,81	79,14	78,60	79,44	79,44	79,11	79,42	79,30	79,50
Fa	20,51	20,42	20,35	20,50	22,93	22,44	22,43	22,60	19,92	19,87	19,77	19,69	20,46	20,98	20,13	20,20	20,45	20,10	20,23	20,05
Ni-oliv	0,42	0,35	0,40	0,40	0,37	0,37	0,39	0,44	0,49	0,47	0,43	0,50	0,40	0,42	0,43	0,36	0,44	0,48	0,47	0,45
TOTAL	100,00	100,00	100,00	100,00	100,00	100,00	100,00	100,00	100,00	100,00	100,00	100,00	100,00	100,00	100,00	100,00	100,00	100,00	100,00	100,00
Ni ppm	3235	2683	3077	3077	2762	2840	2998	3314	3787	3629	3314	3866	2998	3156	31,44	2762	33,14	3623	3623	3472

from a Ni-rich magma and that the sulphides crystallized thereafter.

b) That the magma was so enriched with Ni that this element was partitioned strongly into both the sulphides and olivines.

c) That all the olivine-bearing rock types have sulphides present, and it is therefore pure coincidence that the pothole and lens reefs have apparently higher Ni values. The olivines of normal Merensky Reef have a much larger range of Ni, from 2762-3866 ppm (Figure 21a).

8.3 Pyroxenes

The general formula for the pyroxene group proposed by Berman (1937) and later slightly modified by Hess (1949) may be expressed as follows:

$$(W)_{1-p}(X,Y)_{1+p}Z_2O_6$$

where W = Ca, Na; X = Mg, Fe^{2+}, Mn, Ni, Li; Y = Al, Fe^{3+}, Cr, Ti and Z = Si, Al. In the Mg-Fe pyroxene (orthopyroxene and pigeonite) series, p approaches 1 and the content of Y ions is usually small. In the Mg-Fe-poor pyroxenes the value of p varies from zero to 1. This expression of the structural formula implies a too-rigid partitioning of the various cations into the different sites, and the general formula used by Cameron and Papike (1980) is perhaps more suitable in the light of more modern information on element partitioning within minerals. This latter formula is as follows:

$$XYZ_2O_6$$

where X represents Na, Ca, Mn^{2+}, Fe^{2+}, Mg and Li in the distorted 6 to 8 - coordinated M2 sites;

Y represents Mn^{2+}, Fe^{2+}, Mg, Fe^{3+}, Al, Cr and Ti in the octahedral M1 site;

Z represents Si and Al in the tetrahedral site. The cations mentioned above are the most common ones in the rock-forming pyroxenes; however, others do occur in trace amounts.

The Ca-Mg-Fe ternary diagrams for all the pyroxenes analysed are plotted in Figure 22a and b. Although the nomenclature of Poldervaart and Hess (1951) for the Ca-poor pyroxenes series (viz., enstatite Fs_{0-10}, bronzite Fs_{10-30}, hypersthene Fs_{30-50}, ferrohypersthene Fs_{50-70}, eulite Fs_{70-90} and orthoferrosilite Fs_{90-100}) has been widely adopted, it is not completely followed here. The division between enstatite and bronzite, and between eulite and orthoferrosilite is placed at the change in optic sign, i.e. at Fs_{12} and Fs_{88} (Deer, Howie and Zussman, 1978). The pyroxenes analysed from the Merensky Reef (B235/15, 15a and 16) and Merensky Unit (B235/7-14) are plotted in Figure 22a. The remaining pyroxenes from the Pseudo Marker (B235/24), Pseudo Reef (B235/25-27), Lens Reef (B222/22), Pothole Reef (B232/1), UG 2 hanging wall (B235/31) and UG 1 leader pyroxenite (B222/3) are plotted in Figure 22b.

In Figure 22a the pyroxenes in the Merensky Reef pegmatoid are all found to be less evolved than those of the pyroxenites and norites of the Merensky Unit. This observation is in marked contrast to the findings of Buchanan et al. (1981) where they postulate the opposite to be true. They suggest that iron depletion in the pyroxenes of the Merensky Reef, associated with a chromitite layer, reflects iron depletion in the original magma, caused by the crystallization of the spinel phase. Buchanan et al. (op.cit.) go further to say that this would lead to the magma becoming saturated in sulphur which would result in the precipitation of

Figure 22 a and b: Ca-Mg-Fe plots for Union Section pyroxenes

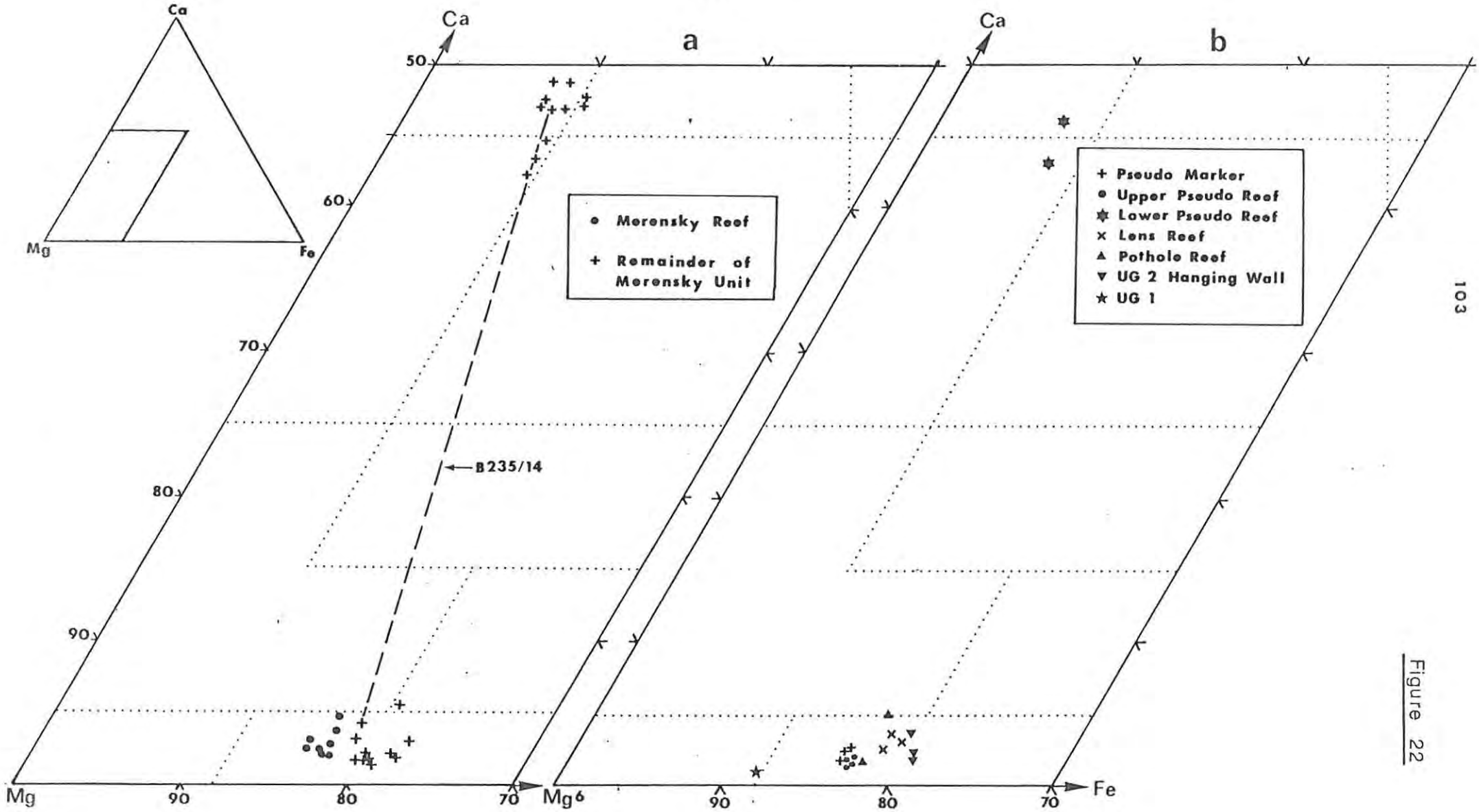

Figure 22

an immiscible sulphide phase, which would further deplete the magma in iron.

The Ca-poor pyroxenes are all plotted against stratigraphic height in Figure 23. The analyses from the normal succession reveal a pattern of Mg/Fe variations similar to that of the olivines from the UG 2 hanging wall to the Pseudo Marker layer. There is a general upward increase in Mg content from $En_{76,8}$ to $En_{82,0}$ for extreme samples ($Fo_{76,7}$ to $Fo_{81,6}$). This sympathetic variation in the orthopyroxenes and the olivines would suggest that they crystallized under conditions of equilibrium. This upward increase in Mg from the UG 2 to Pseudo Marker in both the olivine and the orthopyroxene is a reversal of the normally expected trend. Jackson (1970, p.420) quotes a similar case from the lower part of the Western Bushveld Complex and, in his opinion, the reversal is due to super-cooling at the lower margin. Buchanan (1972) also found this type of reversal between -124 m and -115 m in his Basal Zone of the Bethal area. With the upward Mg-enrichment he noted a corresponding decrease in the An content of the plagioclase. This latter observation is not found to be the case in this study, although there is a wide range of An values.

The orthopyroxenes of the Merensky Reef show a somewhat more scattered composition from $En_{81,0}$ to $En_{78,8}$ for extreme samples. This range in composition is mainly due to the zonal variations in composition. In the Merensky Unit as a whole (B235/14-10), there is a general decrease in the Mg end member from $En_{78,5}$ to $_{74,1}$ in extreme samples. This is the pattern of crystallization one would expect in a magma undergoing fractional crystallization. As the modal percentage of plagioclase increases upward, so the relative abundance of intercumulus clinopyroxene also increases at the

Figure 23

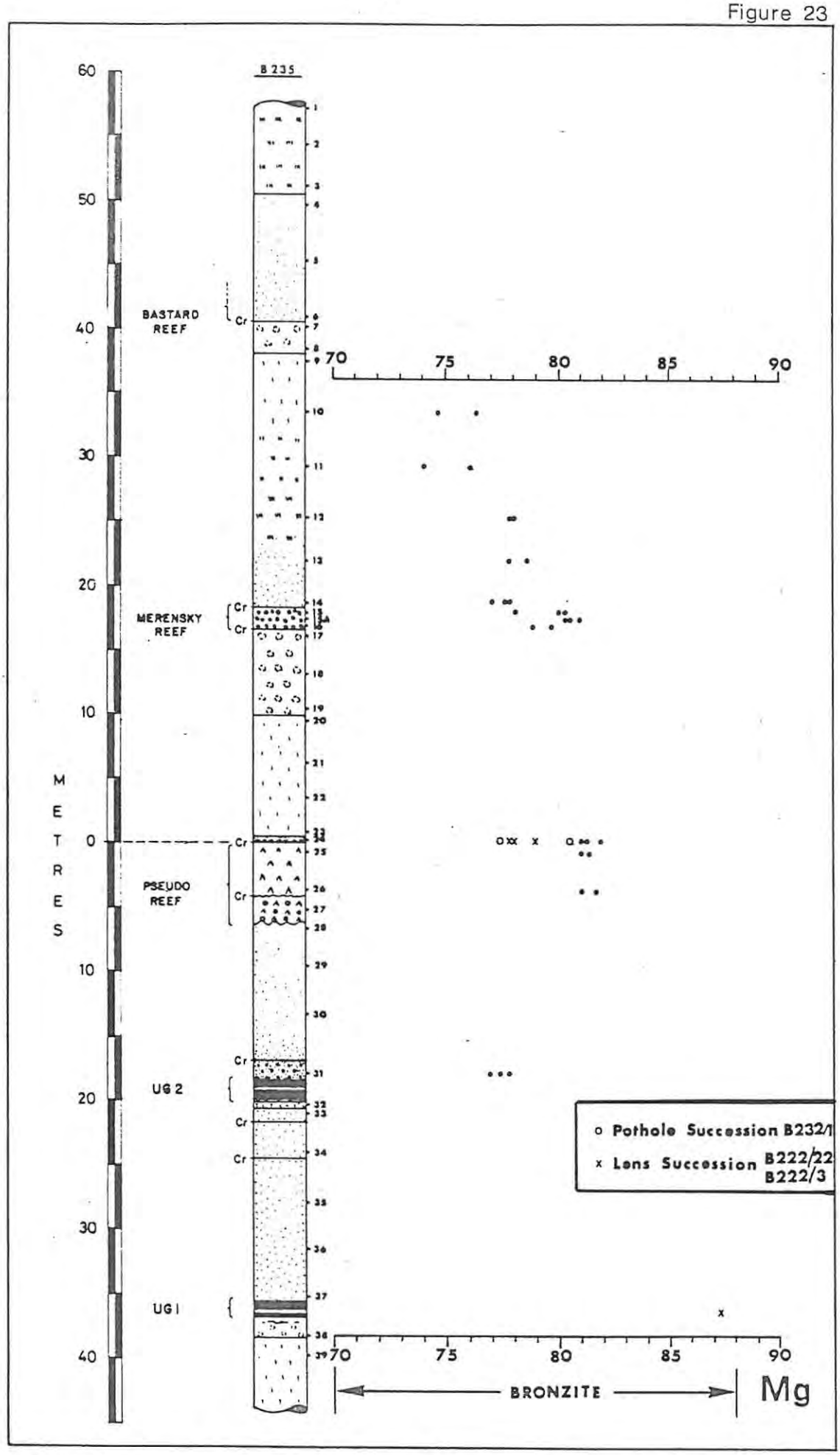

Figure 23: Plot of Atomic % Mg in orthopyroxenes, against stratigraphic height for Normal(•), Pothole-B232/1 (o) and Lens-B222/22 and 3 (x) successions.

expense of cumulus orthopyroxene. Consequently no cumulus orthopyroxene was observed in samples B235/9-7.

Buseck, Nord and Veblen (1980) have pointed out that when pyroxenes cool from igneous temperatures at which they form, they undergo structural and chemical changes in order to remain in equilibrium. Exsolution features in the pyroxene arise from the attempts of individual crystals to lower their total free-energies upon cooling. When a crystal enters a two-phase field from a single-phase field, the reduction of free-energy is the driving force for exsolution and any subsequent microstructural changes.

The ubiquitous presence of exsolution textures in the orthopyroxenes is evidence of their having undergone sub-solidus re-equilibration. Minimum temperatures of crystallization determined using the Ca-poor and Ca-rich pyroxene geothermometer, developed by Wood and Banno (1973), and Wells (1977), were calculated for the Merensky unit rocks (B235/10, 11, 12 and 14), using a computer programme written by G. Davies (WITS.). The clinopyroxene analysed in sample B235/14 is a large oikocryst, whereas that in the other samples analysed was found to consist of anhedral intercumulus crystals, which could, in some instances, have been exsolution products during sub-solidus re-equilibration.

In all cases, the clinopyroxene-orthopyroxene pairs have undergone a certain amount of sub-solidus re-equilibration, and the most reliable temperatures obtained are 1050°C (Wood and Banno, 1973) and 1030°C (Wells, 1977) for this re-equilibration event. Flynn et al. (1978) determined oxygen fugacity and temperature of last equilibration for material from the Critical zone using an oxygen fugacity electrolytic cell. Separate oxygen fugacity-temperature lines were established for bronzite,

plagioclase, whole-rock pyroxenite and whole-rock anorthosite. The intersection of these lines with a chromitite-chromite line was used, by Flynn et al. (1978), to establish a last equilibration at an oxygen fugacity value of $10^{-11,82}$ and at a temperature of 1091°C. This latter temperature value is in fair agreement with the Wood and Banno (1973) temperature of 1050°C, quoted above.

Mitchell (1980) has pointed out that a shortcoming of the Ca-Mg-Fe ternary diagram (Figure 22) is that it does not take into account the minor elements which substitute for Fe, Mg, Ca and Si in the pyroxene structure. The most important elements in this category are Mn, Cr, Ti and Al. Variations of these elements are presented for both the clinopyroxenes and orthopyroxenes in Figures 24a - f.

Manganese (Mn^{2+}) is partitioned more favourably into the orthopyroxenes (Figure 24d) and there does appear to be a linear increase in Mn^{2+}, with increasing Fs content (Campbell and Borley, 1974). The clinopyroxenes increase from 0,13% to 0,20%, with one anomalously high value of 0,27% while the bulk of the orthopyroxenes increase in MnO from 0,20% to 0,31%, with one low sample with only 0,07% MnO. The Feo increases from 4,6% to 14,5%.

Chromium (Cr^{3+}), which partitions more favourably into clinopyroxene ($D^{cpx}_{Cr} \leqslant 40$, Campbell and Borley, 1974) rather than orthopyroxene (Table 8), produces an inverse relationship of Cr_2O_3 to FeO. Cr^{3+} substitution for Mg^{2+} or Fe^{2+} in pyroxenes requires the simultaneous replacement of Si^{4+} by Al^{3+} so that charge balance can be maintained (Campbell, 1977). When Al_2O_3 and Cr_2O_3 are plotted against each other there is a broad linear relationship (Figure 24f).

Figure 24 a-f: Variation diagrams for Union Section orthopyroxene (●) and clinopyroxene (▼)

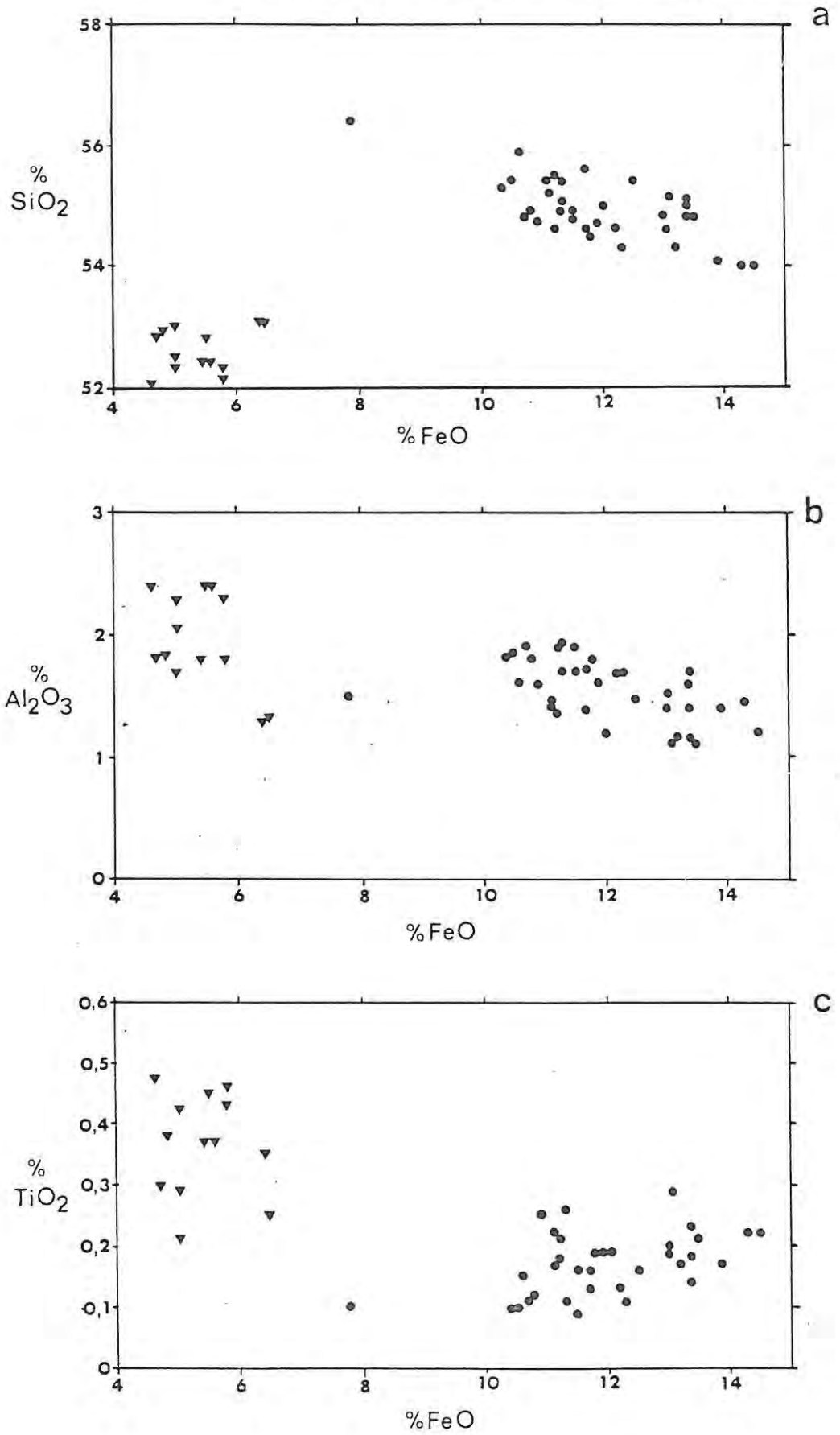

Figure 24 a-f: Variation diagrams for Union Section orthopyroxene (●) and clinopyroxene (▼).

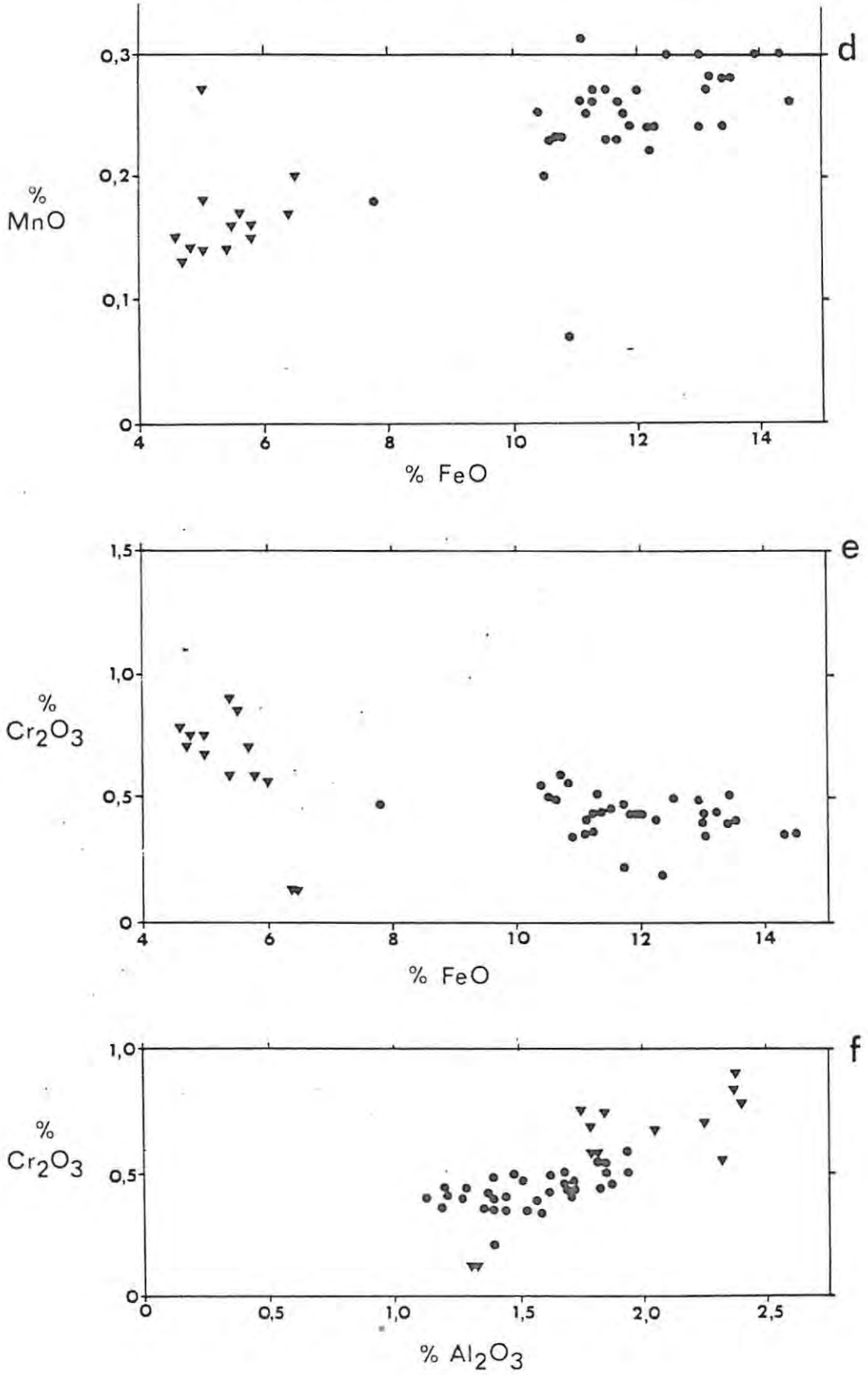

TABLE 2: PYROXENE ANALYSES BY MICROPROBE

	B232/1(1) CORE	B232/1(1) MARGIN	B222/22 CORE	B222/22 CORE	B222/22 CORE	B235/24 MARGIN	B235/24 CORE	B235/24 CORE	B235/25(1) MARGIN	B235/25(1) CORE	B235/26(1) MARGIN	B235/26(1) CORE	B235/27 MARGIN	B235/27 CORE	B235/31 CORE	B235/31 MARGIN
SiO_2	54,65	55,60	54,30	54,60	54,57	55,85	55,28	55,39	55,53	55,37	55,18	55,44	52,51	52,04	54,60	55,02
TiO_2	0,25	0,13	0,11	0,13	0,16	0,15	0,10	0,10	0,18	0,11	0,22	0,17	0,29	0,47	0,20	0,23
Al_2O_3	1,58	1,39	1,71	1,72	1,73	1,63	1,84	1,86	1,36	1,94	1,40	1,45	2,05	2,41	1,53	1,57
FeO	10,86	11,69	12,31	12,17	11,72	10,56	10,35	10,54	11,16	11,33	11,10	11,14	4,99	4,60	13,05	13,36
MnO	0,07	0,26	0,24	0,22	0,23	0,23	0,25	0,20	0,25	0,27	0,26	0,31	0,18	0,15	0,24	0,24
MgO	28,46	30,22	29,90	28,03	28,39	29,77	29,82	30,21	30,48	30,75	30,86	31,10	17,70	16,68	28,84	28,68
CaO	2,98	0,79	1,09	1,46	1,79	1,21	1,24	0,81	0,97	0,73	1,12	0,74	21,67	22,81	1,75	1,21
Na_2O	0,01	0,02	0,05	0,02	0,08	ND	ND	ND	ND	0,07	0,12	ND	0,36	0,39	0,09	0,04
Cr_2O_3	0,34	0,21	0,18	0,41	0,47	0,49	0,54	0,50	0,36	0,51	0,35	0,41	0,67	0,78	0,35	0,39
TOTAL	99,20	100,31	99,89	98,76	99,14	99,89	99,42	99,61	100,29	101,08	100,61	100,76	100,42	100,33	100,64	100,73
Recalculated as cations per 6 Oxygens (Z=2)																
Si	1,956	1,963	1,936	1,966	1,957	1,970	1,966	1,959	1,958	1,939	1,943	1,946	1,920	1,908	1,942	1,953
Al	0,044	0,037	0,064	0,034	0,043	0,030	0,034	0,041	0,042	0,061	0,057	0,054	0,080	0,092	0,058	0,047
Ti	0,007	0,004	0,003	0,004	0,004	0,004	0,003	0,003	0,005	0,003	0,006	0,005	0,008	0,013	0,005	0,006
Al	0,023	0,021	0,008	0,039	0,030	0,038	0,043	0,037	0,015	0,019	0,001	0,006	0,008	0,012	0,006	0,019
Fe	0,325	0,345	0,367	0,367	0,352	0,312	0,307	0,312	0,329	0,332	0,327	0,327	0,153	0,141	0,388	0,397
Mn	0,002	0,008	0,007	0,007	0,007	0,007	0,008	0,006	0,008	0,008	0,008	0,009	0,006	0,005	0,007	0,007
Mg	1,518	1,589	1,588	1,504	1,517	1,565	1,575	1,592	1,601	1,605	1,619	1,627	0,964	0,911	1,528	1,516
Ca	0,114	0,030	0,047	0,056	0,069	0,046	0,047	0,031	0,037	0,027	0,042	0,028	0,849	0,896	0,067	0,046
Na	0,001	0,001	0,004	0,001	0,006	0,001	0,001	0,001	0,001	0,005	0,008	0,001	0,026	0,028	0,006	0,003
Cr	0,010	0,006	0,005	0,012	0,013	0,014	0,015	0,014	0,010	0,014	0,010	0,011	0,019	0,023	0,010	0,011
X+Y	2,000	2,004	2,029	1,990	1,998	1,987	1,999	1,996	2,006	2,013	2,021	2,014	2,033	2,029	2,017	2,005
At%Ca	5,82	1,52	2,34	2,89	3,55	2,38	2,43	1,60	1,88	1,37	2,11	1,40	43,06	45,88	3,37	2,34
Mg	77,49	80,58	79,04	77,77	77,99	81,09	81,31	82,02	81,06	81,39	81,11	81,72	48,88	46,64	76,78	77,11
Fe	16,69	17,90	18,62	19,34	18,46	16,53	16,26	16,38	17,06	17,24	16,78	16,88	8,06	7,48	19,85	20,55

TABLE 2: PYROXENE ANALYSES BY MICROPROBE

	B235/31 CORE	B235/15 MARGIN	B235/15 MID	B235/15 CORE	B235/15A MARGIN	B235/15A MID	B235/15A CORE	B235/16 MARGIN	B235/16 CORE	B235/14 CORE	B235/14 MARGIN	B235/14 CORE	B235/14 MARGIN	B235/14 MID	B235/14 CORE	B222/3 CORE
SiO_2	54,76	54,86	54,45	54,72	54,86	54,85	54,79	54,62	54,81	54,84	55,05	55,00	52,81	52,39	52,30	56,43
TiO_2	0,14	0,26	0,19	0,19	0,09	0,12	0,11	0,21	0,16	0,19	0,18	0,19	0,45	0,37	0,21	0,10
Al_2O_3	1,68	1,72	1,69	1,62	1,87	1,82	1,94	1,83	1.68	1,38	1,39	1,20	2,37	2,37	2,33	1,51
FeO	13,36	11,32	11,84	11,92	11,45	10,80	10,69	11,21	11,49	13,03	13,39	12,04	5,54	5,59	4,97	7,84
MnO	0,24	0,26	0,25	0,24	0,27	0,23	0,23	0,24	0,23	0,30	0,28	0,27	0,16	0,17	0,27	0,18
MgO	28,48	29,57	30,43	30,26	30,32	30,34	30,54	28,96	29,61	28,96	28,72	28,29	16,69	16,59	15,50	33,43
CaO	0,98	2,53	1,01	1,01	1,22	1,62	1,44	1,91	1,37	1,18	0,76	2,17	20,26	21,09	22,65	0,48
Na_2O	0,10	0,10	ND	0,02	0,18	0,15	0,08	ND	ND	0,19	0,06	0,07	0,50	0,33	0,11	0,11
Cr_2O_3	0,51	0,44	0,44	0,43	0,46	0,55	0,59	0,44	0,46	0,43	0,40	0,44	0,84	0,90	0,55	0,47
TOTAL	100,24	101,06	100,30	100,41	100,71	100,48	100,41	99,42	99,81	100,50	100,23	99,67	99,62	99,80	98,89	100,55
Recalculated as cations per 6 oxygens (Z=2)																
Si	1,953	1,934	1,930	1,938	1,934	1,935	1,932	1,950	1,949	1,951	1,961	1,967	1,940	1,928	1,943	1,953
Al	0,047	0,066	0,070	0,062	0,066	0,065	0,068	0,050	0,051	0,049	0,039	0,033	0,060	0,072	0,057	0,047
Ti	0,004	0,007	0,005	0,005	0,002	0,003	0,003	0,006	0,004	0,005	0,005	0,005	0,012	0,010	0,006	0,003
Al	0,024	0,006	0,001	0,006	0,012	0,011	0,013	0,027	0,019	0,009	0,019	0,018	0,043	0,031	0,045	0,015
Fe	0,398	0,334	0,351	0,353	0,338	0,319	0,315	0,335	0,342	0,388	0,399	0,360	0,170	0,172	0,154	0,227
Mn	0,007	0,008	0,008	0,007	0,008	0,007	0,007	0,007	0,007	0,009	0,009	0,008	0,005	0,005	0,009	0,005
Mg	1,513	1,553	1,607	1,596	1,593	1,595	1,605	1,540	1,568	1,535	1,525	1,507	0,914	0,910	0,858	1,724
Ca	0,037	0,096	0,038	0,038	0,046	0,061	0,054	0,073	0,052	0,045	0,029	0,083	0,798	0,832	0,901	0,018
Na	0,007	0,007	0,001	0,001	0,012	0,010	0,004	0,001	0,001	0,013	0,004	0,/05	0,036	0,024	0,008	0,007
Cr	0,014	0,012	0,012	0,012	0,013	0,015	0,017	0,012	0,013	0,012	0,011	0,012	0,024	0,026	0,015	0,013
X+Y	2,004	2,023	2,023	2,018	2,024	2,021	2,018	2,001	2,006	2,016	2,001	1,998	2,002	2,010	1,997	2,012
At%Ca	1,98	4,82	1,90	1,91	2,32	3,08	2,73	3,74	2,65	2,28	1,47	4,24	42,29	43,36	46,88	0,91
Mg	77,39	78,00	80,19	80,04	80,25	80,47	81,02	78,77	79,63	77,64	77,73	76,97	48,44	47,42	44,64	87,34
Fe	20,72	17,18	17,91	18,05	17,43	16,45	16,25	17,49	17,72	20,08	20,80	18,79	9,27	9,22	8,48	11,75

TABLE 2: PYROXENE ANALYSES BY MICROPROBE

	B235/13 MARGIN	B235/13 CORE	B235/12 MARGIN	B235/12 CORE	B235/12 MARGIN	B235/12 MARGIN	B235/11 MARGIN	B235/11 CORE	B235/11 MARGIN	B235/11 MARGIN	B235/10 CORE	B235/10 MARGIN	B235/10 MARGIN	B235/10 CORE	B235/9 MARGIN	B235/9 MARGIN
SiO_2	55,14	55,35	54,81	54,82	52,92	52,97	54,05	54,32	52,81	52,13	54,06	53,98	52,37	52,32	53,06	53,13
TiO_2	0,29	0,16	0,21	0,18	0,38	0,42	0,22	0,17	0,30	0,43	0,17	0,22	0,37	0,46	0,25	0,35
Al_2O_3	1,13	1,48	1,21	1,27	1,84	1,74	1,45	1,29	1,78	2,25	1,40	1,19	1,79	1,81	1,34	1,31
FeO	13,07	12,49	13,51	13,36	4,75	4,98	14,33	13,17	4,71	5,77	13,88	14,49	5,44	5,83	6,51	6,35
MnO	0,27	0,30	0,28	0,28	0,14	0,14	0,30	0,28	0,13	0,16	0,30	0,26	0,14	0,15	0,20	0,17
MgO	29,17	29,39	29,31	29,48	16,14	16,31	28,28	27,72	15,65	16,53	28,00	27,82	15,44	15,89	15,57	15,22
CaO	0,89	1,72	0,95	1,00	23,79	23,41	0,95	2,93	24,41	22,29	1,07	1,60	24,49	23,45	23,95	23,93
Na_2O	0,04	ND	0,09	0,01	0,39	0,34	0,01	0,04	0,54	0,22	ND	ND	0,27	0,40	0,11	0,21
Cr_2O_3	0,40	0,50	0,41	0,40	0,74	0,75	0,35	0,44	0,69	0,70	0,48	0,36	0,57	0,57	0,12	0,12
TOTAL	100,94	101,39	100,78	100,80	101,09	101,05	99,94	100,36	101,02	100,48	99,36	99,92	100,88	100,87	101,10	100.80
Recalculated as cations per 6 oxygens (Z=2)																
Si	1,951	1,948	1,947	1,946	1,930	1,932	1,944	1,947	1,931	1,914	1,952	1,947	1,924	1,921	1,946	1,953
Al	0,049	0,052	0,053	0,055	0,070	0,068	0,056	0,053	0,069	0,084	0,048	0,053	0,076	0,079	0,054	0,047
Ti	0,006	0,004	0,004	0,003	0,010	0,012	0,006	0,005	0,008	0,012	0,005	0,004	0,010	0,012	0,007	0,010
Al	-	0,009	-	-	0,009	0,007	0,006	0,002	0,008	0,008	0,012	-	0,002	-	0,004	0,010
Fe	0,387	0,368	0,401	0,397	0,145	0,152	0,431	0,395	0,144	0,177	0,419	0,437	0,167	0,179	0,200	0,196
Mn	0,008	0,009	0,008	0,008	0,004	0,004	0,009	0,009	0,004	0,005	0,009	0,008	0,004	0,005	0,006	0,005
Mg	1,566	1,541	1,552	1,559	0,877	0,886	1,516	1,480	0,853	0,904	1,506	1,495	0,845	0,869	0,851	0,834
Ca	0,034	0,065	0,036	0,038	0,929	0,915	0,037	0,113	0,956	0,877	0,041	0,062	0,964	0,923	0,914	0,943
Na	0,003	0,001	0,006	0,001	0,028	0,024	0,001	0,003	0,038	0,016	0,001	0,001	0,019	0,029	0,008	0,015
Cr	0,011	0,014	0,012	0,011	0,021	0,022	0,010	0,013	0,020	0,020	0,014	0,010	0,017	0,017	0,004	0,004
X+Y	2,015	2,011	1,989	2,017	2,023	2,022	2,016	2,020	2,031	2,019	2,007	2,017	2,028	2,034	2,021	2,017
AT%Ca	1,70	3,28	1,80	1,90	47,52	46,76	1,85	5,66	48,85	44,68	2,08	3,09	48,68	46,71	47,10	47,68
Mg	78,50	77,71	77,72	77,87	44,86	45,27	76,07	74,11	43,59	46,05	76,25	74,68	42,68	43,98	42,59	42,16
Fe	19,80	19,01	20,48	20,23	7,62	7,97	22,08	20,23	7,56	9,27	21,67	22,23	8,64	9,31	10,31	10,16

The Ti and Al contents of the clinopyroxenes are, in both cases, higher than for the orthopyroxenes. Mitchell (1980) has pointed out that Ti can only enter the pyroxene structure if its charge is balanced, and this can be achieved by the simultaneous entry of two Al^{3+} ions in the tetrahedral site and one Ti^{4+} ion in the octahedral sites. Ti cannot commpete with Cr for charge-deficient octahedral sites, and therefore Ti only becomes an important constituent of pyroxene once the Cr is depleted in the melt (Campbell and Borley, 1974).

8.4 Feldspars

The minerals of the feldspar group are framework silicates, in which small, high-charged cations in tetrahedral coordination with oxygen form the basic structure. Large, irregular cavities in the tetrahedral framework are filled by univalent or divalent cations with radii of close to or greater than 1,0 Å. The general formula is MT_4O_8, where the T site is filled primarily by Al and Si, with minor substitution of B, Ga, Ge and Fe^{3+} (Smith, 1975). The stoichiometry of the tetrahedral group changes from Al_2Si_2, for calcic plagioclase (anorthite) to $AlSi_3$ in albite. The M group in the general formula is filled by Na, K, Ca, Rb, Sr, Pb, Ba and NH_4 (Smith, op. cit.), the most important of these being Na, K and Ca. Other elements which might enter the feldspar structure are Fe^{2+}, Mg, Ti and P. Smith regards this latter group of elements as capable of entering either the M or the T sites.

Fifty-two electron microprobe analyses of the plagioclase feldspars from the study section are presented in Table 3. Plagioclase samples from all the rock types represented in the upper Critical zone, which include

anorthosites, poikilitic anorthosite, norites, feldspathic pyroxenite and feldspathic harzburgite were analysed. The positions of the samples used for plagioclase analyses are illustrated in Figure 19, and once again emphasis on the mineralogy of the Merensky unit prompted more analyses from this unit. Furthermore, the plagioclase in all olivine-bearing rock types plus two samples from the Lens succession in the vicinity of the UG 1 chromitite were also analysed.

In the majority of samples, analyses of both the core and margin of the plagioclase crystals were performed.

All the plagioclase analyses have been recalculated in terms of cations per 8 oxygens, and also in terms of the feldspar end members - orthoclase, albite and anorthite (molecular %). The plagioclase compositions in terms of the end members are plotted in Figure 25a, b and c. The molecular % An of all analyses from both the normal (B235) and potholed successions (B232 and B222) are plotted against stratigraphic height and presented in Figure 26.

The cumulus plagioclase (B235/7, 8, 9, 10, 11, 12 and B222/2) is generally more calcic than the intercumulus plagioclase, and has a range of $An_{72,8-81,7}$, well within the bytownite field (Figure 26). The rest of the analyses, all representing intercumulus plagioclase from feldspathic harzburgites and pyroxenites, have a range of $An_{56,3-71,9}$ with one sample from the Lens reef (B222/22, core) having an abnormally low value of $An_{43,6}$. It would thus appear that the majority of intercumulus plagioclase falls within the labradorite field, with a slight overlap into the more sodic bytownite field. The ranges in An content for both the cumulus and intercumulus plagioclase are in agreement with Van Zyl's (1970) value in the norite-

Figure 25 a, b and c: Or-Ab-An Plots for Union Section Plagioclase Feldspars. Cumulus (▲) and intercumulus plagioclase (●).

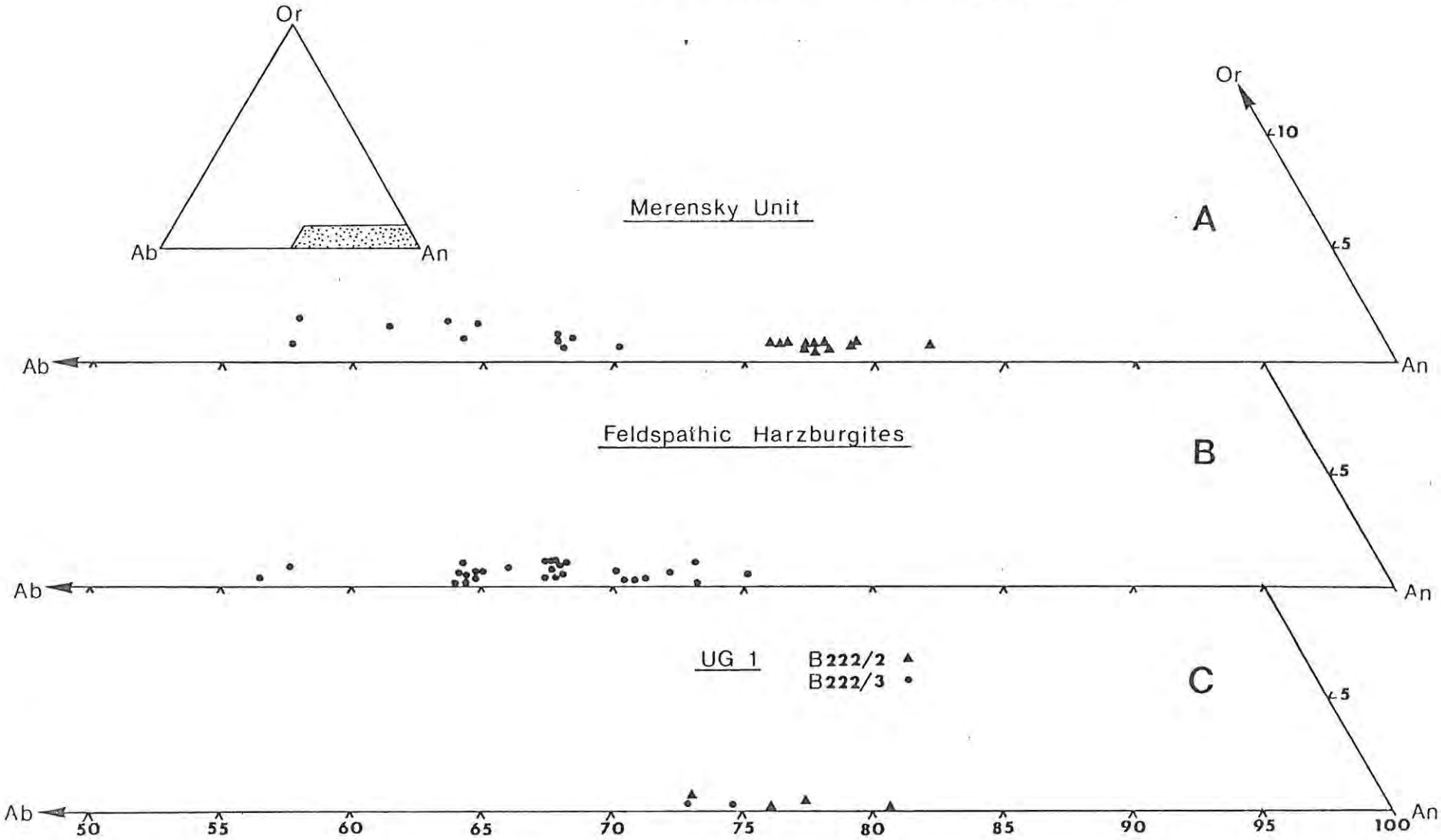

Figure 25

Figure 26

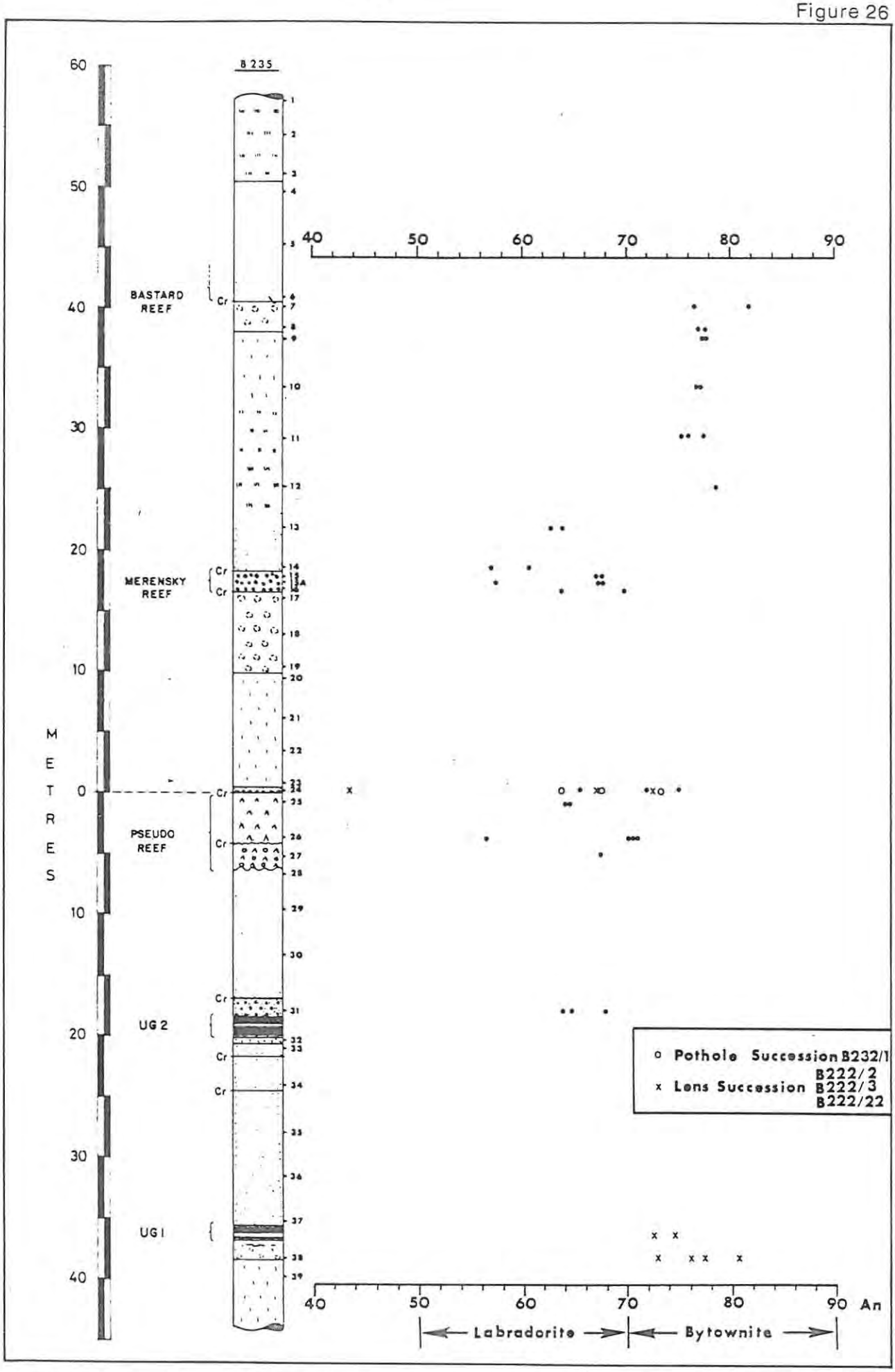

Figure 26: Plot of Mol % An for Union Section plagioclase against stratigraphic height for Normal (•), Pothole-B232/1 (o) and Lens-B222/22, 2 and 3 (×) successions.

anorthosite unit of An_{64-82} (see Figure 1).

Kruger (1981, pers. comm.) in an extensive study of the Merensky unit in the Rustenburg area, has noted that the plagioclase exhibits extensive zoning and has pointed out that a single high-quality microprobe analysis has only limited value. As was noted earlier, a minimum of 2 analyses was done per crystal (core and margin) and if one considers only the cumulus plagioclase, with its limited adcumulus overgrowth, the margins of almost all the crystals in the Merensky unit are enriched in the An component, relative to the cores (Figure 27 a). The pattern does, however, appear to be more complex for the intercumulus plagioclase (Figure 27 b), and this could indicate that nucleation in intercumulus space is probably achieved on the surface of surrounding crystals of orthopyroxene.

Ferguson and Wright (1970) in their study of plagioclase from a 152 m borehole core, 132 m below the Merensky Reef in the Brits district, also observed this unusual zonation pattern, where the cumulus plagioclase has margins which are more calcic than the cores. They conclude from their study that the generally more calcic bulk composition of the plagioclase from the plagioclase-rich cumulates, as compared with those from the other cumulates, is due to a larger and more calcic development of the outer margin. Reversed zoning of cumulus plagioclase has also been noted by Liebenberg (1942) and Wager and Brown (1968, p.385). Normal zoning in plagioclase orthocumulates results when low temperature (Ca-poor) rims form because the residual trapped liquid fails to react with the cumulus crystals over a range of falling temperature (Wager and Brown, 1968, p.65). Although only a limited number of analyses was done on each plagioclase crystal, there is a strong likelihood that these plagioclase crystals display oscillatory zoning. Buchanan

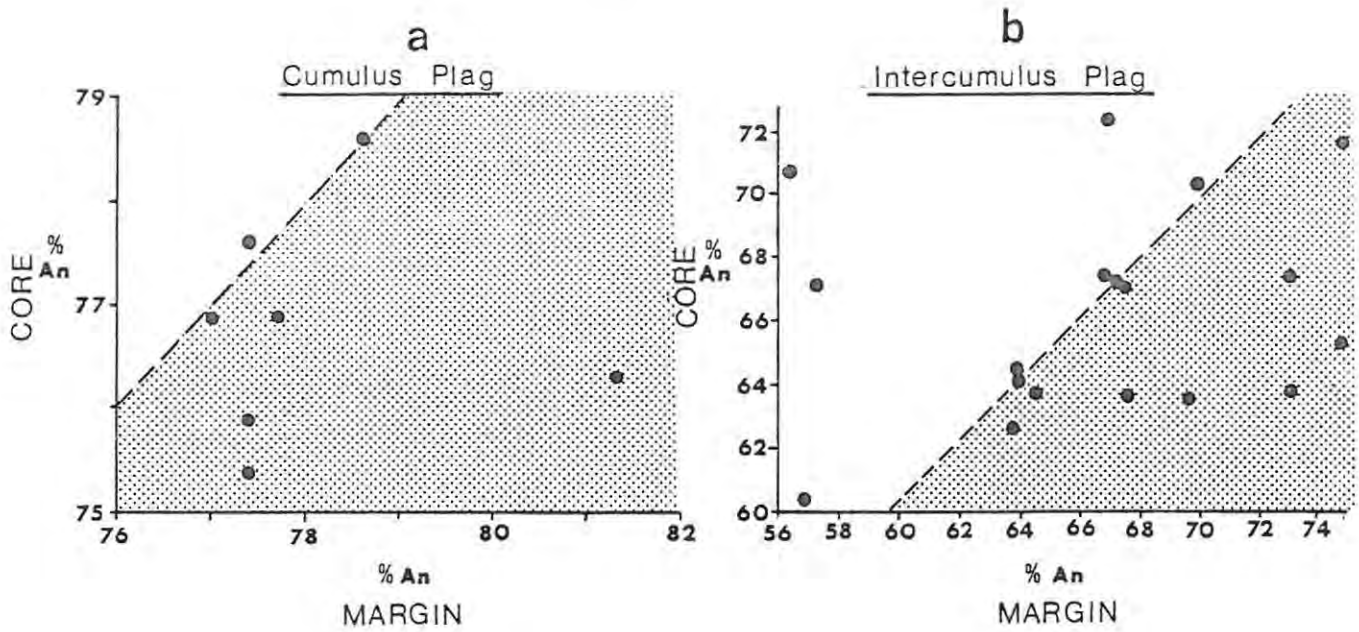

FIGURE 27: (a and b) Diagrams illustrating the pronounced An enrichment on the margins of cumulus plagioclase (a), while no apparent enrichment in either the core or margins is seen in the intercumulus plagioclase (b). Broken lines depict uniform compositions of cores and margins. The shaded areas represent Ca-enrichment on the margins while the unshaded areas represent Ca-enrichment in the cores.

(1972, p.30) has noted that Phemister (1934, p.553) gives four possible causes for oscillatory zoning, namely:

a) Movement of crystals in the magma, whether by gravitational settling or by convection currents.

b) Movement of the magma, as a whole, into a region where different conditions of temperature and pressure prevail.

c) Irruption of additional magma into the crystallizing liquid.

d) Loss of volatile constituents.

In their discussion of oscillatory zoning, Bottinga

et al. (1966) have indicated that supercooling is required for the development of this type of zoning. It follows therefore that the upper Critical zone as a whole formed under supercooled crystallization conditions. The evidence of supercooled crystallization conditions is interesting, as the formation of rhythmic layering may be related to supercooled crystallization (Maaløe, 1976).

A notable feature of the plagioclase composition in the Merensky unit is an apparent increase in An upward in the succession (Figure 26). There is a marked increase from the intercumulus plagioclase in the Merensky pyroxenite (B235/14 and 13) to the cumulus plagioclase in the norites and anorthosites higher in the succession ($\bar{x}$ An 61,0 - $\bar{x}$ An 77,5, difference of 16,5 mol % An). Unfortunately not enough data points were gathered to establish beyond doubt a definite increase in the An component or the cumulus plagioclase, and what data are available could be biased by the effects of zoning.

The phenomenon of an upward increase in the An content within layered units of the Critical zone is by no means unusual, and has been documented by various workers (Vermaak and Hendriks, 1976; Cameron, 1980; Ferguson and Wright, 1970). In their study of the Critical zone in the Brits district, Ferguson and Wright (1970) concluded that the most notable feature of the cumulus minerals is the increase of An with differentiation in a 152 m section, some 132 m below the Merensky Reef. They suggest that this reversal of the normal differentiation trend was produced by an increase in P_{H_2O}. Vermaak (1976) explains the reversal by the flotation of plagioclase in a magma of similar density. He goes further to suggest that if the floating were arrested by a compositional, density, or temperature inversion, it

would seem reasonable that a mat of crystals would form, and that later crystals floated would underplate the mat to form the anorthosite layer. The early plagioclase crystals at the top of the layer would have the highest An content and this would decrease progressively as later crystals were added from below. Lee (1982) (in press) has also noted the upward increase in An in the Merensky unit in the Rustenburg area, and has pointed out that this type of reversal is not uncommon in the Eastern Bushveld Complex, as is indicated by the work of Cameron (1980).

In Figure 28 the plagioclase analyses are plotted in terms of orthoclase vs. anorthite (molecular %). On the basis of this diagram, the various rock types, in terms of cumulate types, fall into distinct, separate fields. The intercumulus plagioclase in the feldspathic pyroxenites (B235/14 and 13), both heteradcumulates, have much higher orthoclase components than the cumulus plagioclase of the norites, leuconorites and anorthosites which are all mesocumulates and adcumulates. The intercumulus plagioclase in all the feldspathic harzburgites is intermediate between the above two extremes. A possible explanation for the K-enrichment of the intercumulus plagioclase in the feldspathic pyroxenites (235/14 and 13), is that it was the last phase to crystallize from an intercumulus liquid which was by then K-enriched. The intercumulus plagioclase from the feldspathic harzburgites may represent a more complex paragenesis.

TABLE 3: PLAGIOCLASE ANALYSES BY MICROPROBE

	B232/1 CORE	B232/1 MARGIN	B232/1 CORE	B222/22 CORE	B222/22(1) MARGIN	B222/22(1) CORE	B235/24 CORE	B235/24 MARGIN	B235/24 CORE	B235/25 CORE	B235/25 MARGIN	B235/25 CORE	B235/26 MARGIN	B235/26 CORE	B235/26 MARGIN	B235/26 CORE	B235/27 MARGIN	B235/27 CORE
SiO_2	51,49	49,06	50,4	56,21	50,87	49,39	49,65	48,99	50,92	51,36	52,30	51,51	50,62	50,43	54,87	50,81	51,00	50,69
Al_2O_3	30,14	31,66	30,86	26,91	30,75	31,49	31,79	32,09	30,99	30,14	30,09	29,91	30,99	31,02	28,36	31,10	30,11	30,49
FeO	0,35	0,27	0,38	0,16	0,28	0,24	0,16	0,13	0,15	0,09	0,13	0,10	0,09	0,07	0,36	0,12	0,14	0,16
CaO	13,83	15,52	14,31	9,83	14,57	15,46	15,29	15,83	14,03	13,75	13,45	13,78	14,87	14,85	11,37	14,77	14,14	14,08
Na_2O	4,31	3,11	3,73	7,00	3,79	3,08	3,24	2,88	3,99	4,14	4,12	4,19	3,48	3,41	4,84	3,28	3,72	3,71
K_2O	ND	0,05	0,10	0,03	0,23	0,23	0,11	0,09	0,13	0,06	0,08	0,05	0,04	0,02	0,05	0,06	0,10	0,09
TOTAL	100,12	99,67	99,78	100,14	100,49	99,89	100,24	100,00	100,21	99,54	100,17	99,54	100,09	99,80	99,85	100,13	99,20	99,22
Recalculated as cations per 8 oxygens.																		
Si	2,346	2,256	2,308	2,534	2,315	2,266	2,267	2,244	2,318	2,350	2,372	2,357	2,308	2,306	2,479	2,313	1,343	2,329
Al	1,619	1,716	1,666	1,430	1,650	1,703	1,710	1,733	1,633	1,625	1,609	1,613	1,666	1,671	1,510	1,669	1,630	1,651
Fe	0,013	0,010	0,016	0,006	0,010	0,009	0,006	0,005	0,006	0,003	0,005	0,004	0,003	0,003	0,014	0,005	0,005	0,006
Ca	0,675	0,765	0,702	0,475	0,710	0,760	0,748	0,777	0,684	0,674	0,654	0,676	0,727	0,727	0,550	0,720	0,696	0,693
Na	0,381	0,277	0,331	0,612	0,335	0,274	0,287	0,256	0,352	0,367	0,362	0,372	0,308	0,302	0,424	0,290	0,331	0,330
K	0,001	0,003	0,006	0,002	0,013	0,014	0,006	0,005	0,008	0,004	0,005	0,003	0,002	0,001	0,003	0,004	0,006	0,005
SUM	5,035	5,027	5,029	5,059	5,033	5,026	5,024	5,020	5,031	5,023	5,007	0,025	5,014	5,010	4,980	5,001	5,011	5,014
Mol %																		
An	63,86	73,21	67,56	43,62	67,11	72,52	71,85	74,86	65,52	64,50	64,05	64,32	70,11	70,58	56,29	71,01	67,38	67,41
Ab	36,05	26,51	31,86	56,20	31,66	26,15	27,57	24,66	33,72	35,12	35,46	35,39	29,70	29,32	43,40	28,60	32,04	32,10
Or	0,09	0,28	0,58	0,18	1,23	1,33	0,58	0,48	0,76	0,38	0,49	0,29	0,19	0,10	0,31	0,39	0,58	0,49

TABLE 3: PLAGIOCLASE ANALYSES BY MICROPROBE

	B235/31 MARGIN	B235/31 MARGIN	B235/31 CORE	B235/31 MARGIN	B235/15 MARGIN	B235/15 CORE	B235/15A MARGIN	B235/15A MARGIN	B235/15A CORE	B235/16 MARGIN	B235/16 CORE	B222/2 CORE	B222/2 CORE	B222/2 CORE	B222/2 CORE	B222/3 CORE
SiO_2	52,06	51,20	51,00	50,89	51,12	50,81	53,13	51,08	50,32	50,00	52,10	48,59	49,65	50,26	49,37	48,83
Al_2O_3	30,88	31,22	29,74	31,37	30,36	30,09	29,58	31,06	31,25	30,34	28,93	32,66	32,12	31,70	32,26	32,11
FeO	0,12	0,15	0,10	0,14	0,32	0,24	0,45	0,22	0,20	0,41	0,23	0,01	0,03	0,01	0,02	0,02
CaO	13,67	13,63	13,83	14,19	14,03	14,22	12,15	13,83	14,46	14,85	13,22	15,81	16,57	15,07	15,81	15,46
Na_2O	4,06	4,07	4,28	3,67	3,66	3,62	4,91	3,59	3,76	3,45	4,05	2,74	2,19	3,02	2,53	2,89
K_2O	0,11	0,10	0,10	0,08	0,23	0,19	0,17	0,11	0,19	0,13	0,19	0,02	0,02	0,13	0,09	0,07
TOTAL	100,90	100,37	99,05	100,34	99,72	99,17	100,38	99,89	100,18	99,18	98,72	99,83	100,58	100,19	100,08	99,38
Recalculated as cations per 8 oxygens																
Si	2,347	2,323	2,349	2,311	2,338	2,338	2,404	2,327	2,296	2,308	2,399	2,227	2,257	2,288	2,254	2,247
Al	1,641	1,669	1,614	1,679	1,637	1,632	1,577	1,668	1,681	1,651	1,570	1,764	1,721	1,701	1,736	1,741
Fe	0,005	0,006	0,004	0,005	0,012	0,009	0,017	0,008	0,008	0,016	0,009	0,000	000,1	-	0,001	0,001
Ca	0,660	0,663	0,683	0,690	0,688	0,701	0,589	0,675	0,707	0,734	0,652	0,776	0,807	0,735	0,773	0,762
Na	0,355	0,358	0,382	0,323	0,325	0,323	0,431	0,317	0,333	0,309	0,362	0,244	0,193	0,267	0,224	0,258
K	0,006	0,006	0,006	0,005	0,013	0,011	0,010	0,006	0,011	0,008	0,011	0,001	0,001	0,008	0,005	0,004
SUM	5,014	5,025	5,038	5,013	5,013	5,014	5,028	5,001	5,036	5,026	5,003	5,012	4,980	4,999	4,993	5,013
Mol %																
An	64,64	64,56	63,77	67,78	67,05	67,73	57,18	67,64	67,27	69,84	63,61	76,00	80,62	72,77	77,15	74,41
Ab	34,77	34,86	35,67	31,73	31,68	31,21	41,84	31,76	31,68	29,40	35,32	23,90	19,28	26,44	22,35	25,20
Or	0,59	0,58	0,56	0,49	1,27	1,06	0,98	0,60	1,05	0,76	1,07	0,10	0,10	0,79	0,50	0,39

TABLE 3: PLAGIOCLASE ANALYSES BY MICROPROBE

	B222/3 CORE	B235/13 MARGIN	B235/13 CORE	B235/14 MARGIN	B235/14 CORE	B235/12 CORE	B235/12 MARGIN	B235/11 MARGIN	B235/11 CORE	B235/11 CORE	B235/10 CORE	B235/10 MARGIN	B235/9 CORE	B235/9 MARGIN	B235/8 CORE	B235/8 MARGIN	B235/7 MARGIN	B235/7 CORE
SiO_2	49,03	51,74	51,86	53,99	52,60	48,30	48,38	48,62	48,71	48,08	48,79	48,71	48,65	48,73	48,90	48,94	47,7	49,28
Al_2O_3	31,84	30,00	30,07	28,92	29,41	32,32	32,70	32,61	32,17	31,41	32,17	32,23	32,28	32,25	32,07	32,14	32,85	31,89
FeO	0,02	0,15	0,16	0,16	0,13	0,30	0,27	0,26	0,23	0,84	0,32	0,28	0,37	0,31	0,46	0,35	0,44	0,43
CaO	15,05	13,47	13,60	11,68	12,82	16,71	17,02	16,65	16,47	15,81	16,88	16,97	16,24	16,38	16,12	16,15	16,90	15,89
Na_2O	3,06	4,00	4,26	4,67	4,44	2,43	2,40	2,59	2,78	2,76	2,72	2,69	2,51	2,57	2,58	2,48	2,01	2,62
K_2O	0,10	0,30	0,35	0,35	0,30	0,14	0,15	0,14	0,17	0,13	0,12	0,15	0,14	0,10	0,15	0,12	0,13	0,18
TOTAL	99,10	99,66	100,3	99,77	99,7	100,20	100,92	100,87	100,53	99,03	101,00	101,03	100,19	100,34	100,28	100,18	100,03	100,29
Recalculated as cations per 8 oxygens																		
Si	2,261	2,363	2,358	2,447	2,397	2,216	2,206	2,216	2,228	2,235	2,224	2,220	2,230	2,230	2,239	2,240	2,193	2,253
Al	1,730	1,615	1,612	1,545	1,580	1,748	1,757	1,752	1,734	1,721	1,728	1,731	1,741	1,739	1,730	1,734	1,780	1,718
Fe	0,001	0,006	0,006	0,006	0,005	0,012	0,010	0,010	0,009	0,033	0,012	0,010	0,014	0,012	0,018	0,013	0,017	0,016
Ca	0,743	0,659	0,663	0,567	0,626	0,822	0,831	0,813	0,807	0,788	0,824	0,829	0,798	0,803	0,791	0,792	0,833	0,778
Na	0,274	0,354	0,376	0,410	0,392	0,216	0,212	0,229	0,247	0,249	0,240	0,238	0,223	0,228	0,229	0,220	0,179	0,232
K	0,006	0,018	0,020	0,020	0,017	0,008	0,009	0,008	0,010	0,008	0,007	0,009	0,008	0,006	0,009	0,007	0,008	0,010
SUM	5,015	5;015	5,035	4,995	5,017	5,022	5,025	5,028	5,035	5,034	5,035	5,037	5,014	5,018	5,016	5,006	5,010	5,007
Mol %																		
An	72,63	63,92	62,61	56,87	60,48	78,59	78,63	77,43	75,85	75,41	76,94	77,04	77,55	77,43	76,87	77,72	81,67	76,27
Ab	26,78	34,34	35,51	41,12	37,87	20,65	20,50	21,81	23,21	23,83	22,41	22,12	21,67	21,99	22,25	21,59	17,55	22,75
Or	0,59	1,74	1,88	2,01	1,65	0,76	0,87	0,76	0,94	0,76	0,65	0,84	0,78	0,58	0,88	0,69	0,78	0,98

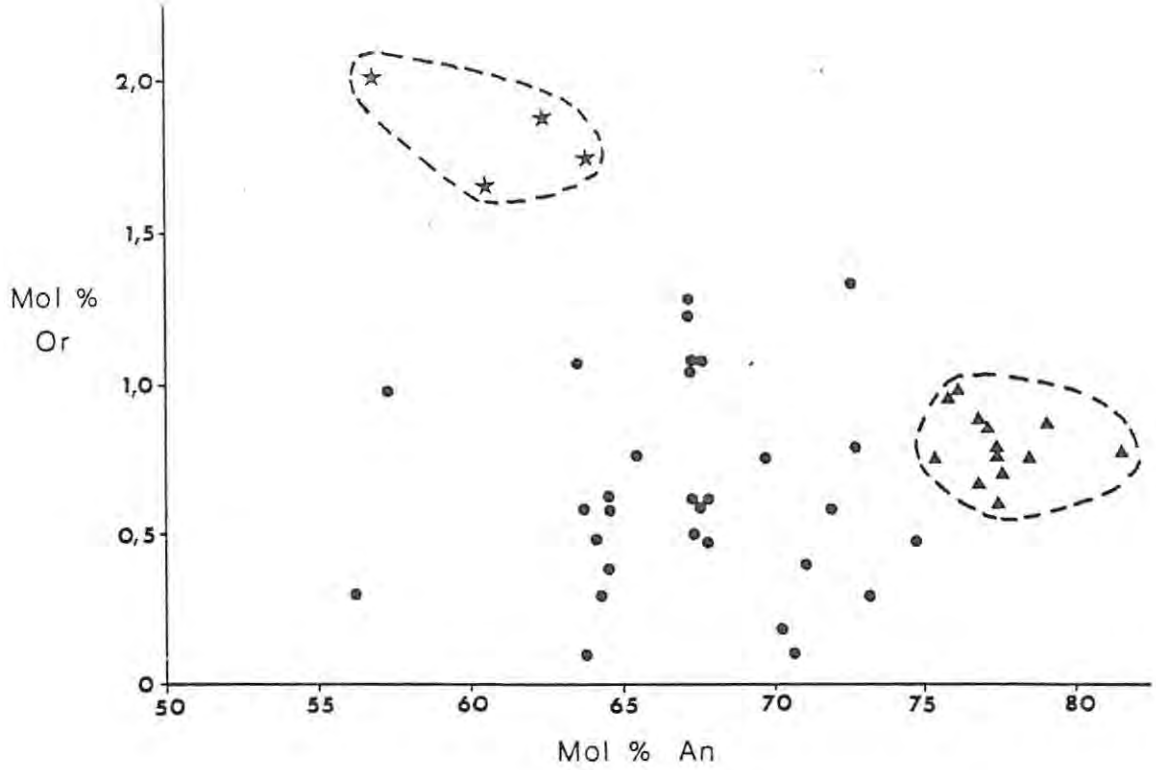

FIGURE 28: Diagram showing variation in Mol % Or and An from the Merensky unit feldspathic pyroxenites, B235/13 and 14 (★); intercumulus plagioclase for all harzburgites (●); and cumulus plagioclase in the Merensky unit B235/7-12 (▲).

8.5 Spinels

Although a detailed study of the oxide phases from the upper Critical zone was not attempted at this stage, 16 chromite analyses were performed by the author while learning how to operate the electron microprobe analyser. An additional 2 analyses were kindly made available by Dr. I. Reynolds (Table 4).

The bulk of the chromite data is from the UG 1 chromitite and associated country rocks, which were exposed

in borehole H212. This borehole was drilled only 50 m south-west of the composite pothole succession used in this study (B232 and B222). Eight chromite analyses from sample H212/1 in the anorthositic footwall of the main UG 1 chromitite were done, and all these disseminated chromite grains are hosted by cumulus plagioclase. Sample H212/3, from the feldspathic pyroxenite between the main UG 1 chromitite layers, has a rather high concentration (5% modal) of disseminated cumulus chromite. Eight analyses were done on this sample and of these, 5 were poikilitically enclosed in cumulus orthopyroxenes. The remainder are hosted by the intercumulus plagioclase.

The two analyses of sample B235/A are from a thin (2 cm) chromitite layer, situated in the pegmatoidal feldspathic pyroxenite below the main UG 2 layer. This sample is located in the normal Merensky Reef succession (B235) used in this study. For analytical methods refer to Appendix 2.

Microprobe data yield no information on the Fe^{3+}/Fe^{2+} ratio, which has to be assigned on a basis of calculation. The procedure followed by Eales et al. (1980) is adopted, where Ti is assigned to the ulvöspinel molecule when grains are optically isotropic, or ilmenite when weak, patchy anisotropism is apparent. The remaining elements are then assigned to spinels on the assumption of stoichiometry.

The generalised formula for the spinel-group minerals may be represented by the formula AB_2O_4, where cations of the A group include Fe^{2+}, Mg, Mn, Ni and Zn, those of the B group Cr, Al, Fe^{3+}, V and $(Fe^{2+}+Ti^{4+})$ (Eales, 1979). Wide variations exist in the relative proportions of the cations. Irvine (1965), pointed out that because chromite was a complex solid-solution series it should be a sensitive indicator of the course of fractionation. The

reaction relations of chromite with associated silicates, complicates the pattern of compositional variation (Cameron, 1977). Variations in composition with modal amounts of coexisting olivine and bronzite are well established (Van der Walt, 1941; Cameron and Desborough, 1969; Jackson, 1969) while compositional variations of chromites in plagioclase have been noted (Cameron, 1975).

Variations in the composition of the chromite analysed from the upper Critical zone are presented in Figures 29 and 30. In Figure 29, the Cr/Fe ratio, the Fe^{3+}/Fe^{3+}+Al+Cr ratio and the Mg/Mg+Tot Fe^{2+} ratios are all plotted against stratigraphic height. The chromites which are hosted by cumulus plagioclase in sample H212/1 appear to have a somewhat different composition to those hosted by cumulus orthopyroxene and intercumulus plagioclase in both H212/3 and B235/A. The Cr/Fe ratio and the Fe^{3+}/Fe^{3+}+Al+Cr ratio are marginally higher in H212/1 than the other analyses, while the Mg/Mg+Tot Fe^{2+} ratio is somewhat lower (Figure 29).

Figure 30 represents a portion of the ternary diagram Cr-Al-(Fe^{3}+2Ti). All 18 analyses plot in a very tight cluster. Insufficient data exist for a detailed discussion of the chromite composition variations. It appears however that the chromite which is hosted by cumulus plagioclase (H212/1) has a lower (Fe^{3}+2Ti) component and would appear to be slightly depleted in Al relative to the rest of the analyses.

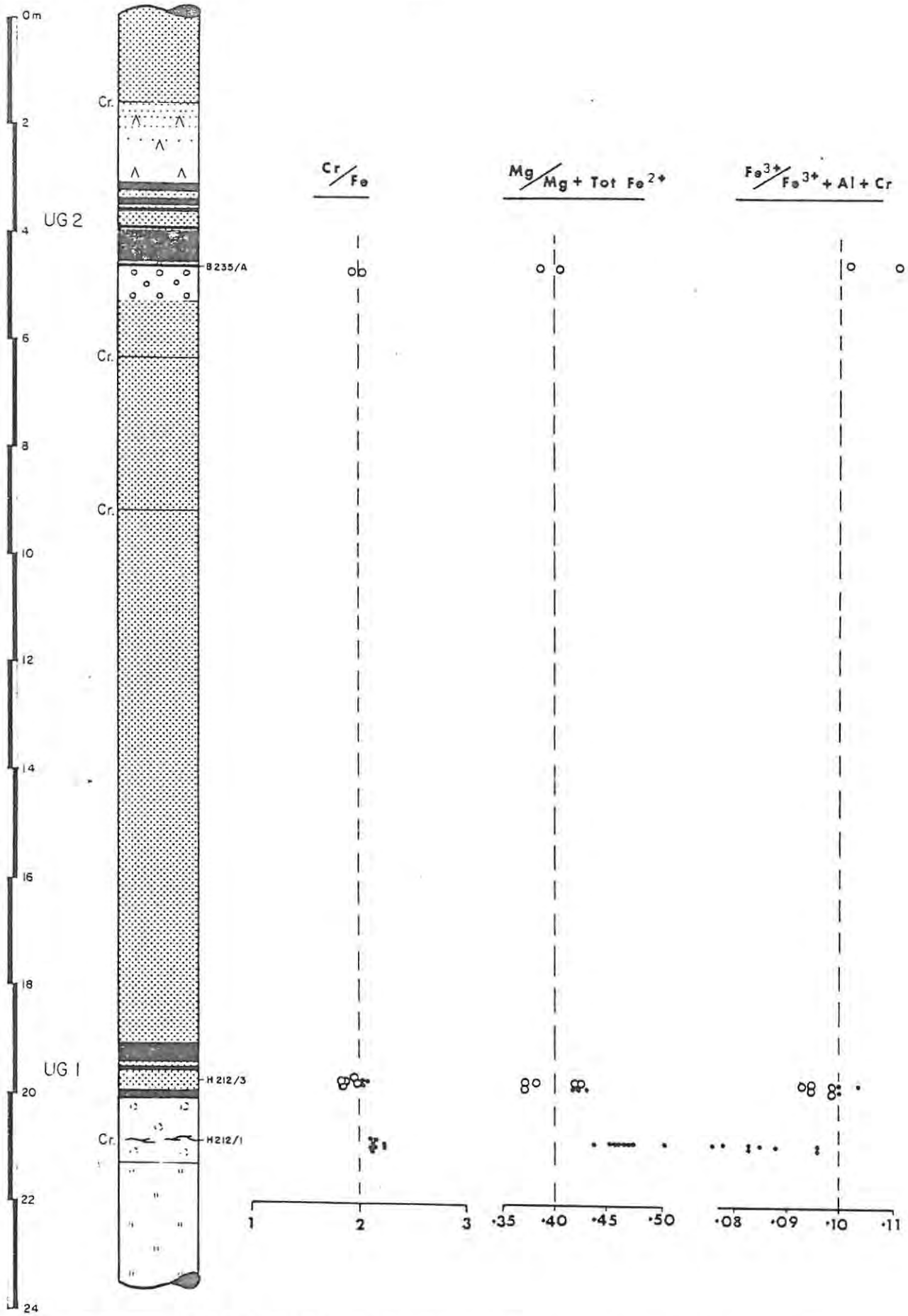

FIGURE 29: Stratigraphic variations in composition of some chromites from the upper critical zone. The chromite grains are hosted by both orthopyroxene (o) and plagioclase (·).

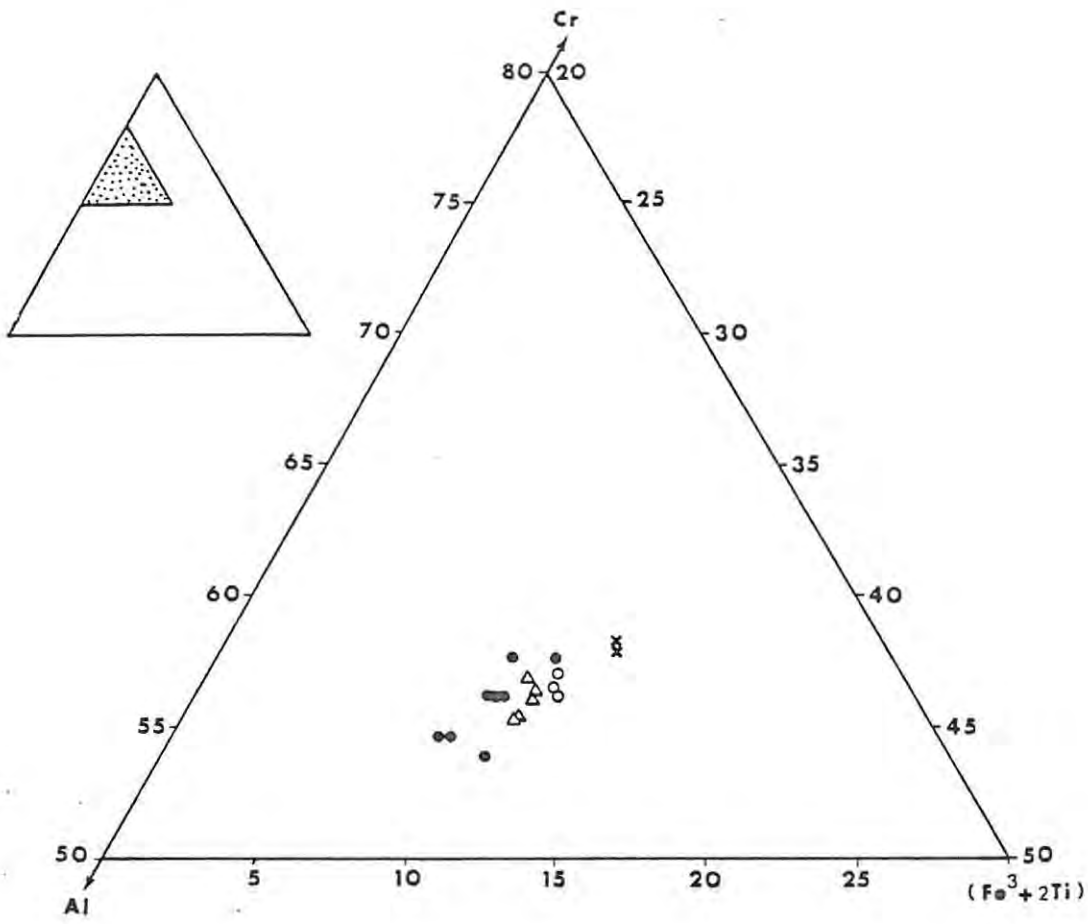

FIGURE 30: Cation percentages for 18 microprobe analyses of spinels from the upper Critical zone.

x B235/A in orthopyroxene

• H212/1 in cumulus plag.

o H212/3 in intercumulus plag.

△ H212/3 in cumulus opx.

TABLE 4: CHROMITE ANALYSES BY MICROPROBE

	B235/A* CORE	B235/A* MARGIN	H212/1 GRAIN 1	H212/1 GRAIN 2	H212/1 GRAIN 3	H212/1 GRAIN 4	H212/1 GRAIN 5	H212/1 GRAIN 6	H212/1 GRAIN 7	H212/1 GRAIN 8	H212/3 GRAIN 1	H212/3 GRAIN 2	H212/3 GRAIN 3	H212/3 GRAIN 4	H212/3 GRAIN 5	H212/3 GRAIN 6	H212/3 GRAIN 7	H212/3 GRAIN 8
TiO_2	0.89	1.21	0.70	0.53	0.67	0.63	0.68	0.69	0.70	0.62	0.75	0.74	0.60	0.64	0.60	0.75	0.69	0,72
Al_2O_3	15,01	14,81	19,23	19,45	18,88	17,93	17,53	17,85	16,29	17,02	17,44	17,66	16,65	16,78	16,59	16,42	16,29	16,52
Fe_2O_3	8,86	8,03	6,44	6,25	7,55	6,75	7,15	6,81	7,79	6,87	7,66	7,66	7,92	7,89	7,33	7,98	7,98	8,38
FeO	21,67	22,37	19,78	19,68	18,69	20,02	19,93	20,36	19,57	20,60	21,05	21,30	22,64	22,20	22,48	21,08	21,13	20,79
MnO	0,51	0,50	0,45	0,48	0,45	0,47	0,53	0,50	0,51	0,50	0,54	0,55	0,60	0,56	0,58	0,56	0,52	0,55
MgO	8,36	8,01	10,01	9,87	10,60	9,51	9,51	9,44	9,67	9,08	8,82	8,76	7,53	7,82	7,44	8,60	8,60	8,85
Cr_2O_3	44,62	44,56	43,42	43,17	42,81	43,91	43,87	44,25	44,83	44,90	43,19	43,18	43,31	43,04	43,23	43,62	44,10	43,60
NiO	0,17	0,14	0,16	0,12	0,10	0,11	0,11	0,11	0,11	0,13	0,19	0,16	0,18	0,17	0,18	0,16	0,17	0,20
TOTAL	100,09	99,63	100,19	99,55	99,76	99,33	99,31	100,01	99,48	99,73	99,64	100,02	99,43	99,11	98,43	99,18	99,48	99,62
Recalculated as cations per 32 oxygens.																		
Ti	0,18	0,24	0,13	0,10	0,13	0,12	0,13	0,13	0,14	0,12	0,15	0,14	0,12	0,13	0,12	0,15	0,14	0,14
Fe^2	0,18	0,24	0,13	0,10	0,13	0,12	0,13	0,13	0,14	0,12	0,15	0,14	0,12	0,13	0,12	0,15	0,14	0,14
Cr	9,26	9,31	8,73	8,73	8,62	8,98	8,99	9,00	9,21	9,21	8,87	8,83	9,02	8,97	9,09	9,05	9,13	8,99
Al	4,64	4,61	5,76	5,86	5,67	5,46	5,35	5,41	4,99	5,20	5,34	5,38	5,17	5.21	5.20	5.08	5.03	5,08
Fe^3	1,75	1,60	1,23	1,20	1,45	1,31	1,39	1,32	1,52	1,34	1,50	1,49	1,57	1,57	1,47	1,58	1,57	1,65
Fe^2	4,58	4,70	4,07	4,11	3,86	4,21	4,19	4,25	4,12	4,35	4,43	4,47	4,87	4,77	4,88	4,48	4,49	4,40
Mg	3,27	3,16	3,80	3,76	4,03	3,67	3,67	3,63	3,75	3,51	3,42	3,38	2,96	3,07	2,95	3,36	3,36	3,44
Mn	0,11	0,11	0,10	0,10	0,10	0,10	0,12	0,11	0,11	0,11	0,12	0,12	0,13	0,13	0,13	0,12	0,12	0,12
Ni	0,04	0,03	0,03	0,02	0,02	0,02	0,02	0,02	0,02	0,03	0,04	0,03	0,04	0,04	0,04	0,03	0,04	0,04
Host	OPX	OPX	PLAG	PLAG	PLAG	PLAG	PLAG	PLAG	PLAG	PLAG	OPX	OPX	OPX	OPX	OPX	PLAG	PLAG	PLAG

* Analyses done by Dr. I. Reynolds.

9. MAJOR ELEMENT GEOCHEMISTRY

9.1 Introduction

Major element analyses are presented for 47 samples from the upper Critical zone of the Bushveld Complex. A representative suite of 40 samples from the normal succession and 7 samples from comparable positions in the potholed succession was analysed, and all the results are presented in Tables 5 and 6. The positions of all 47 samples analysed are presented in Figure 14. The analyses were performed by Bergstrom and Bakker (analytical chemists), using conventional X-ray fluorescence spectrometry. Total Fe was determined as Fe_2O_3. FeO, which was also determined, enabled the recalculation of true Fe_2O_3 (Total Fe, expressed as Fe_2O_3 x 0,89981 ÷ FeO 0,89981 = True Fe_2O_3).

Two sets of C.I.P.W. weight percent norms were calculated. The first (Table 5) was done, using the analysed FeO and recalculated Fe_2O_3 values. The quality of the FeO analytical data is suspect here, as the C.I.P.W. norm indicates substantial magnetite and haematite, which is not apparent in thin section. In the second norm calculations (Table 6), an Fe_2O_3/FeO ratio of 0,2 was used, in keeping with previous work in this department by Robey (1976), Mitchell (1980) and others. An approach similar to that used by Irvine and Baragar (1971) for volcanic rocks, where they set an upper limit on Fe_2O_3 according to the equation

$$\% \ Fe_2O_3 = \% \ TiO_2 + 1{,}5$$

could have been used to obtain a more realistic norm.

9.2 Major Element Variation Diagrams

Major element variations are represented diagramma-

tically, using MgO weight percent as the abscissa, as it reflects the percentage of ferromagnesian minerals in the rocks (Figure 31 a to l). Major elements are also plotted against stratigraphic height to illustrate differences in chemistry between individual units (Figure 32 a to p).

Variations in the concentration of the major elements, with increasing MgO, clearly separate the different rock types into distinct chemical fields. The major elements are strongly influenced by the modal proportions of the major mineral phases - olivine, orthopyroxene, clinopyroxene and plagioclase, and the presence of base metal sulphides and oxides to a lesser degree. The rock types which have no olivine present include anorthosite, poikilitic anorthosites, norite (leuco- to mela-) and feldspathic pyroxenite, and the major elements of these rock types all fall on a straight line when plotted against MgO. The nine medium-grained and coarse pegmatoidal feldspathic harzburgites all plot in a field distinctly separate from the other samples.

SiO_2, TiO_2, FeO, Fe_2O_3 and MnO all increase with increasing MgO content. The feldspathic harzburgites all have SiO_2, TiO_2 (and to a lesser degree MnO) values that diverge sharply from the trend established for the pyroxene-plagioclase cumulates. There is a suggestion of a negative correlation of SiO_2 and TiO_2 for the 9 feldspathic harzburgites, with increasing MgO.

Al_2O_3, CaO, Na_2O and total alkalis all decrease in concentration with increasing MgO (Figures 31 c, h, j and l). In each case the feldspathic harzburgites reinforce the general trend at higher MgO levels. P_2O_5 and K_2O have extremely low concentrations and hence no clear correlation with MgO is observed (Figures 31 i and k).

Total Fe expressed as Fe_2O_3 has a definite positive correlation with MgO but when one considers FeO and Fe_2O_3 individually, the plot for Fe_2O_3 against MgO shows increasing slope (Figure 31 f), whereas that for FeO shows decreasing slope (Figure 31 e). The quality of the analytical data is suspect here, as these data imply either a modal increase in Fe oxides, or late-stage oxidation. Neither of these phenomena are apparent in thin section.

9.3 Major elements vs. stratigraphic height

Variations in the whole-rock major element chemistry between individual rhythmic units are presented in Figure 32 a to p. These variations must be interpreted with caution because they are influenced by the modal proportion of the major mineral phases. Trends are summarised as follows.

SiO_2, TiO_2, MnO, MgO and iron generally all increase toward the base of each unit, in Bastard Merensky and Footwall units. In the feldspathic harzburgite of the Merensky Reef SiO_2, TiO_2 and to a lesser degree MnO are relatively depleted. SiO_2 decreases slightly in the feldspathic harzburgite (Pseudo Marker layer) at the base of the Footwall unit.

Correspondingly, there is a sympathetic downward decrease in the Al_2O, CaO, Na_2O and K_2O contents of the three upper units, the above four elements also being excellent indicators of the unit boundaries. The pronounced breaks in the chemical trends at the base of the individual units are well defined for the upper three units, but distinct chemical breaks are not clearly defined in the Pseudo Reef, UG 2 and UG 1 units.

When one considers the chemical distribution in the Pseudo Reef, UG 2 and UG 1 units, cognizance should be taken

of the fact that one could quite well be dealing with incomplete or beheaded units, i.e. crystallization of the more feldspathic rock types such as norites and anorthosites was interrupted. Demarcation of the lower limits of these units is made rather on the basis of lithological changes or differences. MgO is the only major element which is useful in the demarcation of the boundary between the UG 2 and UG 1 units.

Because only the very basal portions of both the Pseudo units (upper and lower) are present, more data points would be required to establish any cryptic variation.

One feature of interest is a prominent break in the otherwise smooth chemical trend between the poikilitic anorthosite (mottled) and the underlying leuconorite of the Footwall unit. There is a distinct increase in SiO_2. MgO and Fe with a corresponding drop of CaO, Na_2O, K_2O and Al_2O_3 as one moves down across the contact. This break is explained by the abrupt change from intercumulus clino- and lesser orthopyroxene to cumulus orthopyroxene plus intercumulus clinopyroxene.

The level of P_2O_5, where detected by the analytical method used, is in these rocks, in all cases, $\leqslant$0,06%. The higher values of 0,05 and 0,06 are in all cases associated with the anorthosite and leuconorite. These findings are in agreement with those of Henderson (1968), who determined the P_2O_5 content of cumulate rocks, without primary apatite, from Skaergaard, Bushveld and Rhum. He found that the concentration of P_2O_5 was extremely low and that the order of entry of P into the cumulus minerals is olivine>plagioclase >pyroxene. Henderson (1968) pointed out that the use of P as a guide to the amount of interstitial material is feasible, provided a correction is made for the amount of P in the cumulus phases.

No significant variation is observed in the MgO/ MgO+FeO+0,9Fe_2O_3. Deviations from an average value of 0,68 only occur in rocks with very low modal mafic minerals, such as poikilitic anorthosites, and are therefore of dubious significance.

Figure 31 a-l: Major element variations (weight % oxides) using MgO as the abscissa

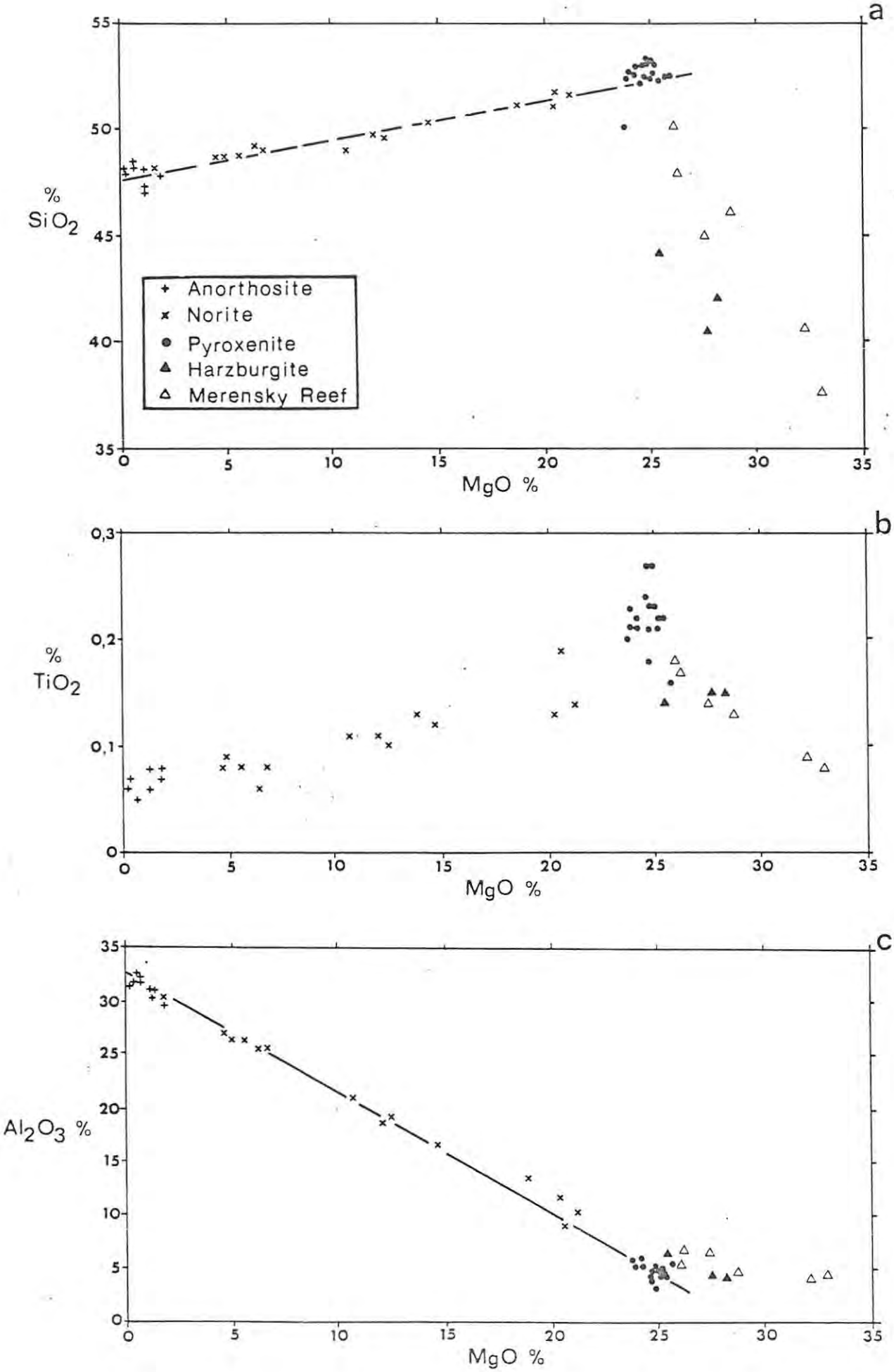

Figure 31 a-l: Major element variations (weight % oxides) using MgO as abscissa

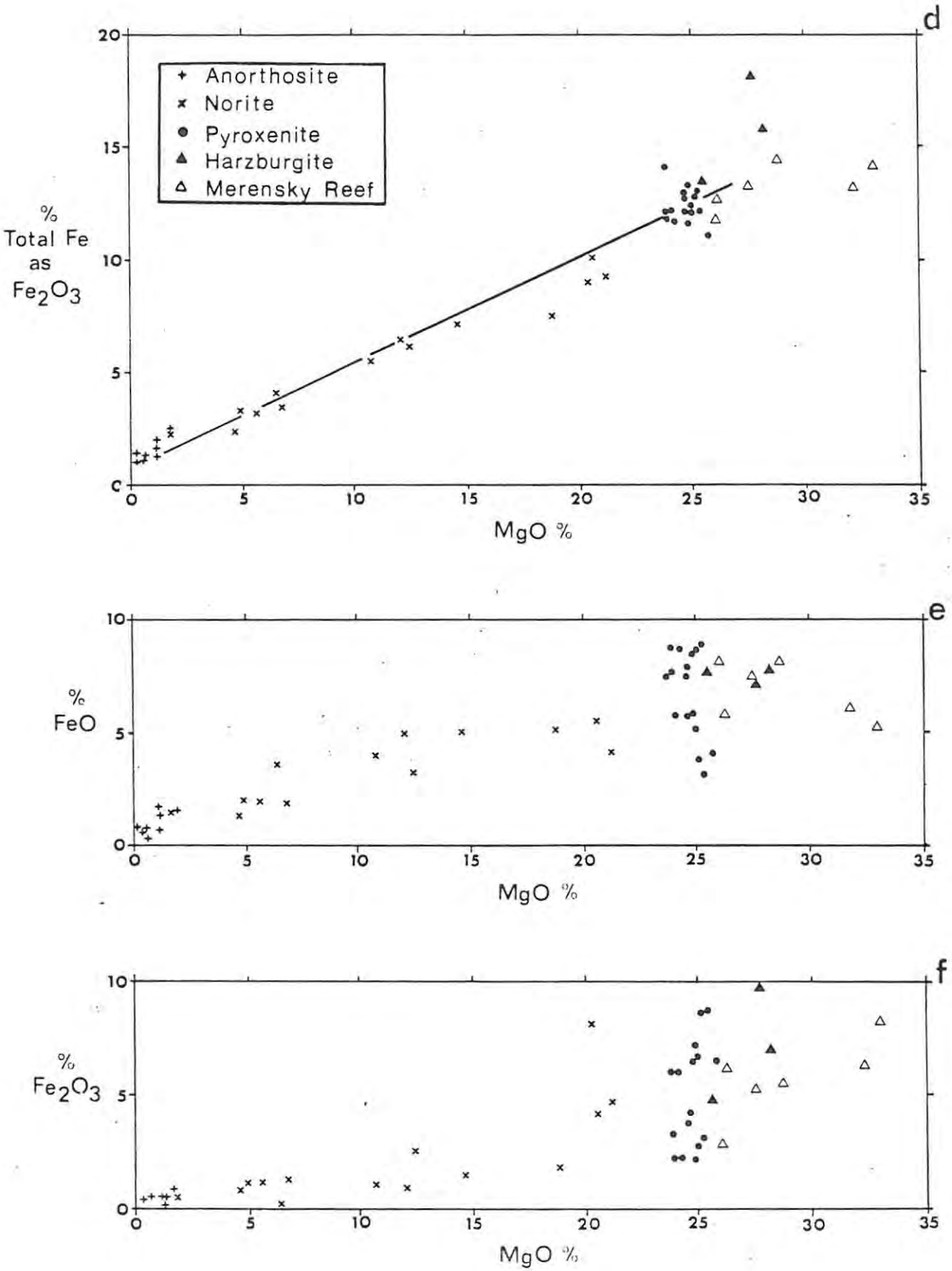

Figure 31 a-l: Major element variations (weight % oxides) using MgO as abscissa

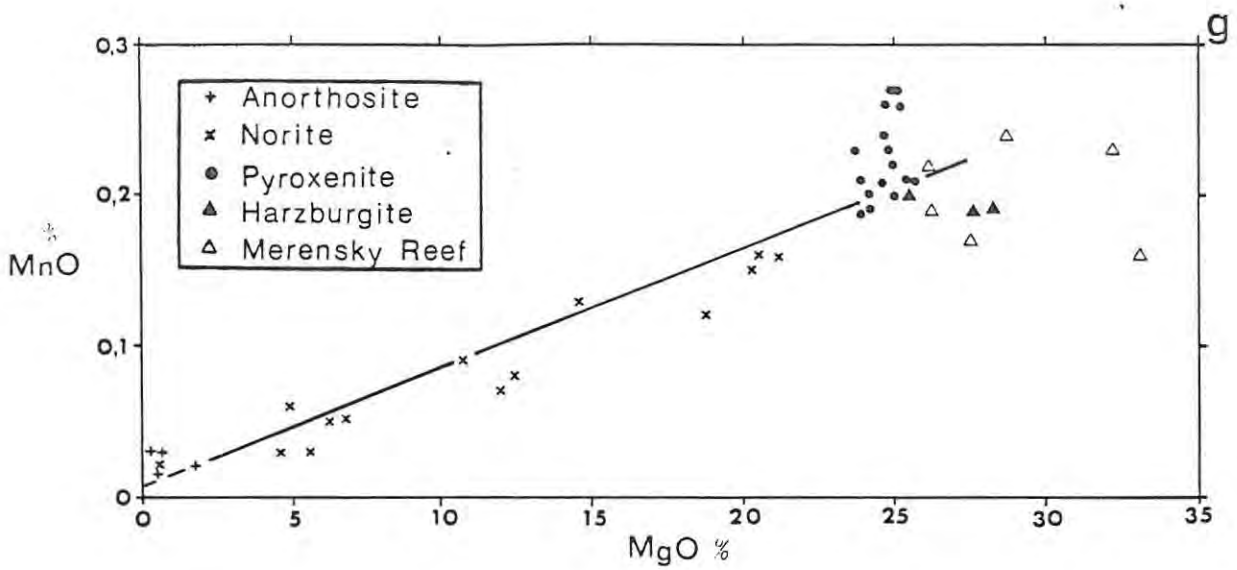

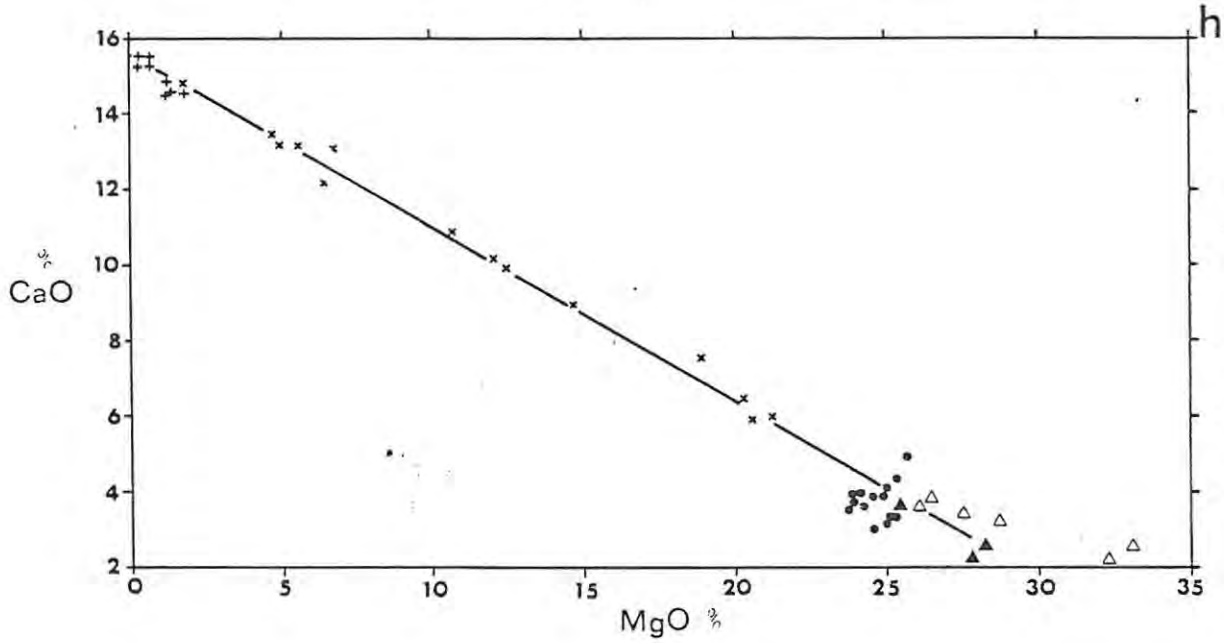

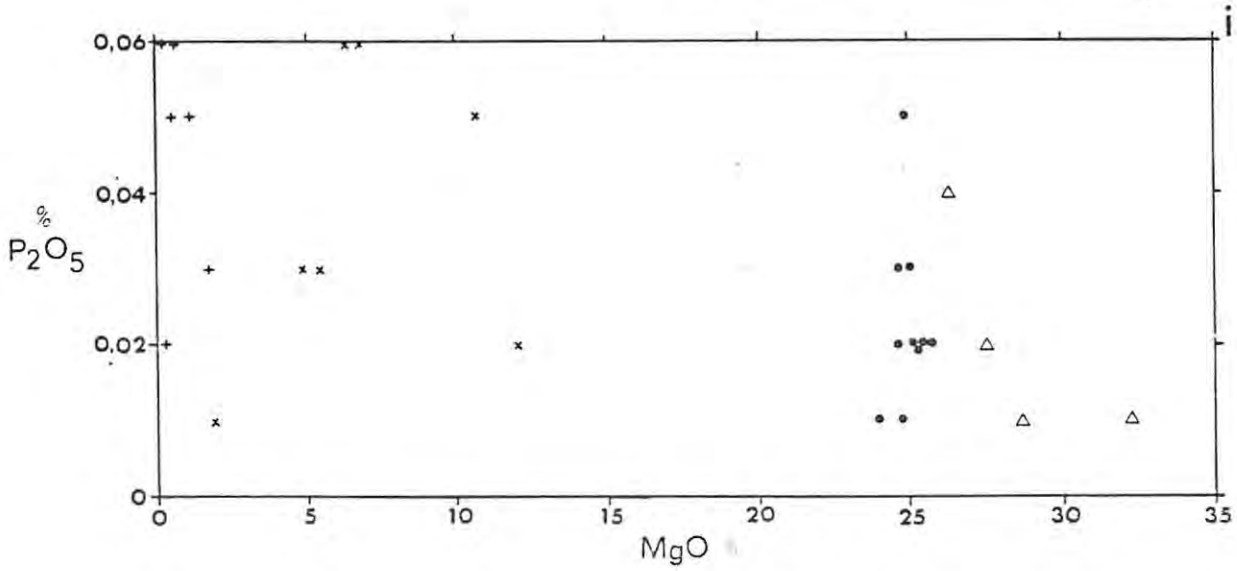

Figure 31 a-l: Major element variations (weight % oxides) using MgO as abscissa

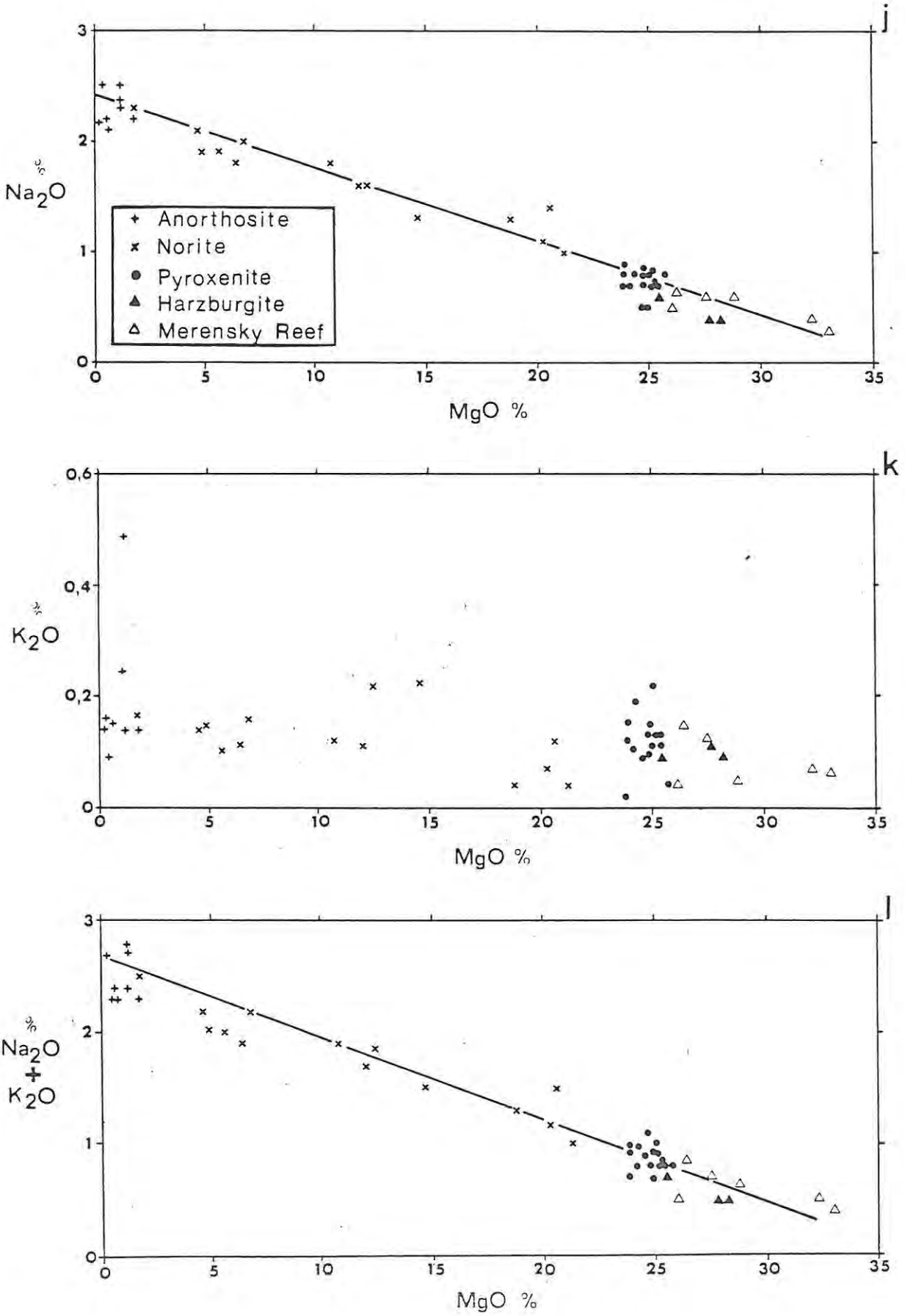

Figure 32 a-p: Major elements vs. stratigraphic height (+ pothole succession)

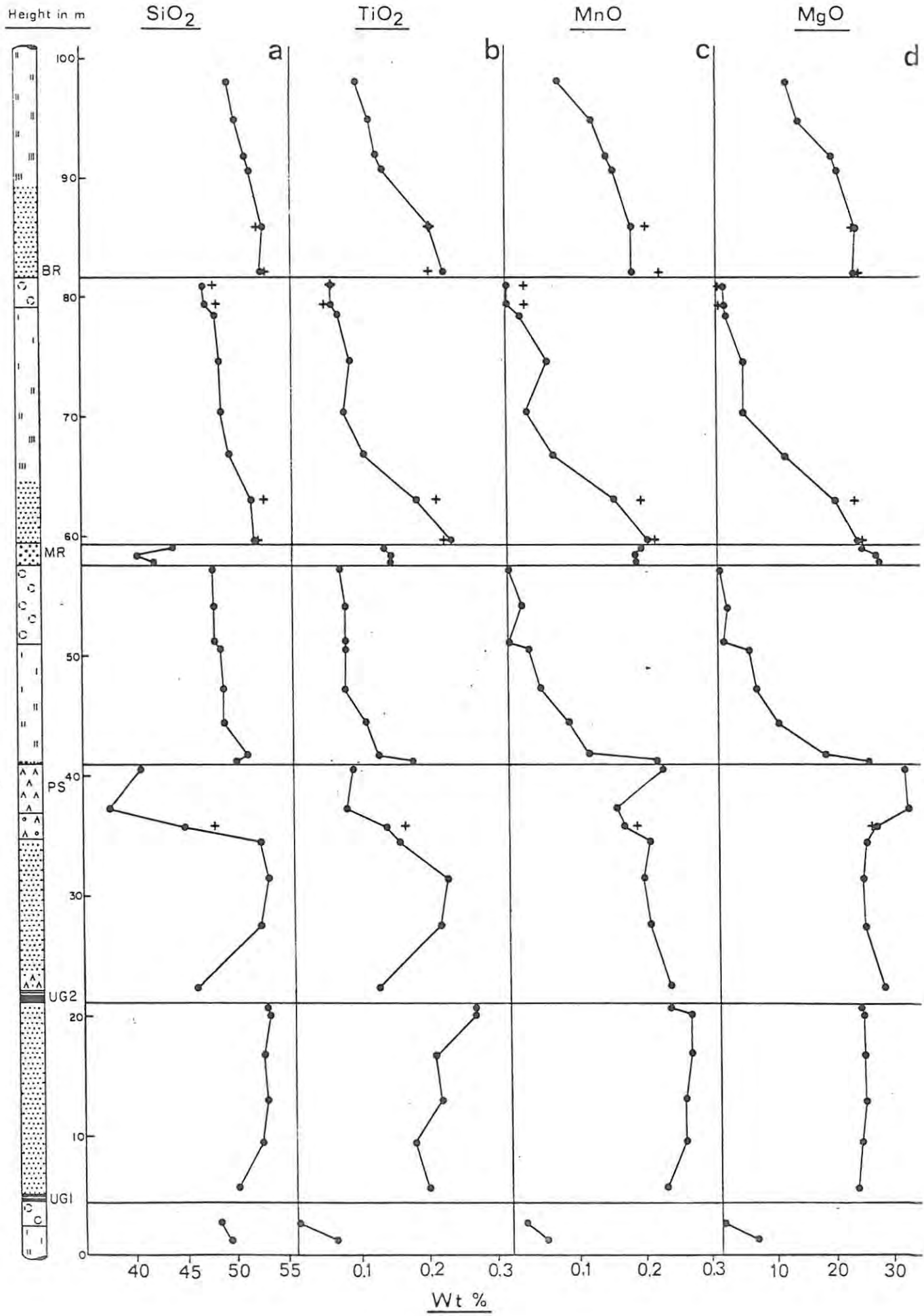

Figure 32 a-p: Major elements vs. stratigraphic height (+ pothole succession)

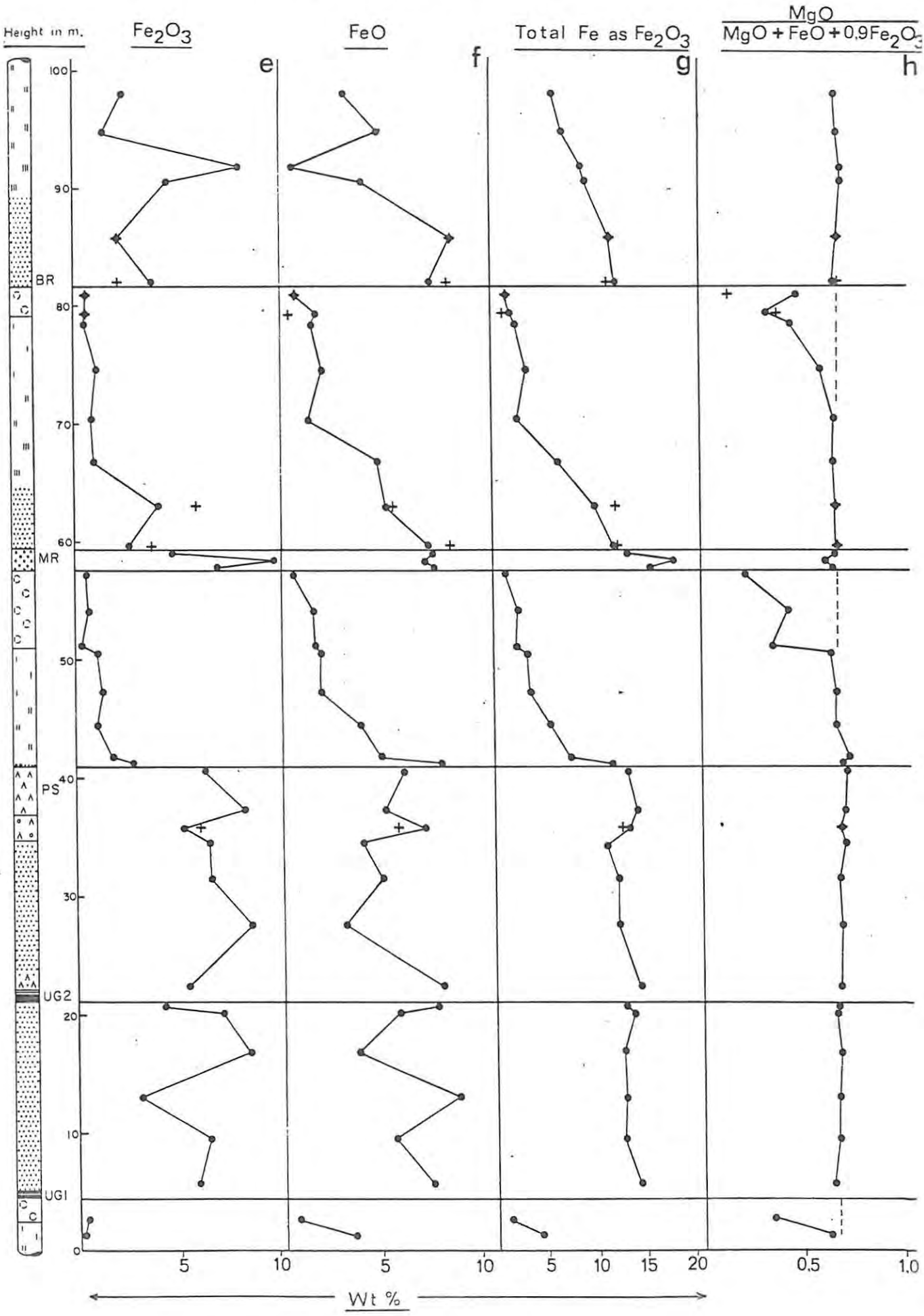

Figure 32 a-p: Major elements vs. stratigraphic height
(+ pothole succession)

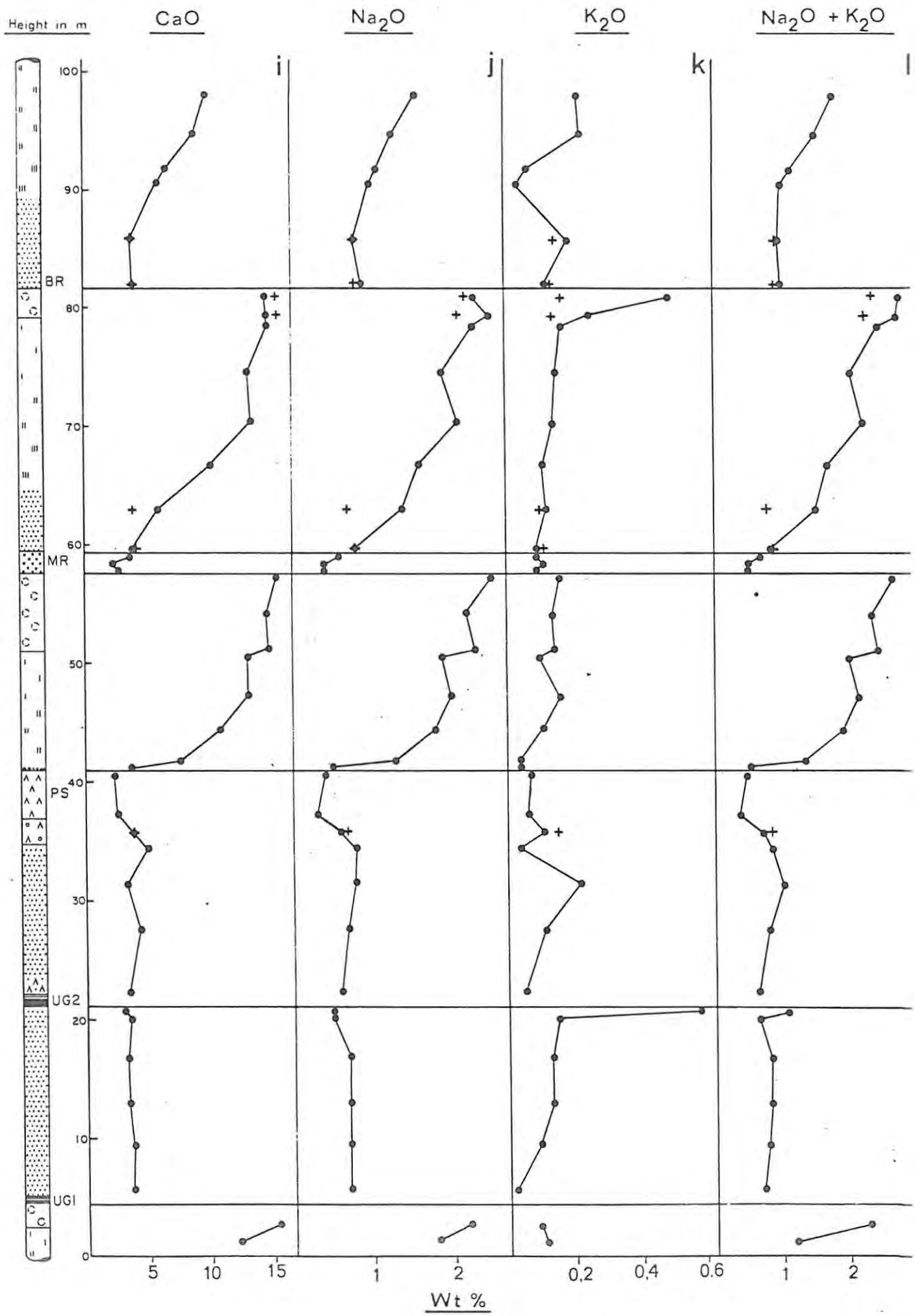

Figure 32 a-p: Major elements vs. stratigraphic height (+ pothole succession)

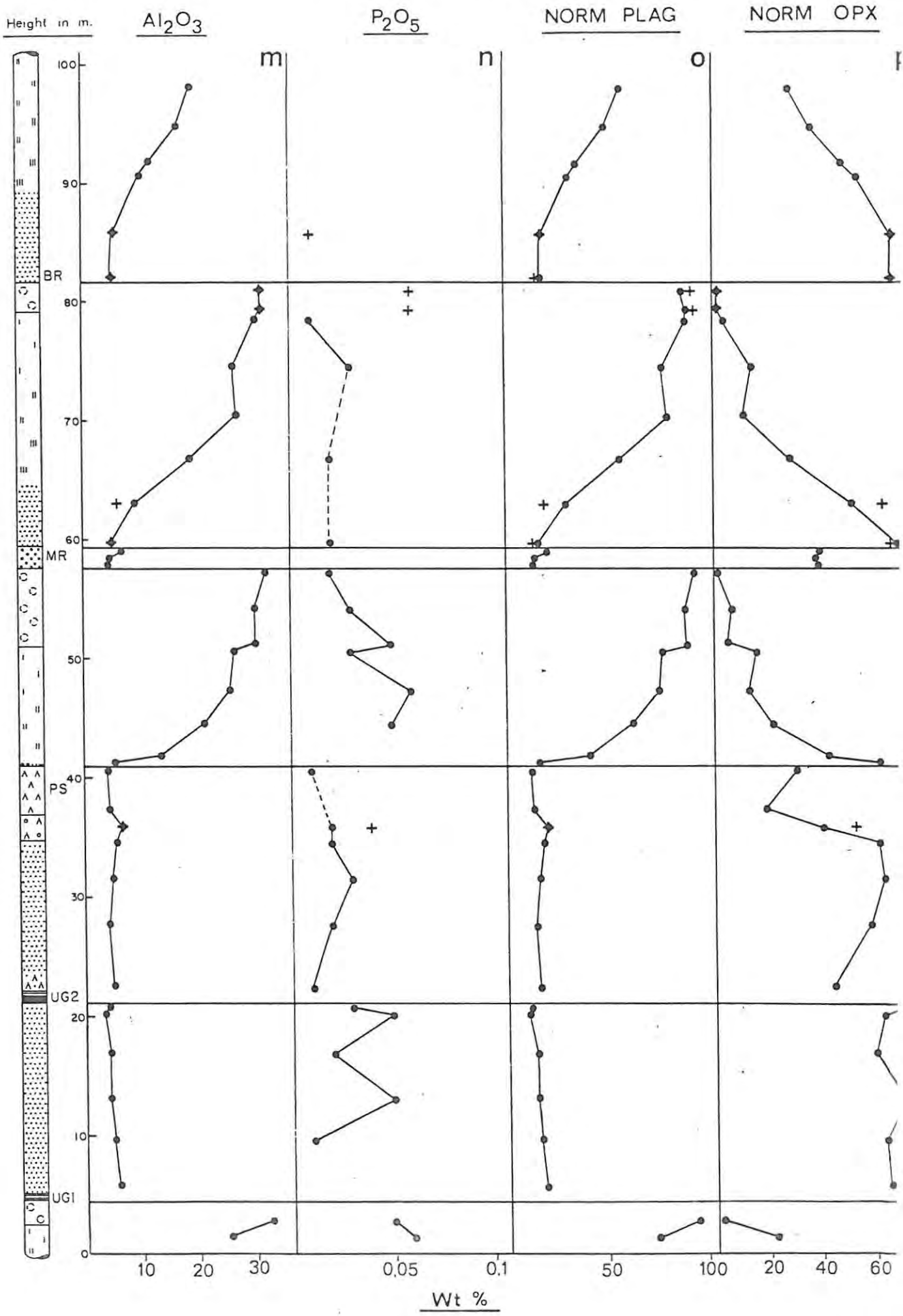

Rock-Type Code For All Rocks Analysed

B235/1 - N	B235/24 - H
2 - N	25 - H
3 - N	26 - H
4 - N	27 - H
5 - Px	28 - Px
6 - Px	29 - Px
7 - A	30 - Px
8 - A	31 - H
9 - N	32 - Px
10 - N	33 - Px
11 - N	34 - Px
12 - N	35 - Px
13 - Px	36 - Px
14 - Px	37 - Px
15 - H	38 - A
15[a] - H	39 - N
16 - H	B232/13 - Px
17 - A	12 - Px
18 - A	10 - A
19 - A	9 - A
20 - N	B222/25 - Px
21 - N	B232/ 2 - Px
22 - N	B222/19 - H
23 - N	

A - Anorthosites
N - Norites
Px - Pyroxenites
H - Harzburgites

TABLE 5 MAJOR ELEMENT ANALYSES (INCLUSIVE OF H_2O^+, CO_2 AND LOI) AND C.I.P.W. WEIGHT PERCENT NORMS

	N B235/1	N B235/2	N B235/3	N B235/4	Px B235/5	Px B235/6	A B235/7	A B235/8	N B235/9	N B235/10	N B235/11	N B235/12	Px B235/13	Px B235/14	H B235/15	H B235/15A
SiO_2	49,6	50,3	51,2	51,7	53,0	52,8	47,1	47,3	48,3	48,7	48,9	49,7	51,8	52,2	44,1	40,5
TiO_2	0,10	0,12	0,13	0,14	0,21	0,23	0,06	0,06	0,07	0,09	0,08	0,11	0,19	0,24	0,14	0,15
Al_2O_3	19,1	16,7	11,8	10,2	5,3	5,3	31,0	31,0	30,2	26,3	27,0	18,7	9,0	4,7	6,62	4,56
Fe_2O_3	2,5	1,5	8,3	4,7	2,2	3,9	0,51	0,50	0,47	1,09	0,84	0,92	4,2	3,8	4,9	10,0
FeO	3,3	5,0	0,6	4,2	8,6	7,6	0,8	1,8	1,6	2,1	1,4	5,0	5,4	7,5	7,7	7,3
MnO	0,08	0,13	0,15	0,16	0,19	0,19	0,0	0,0	0,02	0,06	0,03	0,07	0,16	0,21	0,20	0,19
MgO	12,5	14,6	20,3	21,2	24,3	23,9	1,2	1,2	1,7	4,9	4,6	12,0	20,5	24,5	25,4	27,6
CaO	9,9	8,9	6,7	6,0	3,7	4,0	14,6	14,7	14,8	13,2	13,5	10,2	5,9	3,87	3,66	2,28
Na_2O	1,6	1,3	1,1	1,0	0,8	0,9	2,3	2,5	2,3	1,9	2,1	1,6	1,4	0,8	0,6	0,4
K_2O	0,22	0,23	0,07	0,04	0,19	0,12	0,49	0,25	0,17	0,15	0,14	0,11	0,12	0,09	0,09	0,11
P_2O_5									0,01	0,03		0,02		0,02	ND	ND
H_2O+							2,1								4,91	5,80
CO_2							0,4								0,86	0,60
LOI	0,17	0,27	0,0	0,0	(+0,2)	(+0,1)	1,15	0,68	0,47	0,91	0,33	0,31	0,1	0,22	4,54	5,64
TOTAL	99,07	99,05	100,35	99,37	98,47	98,84	100,56	99,99	100,11	99,43	98,92	98,74	98,77	98,15	99,66	99,91
Ap	-	-	-	-	-	-	-	-	0,02	0,07	-	0,05	-	0,03	-	-
Cc	-	-	-	-	-	-	0,92	-	-	-	-	-	-	-	-	-
Il	0,19	0,23	0,24	0,26	0,39	0,43	0,11	0,11	0,13	0,17	0,15	0,21	0,36	0,46	0,26	0,28
Or	1,30	1,36	0,41	0,24	0,12	0,71	2,90	1,48	1,00	0,89	0,83	0,65	0,71	0,56	0,53	0,65
Ab	13,54	11,00	9,31	8,46	6,77	7,61	19,46	19,03	19,46	16,08	17,77	13,45	11,85	6,77	5,08	3,38
An	44,29	39,06	27,06	23,23	10,31	10,07	69,90	72,63	71,58	62,79	63,84	43,52	17,92	8,96	15,11	10,32
Mt	3,62	2,17	2,06	6,81	3,19	5,65	0,74	2,45	0,68	1,58	1,22	1,33	6,09	5,51	7,01	14,50
Hm	-	-	6,88	-	-	-	-	-	-	-	-	-	-	-	-	-
Di: En	1,54	1,58	2,23	2,23	2,47	3,10	-	0,07	0,44	0,76	1,01	2,07	3,74	3,23	0,98	0,34
Di: Fs	0,26	0,35	-	0,17	0,57	0,56	-	0,04	0,26	0,18	0,16	0,58	0,47	0,57	0,16	0,03
Di: Wo	2,02	2,13	2,58	2,73	3,36	4,08	-	0,12	0,74	1,04	1,31	2,90	4,74	4,24	1,27	0,41
Hy: En	24,34	30,46	48,32	50,56	54,76	56,42	1,46	-	2,19	11,44	10,44	22,24	45,86	57,08	34,20	35,40
Hy: Fs	4,16	6,69	-	3,74	12,66	10,16	0,46	-	1,28	2,74	1,64	6,23	5,78	9,95	5,54	2,71
Q	-	-	1,26	0,91	-	0,15	-	-	-	0,78	0,22	-	-	-	-	-
Fo	3,68	3,03	-	-	2,31	-	1,07	2,04	1,12	-	-	3,91	1,02	0,49	19,67	23,12
Fa	0,69	0,73	-	-	0,59	-	0,38	1,37	0,72	-	-	1,21	0,14	0,10	3,51	1,95

Ap	-	Apatite	Il	-	Ilmenite	Or	-	Orthoclase	Ab	-	Albite
An	-	Anorthite	Mt	-	Magnetite	En	-	Enstatite	Fs	-	Ferrosilite
Di	-	Diopside	Wo	-	Wollastonite	Hy	-	Hypersthene	Q	-	Quartz
Fo	-	Forsterite	Fa	-	Fayalite	Cc	-	Calcite	Hm	-	Haematite

TABLE 5 MAJOR ELEMENT ANALYSES (INCLUSIVE OF H_2O^+, CO_2 AND LOI) AND C.I.P.W. WEIGHT PERCENT NORMS

	H B235/16	A B235/17	A B235/18	A B235/19	N B235/20	N B235/21	N B235/22	N B235/23	H B235/24	H B235/25	H B235/26	H B235/27	Px B235/28	Px B235/29	Px B235/30	H B235/31
SiO_2	42,1	48,0	48,1	48,2	48,7	49,0	49,0	51,2	50,2	40,7	37,6	45,0	52,5	53,3	52,4	46,1
TiO_2	0,15	0,07	0,08	0,08	0,08	0,08	0,11	0,13	0,18	0,09	0,08	0,14	0,16	0,23	0,22	0,13
Al_2O_3	4,10	31,8	30,0	30,2	26,3	25,6	21,0	13,4	5,16	4,0	4,3	6,5	5,5	4,8	4,1	4,9
Fe_2O_3	7,10	0,49	0,61	0,26	1,05	1,28	1,04	1,8	2,8	6,4	8,41	5,3	6,6	6,7	8,7	5,5
FeO	7,8	0,6	1,6	1,7	2,0	2,0	4,0	5,1	8,1	6,2	5,3	7,2	4,1	5,1	3,2	8,1
MnO	0,19	0,0	0,02	0,0	0,03	0,05	0,09	0,12	0,22	0,23	0,16	0,17	0,21	0,20	0,21	0,24
MgO	28,1	0,3	1,7	1,1	5,5	6,7	10,6	18,7	26,0	32,2	33,0	27,5	25,7	25,0	25,4	28,7
CaO	2,62	15,5	14,6	14,8	13,1	13,1	10,8	7,52	3,67	2,23	2,50	3,7	4,9	3,21	4,3	3,4
Na_2O	0,4	2,5	2,2	2,3	1,9	2,0	1,8	1,3	0,5	0,4	0,3	0,6	0,8	0,8	0,7	0,6
K_2O	0,09	0,16	0,14	0,14	0,10	0,16	0,11	0,04	0,04	0,07	0,06	0,11	0,04	0,22	0,11	0,05
P_2O_5	ND	0,02	0,03	0,05	0,03	0,06	0,05	ND	ND	0,01	-	0,02	0,02	0,03	0,02	0,01
H_2O+	5,77							0,86	2,26	6,7	5,2	4,6				2,1
CO_2	1,25							0,43	0,54	0,4	0,2	0,35				0,4
LOI	5,25	0,36	0,13	0,10	0,18	0,20	0,16	0,18	1,35	6,8	7,9	2,94	0,04	0,07	0,19	1,37
TOTAL	100,59	99,80	99,21	98,93	98,97	100,23	98,76	100,65	100,01	99,63	97,11	101,19	100,57	99,66	99,55	100,23
Ap	-	0,05	0,07	0,12	0,07	0,14	0,12	-	-	0,02	-	0,07	0,05	0,07	0,05	0,02
Cc	-	-	-	-	-	-	-	-	-	0,92	0,46	0,80	-	-	-	0,92
Il	0,28	0,13	0,15	0,15	0,15	0,15	0,21	0,24	0,34	0,17	0,15	0,26	0,30	0,43	0,41	0,24
Or	0,53	0,95	0,83	0,83	0,59	0,95	0,65	0,24	0,24	0,41	0,35	0,65	0,24	1,30	0,65	0,30
Ab	3,38	20,09	18,61	19,46	16,08	16,92	15,23	11,00	4,23	3,38	2,54	5,08	6,77	6,77	5,92	5,08
An	9,13	75,08	71,57	71,67	62,94	60,41	48,90	30,61	11,72	8,47	10,21	14,72	11,30	8,86	7,72	10,53
Mt	10,29	0,71	0,88	0,38	1,52	1,86	1,51	2,61	4,06	9,28	12,19	7,86	9,57	9,71	10,38	7,97
Hm	-	-	-	-	-	-	-	-	-	-	-	-	-	-	1,54	-
Di: En	1,28	0,38	0,17	0,29	0,58	1,35	1,32	2,14	2,04	-	0,33	0,42	4,53	2,37	4,87	1,21
Di: Fs	0,16	0,30	0,09	0,29	0,12	0,21	0,32	0,36	0,40	-	0,01	0,06	0,16	0,15	-	0,18
Di: Wo	1,62	0,70	0,28	0,60	0,77	1,75	1,82	2,80	2,71	-	0,39	0,54	5,38	2,87	5,63	1,56
Hy: En	34,67	-	4,07	2,45	13,12	11,14	17,47	36,59	51,25	28,36	18,39	35,83	59,47	59,89	58,39	38,65
Hy: Fs	4,25	-	2,25	2,48	2,62	1,72	4,29	6,20	10,09	2,26	0,66	4,67	2,05	3,69	-	5,71
Q	-	-	0,11	0,12	0,24	-	-	-	-	-	-	-	0,72	3,49	3,81	-
Fo	23,84	0,26	-	-	-	2,94	5,33	5,49	7,84	36,32	44,48	22,58	-	-	-	22,15
Fa	3,22	0,22	-	-	-	0,50	1,44	1,03	1,69	3,18	1,76	3,25	-	-	-	3,61

TABLE 5 MAJOR ELEMENT ANALYSES (INCLUSIVE OF H_2O^+, CO_2 AND LOI) AND C.I.P.W. WEIGHT PERCENT NORMS

	Px B235/32	Px B235/33	Px B235/34	Px B235/35	Px B235/36	Px B235/37	A B235/38	N B235/39	Px B232/13	Px B232/12	A B232/10	A B232/9	Px B222/25	Px B232/2	H B222/19
SiO_2	53,0	53,3	52,7	53,0	52,5	50,0	48,3	49,3	52,5	53,1	48,2	48,5	53,1	52,5	48,0
TiO_2	0,27	0,27	0,21	0,22	0,18	0,20	0,0	0,06	0,21	0,21	0,06	0,05	0,22	0,23	0,17
Al_2O_3	4,0	3,2	4,3	4,1	4,8	5,7	32,6	25,2	5,5	4,85	31,5	31,8	5,9	4,8	6,8
Fe_2O_3	4,3	7,2	8,6	3,1	6,5	6,0	0,36	0,18	2,2	2,2	0,61	0,62	6,0	2,7	6,1
FeO	7,8	5,9	3,8	8,9	5,7	7,5	0,7	3,6	8,7	8,5	0,7	0,4	5,7	8,6	5,9
MnO	0,24	0,27	0,27	0,26	0,26	0,23	0,02	0,05	0,21	0,23	0,03	0,03	0,20	0,22	0,19
MgO	24,6	24,9	25,1	25,3	24,7	23,7	0,5	6,4	23,9	24,8	0,21	0,6	24,1	25,0	26,3
CaO	3,0	3,6	3,25	3,3	3,7	3,6	15,4	12,2	3,72	3,79	15,4	15,6	3,9	4,0	3,8
Na_2O	0,5	0,5	0,7	0,7	0,7	0,7	2,2	1,8	0,8	0,8	2,2	2,1	0,7	0,8	0,7
K_2O	0,58	0,15	0,13	0,13	0,09	0,02	0,09	0,11	0,15	0,13	0,17	0,14	0,1	0,11	0,15
P_2O_5	0,03	0,05	0,02	0,05	0,01	-	0,05	0,06	0,01	ND	0,06	0,06			0,04
H_2O+										0,66					3,6
CO_2										0,37					0,3
LOI	0,24	(+0,1)	0,10	(+0,16)	0,11	(+0,25)	0,12	0,65	(+0,05)	(+0,32)	0,17	0,14	0,13	(+0,11)	1,59
TOTAL	98,56	99,33	99,18	98,90	99,25	97,40	99,98	99,61	97,85	100,13	99,31	100,04	100,05	98,85	102,05
Ap	0,07	0,12	0,05	0,12	0,02	-	0,12	0,14	0,02	-	0,14	0,14	-	-	0,09
Cc	-	-	-	-	-	-	-	-	-	-	-	-	-	-	-
Il	0,51	0,51	0,39	0,41	0,34	0,38	-	0,11	0,39	0,39	0,11	0,09	0,41	0,43	0,32
Or	3,43	0,89	0,77	0,77	0,53	0,12	0,53	0,65	0,89	0,77	1,00	0,83	0,59	0,65	0,89
Ab	4,23	4,23	5,92	5,92	5,92	5,92	18,61	15,23	6,77	6,77	18,61	17,77	5,92	6,77	5,92
An	6,96	6,03	8,21	7,66	9,69	12,35	76,07	60,13	10,97	9,26	75,58	76,93	12,66	9,18	14,97
Mt	6,23	10,44	12,47	4,49	9,42	8,70	0,52	0,26	3,19	3,19	0,88	0,90	8,70	3,91	8,84
Hm	-	-	-	-	-	-	-	-	-	-	-	-	-	-	-
Di: En	2,46	3,91	2,81	2,59	2,91	1,78	-	-	2,26	2,94	0,07	0,02	2,25	3,30	0,58
Di: Fs	0,43	0,31	-	0,57	0,25	0,27	-	-	0,54	0,66	0,11	-	0,21	0,72	0,05
Di: Wo	3,23	4,80	3,25	3,50	3,59	2,30	-	-	3,10	3,98	0,18	0,03	2,79	4,45	0,72
Hy: En	58,80	58,10	59,70	58,33	58,60	57,07	1,25	15,82	53,97	54,84	0,45	1,47	57,76	52,38	48,16
Hy: Fs	10,35	4,64	0,04	12,88	5,04	8,63	1,03	6,41	12,89	12,33	0,63	0,19	5,32	11,44	4,32
Q	1,62	5,36	5,48	-	2,82	-	1,09	-	-	-	1,36	1,52	3,30	-	-
Fo	-	-	-	1,46	-	0,12	-	0,08	2,30	2,79	-	-	-	4,61	11,74
Fa	-	-	-	0,36	-	0,02	-	0,04	0,60	0,69	-	-	-	1,11	1,16

TABLE 6 MAJOR ELEMENT ANALYSES (WHERE $Fe_2O_3/FeO = 0,2$) AND C.I.P.W. WEIGHT PERCENT NORMS

	N B235/1	N B235/2	N B235/3	N B235/4	Px B235/5	Px B235/6	A B235/7	A B235/8	N B235/9	N B235/10	N B235/11	N B235/12	Px B235/13	Px B235/14	H B235/15	H B235/15A
SiO_2	49,6	50,3	51,2	51,7	53,0	52,8	47,1	47,3	48,3	48,7	48,9	49,7	51,8	52,2	44,1	40,5
TiO_2	0,10	0,12	0,13	0,14	0,21	0,23	0,06	0,06	0,07	0,09	0,08	0,11	0,19	0,24	0,14	0,15
Al_2O_3	19,1	16,7	11,8	10,2	5,3	5,3	31,0	31,0	30,2	26,3	27,0	18,7	9,0	4,7	6,62	4,56
Fe_2O_3	0,95	1,08	1,37	1,43	1,80	1,88	0,21	0,26	0,34	0,52	0,37	0,99	1,56	1,85	2,06	2,76
FeO	4,73	5,41	6,86	7,17	9,00	9,38	1,07	1,29	1,72	2,61	1,83	4,94	7,78	9,23	10,30	13,80
MnO	0,08	0,13	0,15	0,16	0,19	0,19	0,0	0,0	0,02	0,06	0,03	0,07	0,16	0,21	0,20	0,19
MgO	12,5	14,6	20,3	21,2	24,3	23,9	1,2	1,2	1,7	4,9	4,6	12,0	20,5	24,5	25,4	27,6
CaO	9,9	8,9	6,7	6,0	3,7	4,0	14,6	14,7	14,8	13,2	13,5	10,2	5,9	3,87	3,66	2,28
Na_2O	1,6	1,3	1,1	1,0	0,8	0,9	2,3	2,5	2,3	1,9	2,1	1,6	1,4	0,8	0,6	0,4
K_2O	0,22	0,23	0,07	0,04	0,19	0,12	0,49	0,25	0,17	0,15	0,14	0,11	0,12	0,09	0,09	0,11
P_2O_5									0,01	0,03		0,02		0,02	ND	ND
H_2O+							2,1								4,91	5,80
CO_2							0,4								0,86	0,60
LOI	0,17	0,27	0,0	0,0	(+0,2)	(+0,1)	1,15	0,68	0,47	0,91	0,33	0,31	0,1	0,22	4,54	5,64
TOTAL	98,95	99,04	99,68	99,04	98,29	98,60	100,53	99,24	100,10	99,37	98,88	98,75	98,51	97,93	98,94	98,75
Ap	-	-	-	-	-	-	-	-	0,02	0,07	-	0,05	-	0,05	-	-
Il	0,19	0,23	0,24	0,26	0,39	0,43	0,11	0,11	0,13	0,17	0,15	0,21	0,36	0,45	0,26	0,28
Or	1,30	1,36	0,41	0,24	1,12	0,71	2,90	1,48	1,00	0,89	0,83	0,65	0,71	0,53	0,53	0,65
Ab	13,54	11,00	9,31	8,46	6,77	7,61	17,89	18,90	19,46	16,08	17,77	13,54	11,85	6,77	5,08	3,38
An	44,29	39,06	25,69	23,23	10,31	10,07	72,43	72,63	71,58	62,79	63,84	43,52	17,92	8,97	15,11	10,32
Mt	1,38	1,57	1,99	2,07	2,61	2,73	0,30	0,38	0,49	0,75	0,54	1,44	2,26	2,68	2,99	4,00
Di: En	1,46	1,55	2,32	2,01	2,44	2,94	-	0,07	0,43	0,71	0,95	2,08	3,43	3,06	0,91	0,28
Di: Fs	0,37	0,39	0,53	0,46	0,61	0,77	-	0,05	0,28	0,25	0,25	0,57	0,87	0,77	0,25	0,10
Di: Wo	2,02	2,13	3,15	2,73	3,36	4,08	-	0,12	0,74	1,04	1,31	2,90	4,74	4,22	1,27	0,41
Hy: En	21,42	29,16	37,70	42,81	53,46	50,72	-	-	1,94	11,49	9,63	22,42	37,93	51,25	27,29	18,96
Hy: Fs	5,43	7,29	8,60	9,78	13,30	13,34	-	-	1,28	4,08	2,51	6,16	9,65	12,96	7,49	6,39
Q	-	-	-	-	-	-	-	-	-	0,14	-	-	-	-	-	-
Fo	5,78	3,96	7,38	5,59	3,24	4,10	2,09	2,04	1,31	-	0,62	3,78	6,79	4,70	24,56	34,68
Fa	1,61	1,09	1,86	1,41	0,89	1,19	1,31	1,55	0,96	-	0,18	1,14	1,90	1,31	7,43	12,88

Ap	-	Apatite	Il	-	Ilmenite	Or	-	Orthoclase
An	-	Anorthosite	Mt	-	Magnetite	En	-	Enstatite
Di	-	Diopside	Wo	-	Wollastonite	Hy	-	Hypersthene
Fo	-	Forsterite	Fa	-	Fayalite	Ab	-	Albite
Fs	-	Ferrosilite	Q	-	Quartz			

TABLE 6 MAJOR ELEMENT ANALYSES (WHERE $Fe_2O_3/FeO = 0,2$) AND C.I.P.W. WEIGHT PERCENT NORMS

	H B235/16	A B235/17	A B235/18	A B235/19	N B235/20	N B235/21	N B235/22	N B235/23	H B235/24	H B235/25	H B235/26	H B235/27	Px B235/28	Px B235/29	Px B235/30	H B235/31
SiO_2	42,1	48,0	48,1	48,2	48,7	49,0	49,0	51,2	50,2	40,7	37,6	45,0	52,5	53,3	52,4	46,1
TiO_2	0,15	0,07	0,08	0,08	0,08	0,08	0,11	0,13	0,18	0,09	0,08	0,14	0,16	0,23	0,22	0,13
Al_2O_3	4,10	31,8	30,0	30,2	26,3	25,6	21,0	13,4	5,16	4,0	4,3	6,5	5,5	4,8	4,1	4,9
Fe_2O_3	2,41	0,18	0,36	0,33	0,50	0,53	0,84	1,14	1,80	2,03	2,18	2,03	1,71	1,89	1,88	2,21
FeO	12,05	0,88	1,82	1,64	2,49	2,67	4,18	5,71	9,00	10,14	10,91	10,14	8,54	9,46	9,38	11,06
MnO	0,19	0,0	0,02	0,0	0,03	0,05	0,09	0,12	0,22	0,23	0,16	0,17	0,21	0,20	0,21	0,24
MgO	28,1	0,3	1,7	1,1	5,5	6,7	10,6	18,7	26,0	32,2	33,0	27,5	25,7	25,0	25,4	28,7
CaO	2,62	15,5	14,6	14,8	13,1	13,1	10,8	7,52	3,67	2,23	2,50	3,7	4,9	3,21	4,3	3,4
Na_2O	0,4	2,5	2,2	2,3	1,9	2,0	1,8	1,3	0,5	0,4	0,3	0,6	0,8	0,8	0,7	0,6
K_2O	0,09	0,16	0,14	0,14	0,10	0,16	0,11	0,04	0,04	0,07	0,06	0,11	0,04	0,22	0,11	0,05
P_2O_5	ND	0,02	0,03	0,05	0,03	0,06	0,05	ND	ND	0,01	-	0,02	0,02	0,03	0,02	0,01
H_2O+	5,77							0,86	2,26	6,7	5,2	4,6				2,1
CO_2	1,25							0,43	0,54	0,4	0,2	0,35				0,4
LOI	5,25	0,36	0,13	0,10	0,18	0,20	0,16	0,18	1,35	6,8	7,9	2,94	0,04	0,07	0,19	1,37
TOTAL	99,23	99,77	99,18	98,94	98,91	100,15	98,74	100,55	100,92	99,20	96,49	100,86	100,12	99,21	98,91	99,90
Ap	-	0,05	0,07	0,12	0,07	0,14	0,12	-	-	0,02	-	0,05	0,05	0,07	0,05	0,02
Il	0,28	0,13	0,15	0,15	0,15	0,15	0,21	0,24	0,34	0,17	0,15	0,26	0,30	0,43	0,41	0,24
Or	0,53	0,95	0,83	0,83	0,59	0,95	0,65	0,24	0,24	0,41	0,35	0,65	0,24	1,30	0,65	0,30
Ab	3,38	19,71	18,61	19,46	16,08	16,92	15,23	11,00	4,23	3,88	2,54	5,08	6,77	6,77	5,92	5,08
An	9,13	75,08	71,57	71,67	62,94	60,41	48,90	30,61	11,72	8,91	10,21	14,72	11,30	8,86	7,72	10,53
Mt	3,49	0,26	0,52	0,48	0,72	0,77	1,22	1,65	2,61	2,94	3,16	2,94	2,48	2,74	2,73	3,20
En (Di)	1,15	0,26	0,16	0,30	0,54	1,26	1,31	2,09	1,99	0,65	0,68	1,06	3,97	2,08	4,09	1,89
Fs (Di)	0,33	0,46	0,11	0,28	0,16	0,33	0,35	0,43	0,47	0,14	0,15	0,26	0,89	0,53	1,02	0,49
Wo (Di)	1,62	0,70	0,28	0,60	0,77	1,75	1,82	2,80	2,71	0,87	0,92	1,46	5,38	2,87	5,63	2,62
En (Hy)	23,78	-	3,71	2,44	12,12	9,18	16,95	34,64	48,64	16,27	4,92	25,92	46,24	54,68	49,75	28,39
Fs (Hy)	6,88	-	2,59	2,33	3,62	2,44	4,48	7,11	11,39	3,49	1,10	6,45	10,41	13,89	12,36	7,44
Q	-	-	-	0,19	-	-	-	-	-	-	-	-	-	-	-	-
Fo	31,57	0,34	0,26	-	0,72	4,38	5.71	6,90	9,89	44,34	53,67	29,08	9,66	3,86	6,59	28,87
Fa	10,07	0,69	0,20	-	0,24	1,28	1,66	1,56	2,55	10,50	13,24	7,97	2,39	1,08	1,80	8,33

TABLE 6 MAJOR ELEMENT ANALYSES (WHERE $Fe_2O_3/FeO = 0,2$) AND C.I.P.W. WEIGHT PERCENT NORMS

	Px B235/32	Px B235/33	Px B235/34	Px B235/35	Px B235/36	Px B235/37	A B235/38	N B235/39	Px B232/13	Px B232/12	A B232/10	A B232/9	Px B222/25	Px B232/2	H B222/19
SiO_2	53,0	53,3	52,7	53,0	52,5	50,0	48,3	49,3	52,5	53,1	48,2	48,5	53,1	52,5	48,0
TiO_2	0,27	0,27	0,21	0,22	0,18	0,20	0,0	0,06	0,21	0,21	0,06	0,05	0,22	0,23	0,17
Al_2O_3	4,0	3,2	4,3	4,1	4,8	5,7	32,6	25,2	5,5	4,85	31,5	31,8	5,9	4,8	6,8
Fe_2O_3	1,98	2,11	1,95	1,98	1,95	2,18	0,17	0,64	1,81	1,77	0,21	0,16	1,88	1,88	1,94
FeO	9,91	10,52	9,76	9,91	9,76	10,91	0,87	3,19	9,07	8,85	1,06	0,81	9,38	9,38	9,69
MnO	0,24	0,27	0,27	0,26	0,26	0,23	0,02	0,05	0,21	0,23	0,03	0,03	0,20	0,22	0,19
MgO	24,6	24,9	25,1	25,3	24,7	23,7	0,5	6,4	23,9	24,8	0,21	0,6	24,1	25,0	26,3
CaO	3,0	3,6	3,25	3,3	3,7	3,6	15,4	12,2	3,72	3,79	15,4	15,6	3,9	4,0	3,8
Na_2O	0,5	0,5	0,7	0,7	0,7	0,7	2,2	1,8	0,8	0,8	2,2	2,1	0,7	0,8	0,7
K_2O	0,58	0,15	0,13	0,13	0,09	0,02	0,09	0,11	0,15	0,13	0,17	0,14	0,1	0,11	0,15
P_2O_5	0,03	0,05	0,02	0,05	0,01	-	0,05	0,06	0,01	ND	0,06	0,06	-	-	0,04
H_2O+										0,66					3,6
CO_2										0,37					0,3
LOI	0,24	(+0,1)	0,10	(+0,16)	0,11	(+0,25)	0,12	0,65	(+0,05)	(+0,32)	0,17	0,14	0,13	(+0,11)	1,59
TOTAL	98,35	98,77	98,49	98,79	98,76	96,99	100,32	99,66	97,83	99,56	99,27	99,99	99,61	98,81	101,68
Ap	0,07	0,12	0,05	0,12	0,02	-	0,12	0,14	0,02	-	0,14	0,14	-	-	0,09
Il	0,51	0,51	0,39	0,41	0,34	0,38	-	0,11	0,39	0,39	0,11	0,09	0,41	0,43	0,32
Or	3,43	0,89	0,77	0,77	0,53	0,12	0,53	0,65	0,89	0,77	1,00	0,83	0,59	0,65	0,89
Ab	4,23	4,23	5,92	5,92	5,92	5,92	18,61	15,23	6,77	6,77	18,61	17,77	5,92	6,77	5,92
An	6,96	6,04	8,21	7,66	9,69	12,35	76,07	60,13	10,97	9,26	75,58	76,93	12,66	9,18	14,97
Mt	2,87	3,06	2,83	2,87	2,83	3,16	0,25	0,93	2,62	2,57	0,30	0,23	2,73	2,73	2,81
En (Di)	2,31	3,41	2,34	2,52	2,58	1,61	-	-	2,24	2,91	0,04	0,01	2,01	3,23	1,10
Fs (Di)	0,63	0,97	0,62	0,67	0,69	0,50	-	-	0,57	0,70	0,15	0,01	0,53	0,81	0,27
Wo (Di)	3,23	4,80	3,25	3,50	3,59	2,30	-	-	3,10	3,98	0,18	0,03	2,79	4,45	1,51
En (Hy)	56,14	57,45	54,58	54,94	52,59	45,67	1,25	15,94	52,76	53,63	0,48	1,48	54,30	49,90	34,89
Fs (Hy)	15,19	16,35	14,39	14,55	14,11	14,19	1,49	5,33	13,48	12,92	1,59	1,32	14,19	12,59	8,67
Q	-	-	-	-	-	-	0,89	0,47	-	-	0,91	1,00	-	-	-
Fo	1,97	0,81	3,91	3,89	4,45	8,23	-	-	3,17	3,66	-	-	2,60	6,40	20,68
Fa	0,59	0,25	1,14	1,14	1,32	2,82	-	-	0,89	0,97	-	-	0,75	1,78	5,66

10. TRACE ELEMENT GEOCHEMISTRY

10.1 Introduction

McCarthy and Lee (1981) have pointed out that the interpretation of trace element abundance data in cumulus rocks is made difficult by the complexity of the origin of such rocks: they consist of one or more cumulus minerals with variable amounts of adcumulate growth; the relative proportions of the cumulus minerals may vary considerably over short vertical or lateral distances; cumulate rocks also contain variable amounts of crystallised interstitial melt. The chemistry of the cumulus minerals therefore does not reflect the composition of the magma body as a whole, but only that portion of melt adjacent to the solid-melt interface.

McCarthy and Lee (op.cit.) also point out that this interstitial melt differs from the magma as a whole by different degrees for different trace elements: differences are large for trace elements with very large bulk partition coefficients, but they are small where the partition coefficients are near unity. All these variables combine to introduce scatter in trace element abundances in cumulates, making interpretation difficult. Quantitative techniques such as have been developed for treating melt abundance data (e.g. Allegre et al., 1977; Minster et al., 1977) cannot readily be applied and it is often necessary to generalise when interpreting data.

The major element data have shown the nature of rhythmic layering and in this chapter the whole-rock trace element data are presented. In the following sections, individual trace elements are discussed in terms of simple

binary diagrams of trace element plotted against MgO (Figure 34 a to i) and against stratigraphic height (Figure 35 a to k). The discussion of the trace element data is broadly divided into incompatible and compatible trace elements. The elements analysed for are Rb, Sr, Y, Zr, Nb, Co, V, Cr, Cu and Ni (Table 7). All these analyses were done by the author, except for Cu and Ni, which were done by Bergström and Bakker. Further information regarding the trace element analyses is presented in Appendix 1.

10.2 Incompatible Trace Elements

Incompatible trace elements are those which have partition coefficients very much less than unity in all the cumulus mineral phases. Included in the study are the elements Rb, Y, Zr and Nb. The abundance of these elements in cumulus rocks is determined principally by the quantity of trapped interstitial melt and the concentrations in that melt at the time of entrapment, the latter varying continually as crystallization proceeds. It is for this reason, McCarthy and Lee (op.cit) point out, that the abundances of such elements correlate positively, irrespective of the mineralogy of the cumulate. Plots of Zr vs Y and Rb vs Y are shown in Figure 33 a and b. Reasonably good positive correlation is evident in spite of gross mineralogical differences.

10.2.1 Rubidium (Rb) Where Rb is high enough in concentration to be analysed with precision, there is a good correlation between Rb and K values (compare Figure 35 a, and Figure 32 k). Rb and K have similar electronegativities and ionization potentials. The size of Rb (1,47 Å) is very

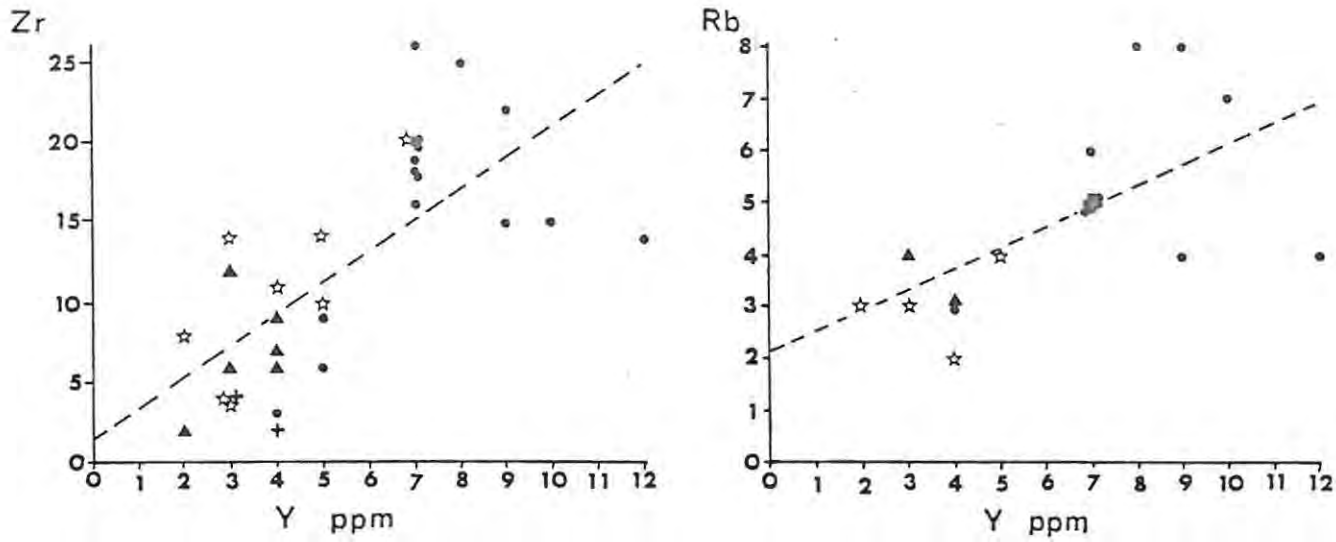

Figure 33 a and b: Plots of Zr vs. Y, and Rb vs. Y for whole-rock analyses. Note that the slope (m), of the curve Y = mx+c, is the interelement ratio. For (a) the Zr/Y = 2,1 and for (b) $\frac{Rb}{Y}$ = 0,6. The symbols for the various rock types are: norite (▲), harzburgite (☆), pyroxenite (•) and anorthosite (+).

close to, but slightly larger than K (1,33 Å). Rb readily enters K positions in alkali-feldspars, but shows a marked preference for entry into the micas (Taylor, 1965). Mitchell (1980) has pointed out that from available partition coefficient data, it may be concluded that Rb will enrich progressively in a differentiating system of basic magma.

Rb values in this study section are generally very low, ranging from 3-22 ppm. The average value is 5 ppm. There does not appear to be any preferred concentration in any one particular rock type, and the highest values obtained were 15 ppm (B235/7) in a poikilitic anorthosite, 8 ppm (B235/29) in a feldspathic pyroxenite and 22 ppm (B235/32) in the pegmatoidal feldspathic pyroxenite footwall of the

UG 2.

In all three cases there is a corresponding high K value. No reasonable explanation is afforded for the anomalously high value in B235/7 (poikilitic anorthosite) except that if one accepts the concept of a bottom-crystallizing magma, then this sample would represent the last crystallization product of the Merensky unit and one could possibly expect Rb enrichment in this fractionating system. This argument is not supported by the observed low Rb values in B232/10, which is the corresponding stratigraphic sample in the potholed succession, nor is it supported by B235/17, which forms the top of the Footwall unit (Figure 35 a). There is, however, a suggestion of a possible Rb increase toward the top of the Bastard unit norites, but unfortunately no poikilitic anorthosites from the top of this unit were sampled.

The high Rb value of 22 ppm, which occurs at the top of the UG 1 unit could be explained by the process of enrichment toward the top of a fractionating system, with the concentration of Rb aided by an alkali-ion enriched fluid towards the end of UG 1 unit crystallization. There is a higher concentration of biotite mica in this layer and, as was pointed out earlier, Rb shows a marked preference for entry into the micas, and partition coefficients of up to 3,1 (Cox et al., 1979) have been quoted (see also Table 8). The assignment of Rb to the "incompatible" group depends therefore on the phases separating during the earlier stages of magma crystallization.

10.2.2 <u>Zirconium (Zr) and Niobium (Nb)</u> Zr, Y and Nb, together with the major element Ti, are all elements with a high field strength, i.e. charge/radius ratio (Pearce and Norry, 1979). Zr, which has an ionic radius of 0,79 Å, does not enter any of the major cation sites in common

cumulus minerals, concentrating itself rather in the residual liquid and ultimately crystallizing as zircon. Zr may substitute to a limited extent for Ti in early Ti-Fe oxides (Taylor, 1965; Walker, 1970), or enter pyroxene and apatite (Table 8). As was pointed out earlier (10.2) Zr and Y show a positive correlation (Figure 33 a),which was also noted by Walker (1970).

The Zr values throughout the succession are quite variable and range from 2-26 ppm, with the pegmatoidal feldspathic pyroxenite footwall of the UG 2 (B235/32) having the highest value of 52 ppm. There is a general increase in the Zr values towards the base of the Bastard and Merensky Units. Other Zr values are quite erratic with no real pattern emerging throughout. As Zr increases in concentration in the intercumulus liquid during fractional crystallization, one could possibly expect an up-section concentration, as the intercumulus liquid migrates upward through the crystalline mush due to compaction effects. This displacement would be stratigraphically higher than the modal breaks, as observed by Irvine (1978) in the Muskox intrusion. He ascribes this to the process of infiltration metasomatism. This model could possibly explain the higher Zr and Y values at the base of the Merensky and Bastard units in their respective feldspathic pyroxenites (Figure 35 c and d).

Although Nb was analysed for in all samples, only one feldspathic pyroxenite in the Bastard unit had a value above the lower limit of analytical detection, namely B 235/5, with a value of 5 ppm.

10.2.3 <u>Yttrium (Y)</u> In comparison with the major elements, Y, which has an ionic radius of 0.98 A, lies between F^{2+} (0,76 Å) and Ca^{2+} (1,01 Å), though closer to the latter. This close assocation of Ca and Y has been

discussed by Lambert and Holland (1974). Compared with average basalt melts, plagioclase and augite have low Y values for their CaO content, while orthopyroxene has high Y values for its CaO content.

In all igneous series the Ca/Y ratio falls as Ca falls. Lambert and Holland (op.cit.) identify Ca minerals as Y-acceptors or rejectors, according to whether their Ca/Y ratio is less or greater than 2000 respectively. Orthopyroxene, which is defined as an acceptor, generally has a range of Y values from 10-30 ppm, with an average of 24 ppm (Green, 1964; Ewart and Taylor, 1969). Olivine has a value of only 1,57 ppm, reported by Schmitt et al. (1963), and would therefore not be of quantitative significance. The important factor governing Y in plagioclase appears to be the inability of the structure to accept trivalent ions.

Much like the Rb values in the study section, Y is rather low in concentration. There is an average value of 6 ppm throughout, with a range of 2-12 ppm. The feldspathic pyroxenites in the succession have the largest range, from 4-12 ppm, and all the other rock types have values below 5 ppm. Where data are sufficiently abundant when plotted against stratigraphic height (Figure 35 c), there is a strong suggestion that Y increases towards the base of the Merensky, Footwall and UG 2 units (excluding B235/31, feldspathic harzburgite at the base of the UG 2 unit). A reverse trend, i.e. a general downward decrease, is evident for the UG 1 unit and the upper two samples of the Basal unit.

10.3 Compatible Trace Elements

Compatible trace elements are those which have partition coefficients greater than unity for a particular

phase. Compatible trace elements in this study include Sr, Cr, Co, V, Ni and to a limited extent Cu. McCarthy and Lee (1981) have pointed out that there are problems in interpreting compatible trace element abundances in cumulate rocks: the problem of the diluting effect of other cumulus phases for which the partition coefficient is small, and the presence of intercumulus melt and of more than one phase into which a particular trace element may be strongly partitioned.

They suggest that ideally, only monomineralic rocks should be used to reduce the problem: alternatively trace element analyses of mineral separates would overcome this problem. Ratios of elements may be used, but these are not entirely satisfactory and do not overcome the effect of intercumulus material. Cawthorn and McCarthy (1980) have also pointed out that the compatible trace elements also tend to be more sensitive to the mechanisms of crystallization - whether by Rayleigh or diffusion control.

A large proportion of the rock units throughout the study section do approach being monomineralic assemblages, while others are only two-phase assemblages, and thus the interpretation of results is made that much simpler.

10.3.1 Strontium (Sr) Because of the intermediate ionic radius of Sr^{2+} (1,18 Å) which lies between that of Ca^{2+} (1,01 Å) and K^{+} (1,33 Å), Sr^{2+} may distribute itself equally between Ca^{2+} and K^{+}-bearing phases. The partition coefficient for Sr (D_{Sr}) between plagioclase and liquid has been measured by various workers (Sun et al., 1974; Philpotts and Schnetzler, 1970; Korringa and Noble, 1971), and data suggest that values of D_{Sr} vary between 1-3 for calcic

plagioclase, while the value increases with decreasing An% of the plagioclase (Jensen, 1973). D_{Sr}, determined by Korringa and Noble (1971) for various An contents, is as follows: An_{30}=7,0; An_{45}=5,4; An_{60}=3,8; An_{75}=2,3 and An_{90}=1,5. As long as Sr cannot enter a fractionating phase, it will be enriched in the residual liquid and act as an incompatible trace element, but because plagioclase occurs throughout the study section, Sr is partitioned into this mineral.

Korringa and Noble (1971) have also pointed out that the separation of plagioclase from mafic and relatively Ca-rich intermediate melts will tend slightly to raise the Sr/Ca ratio of the residual liquid. They go on further to say that a more marked increase in the Sr/Ca ratio will result from the crystallization of clinopyroxene, which does not readily accept Sr into its structure.

The Sr values of all samples analysed range from 33-470 ppm, the lower values being from the poikilitic feldspathic pyroxenites (33 - 81 ppm), the higher values from the more feldspathic rock types such as the poikilitic anorthosites (379 - 470 ppm) and a wide range in norites (114 - 390 ppm). The pegmatoidal and medium-grained feldspathic harzburgites of the Merensky Reef, Pseudo Reef and the UG 2 hanging wall have rather low values, from 58 - 80 ppm, which compares favourably with the Sr in the poikilitic feldspathic pyroxenites throughout the study section of 33-81 ppm (Figure 34 b and Figure 35 b). This could well reflect a similar modal plagioclase count in these two rock types. Stratigraphically equivalent samples in potholed succession are, in all seven cases, very similar to the normal succession (Figure 35 b), except the second sample above the Merensky Reef (B222/25) where a 62 ppm difference occurs.

This anomaly is explained by a lower modal percentage of intercumulus plagioclase at this position in the potholed succession. In each of the well-defined rhythmic units, i.e. the Bastard, Merensky and Footwall units, there is a gradual decrease downwards in the Sr concentration with well-defined breaks at the base of each unit. This pattern is not as clearly defined in the UG 2 and UG 1 units, but a sharp break is observed at the start of the Basal unit.

Ferguson and Wright (1970) noted that Sr appears preferentially to enter the cumulus plagioclase, depriving the later-crystallized intercumulus plagioclase of this trace element. They also note that during cyrstallization of the intercumulus plagioclase, Sr^{2+} appears to distribute itself equally between Ca^{2+} and K^{+}. When allocating the whole-rock Sr to the normative plagioclase, an interesting pattern emerges when plotted against stratigraphic height (Figure 35 k). There is a steady drop in value in the Bastard unit from 406 - 320 ppm at the base. This drop could possibly be explained by the preferential inclusion of Sr in the cumulus plagioclase in the norite at the top of the unit, when compared with the intercumulus plagioclase at the base. The calculated value of 406 ppm Sr in plagioclase compares favourably with values analysed from mineral separates of plagioclase from the top of the Bastard unit in the Rustenburg area (Kruger, 1981).

The average calculated Sr values in plagioclase for the Bastard, Merensky and Footwall units are 358, 433 and 483 ppm respectively, which strongly suggests a progressive depletion of Sr as crystallization proceeded, or if one accepts the concept of new magma influxes or heaves, that these influxes were progressively depleted in Sr. The calculated Sr in plagioclase for the UG 2, UG 1 and Basal units is not as clearly defined as the upper three units, although there is a suggestion of a depletion in the UG 2

and UG 1 units, with average values of 438 and 358 ppm respectively. There is, however, a sharp increase in the Basal unit, up to 493 ppm.

If one plots the whole-rock Sr value against normative plagioclase for all 47 rocks analysed, a value of 464 ppm Sr is obtained when the curve is projected to 100% normative plagioclase.

10.3.2 Chromium (Cr) Cr and Ni partition strongly into the early cumulus phases, and are therefore sensitive indicators of fractionation (Irvine and Smith, 1967; Irvine, 1965). Cr and V also compete with one another for the Fe sites in mineral lattices. Cr partitions readily into clino- and orthopyroxene, but is rejected by plagioclase (Table 8). Mitchell (1980) has suggested that the partition coefficient figures for Cr into olivine (D^{ol}_{Cr}), quoted by Flower (1973), are perhaps unrealistically high and are (perhaps) the result of small Cr-Spinel inclusions in the olivine (Gunn, 1971). In view of this consideration, D^{ol}_{Cr} evaluations should be treated with caution. Experimental data quoted by Irvine (1978) indicate a D^{ol}_{Cr} in the region of unity. The partition coefficient of Cr in pyroxene is sensitive to both temperature and fO_2 (Irvine, 1978), and furthermore its abundance relationship in whole-rocks is complicated by the ubiquitous presence of disseminated cumulus chromite. McCarthy and Lee (1981) suggest therefore that Cr is an unsuitable monitor of fractionation.

The values of Cr in the majority of rocks analysed range between 55 - 4390 ppm (Figure 34 e and Figure 35 e). Those samples that contained disseminated cumulus chromite have values far in excess of the above values, i.e. B235/34 and B235/37, which have values of 6384 and 14555 ppm respectively. As Cr partitions preferentially into the

pyroxenes, it is the feldspathic pyroxenites that have the higher Cr values, which range from 2263 - 4390 ppm. The poikilitic anorthosites, which are low in pyroxene, range from 14 - 178 ppm, with the exception of B235/38, which has a value of 889 ppm. This can be accounted for by disseminated cumulus chromite in the footwall of the UG 1. The norites range in value from 212 - 2786 ppm.

Although there is a lower modal percentage of orthopyroxene in the Merensky reef as compared with the Merensky pyroxenite above it, there is a higher Cr concentration in the Reef itself. This is explained by an abundance of cumulus disseminated chromite throughout the Merensky Reef. There is a notable increase of Cr throughout the succession towards the base of each unit. An identical distribution is quoted for the Macro-rhythmic units of the Jimberlana Intrusion by Campbell (1977).

The poikilitic anorthosites are generally low in Cr, with an average value of 88 ppm because of their lower modal intercumulus pyroxene, but the anorthosite below the UG 1 (B235/38) in the Basal unit, although being almost devoid of pyroxene, has a Cr value of 889 ppm. As has been noted in a previous section (4.5.2) chromite is present in the form of disseminated stringers and irregular blebs, which would account for this anomalously high value.

10.3.3 <u>Cobalt (Co)</u> Co, together with Cr and V, is a member of the first transition series of the periodic table, and all three elements behave essentially compatibly. Co generally substitutes for Mg (Burns, (1970b) and also substitutes fairly readily in olivine and both clino- and orthopyroxene lattices, but it is rejected by plagioclase.

Cobalt, which partitions favourably into both the pyroxenes and olivine (See Table 8), is preferentially concentrated by cumulus processes in the more mafic rocks in the sequence. The range of Co values throughout the succession is from 4 - 201 ppm. Co values are highest in the feldspathic harzburgites, and range in value from 93 - 201 ppm, with all three of the Merensky Reef samples being above 143 ppm in value (Figure 34 f).

As the modal percentage of cumulus orthopyroxene increases in the rest of the cumulates, so the Co value also increases, effectively separating each rock type into distinctive fields (Figure 34 f). The anorthosites have an average Co value of 6 ppm, while the norites range in value from 11 - 86 ppm. The feldspathic pyroxenites have an average value of 103 ppm excluding B235/30 which has an anomalously low Co value of only 60 ppm. When plotted against stratigraphic height (Figure 35 c) Co has a markedly similar trend to that of Cr (Figure 35 e), disregarding the UG 1 unit, which has high Cr values due to disseminated chromite being present. Sharp trend breaks are again evident at the base of all the units.

The approach of allocating the whole-rock Co value entirely to the normative orthopyroxene (as was done with Sr and plagioclase) was attempted, but a rather scattered pattern was obtained when this was plotted against stratigraphic height. A good correlation was, however, obtained between whole-rock Co and normative orthopyroxene, and a value of 150 ppm was obtained by extrapolation for Co in 100% orthopyroxene. The value was calculated without including the 9 feldspathic harzburgite samples.

10.3.4 Nickel (Ni) The partition coefficient of Ni in Ca-poor pyroxenes has been measured experimentally

by several workers. Bird (1971) and Lindstrom (1976) report values in the range of 2 to 3 in melts of appropriate composition (See also Table 8).

Nickel partitions favourably into almost all the ferro-magnesian minerals (Table 8), and therefore behaves in much the same way as the above two elements, Cr and Co. The range of Ni values throughout the succession is from 60 - 4700 ppm. The higher Ni values in the Merensky and Bastard pyroxenite, the Merensky Reef, Pseudo Marker layer and Pseudo reef are not only due to Ni in the pyroxenes and olivines, but due to Ni in the base-metal sulphides of pyrrhotite and pentlandite. The average Ni content of the poikilitic anorthosites is 110 ppm (Ni is also concentrated in finely disseminated base metal sulphides in the immediate footwall of the Bastard and Merensky Reefs), while the range of values in the norites is from 210 - 1030 ppm. The average value in the feldspathic pyroxenite is 835 ppm, if one excludes the samples which have significant base metal sulphide concentrations (B235/6, 13, 14, 32, B232/2, 12 and B222/25 which all have values >1000 ppm.

Because Ni partitions strongly into olivine and base metal sulphides, a wide scatter is observed if whole rock Ni is allocated to the normative orthopyroxene. When Ni is plotted against normative orthopyroxene for those rocks which are devoid of olivine and visible sulphide, a value of 1238 ppm Ni is obtained at 100% normative orthopyroxene.

Campbell (1976) noted that the Ni values in the Jimberlana intrusion are highest at, or a little below, the base of each macro-rhythmic unit, and fall towards the top of the unit. He also noted that the Ni variations in the olivines do not follow the Ni variations in the rocks.

10.3.5 Copper (Cu) Copper is generally low in value throughout the succession, never being higher than 100 ppm in those rocks containing very little or no base metal sulphides (See Figure 34 h). The ten samples taken from the vicinity of or within mineralised layers, contain significantly high base metal sulphides, specifically chalcopyrite, and all ten samples have values in excess of 200 ppm (range 220 - 1100 ppm). When Cu is plotted against height (Figure 35 h) it is only at the base of the Bastard, Merensky and Footwall units that the Cu values increase. An interesting feature of the Cu values throughout the succession is that samples from the upper parts of the Merensky unit have an average Cu value of 54 ppm, whereas the average value for equivalent rocks in the other units is only 16 ppm. It would thus appear that the Merensky unit as a whole is enriched in Cu and sulphides by a factor of about 3,5, relative to the rest of the succession.

Campbell (1976) in his discussion of the Jimberlana Intrusion noted that chalcopyrite is present in samples with >10 ppm Cu, which indicates that the average Cu content of the cumulus phases is <10 ppm. Cu values above this level indicate the presence of sulphides. He found four zones of high Cu concentration, each of these zones being at the bottom of the Jimberlana macro-rhythmic units. He further noted that these Cu concentrations were not entirely confined to the base of each macro-rhythmic unit, but that they extended a little beneath the bottoms of each unit into the top of the unit below, much the same as what is found in the top of the Footwall unit (footwall of the Merensky Reef, B235/17).

The presence of base-metal sulphides in the immediate footwall anorthosites of the Bastard and Merensky Reef is not too clearly defined in this study section, but from

many on-mine evaluation samples, the presence of these disseminated sulphides in the respective footwalls is well documented.

10.3.6 Vanadium (V) Cr and V compete with one another for the Fe sites in mineral lattices. V partitions favourably into the clino- and orthopyroxenes (Table 8), but is again rejected by plagioclase. V is not, however, accepted by the olivine lattice, due to charge imbalance restrictions set up by the substitution of V^{3+} for Fe^{2+} (Taylor, 1965 as quoted in Mitchell, 1980).

There is a progressive increase in V content with increasing modal pyroxene content of the various rock types. Walker (1970) pointed out that V enters minerals preferentially in the following order: magnetite, clinopyroxene and orthopyroxene. The total range of V in all the samples is from 9 - 158 ppm, excluding B235/37 (231 ppm), in which disseminated cumulus chromite is found. The anorthosites, being low in modal pyroxene, have an average V content of 14 ppm, while the various norites range in value from 19 - 117 ppm. The feldspathic pyroxenites have an average V content of 133 ppm, while in the feldspathic harzburgites the value is somewhat lower, being in the range of 38 - 106 ppm. The reason for the lower V content in the feldspathic harzburgites is, firstly, that there is a lower modal percentage of orthopyroxene than in the feldspathic harzburgite, and, secondly, that the partition coefficient (D_V^{ol}) of V into olivine is only 0,05 (Duke, 1976).

When plotted against height (Figure 35 i), V displays a trend which is similar to that of Cr, Co and Ni, except that a decrease in V content is quite apparent in the olivine-bearing rock types. Sharp contacts are defined at the bases of all the units defined in the succession.

When whole-rock V is allocated only to the normative orthopyroxene, an extremely constant value from the feldspathic pyroxenites and norites is obtained (Figure 35 j). The higher values within the anorthosite below the Bastard Reef, Merensky Reef and UG 1 are due to a very low percentage of mafic mineral phases of these rocks. A value of 194 ppm is obtained for V in 100% normative orthopyroxene (ignoring the high value of 231 ppm in sample B235/37 which is the immediate hangingwall of the UG 1).

Co, V and Ni inter-element variations for the upper Critical zone are shown in Figure 36 b. Also shown (Figure 36 a) are the trends for the Dillsburg sill and the Skaergaard complex as presented in Ishikawa (1968) and the trend for the Birds River intrusion (Robey, 1976). In Figure 36 b the Main zone inter-element variations are also presented using the data of Marais, (1977).

The harzburgites from the study section all fall in Ishikawa's (op.cit.) field I, where Ni>Co>V, while all the other rock types, pyroxenites, norites and anorthosites fall in field II where V>Ni>Co.

Ishikawa (1968) has pointed out that the general trend during differentiation is that of enrichment of V at the expense of Ni in the intermediate and late stages of differentiation. The trend of the ratios moves almost parallel to the V-Ni boundary, e.g. Dillsburg, Skaergaard and Birds River (Figure 36 a). This constant ratio is also reflected in the Critical and Main zone rocks of the Bushveld Complex (Figure 36 b). The very last differentiates of the Dillsburg and Skaergaard intrusions show an enrichment of Co. The data for the Bushveld rocks (Liebenberg, 1960; Marais, 1977, this study) show an overall V enrichment, but no enrichment of Co is observed.

Figure 34 a-i: Trace element variations (in ppm) using weight % MgO as the abscissa

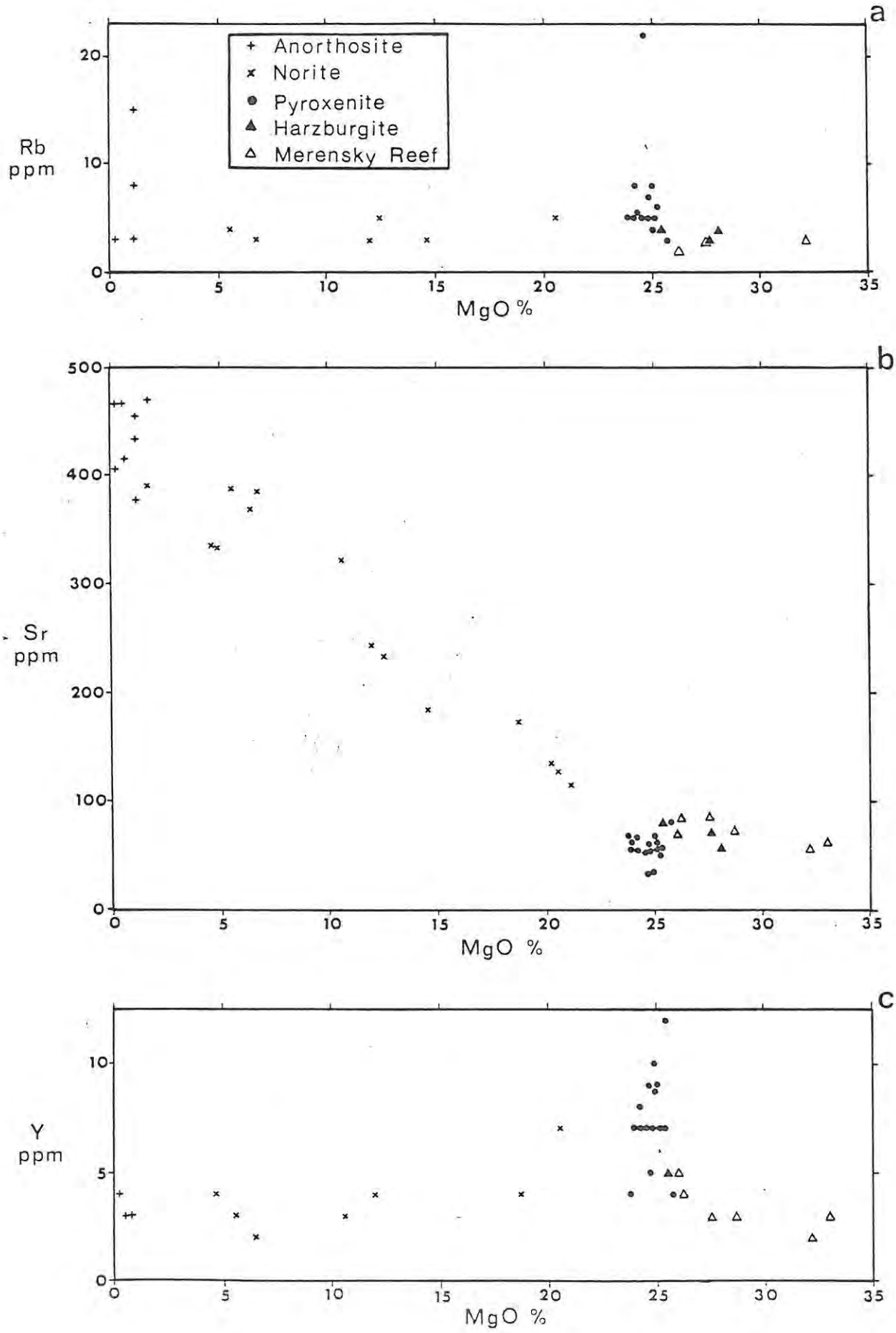

Figure 34 a-i: Trace element variations (in ppm) using weight % MgO as the abscissa

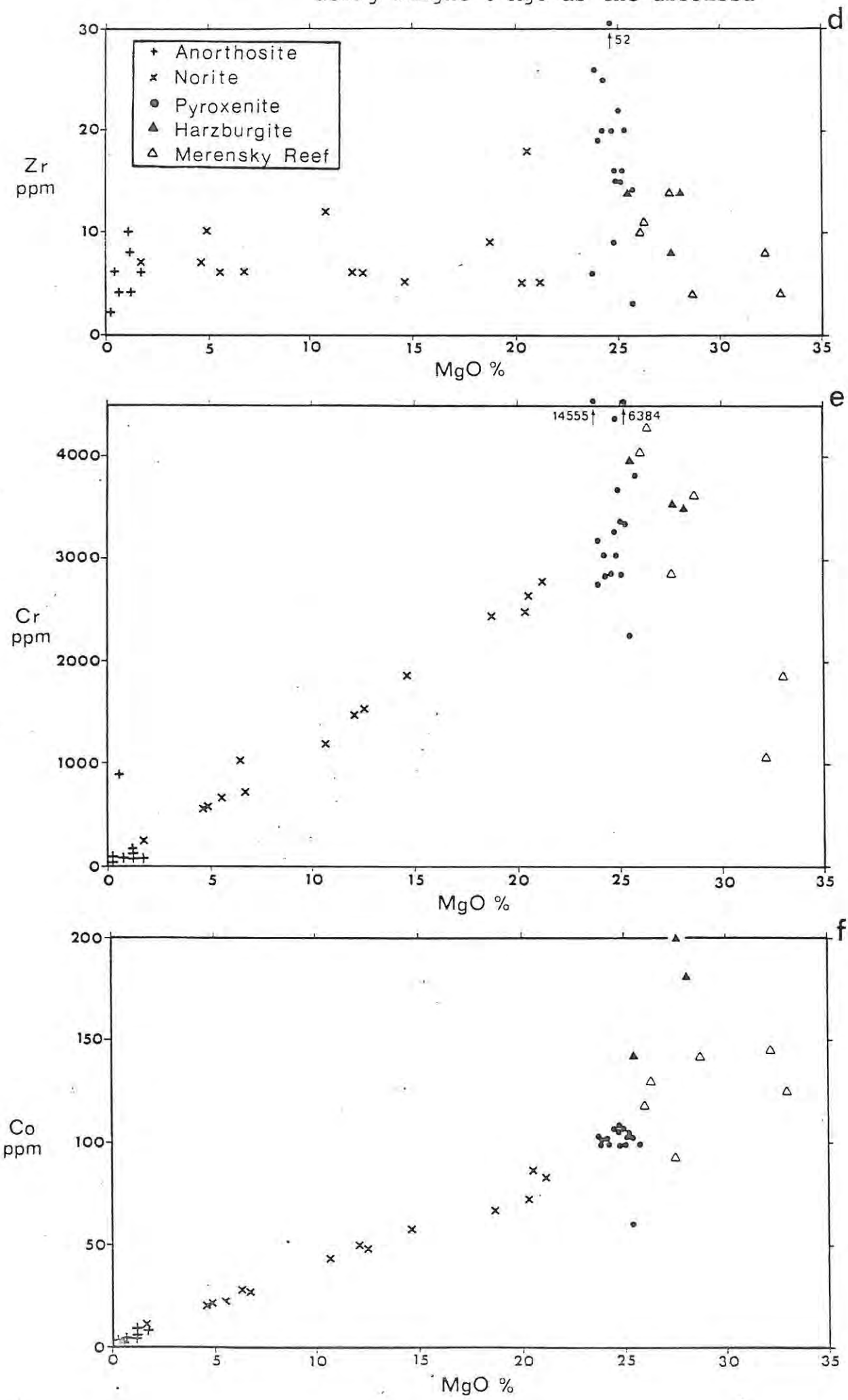

Figure 34 a-i: Trace element variations (in ppm) using weight % MgO as the abscissa

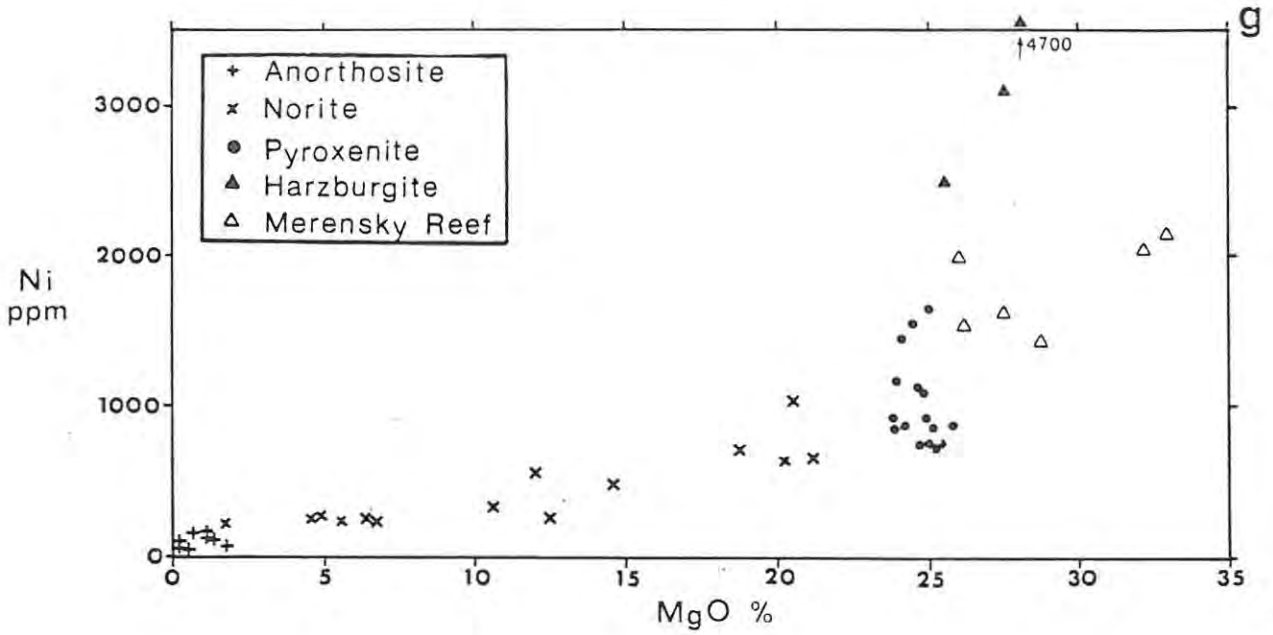

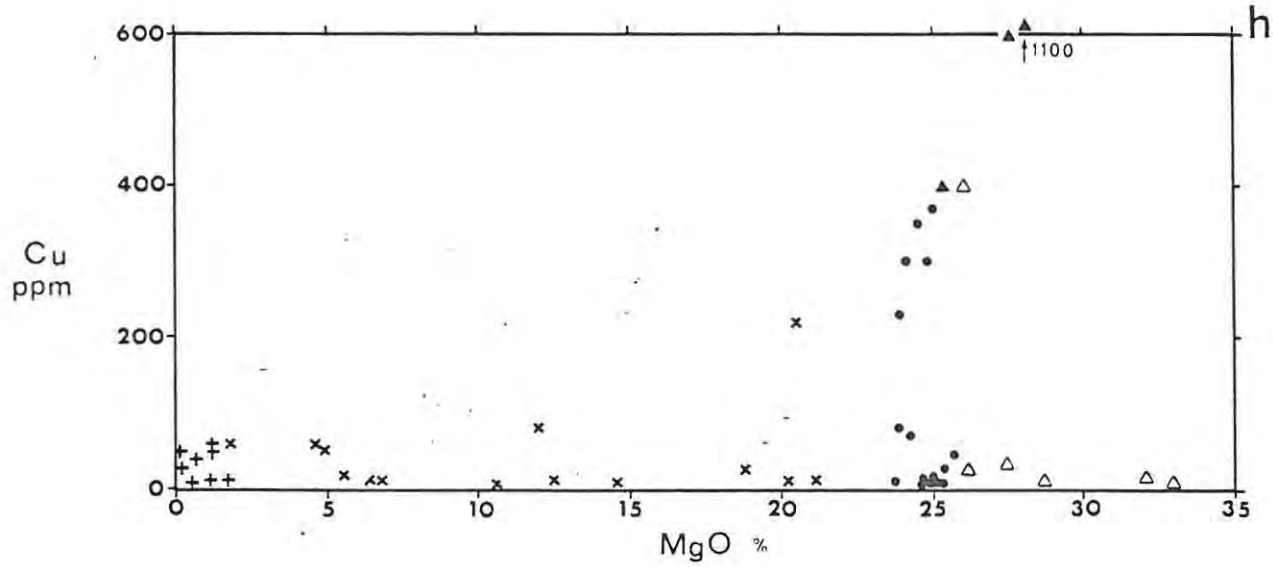

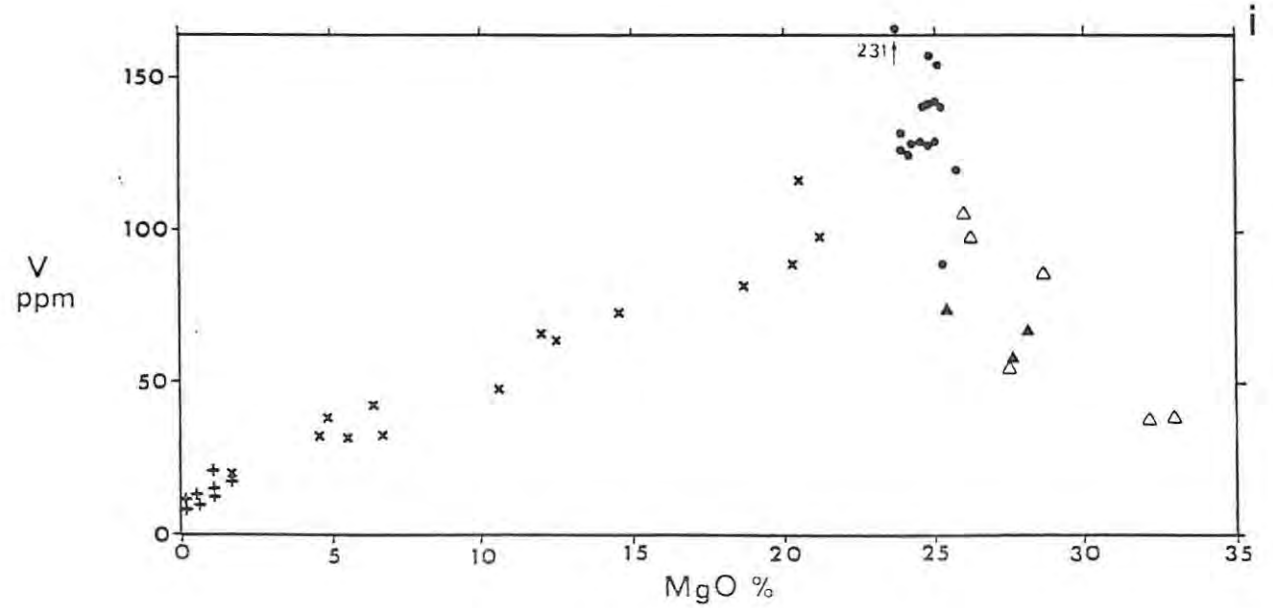

Figure 35 a-k: Trace element vs. Stratigraphic height
(+ pothole succession)

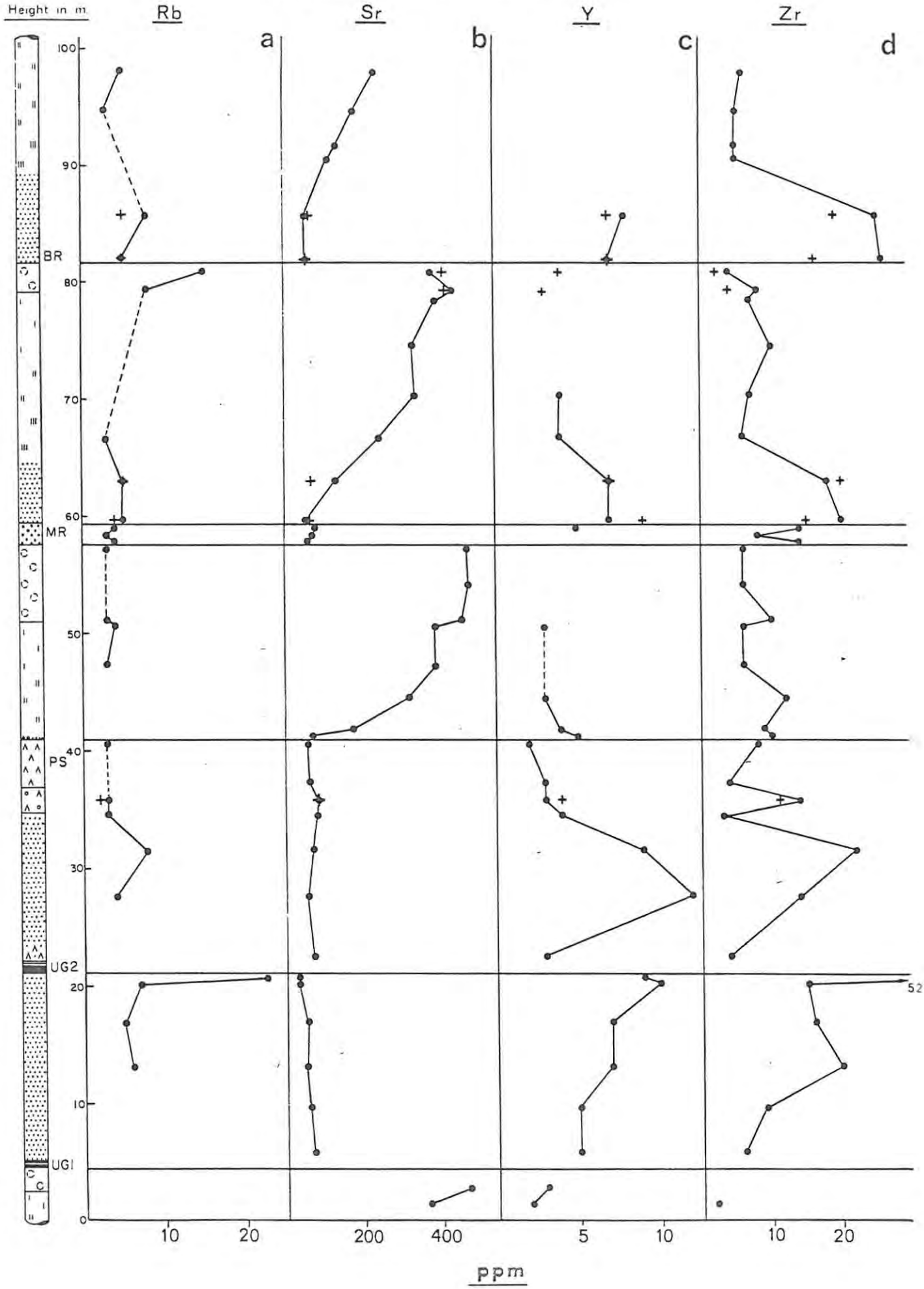

Figure 35 a-k: Trace element vs. Stratigraphic height
(+ pothole succession)

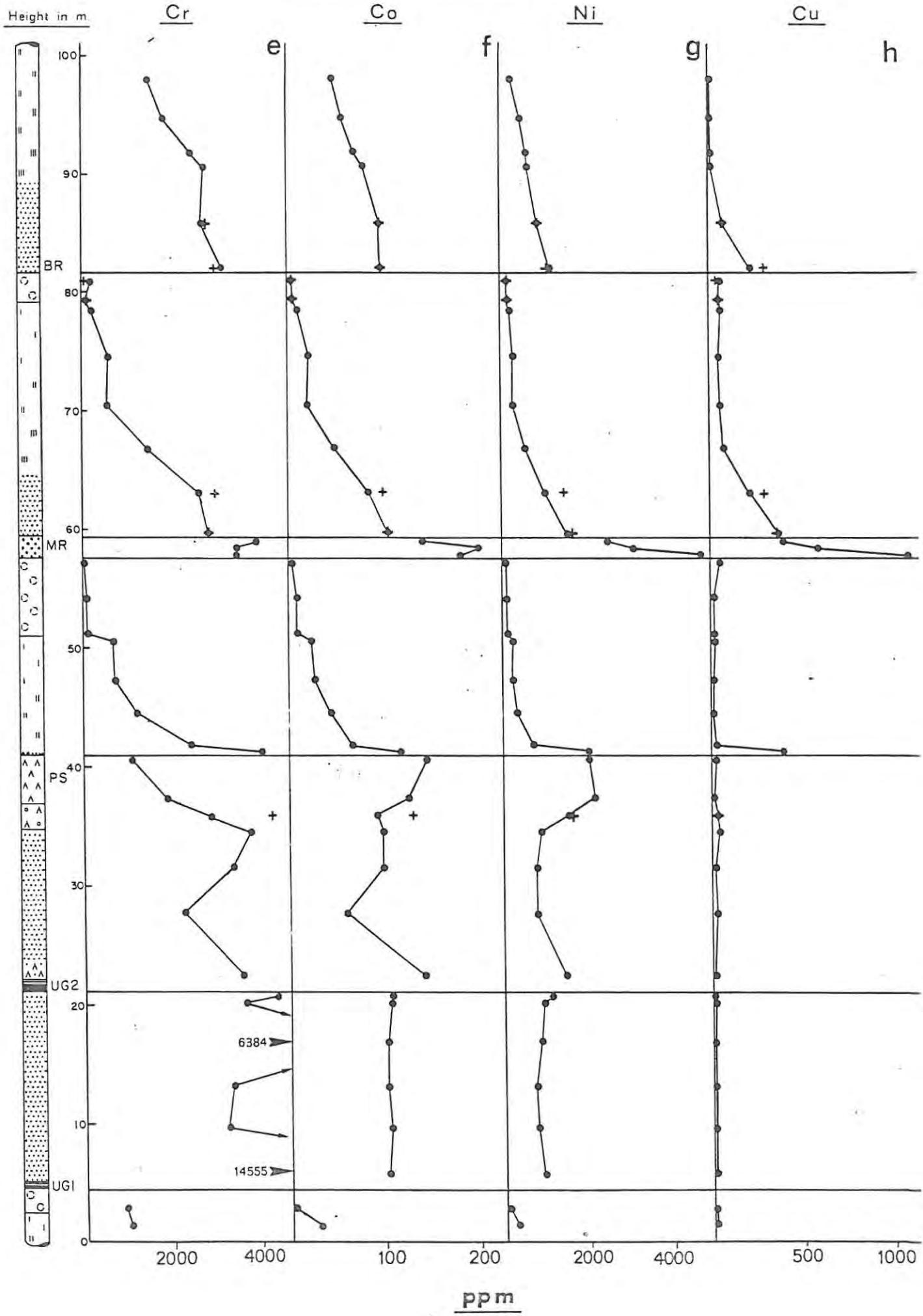

Figure 35 a-k: Trace element vs. stratigraphic height (+ pothole succession)

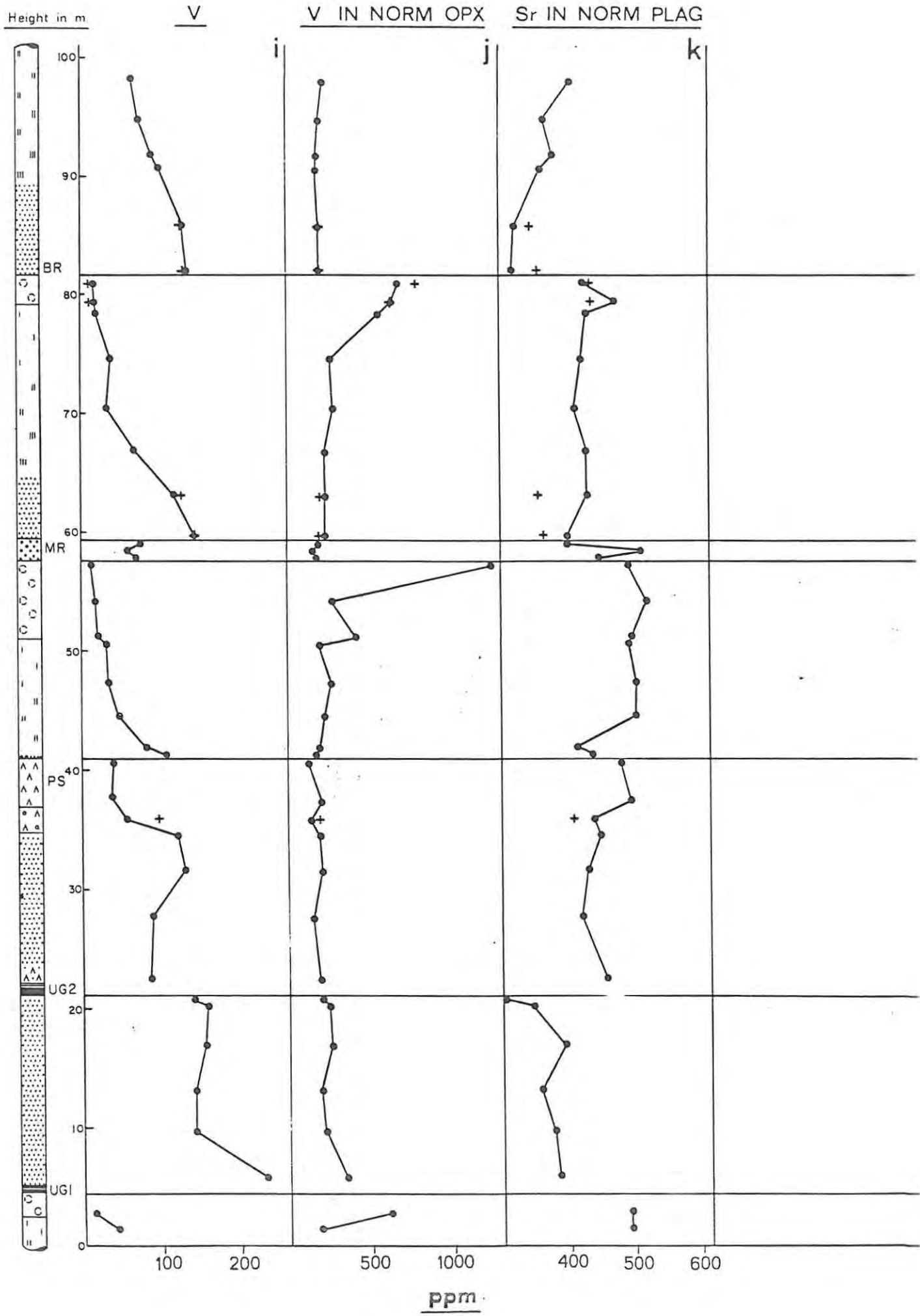

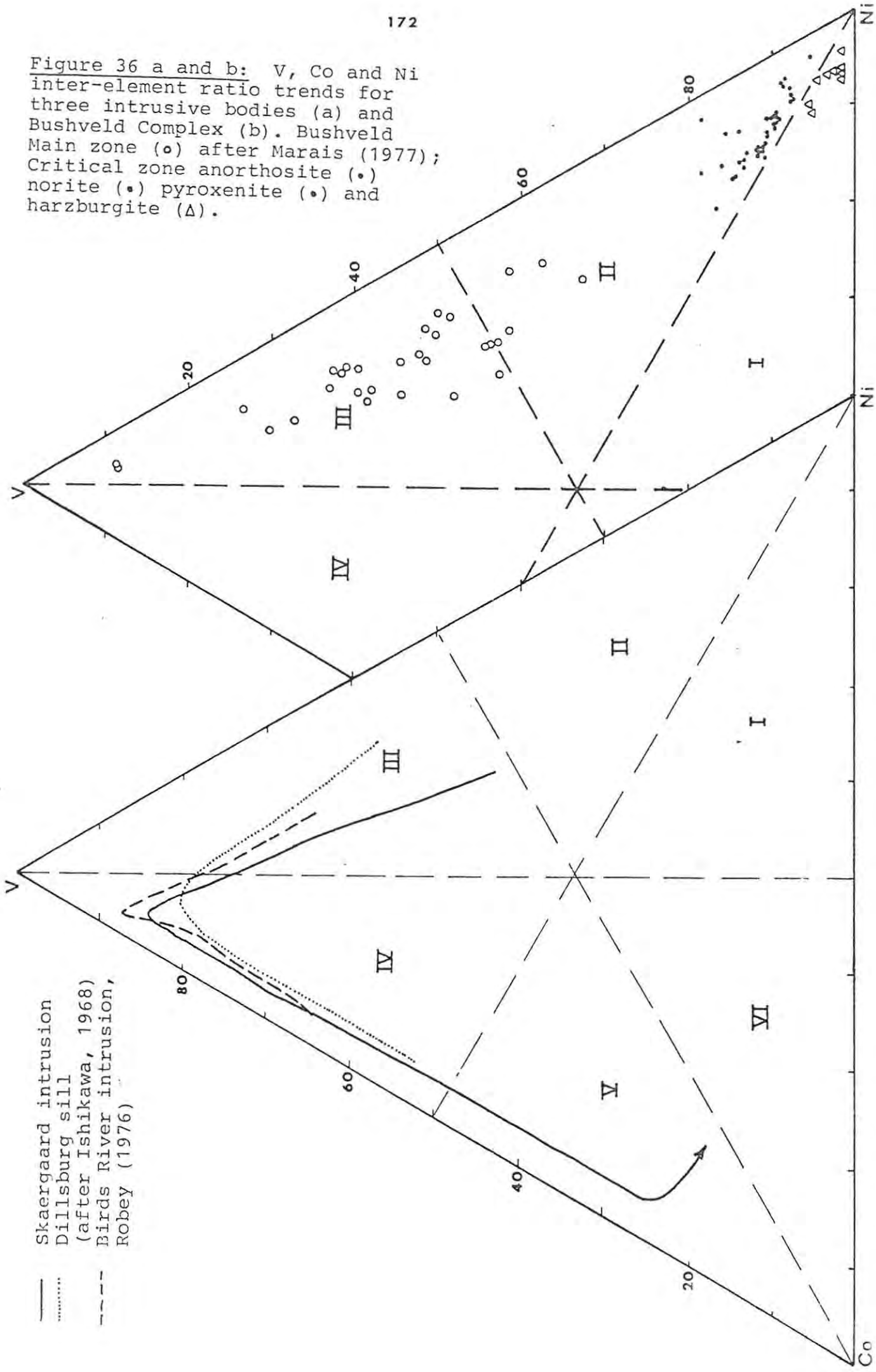

Figure 36 a and b: V, Co and Ni inter-element ratio trends for three intrusive bodies (a) and Bushveld Complex (b). Bushveld Main zone (o) after Marais (1977); Critical zone anorthosite (•) norite (•) pyroxenite (•) and harzburgite (Δ).

TABLE 7 WHOLE ROCK TRACE ELEMENT ANALYSES IN PPM

	N B235/1	N B235/2	N B235/3	N B235/4	Px B235/5	Px B235/6	A B235/7	A B235/8	N B235/9	N B235/10	N B235/11	N B235/12	Px B235/13	Px B235/14
Sr	235	183	138	114	55	55	379	433	390	333	337	245	129	52
Rb	5	3	ND	ND	8	5	15	8	ND	ND	ND	3	5	5
Y	ND	ND	ND	ND	8	7	ND	ND	ND	ND	4	4	7	7
Zr	6	5	5	5	25	26	4	8	7	10	7	6	18	20
Nb	ND	ND	ND	ND	5	ND	ND	ND	ND	ND	ND	ND	ND	ND
Co	49	58	72	82	99	101	5	6	11	22	21	50	86	107
Cr	1515	1869	2483	2786	2813	3192	178	79	212	593	560	1480	2628	2856
V	64	73	89	98	129	133	13	15	19	37	32	66	117	130
Cu	10	6	12	14	70	230	60	50	60	50	60	80	220	350
Ni	270	490	640	660	890	1180	140	150	210	290	280	570	1030	1540

	H B235/15	H B235/15A	H B235/16	A B235/17	A B235/18	A B235/19	N B235/20	N B235/21	N B235/22	N B235/23	H B235/24	H B235/25	H B235/26	H B235/27
Sr	80	72	58	468	470	454	389	387	322	174	70	58	64	88
Rb	4	3	4	3	ND	3	4	3	ND	ND	ND	3	ND	3
Y	5	ND	ND	ND	ND	ND	3	ND	3	4	5	2	3	3
Zr	14	8	14	6	6	10	6	6	12	9	10	8	4	14
Nb	ND	ND	ND	ND	ND	ND	ND	ND	ND	ND	ND	ND	ND	ND
Co	143	201	182	4	9	9	23	27	44	67	118	145	126	93
Cr	3975	3523	3503	14	66	112	659	704	1193	2419	4047	1079	1881	2871
V	74	58	68	12	17	21	31	33	47	82	106	39	38	56
Cu	400	600	1100	50	16	17	20	10	4	25	400	19	1	37
Ni	2500	3100	4700	60	80	120	240	230	340	700	2000	2030	2150	1610

ND= VALUES BELOW THE LOWER LIMITS OF DETECTION

TABLE 7 WHOLE ROCK TRACE ELEMENT ANALYSES IN PPM

	Px B235/28	Px B235/29	Px B235/30	H B235/31	Px B235/32	Px B235/33	Px B235/34	Px B235/35	Px B235/36	Px B235/37
Sr	81	69	59	73	33	34	55	50	60	69
Rb	3	8	4	ND	22	7	5	6	ND	ND
Y	4	9	12	3	9	10	7	7	5	5
Zr	3	22	14	4	52	15	16	20	9	6
Nb	ND	ND	ND	ND	ND	ND	ND	ND	ND	ND
Co	99	99	60	142	108	107	103	103	106	103
Cr	3807	3386	2263	3624	4390	3670	6384	3376	3264	14555
V	120	130	88	86	141	158	155	141	142	231
Cu	43	16	26	10	4	11	9	8	4	9
Ni	890	760	760	1440	1120	920	860	720	750	930

	A B235/38	N B235/39	Px B232/13	Px B232/12	A B232/10	A B232/9	Px B222/25	Px B232/2	H B222/19
Sr	468	370	62	57	407	415	67	59	85
Rb	ND	ND	5	5	ND	ND	5	4	2
Y	3	2	7	7	4	3	7	9	4
Zr	ND	2	19	16	2	4	20	15	11
Nb	ND	ND	ND	ND	ND	ND	ND	ND	ND
Co	2	29	99	99	4	5	101	106	130
Cr	889	1009	2736	3009	55	73	3023	2843	4297
V	14	43	127	129	9	10	125	143	97
Cu	4	10	80	300	30	40	300	370	24
Ni	60	260	870	1100	90	180	1450	1630	1540

TABLE 8: Partition coefficients for trace elements in plagioclase, clinopyroxene, orthopyroxene, olivine and biotite.

	Plagioclase	Clinopyroxene	Orthopyroxene	Olivine	Biotite
D_{Sr}	1,5-2,2 [4] 2,2 [18] 3,06 [21]	0,1 [3] 0,16-0,28 [4] 0,07 [18]	0,01 [18]	0,01 [1] 0,001 [3+18]	0,08 [18]
D_{Rb}	0,03 [1] 0,03-0,0002 [3] 0,07 [18]	0,03 [3] 0,001 [18]	0,001 [18]	0,01 [1] 0,002 [3] 0,001 [18]	0,94-3,3 [1] 1,26-1,58 [2] 3,1 [18]
D_{Zr}	0,01 [5]	0,1 [5]	0,03 [5]	0,01 [5]	[5]
D_{Y}	0,03 [5] 0,014 [21]	0,5 [5]	0,2 [5]	0,01 [5]	0,03 [5]
D_{Ti}	0,04 [5]	0,3 [5] 0,34 [20]		0,02 [5] 0,07 [20]	
D_{Co}	0,1 [6] 0,026 [19]	0,5-2,0 [7] 1,7-4,9 [8] 1,2 [19] 1,2 [20]		1-7 [9] 3,1 [19] 4,8 [20]	
D_{Cr}	0,1 [10] 0,01 [18] 0,026 [19]	40 [11] 10 [18] 1,2 [19] 20 [20]	2 [18]	~1 [9] 3,1-10 [12] 0,2 [18] 3,1 [19] 2,7 [20]	7 [18]
D_{V}	0,1 [10]	0,94-4,1 [8] 0,06-3,4 [13] 1,3 [20]	0,5-2,3 [8]	0,05 [14] 0,05 [20]	
D_{Cu}	0,24 [8] 0,004 [19]	1,5-2,4 [15] 0,071 [19]		0,3-0,5 [9] 0,023 [19]	
D_{Ni}	0,2 [16] 0,01 [18]	6,5 [8] 2 [18] 4,5 [20]	4 [18]	4,8-34 [17] 10 [18] 23,8 [20]	3,5 [18]
D_{K}	0,2 [18]	0,002 [18]	0,001 [18]	0,001 [18]	2,7 [18]
D_{Mn}	0,016 [19]	0,63 [20]		2,6 [19] 1,25 [20]	
D_{Nb}	0,01 [5]	0,1 [5]	0,15 [5]	0,01 [5]	

[1] Philpotts and Schnetzler (1970)
[2] Dupay (Marsh, 1973)
[3] Hart and Brooks (1974)
[4] Sun, Williams and Sun (1974)
[5] Pearce and Norry (1979)
[6] Jensen (1973)
[7] Lindstrom and Weill (1978)
[8] Ewart et al. (1973)
[9] Irving (1978)
[10] Walker (1979)
[11] Cambell and Borley (1974)
[12] Flower (1973)
[13] Ringwood (1970)
[14] Duke (1976)
[15] Seward (1971)
[16] De Long (1974)
[17] Leeman and Lindstrom (1978)
[18] Cox, Bell and Parkhurst (1979)
[19] Paster et al. (1974)
[20] Duke (1976)
[21] Drake (1975)

11. DISCUSSION AND CONCLUSIONS

McBirney and Noyes (1979) have pointed out that two basic processes have been proposed to account for crystal fractionation during the solidification of large intrusions. The most widely accepted of these is the one that Wager (1963) described in which crystals nucleate and grow, mainly under the roof, and move under the influence of gravity to accumulate on the floor, in a similar fashion to the fragments of a clastic sediment. This process has been under critical review over the past few years. Bottinga and Weill (1970) and Morse (1973) have shown that in some gabbroic layered intrusions (e.g. Skaergaard and Kiglapait), much of the plagioclase that has been classed as "cumulus" was actually less dense than its parental liquid and so could not have settled. Irvine (1979) has pointed out that even in basaltic magma in which plagioclase might be denser than the liquid, the settling velocity of the typical feldspar would be practically negligible.

A mechanism of bottom crystallization in layered intrusions was proposed by Jackson (1961) in his work on the Stillwater Complex. This was based on the observation that the liquidus temperature of a magma increases more rapidly with depth than the adiabatic temperature gradient anticipated if the magma was convecting. Irvine (1980) points out that the problem with this formulation is that the depth dependence of even the liquidus temperature is only about 3°C/km; consequently, in the case of layers, perhaps 300 m below the roof contact of an intrusion, one is faced with the unlikely postulate that crystallization occurred at the bottom rather than the roof because of a temperature increase of 1°C.

A very different perspective on the mechanism of

layering is obtained, however, in the light of a phenomenon known as double-diffusive convection. This process is not only an efficient means of transferring heat, it is also a highly effective mechanism for mixing contrasting liquids and transmitting compositional changes. Theoretically at least, it can lead to bottom crystallization because it can operate in circumstances whereby the liquidus temperature increases with depth through compositional effects as well as pressure (Irvine, 1980). Irvine also believes that many, if not most, uniform cumulates have formed by in situ crystallization. In the case of gabbroic and anorthositic cumulates the plagioclase - flotation problem effectively vanishes.

This investigation has highlighted the prominant cyclical nature of the various units which make up the stratigraphic succession at Union Section. This is borne out especially by the distribution of the trace elements. Campbell (1976) has pointed out that macro-cycles of crystallization or macro-rhythmic layers are a prominent feature of many layered intrusions including the Stillwater Complex (Jackson, 1961), the Rhum Intrusion (Wager and Brown, 1968), the Jimberlana Complex (Campbell, 1976), and the Bushveld Complex. Many of these cyclical units begin with the crystallization of chromite and olivine at the base, passing upward gradationally or abruptly into pyroxene or plagioclase cumulates at the top.

Although cyclical layering has been widely recognised and documented, its origin remains uncertain. Campbell (1976) has noted that three contrasting hypotheses have been used to explain the cyclical nature of layering:

1) the units are due to the periodic influxes of undifferentiated magma (Brown, 1956; Irvine and Smith, 1967). Each influx mixes with the fractionated magma in the chamber which makes it more

ultrabasic and raises the temperature resulting in a repetition of the mineral assemblage.

2) In Jackson's (1961) bottom crystallization model, crystallization occurs from a layer of supercooled magma. Crystallization takes place close to the crystal pile in a stagnant zone below the convecting magma. Continued crystallization of olivine from the lower stagnant layer of the magma raises its SiO_2 and lowers its MgO content until, eventually, olivine is replaced by bronzite as the stable liquidus phase. The cycle ends when the released latent heat of crystallization raises the temperature of the stagnant layer to that of the melting point curve, making further crystallization impossible. The stagnant layer is now at a superadiabatic temperature and, when crystal settling is complete, is in a favourable condition to join the convection of the main body of magma. The cycle is restarted when a major convectional overturn sweeps away the stagnant layer and replaces it with a magma, higher in MgO and lower in SiO_2, from the convecting upper layer.

3) Wager (1959) and Wager and Brown (1968) believe that the type of layering found in Rhum and the Bushveld may be the result of the order of nucleation of the cumulus phases from a supercooled magma.

In the case of the cyclical units of the upper Critical zone at Union Section a combination of all three hypotheses could well explain the cyclicity.

A number of units within the 100 m study section are, however, only represented by the very basal portion of the column of magma from which they crystallized, notably the

UG 1, UG 2 and Pseudo units. The UG 1 unit has an average of 85 cm of chromite over a total thickness of 15 m. Assuming that the chromite has a Cr_2O_3 (wt%) value of 44% and that very little Cr has been partitioned into the pyroxenes (2000 ppm), then the net amount of Cr_2O_3 in the unit would be 2,68%. This value is far above the highest Cr content in natural systems. By using a value of 970 ppm Cr (or 1417 ppm Cr_2O_3) in a primary magma for the Bushveld Complex (Davies et al., 1981) then a 284 m column of liquid would have been required to precipitate the total 85 cm of chromitite which is found at the base of the UG 1 unit.

This line of evidence suggests that only the roots of the individual units (apart from the Footwall, Merensky and Bastard units) are now evident and that the rest of the material which would have made up the full unit has either been removed, or that crystallization never occurred for the bulk of the unit. A possible sequence of crystallization for this study section is illustrated in Figure 37.

It would appear that for the Footwall unit, definite removal of crystalline material did take place. This is now evident in the form of potholes, where isolated remnant Footwall unit layers, e.g. "Strepies", is still preserved and found in lenses in the larger potholes on the mine.

In summary, this investigation has highlighted a number of points.

1) The cyclical nature of the various units which make up the stratigraphic succession which is borne out by the distribution of trace elements.

2) The apparent truncation of certain of the cyc-

FIGURE 37: Possible crystallization sequence of the Upper Critical zone at Union Section. The word "removal" could in all cases be supplemented by "non-crystallization".

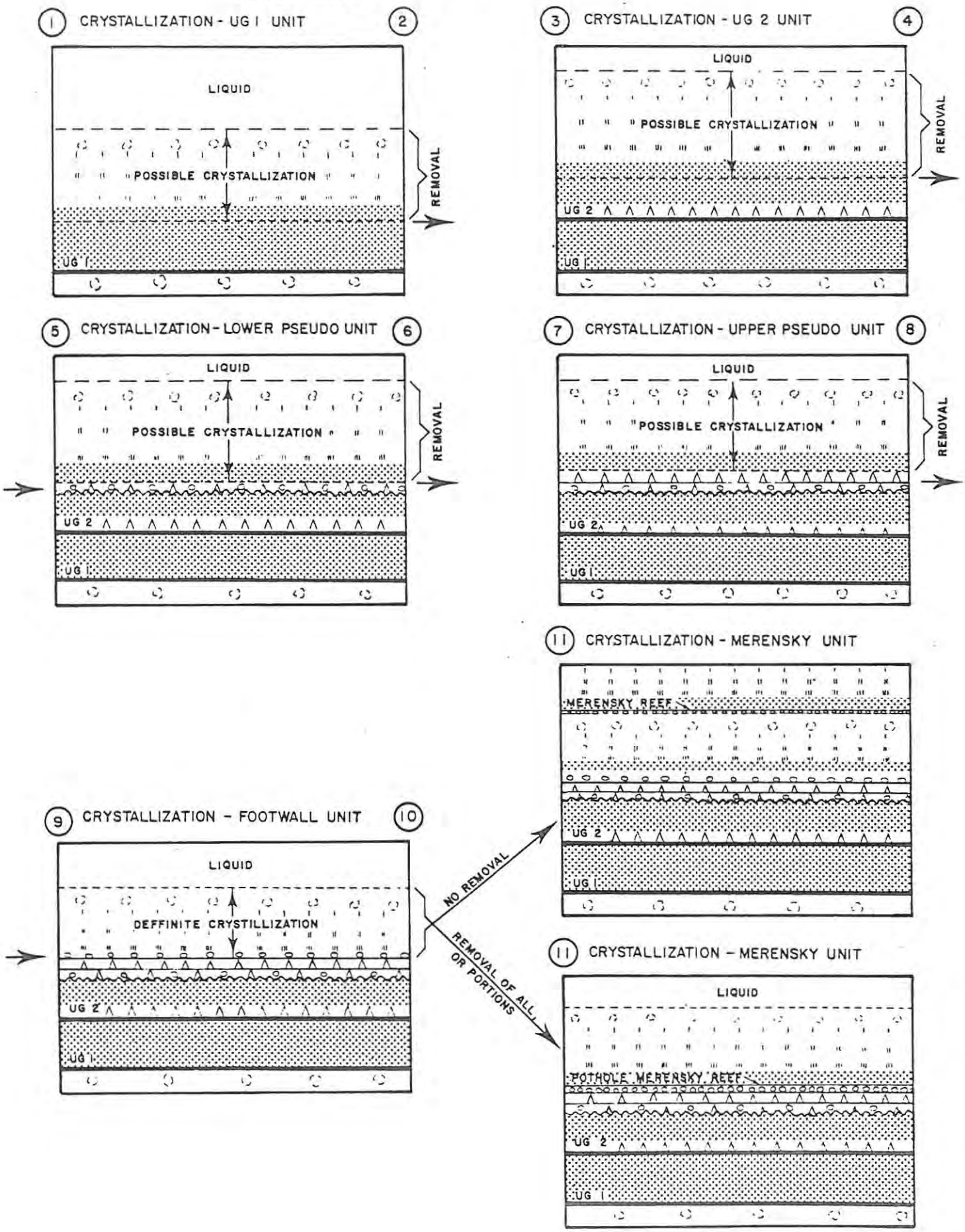

lical units, e.g. an ideal sequence being the Bastard, Merensky or Footwall units whereas the UG 2 and UG 1 units have been truncated.

3) Despite variations of individual trace elements, variations are controlled by modal proportions of the more important mineral phases. Some of the more important ratios show no variation at all throughout the succession, e.g. Mg/Mg+Fe.

4) There is a change in habit of some of the more important mineral phases, e.g. plagioclase occurs as both a cumulus phase and also as an intercumulus phase.

5) Enigmatic nature of pothole structure. These are of particular importance as they reveal the elimination of significant parts of the sequence and cause the hanging wall and footwall units to come into close juxtaposition. These features are possibly due to some process of erosive scour, or inhibited crystallization.

Many of the features observed can be partially explained either by the approach of crystal settling or by the newer approach of bottom in situ crystallization.

The present thesis is not directed at either of these problems but is more concerned with the documentation of basic factual data.

There is a degree of dissension among the proponents of the various hypotheses, and there are no rigid criteria at this stage on the basis of which any one of the hypotheses could be accepted.

There are many aspects of this investigation that need further detailed research and amongst these might be listed:

1) Detailed geochemical studies of the various mineral phases within individual units.
2) Study of the variations of chromite and other spinels.
3) Determination of additional trace elements not reported, e.g. Sc, Ba, Pb, Zr, PGE, Au, etc.
4) Study of Sr isotope variations throughout the succession.
5) Study of trace element variations on mineral separates from individual units.
6) Comprehensive study of all sulphide phases throughout the succession.

These are aspects which should be examined in the future, but would have extended the mandate of the present study well beyond the planned framework. The author wishes, however, to stress the importance of examining all aspects of the evidence offered by mapping, correlation of borehole sections, petrography, mineralogy and geochemistry.

APPENDIX 1

X-Ray Fluorescence Spectrometry

All major elements, including FeO, and trace elements Cu and Ni, were determined by Messrs. Bergström and Bakker, Johannesburg. The major elements, apart from sodium, were determined on fusion discs. Sodium, together with the trace elements Cu and Ni, were determined separately on pressed powder briquettes. Total iron was determined as Fe_2O_3 and FeO was determined separately by titration. A Phillips PW-1450 spectrometer was used in all cases.

The remaining trace element analyses Sr, Rb, Zr, Y, Co, Cr and V were performed by the author in the laboratory at Rhodes University. Data were processed by computer, and corrections were made for position factors, dead-time, background, instrumental drift and spectral line interferences. Mass absorbtion coefficients, used in trace element data reduction, were derived from the major element data, using Heinrich's (1966) values.

Working curves were calculated using the international rock standards AGV-1, GSP-1, DTS-1, G2, BCR-1, PCC-1, S-12 and S-9 plus NIM standards. Details of the analytical conditions for trace element runs performed at Rhodes University are tabulated overleaf (Table A), and the lower limits of determination and average absolute errors for the trace element runs are given in Table B.

TABLE A : X-RAY FLUORESCENCE ANALYTICAL CONDITIONS

Element	Emission line	Tube	KV	mA	Crystal	Time (secs)	Counter	Collimator	Specimen
Sr	Kα	W	55	40	LiF(220)	200	scint.	fine	powder pellet
Rb	Kα	W	55	40	LiF(220)	200	scint.	fine	powder pellet
Zr	Kα	W	55	40	LiF(220)	200	scint.	fine	powder pellet
Y	Kα	W	55	40	LiF(220)	200	scint.	fine	powder pellet
Nb	Kα	W	55	40	LiF(220)	200	scint.	fine	powder pellet
Co	Kα	W	55	40	LiF(220)	200	flow	fine	powder pellet
Cr	Kα	W	55	40	LiF(220)	200	flow	fine	powder pellet
V	Kα	W	55	40	LiF(220)	200	flow	fine	powder pellet

TABLE B : AVERAGE AND STANDARD DEVIATION (S.D.) OF LOWER LIMITS OF DETERMINATION (L.L.D.) AND ERRORS OF DETERMINATION FOR TRACE ELEMENT ANALYSES BY X-RAY FLUORESCENCE SPECTROMETRY

ELEMENT	L.L.D.	S.D.	ABSOLUTE ERROR	S.D.
Sr	2.30	0.42	0.91	0.23
Rb	2.46	0.42	0.72	0.12
Y	2.67	0.57	0.78	0.16
Zr	2.07	0.32	0.61	0.09
Nb	2.68	0.33	0.77	0.10
Co	2.76	0.47	0.95	0.22
Cr	2.52	0.29	3.98	1.87
V	3.10	0.38	1.06	0.24

APPENDIX 2

Electron Microprobe Analysis

Microprobe studies were carried out on Rhodes University's Cambridge Scientific Instruments Microscan V instrument. Polished specimen slides were vacuum-coated to a maximum thickness of 25 nM with carbon. Specimen current was monitored at regular intervals by means of a Faraday Cage.

Nominal concentrations were corrected by using a computer programme which applies the Bence-Albee correction routine (Bence & Albee, 1968), using the α-factors of Albee and Ray (1970) in the programme HVE:MARK III which also makes corrections for dead-time counting losses.

An accelerating potential of 20 kv, a specimen current of 30 nA and a flow counter were used in all microprobe analyses.

Analytical conditions and standards employed for pyroxene, feldspar and olivine analyses are tabulated overleaf (Table C). Standards used for chromite analyses were synthetic $MgO.Al_2O_3$ and Fe_3O_4, Stillwater chromite and a well analysed kimberlite ilmenite.

The count rates, quoted in Table C, are for 10 seconds, but actual counting times varied from 30-70 seconds. The standards listed (Table C) are all well authenticated and supplied from various operating laboratories.

TABLE C : MICROPROBE ANALYTICAL CONDITIONS FOR OLIVINE

ELEMENT	CRYSTAL	STANDARD	AV.STD COUNTS
Si	KAP	St.J.Is.01	3547.1
Mg	KAP	St.J.Is.01	7945.5
Fe	LiF(220)	Ni-Magnetite	2818.6
Ni	LiF(220)	Ni-Magnetite	115.6

MICROPROBE ANALYTICAL CONDITIONS FOR PYROXENE

ELEMENT	CRYSTAL	STANDARD	AV.STD. COUNTS.
Si	KAP	Jadeite	5203.2
Ti	Qtz.	K.K.Hb1	290.6
A1	KAP	Spinel	6074.5
Fe	Qtz	Ni-Magnetite	6777.4
Mn	Qtz	Rhodonite	3170.2
Mg	KAP	Spinel	1768.4
Ca	Qtz	Wollastonite	2577.4
Na	KAP	Jadeite	306.5
Cr	Qtz	Chromite	4018.4

MICROPROBE ANALYTICAL CONDITIONS FOR PLAGIOCLASE

ELEMENT	CRYSTAL	STANDARD	AV.STD COUNTS.
Si	KAP	Jadeite	5525.9
A1	KAP	Jadeite	2300.8
Fe	Qtz	Ni-Magnetite	6675.0
Ca	Qtz	Wollastonite	2578.3
Na	KAP	Jadeite	301.5
K	Qtz	Orthoclase 1A	678.9

ACKNOWLEDGEMENTS

I wish to thank the management of the Johannesburg Consolidated Investment Co. and Rustenburg Platinum Mines Ltd., for affording me the opportunity of undertaking this study, and for financial assistance throughout. Special thanks are extended to the manager of Union Section, Mr. C. Stott, for his cooperation throughout the project and to Mr. P. Coetzer, chief geologist on the Mine and Dr. M.J. Viljoen of the Platinum division for their continued interest and help. Colleagues on the various platinum mines and the J.C.I. Fundamental Research Unit, and especially Drs. R.P. Viljoen and C.A. Lee are thanked for their helpful comments and encouragement throughout the investigation.

I wish also to express my sincere appreciation to Professor H.V. Eales for his patient and good-humoured assistance and guidance, and to Rhodes geological staff and post-graduate students for their help during time spent in the laboratory.

Thanks too, to a very patient typist, Mrs. V. Ainslie, and to my wife Vivian for her cheerful willingness to help in any way she could.

REFERENCES

Albee, A.L. and Ray, L., 1970, Correction factors for electron probe microanalysis : Analyt. Chem., v. 42, p. 1408-1414.

Allegre, C.J., Treuil, M., Minster, J.F., Minster, B. and Albarede, F., 1977, Systematic use of trace elements in igneous processes : Contrib. Miner. Petrol., v. 60, p.57-75.

Bence, A.E., and Albee, A.L., 1968, Empirical correction factors for the electron microanalysis of silicates and oxides : Jour. of Geol., v. 76, p.382-403.

Berman, H., 1937, Constitution and classification of the natural silicates : Amer. Min., v. 22, p.342-408.

Bird, M.L., 1971, Distribution of trace elements in olivines and pyroxenes - an experimental study : Ph.D. Thesis, University of Missouri Rolla, 244 p.

Birle, J.D., Gibbs, G.V., Moore, P.B. and Smith, J.V., 1968, Crystal structure of natural olivines : Amer. Min., v. 47, p. 383-394.

Bottinga, Y., Kudo, A. and Weill, D., 1966, Some observations on oscillatory zoning and crystallization of a magmatic plagioclase : Amer. Min., v. 51, p.792-806.

Bottinga, Y. and Weill, D.F., 1970, Densities of liquid silicate systems calculated from partial molar volumes of oxide components : Amer. Jour. Sci., v. 269, p.169-182.

Brown, G.M., 1956, The layered ultrabasic rocks of Rhum, Inner Hebrides : Phil. Trans. Roy. Soc. Lond. B. 240, p.1-53.

Burns, R.G., 1970a, Crystal Field Spectra and evidence of cation disordering in olivine minerals : Amer. Min., v. 55, p.1608-1632.

Burns, R.G., 1970b, Mineralogical applications of Crystal Field Theory : Cambridge University Press, 224p.

Buchanan, D.L., 1972, The petrography of rocks of the Bushveld Complex type intersected by boreholes in the Bethal area : Unpubl. M.Sc. Thesis, Pretoria University.

Buchanan, D.L., Suddaby, P., Nolan, J., Lee, C.A., Viljoen, M.J. and Davenport, J.W.J., 1981, The chemistry of spinel and silicate phases associated with platinum - rich horizons in the Bushveld Complex: Abstracts, 3rd International Platinum Symposium, p.7-8.

Buseck, P.R., Nord, G.L. and Veblen, D.R., 1980, Subsolidus phenomena in pyroxenes : In, Prewitt, C.T. (ed.), Reviews in Mineralogy; Pyroxenes : Min. Soc. Amer., v. 7, p.117-204.

Button, A., 1975, Stratigraphy and attitude of the floor of the Bushveld Complex in the Eastern Transvaal : Econ. Geol. Research Unit, Univ. Witwatersrand Information Circular No. 96, 13p.

Cameron, E.N. and Desborough, G.A., 1969, Occurrence and characteristics of chromite deposits - Eastern Bushveld Complex : Econ. Geol. Monogr. 4, p.23-40.

Cameron, E.N., 1975, Postcumulus and subsolidus equilibration of chromite and co-existing silicates in the Eastern Bushveld Complex : Geochim. et Cosmochim., v. 39, p.1021-1033.

Cameron, E.N., 1977, Chromite in the central sector of the Eastern Bushveld Complex, South Africa : Amer. Min., v. 62, p.1082-1096.

Cameron, E.N., 1978, The lower zone of the Eastern Bushveld Complex in the Oliphants river trough: Jour. of Pet., v. 19, p.437-462.

Cameron, E.N., 1980, Evolution of the lower Critical zone, Central sector, Eastern Bushveld Complex, and its chromite deposits : Econ. Geol., v. 75, p.845-871.

Cameron, M., and Papike, J.J., 1980, Crystal chemistry of silicate pyroxenes : In, Prewitt, C.T. (ed.), Reviews in Mineralogy; Pyroxenes : Min. Soc. Amer., v. 7, p.5-87.

Campbell, I.H. and Borley, G.D., 1974, The geochemistry of pyroxenes from the Lower Layered Series of the Jimberlana Intrusion, Western Australia : Contrib. Miner. Petrol., v. 47, p.281-297.

Campbell, I.H., 1977, A study of Macro-Rhythmic layering and cumulate processes in the Jimberlana Intrusion, Western Australia, Part 1 - The upper layer series : Jour. of Pet., v. 18, p.183-215.

Cawthorn, R.G. and McCarthy, T.S., 1980, Variations in the Cr content of magnetite from the Upper zone of the Bushveld Complex - evidence for heterogeneity and convection currents in magma chambers : Earth. Planet. Sci. Lett., v. 46, p.335-343.

Coertzer, F.J., 1958, Intrusive relationships and ore deposits in the western part of the Bushveld Igneous Complex : Trans. Geol. Soc. South Africa, v. 61, p.387-400.

Coertzer, F.J., 1959, Discussion of Feringa, G., 1959, The geological succession in a portion of the Northwestern Bushveld (Union Section) and its interpretation: Trans. Geol. Soc. South Africa, v. 62, p.233.

Coertzer, F.J., and Schumann, F.W., 1962, The Basic portion and associated minerals of the Bushveld Igneous Complex north of Pilanesberg : Dept. of Mines S.A. Geol. Survey Bulletin 38, p.1-48.

Coertzer, F.J., 1970, The geology of the western part of the Bushveld Igneous Complex : In, Visser, D.J.L., and von Gruenewaldt, G. (eds.), Symposium on the Bushveld Igneous Complex and other layered intrusions : Geol. Soc. South Africa, Spec. Publ. 1, p.1-22.

Coertzer, F.J., 1974, The geology of the basic portion of the Western Bushveld Igneous Complex : Dept. Mines S.A. Geol. Survey, Memoir 66, 148p.

Cousins, C.A., 1959, Discussion of Feringa, G., 1959, The geological succession in a portion of the Northwestern Bushveld (Union Section) and its interpretation : Trans. Geol. Soc. South Africa, v. 62, p.233-236.

Cousins, C.A., 1959, The structure of the mafic portion of the Bushveld Igneous Complex : Trans. Geol. Soc. South Africa, v. 62, p.179-189.

Cousins, C.A., 1964, The platinum deposits of the Merensky Reef : In, Haughton, S.H. (ed.), The geology of some ore deposits in Southern Africa, v. 2, Geol. Soc. South Africa, p.225-237.

Cousins, C.A., and Feringa, G., 1964, The chromite deposits of the western belt of the Bushveld Complex : In, Haughton, S.H. (ed.), The geology of some ore deposits in Southern Africa, v. 2, Geol. Soc. South Africa, p.183-202.

Cox, K.G., Bell, J.D. and Pankhurst, R.J., 1979, The interpretation of igneous rocks : George Allen and Unwin, London, 450p.

Davies, G., Cawthorn, G.R., Barton, J.M. Jr. and Morton, M., 1980, Parental magma to the Bushveld Complex : Nature, v. 287, p.33-35.

Deer, W.A., Howie, R.A. and Zussman, J., 1978, Rock-Forming Minerals, Volume 2A; Single-chain Silicates : Longman, London, 668p.

de Long, S.E., 1974, Distribution of Rb, Sr and Ni in igneous rocks, central and western Aleutian islands, Alaska : Geochim. et Cosmochim., v. 38, p.245-266.

Drake, M.J., 1975, Partition of Sr, Ba, Ca, Y, Eu^{2+}, Eu^{3+}, and other REE between plagioclase feldspar and magmatic liquid : an experimental study : Geochim. et Cosmochim., v. 39, p.689-712.

Duke, J.M., 1976, Distribution of the period four transition elements among olivine, calcic pyroxene and mafic silicate liquid : Experimental results: Jour. of Pet., v. 17, p.499-521.

Eales, H.V., 1979, Anomalous Karoo spinels along the chromite-titanomagnetite join : South African Jour. Sci., v. 75, p.24-29.

Eales, H.V., and Marsh, J.S., 1979, High-Mg tholeiitic rocks and their significance in the Karoo Central Province : South African Jour. of Sci., v. 75, p.400-404.

Eales, H.V., Reynolds, I.M. and Gouws, D.A., 1980, The spinel-group minerals of the central Karoo tholeiitic province : Trans. Geol. Soc. South Africa, v. 83, p.243-253.

Ewart, A. and Taylor, S.R., 1969, Trace element geochemistry of the rhyolitic volcanic rocks, central North Island, New Zealand, phenocryst data : Contrib. Miner. Petrol., v. 22, p.127-146.

Ewart, A., Bryan, W.B. and Gill, J.B., 1973, Mineralogy and geochemistry of the younger volcanic islands of Tonga, S.W. Pacific : Jour. of Pet., v. 14, p.429-465.

Ferguson, J., and Botha, E., 1963, Some aspects of igneous layering in the Basic zones of the Bushveld Complex : Trans. Geol. Soc. South Africa, v. 66, p.259-278.

Ferguson, J. and Wright, J., 1970, Composition variation of plagioclase in the Critical Series, Bushveld Complex : In, Visser, D.J.L. and von Gruenewaldt, G. (eds.), Symposium on the Bushveld Igneous Complex and other layered intrusions, Geol. Soc. South Africa, Spec. Pub. 1, p.59-66.

Ferguson, J., 1973, The Pilanesberg Alkaline Province, Southern Africa : Trans. Geol. Soc. South Africa, v. 76, p.249-270.

Feringa, G., 1958, Report on the chromite deposits of the Pilanesberg area : Geological investigation of the differentiated zone of the Western belt of the Bushveld Igneous Complex : J.C.I. Internal Report, 33p.

Feringa, G., 1959, The Geological succession in a portion of the Northwestern Bushveld (Union Section) and its interpretation : Trans. Geol. Soc. South Africa, v. 62, p.219-233.

Flower, M.J., 1973, Trace element distribution in lava flows from Anjouan and Grande Comore, Western Indian Ocean : Chem. Geol., v. 12, p.81-98.

Flynn , R.T., Ulmer, G.C. and Sutphen, C.F., 1978, Petrogeneses of the Eastern Bushveld Complex : Crystallization of the middle Critical zone : Jour. of Pet., v. 19, p.136-152.

Fuller, A.O., 1951, The Critical zone of the Bushveld Complex at the Swartkop chrome mine, Rustenburg district : Unpubl. M.Sc. Thesis, Cape Town University.

Gunn, B.M., 1971, Trace element partition during fractionation of Hawaiian basalts : Chem. Geol., v. 8, p.1-13.

Green, D.H., 1964, The petrogenesis of the high-temperature peridotite intrusion in the Lizard area, Cornwell : Jour. of Pet., v. 5, p.134-188.

Gough, D.L., 1956, Study of the palaeomagnetism of the Pilanesberg Dykes : Mon. Nat. Roy. Austr. Soc. Geophys., v. 7, p.193-213.

Hart, S.R. and Brooks, C., 1974, Clinopyroxene-matrix partitioning of K, Rb, Cs, Sr and Ba : Geochim. et Cosmochim., v. 38, p.1799-1806.

Hart, S.R. and Davis, K.E., 1978, Nickel partitioning between olivine and silicate melt : Earth Planet. Sci. Lett., v. 40, p.203-219.

Heinrich, K.F.J., 1966, X-ray absorbtion uncertainty : In, McKinley, T.D., Heinrich, K.F.J. and Wittry, D.B. (eds.), : The Electron Microprobe, Wiley, New York.

Henderson, P., 1968, The distribution of phosphorous in the early and middle stages of fractionation of some basic layered intrusions : Geochim. et Cosmochim., v. 32, p.897-911.

Henderson, P., 1975, Reaction trends shown by Chrome-spinels of the Rhum layered intrusion : Geochim. et Cosmochim., v. 39, p.1035-1044.

Hess, H.H., 1949, Chemical composition and optical properties of common clinopyroxenes : Amer. Min.,v. 34, p.621-666.

Hess, H.H., 1960, Stillwater igneous complex, Montana : Geol. Soc. of Amer., Memoir 80, p.230.

Irvine, T.N., 1965, Chromian spinel as a petrogenetic indicator, Part 1, Theory : Canad. Jour. Earth Sci., v. 4, p.71-103.

Irvine, T.N. and Smith, C.H., 1967, The ultramafic rocks of the Muskox intrusion Northwest Territories, Canada : In, Wyllie., P.J., (ed.), Ultramafic and related rocks, Wiley, New York, p.38-49.

Irvine, T.N. and Baragar, W.R.A., 1971, A guide to the chemical classification of the common volcanic rocks : Canad. Jour. Earth Sci., v. 8, p.523-548.

Irvine, T.N., 1978, Infiltration metasomatism, adcumulus growth, and secondary differentiation in the Muskox intrusion : Carnegie Inst. Wash. Year Book, v. 77, p.743-751.

Irvine, T.N., 1979, Rocks whose composition is determined by crystal accumulation and sorting : In, Yoder, H.S. (ed.), The evolution of the igneous rocks, Princeton Univ. Press. P.245-306.

Irvine, T.N., 1980, Magmatic infiltration metasomatism, double-diffusive fractional crystallization, and adcumulus growth in the Muskox intrusion and other layered intrusions : In, Hargraves, R.B., (ed.), Physics of Magmatic Processes, Princeton University Press, Princeton, New Jersey, p.325-383.

Ishikwawa, H., 1976, Some aspects of geochemical trends and fields of ratios of V, Ni and Co : Geochim. et Cosmochim., v. 32, p.913-917.

Jackson, E.D., 1961, Primary textures and mineral associations in the ultramafic zone of the Stillwater Complex, Montana: U.S. Geol. Survey Prof. Paper, No. 358, p.106.

Jackson, E.D., 1969, Chemical variation in coexisting chromite and olivine and chromitite zones of the Stillwater Complex : Econ. Geol. Monogr. 4, p.41-71.

Jackson, E.D., 1970, The cyclic unit in layered intrusions - a comparison of repetitive stratigraphy in the ultramafic part of the Stillwater, Muskox, Great Dyke and Bushveld Complexes : In, Visser, D.J.L. and von Gruenewaldt, G. (eds.), Symposium on the Bushveld Igneous Complex and other layered intrusions, Geol. Soc. South Africa, Spec. Pub. 1, p.391-424.

Jensen, B.B., 1973, Patterns of trace element partitioning : Geochim. et Cosmochim., v. 37, p.2227-2242.

Korringa, M.K. and Noble, D.C., 1971, Distribution of Sr and Ba between natural feldspar and igneous melt : Earth Planet. Sci. Lett., v. 11, p.147-151.

Kruger, F.J., 1981, Ph.D. Study on Rustenburg Platinum mines, in progress : Rhodes University.

Lambert, R. St. J. and Holland, J.G., 1974, Yttrium geochemistry applied to petrogenesis utilizing calcium-yttrium relationships in minerals and rocks : Geochim. et Cosmochim., v. 38, p.1393-1414.

Leeman, W.P. and Lindstrom, D.J., 1978, Partitioning of Ni^{2+} between basaltic and synthetic melts and olivines - an experimental study : Geochim. et Cosmochim., v. 42, p.801-816.

Lee, C.A., 1981, Post-depositional structures in the Bushveld Complex mafic sequence : Jour. Geol. Soc. London, v. 138, p.327-341.

Lee, C.A., 1981, Landsat imagery and the Bushveld Complex : J.C.I. Fundamental Res., Report No.116, (Unpubl.).

Lee, C.A., 1982, Trace and platinum group element geochemistry and the development of the Merensky Unit of the Western Bushveld Complex : J.C.I. Fundamental Res., Report No. 133, 24 p., (Unpubl.).

Liebenberg, C.J., 1960, The trace elements of the rocks of the Bushveld Igneous Complex : Univ. Pretoria Nuwe Reeks, v. 12, 69p.

Liebenberg, W.R., 1942, The basal rocks of the Bushveld Complex in the Marico district south of Dwarsberg : Trans. Geol. Soc. South Africa, v. 45, p.81-108.

Lindstrom, D.J., 1976, Experimental study of the partitioning of the transition metals between clinopyroxene and coexisting silicate liquids : Ph.D. Thesis, University of Oregon, 188p.

Lindstrom, D.J. and Weill, D.F., 1978, Partitioning of transition metals between diopside and coexisting silicate liquids - 1. Nickel, cobalt and manganese : Geochim. et. Cosmochim. v. 42, p.817-832.

Maaløe, S., 1976, The zoned plagioclase of the Skaergaard intrusion, East Greenland : Jour. of Pet., v. 17, p.398-419.

Marais, C.L., 1977, An investigation of the Pyroxenite Marker and the associated rocks in the Main zone of the Eastern Bushveld Complex : Unpubl. M.Sc. Thesis, Pretoria University.

McBirney, A.R., 1975, Differentiation of the Skaergaard Intrusion : Nature, v. 253, p.691-694.

McBirney, A.R. and Noyes, R.M., 1979, Crystallization and layering of the Skaergaard Intrusion : Jour. of Pet., v. 20, p.487-554.

McCarthy, T.S., and Lee, C.A., 1981, Sulphur saturation in the Lower and Critical zones of the Bushveld Complex : In press.

Minster, J.F., Minster, J.B., Treuil, M. and Allegré, C.J., 1977, Systematic use of trace elements in igneous processes, Part II : Contrib. Miner. Petrol., v. 61, p.49-77.

Mitchell, A.A., 1980, The extrusive and intrusive basaltic rocks of the Molteno-Jamestown area : Unpubl. M.Sc. Thesis, Rhodes University.

Morse, S.A., 1973, The Nair anorthosite project, Labrador : Field Report, Contr. 11, Geol. Dept. Univ. Massachusetts, p.156.

Paster, T.P., Schauwecker, D.S. and Haskin, L.A., 1974, The behaviour of some trace elements during solidification of the Skaergaard layered series : Geochim. et Cosmochim., v. 34, p.307-322.

Pearce, J.A. and Norry, M.J., 1979, Petrogenetic implications of Ti, Zr, Y and Nb variations in volcanic rocks : Contrib. Miner. Petrol., v. 69, p.33-47.

Phemister, J., 1934, Zoning of plagioclase feldspar : Min. Mag., v.23, p.541-555.

Philpotts, J.A. and Schnetzler, C.C., 1970, Phenocryst-matrix partition coefficients for K, Rb, Sr, and Ba, with applications to anorthosite and basalt genesis : Geochim. et Cosmochim., v. 34, p.307-322.

Poldervaart, A. and Hess, H.H., 1951, Pyroxenes in the crystallization of basaltic magmas : Jour. Geol., v. 59, p.472-489.

Ringwood, A.E., 1970, Petrogenesis of Apollo 11 basalts and implications for lunar origin : Jour. Geophys. Res., v. 75, p.6453-6479.

Robey, J. v. A., 1976, Aspects of the geochemistry of the dolerites and basalts of the north-eastern Cape Province, South Africa : Unpubl. M.Sc. Thesis, Rhodes University.

Sampson, E., 1932, Magmatic chromite deposits in Southern Africa : Econ. Geol, v. 27, p.113-144.

Sato, H., 1977, Nickel content of basaltic magmas : identification of primary magmas and a measure of the degree of olivine fractionation : Lithos, v. 10, p.113-120.

Seward, T.M., 1971, The distribution of transition elements in the system $CaMgSi_2O_6$-$Na_2Si_2O_5$-H_2O at 1000 bars pressure : Chem. Geol., v. 7, p.73-95.

Schmitt, R.A., Smith, R.H., Lasch, J.E., Mosen, A.W., Olehy, D.A. and Vasilerskis, J., 1963, Abundances of the fourteen rare-earth elements, scandium and yttrium in meteorites and terrestrial matter: Geochim. et Cosmochim., v. 27, p.577-622.

Schwellnus, J.S.I., 1956, The basal portion of the Bushveld Igneous Complex and the adjoining metamorphosed sediments in the Northeastern Transvaal : Unpubl. D.Sc. Thesis, Pretoria University.

Shand, S.J., 1943, Eruptive Rocks : Murby and Co., London, 488p.

Smith, J.V., 1975, Some chemical properties of feldspars : In, P.H. Ribbe (ed.), Feldspar mineralogy, v. 2, Min. Soc. Amer.

Streckeisen, A., 1976, To each plutonic rock its proper name : Earth. Sci. Reviews, v. 12, p.1-33.

Sun, C.O., Williams, R.J., and Sun, S.S., 1974, Distribution coefficients of Eu and Sr for plagioclase-liquid and clinopyroxene-liquid equilibria in ocean ridge basalt: an experimental study : Geochim. et Cosmochim., v. 38, p.1415-1433.

Taylor, S.R., 1965, The application of trace element data to problems in petrology : Phys. Chem. Earth, v. 6, p.133-214.

Van der Walt, C.F.J., 1941, Chrome ores of the Western Bushveld Complex: Trans. Geol. Soc. South Africa, v. 44, p.79-112.

Van Zyl, J.P., 1970, The petrology of the Merensky Reef and the associated rocks on Swartklip 988, Rustenburg district : In, Visser, D.J.L., and von Gruenewaldt, G. (eds.), Symposium on the Bushveld Igneous Complex and other layered intrusions, Geol. Soc. South Africa, Spec. Pub. 1, p.80-107.

Vermaak, C.F. and Hendricks, L.P., 1976, Review of the mineralogy of the Merensky Reef, with the specific reference to new data on the precious metal mineralogy : Econ. Geol., v. 71, No. 7, p.1244-1269.

Vermaak, C.F., 1976, The Merensky Reef - Thoughts on its environment and genesis : Econ. Geol., v. 71, No. 7, p.1270-1298.

Viljoen, M.J. and Feuchtwanger, T., 1977, The northern Gap area of the B.I.C., results of a thermal scanner survey and a summary of available information : J.C.I. Fundamental Res., Report No. 65, (unpubl.) 14p.

Wager, L.R., 1959, Differing powers of crystal nucleation as a factor producing diversity in layered igneous intrusions : Geol. Mag., v. 96, p.75-80.

Wager, L.R., Brown, G.M. and Wadsworth, W.J., 1960, Types of igneous cumulates : Jour. of Pet., v. 1, p.73-85.

Wager, L.R., 1963, The mechanism of adcumulus growth in the layered series of the Skaergaard intrusion : Spec. Paper Mineralog. Soc. Amer., v. 1, p.1-9.

Wager, L.R., 1968, Rhythmic and cryptic layering in mafic and ultramafic plutons : In, Hess, H.H. and Poldervaart, A, (eds.), Basalts,Volume 2, Wiley Interscience.

Wager, L.R. and Brown, G.M., 1968, Layered Igneous Rocks : Oliver and Boyd, Edinburgh and Lond., 588p.

Wagner, P.A., 1929, The platinum deposits and mines of South Africa : Oliver and Boyd, Edinburgh, 326p.

Walker, K.R., 1970, The Palisade sill, New Jersey : A reinvestigation : Geol. Soc. Amer. Special Paper III, p.178.

Walraven, F., and Darracott, B.W., 1976, Quantitative interpretation of a gravity profile across the Western Bushveld Complex : Trans. Geol. Soc. South Africa, v. 79, p.22-26.

Wasserstein, B., 1936, Some notes on the Critical zone of the Bushveld gabbro at the Swartkop chrome mine in the Rustenburg district : Trans. Geol. Soc. South Africa, v. 39, p.215-222.

Wells, R.A., 1977, Pyroxene thermometry in simple and complex systems : Contrib. Miner. Petrol., v. 62, p.129-139.

Willemse, J., 1969, The geology of the Bushveld Igneous Complex, the largest repository of magmatic ore deposits in the world : Econ. Geol. Monogr. 4 p.1-22.

Wood, B.J. and Banno, S., 1973, Garnet - orthopyroxene and orthopyroxene - clinopyroxene relationships in simple and complex systems : Contrib. Miner. Petrol., v. 42, p.109-124.

Osborn, E.F., 1980, On the cause of the reversal of the normal fractionation trend - an addendum to the paper by E.N. Cameron, "Evolution of the Lower Critical Zone, Central sector, Eastern Bushveld Complex, and its chromite deposits": Econ. Geol., v. 75, p. 872-875.

Paster, T.P., Schauwecker, D.S. and Haskin, L.A., 1974, The behaviour of some trace elements during solidification of the Skaergaard layered series : Geochim. et Cosmochim., v. 34, p. 307-322.

Pearce, J.A. and Norry, M.J., 1979, Petrogenetic implications of Ti, Zr, Y and Nb variations in volcanic rocks : Contrib. Miner. Petrol., v. 69, p. 33-47.

Philpotts, J.A. and Schnetzler, C.C., 1970, Phenocryst-matrix partition coefficients for K, Rb, Sr, and Ba, with applications to anorthosite and basalt genesis : Geochim. et Cosmochim., v. 34, p. 307-322.

Pringle, G.J., Trembath, L.T. and Pajari, G.J., 1974, Crystallization history of a zoned plagioclase (Microprobe analysis of a zoned plagioclase from the Grand Manan tholeiite sheet) : Min. Mag., v. 39, p. 867-877.

Richards, D.J., 1974, Some aspects of the Pilanesberg dyke system deduced from aeromagnetic, ground magnetic and photogeological studies : S.A. Dept. of Mines, Annals of the Geol. Survey, v. 10, p. 97-99.

Ringwood, A.E., 1970, Petrogenesis of Apollo 11 basalts and implications for lunar origin : Jour. Geophys. Res., v. 75, p. 6453-6479.

Robey, J. v. A., 1976, Aspects of the geochemistry of the dolerites and basalts of the north-eastern Cape Province, South Africa : Unpubl. M.Sc. Thesis, Rhodes University.

Roeder, P.L. and Emslie, R.F., 1970, Olivine-liquid equilibrium : Contrib. Miner. Petrol., v. 29, p. 275-289.

Sampson, E., 1932, Magmatic chromite deposits in Southern Africa : Econ. Geol., v. 27, p. 113-144.

Sato, H., 1977, Nickel content of basaltic magmas : identification of primary magmas and a measure of the degree of olivine fractionation : Lithos, v. 10, p. 113-120

Seward, T.M., 1971, The distribution of transition elements in the system $CaMgSi_2O_6$-$Na_2Si_2O_5$-H_2O at 1000 bars pressure : Chem. Geol., v. 7, p. 73-95.

Schmitt, R.A., Smith, R.H., Lasch, J.E., Mosen, A.W., Olehy, D.A. and Vasilerskis, J., 1963, Abundances of the fourteen rare-earth elements, scandium and yttrium in meteorites and terrestrial matter : Geochim. et Cosmochim., v. 27, p. 577-622.

Schwellnus, J.S.I., 1956, The basal portion of the Bushveld Igneous Complex and the adjoining metamorphosed sediments in the Northeastern Transvaal : Unpubl. D.Sc. Thesis, Pretoria University.

Schwellnus, J.S.I., Hiemstra, S.A. and Gasparrini, E., 1976, Merensky Reef at the Atok Platinum mine and its environs : Econ. Geol., v. 71, No. 1, P. 249-260.

Shand, S.J., 1943, Eruptive Rocks : Murby and Co., London, 488p.

Sharkov, Ye. V., 1971, Rhythmic stratification in layered intrusions and its origin : International Geology Review, v. 14, No. 6, p. 592-598.

Shaw, D.M., 1961, Element distribution laws in geochemistry : Geochim. et Cosmochim., v. 23, p. 116-134.

Shaw, D.M., 1977, Trace element melting models : In, Ahrens, L.H. (ed.), Origin and distribution of the elements, Pergamon Press, Oxford, p. 577-586.

Smith, J.V., 1975, Some chemical properties of feldspars : In, P.H. Ribbe (ed.), Feldspar mineralogy, v. 2, Min. Soc. Amer.

Streckeisen, A., 1976, To each plutonic rock its proper name : Earth. Sci. Reviews, v. 12, p. 1-33.

Sun, C.O., Williams, R.J., and Sun, S.S, 1974, Distribution coefficients of Eu and Sr for plagioclase-liquid and clinopyroxene-liquid equilibria in ocean ridge basalt : an experimental study : Geochim. et Cosmochim., v. 38, p. 1415-1433.

Taylor, S.R., 1965, The application of trace element data to problems in petrology : Phys. Chem. Earth, v. 6, p. 133-214.

Thayer, T.P., and Jackson, E.D., 1972, A classification of igneous rocks by their history of crystallization and emplacement : U.S. Geol. Surv. Prof. Paper 800-B, p. B79-B83.

Van der Walt, C.F.J., 1941, Chrome ores of the Western Bushveld Complex : Trans. Geol. Soc. South Africa, v. 44, p. 79-112.

Van Zyl, J.P., 1970, The petrology of the Merensky Reef and the associated rocks on Swartklip 988, Rustenburg district : In, Visser, D.J.L., and von Gruenewaldt, G. (eds.), Symposium on the Bushveld Igneous Complex and other layered intrusions, Geol. Soc. South Africa, Spec. Pub. 1, p. 80-107.

Vermaak, C.F. and Hendricks, L.P., 1976, Review of the mineralogy of the Merensky Reef, with the specific reference to new data on the precious metal mineralogy : Econ. Geol.,v. 71, No. 7, p. 1244-1269.

Vermaak, C.F., 1976, The Merensky Reef - Thoughts on its environment and genesis : Econ. Geol., v. 71, No. 7, p. 1270-1298.

Viljoen, M.J. and Feuchtwanger, T., 1977, The northern Gap area of the B.I.C., results of a thermal scanner survey and a summary of available information : J.C.I. Fundamental Res., Report No. 65, (unpubl.) 14p.

Viljoen, M.J., De Klerk, W.J., Coetzer, P.M., and Hatch, N.P., 1981, The geology of Union Section of Rustenburg Platinum mines with special reference to the Merensky Reef : In press.

Wadsworth, W.J., 1973, Magmatic Sediments : Min. Sci. and Eng., v. 5, p. 25-35.

Wager, L.R., 1959, Differing powers of crystal nucleation as a factor producing diversity in layered igneous intrusions : Geol. Mag., v. 96, p. 75-80.

Wager, L.R., Brown, G.M. and Wadsworth, W.J., 1960, Types of igneous cumulates : Jour. of Pet., v. 1, p. 73-85.

Wager, L.R., 1963, The mechanism of adcumulus growth in the layered series of the Skaergaard intrusion : Spec. Paper Mineralog. Soc. Amer., v. 1, p. 1-9.

Wager, L.R. and Brown, G.M., 1968, Layered Igneous Rocks : Oliver and Boyd, Edinburgh and Lond, 588p.

Wagner, P.A., 1929, The platinum deposits and mines of South Africa : Oliver and Boyd, Edinburgh, 326p.

Walker, K.R., 1970, The Palisade sill, New Jersey : A reinvestigation : Geol. Soc. Amer. Special Paper III, p. 178.

Wasserstein, B., 1936, Some notes on the Critical zone of the Bushveld gabbro at the Swartkop chrome mine in the Rustenburg district : Trans. Geol. Soc. South Africa, v. 39, p. 215-222.

Walraven, F., 1976, Notes on the late stage history of the Western Bushveld Complex : Trans. Geol. Soc. South Africa, v. 79, p. 13-21.

Walraven, F., and Darracott, B.W., 1976, Quantitative interpretation of a gravity profile across the Western Bushveld Complex : Trans. Geol. Soc. South Africa, v. 79, p. 22-26.

Wells, R.A., 1977, Pyroxene thermometry in simple and complex systems : Contrib. Miner. Petrol., v. 62, p. 129-139.

Willemse, J., 1969, The geology of the Bushveld Igneous Complex, the largest repository of magmatic ore deposits in the world : Econ. Geol. Monogr. 4, p. 1-22.

Wood, B.J. and Banno, S., 1973, Garnet - orthopyroxene and orthopyroxene-clinopyroxene relationships in simple and complex systems : Contrib. Miner. Petrol., v. 42, p. 109-124.

Wright, T.L., 1974, Presentation and interpretation of chemical data for igneous rocks : Contrib. Miner. Petrol., v. 48, p. 233-248.